LMD THESIS

Submitted to the

FACULTY OF SCIENCE - DEPARTMENT OF CHEMISTRY

For the Degree of

DOCTOR OF PHILOSOPHY

Specialty: Polymeric Materials and Environment

By

Mr BAOUCH Zakarya

On the Theme

Preparation and Characterization of Hybrid Materials Composites Based on Biopolymers and Clays, Application to the Adsorption of Dyes.

Defended publicly on March 2021 in Tlemcen before the jury composed of :

Mr. MEDJAHED Kouider	Professor	University of Tlemcen	Chairman
Mr. BENABADJI Kamel Ismat	Professor	University of Tlemcen	Supervisor
Mr. BOURAS Brahim	Associate Professor	University of Tlemcen	Co-Supervisor
Mr. BENMANSOUR Kamel	Professor	University of Tlemcen	Examiner
Mr. BOUSALEM Smain	Professor	University of Ain Temouchent	External Examiner
Mr. MORSLI Amine	Associate Professor	University of Oran USTOMB	External Examiner

UNIVERSITE ABOU-BEKR BELKAID – TLEMCEN

THÈSE LMD

Présentée à :

FACULTE DES SCIENCES – DEPARTEMENT DE CHIMIE

Pour l'obtention du diplôme de :

DOCTORAT

Spécialité : Matériaux Polymères et Environnement

Par :

Mr BAOUCH Zakarya

Sur le thème

Préparation et Caractérisation de Matériaux Composites Hybrides à base de Biopolymères et d'Argiles, Application à l'adsorption des Colorants.

Soutenue publiquement le Mars 2021 à Tlemcen devant le jury composé de :

Mr MEDJAHED Kouider	Professeur	Université de Tlemcen	Président
Mr BENABADJI Kamel Ismat	Professeur	Université de Tlemcen	Directeur de Thèse
Mr BOURAS Brahim	Maître de Conférences A	Université de Tlemcen	Co-Directeur de Thèse
Mr BENMANSOUR Kamel	Professeur	Université de Tlemcen	Examinateur
Mr BOUSALEM Smain	Professeur	Centre Universitaire Ain Temouchent	Examinateur
Mr MORSLI Amine	Maître de Conférences A	Université d'Oran USTOMB	Examinateur

This Work is Dedicated to My Parents

GHEMADI **Fatiha** & BAOUCH **Tayeb.**

TABLE OF CONTENTS

CHAPTER I: INTRODUCTION

CHAPTER II: LITERATURE REVIEW

PART I: DYES

CHAPTER III: MATERIALS, CHARACTERISATION AND EXPERIMENT METHODS

PART III
STUDY OF THE DECOLORIZATION AND COD REDUCTION EFFICIENCY OF THE MIXTURE OF THE THREE DYES (MB, BZR, AND TB).

ACKNOWLEDGEMENTS

LIST OF FIGURES

CHAPTER II: LITERATURE REVIEW

PART I: DYES

PART II: CLAYS

PART III: BIOPOLYMERS

PART IV: SORPTION

CHAPTER III: MATERIALS, CHARACTERISATION AND EXPERIMENT METHODS

PART I: ORGANO-BENTONITE

PART II

ORGANO-BENTONITE/CMC (BAS/CMC)

PART III

STUDY OF THE DECOLORIZATION AND COD REDUCTION EFFICIENCY OF THE MIXTURE OF THE THREE DYES (MB, BZR, AND TB)

LIST OF TABLES

NOMENCLATURE

IUPAC	Union of Pure and Applied Chemistry
HDTMA-Br	Hexadecyltrimethylammonium Bromide
CMC	CarboxyMethyl Cellulose
MB	Methylene Blue
BzR	Bezathren Red
TB	Telon Blue
BN	Natural Bentonite
BA	Activated Bentonite
CEC	Cation exchange capacity meq g /100 g
BAS	OrganoBentonites (Bentonite modified with HDTMA-Br)
BAS X	X : The initial amounts of HDTMA-Br vs. the CEC of Bentonite
BAS/CMC	OrganoBentonites modified with CMC
BAS/CMC X/Y	X: is the amount of BAS in grams, Y: is the amount of CMC in grams
C_0	Initial dye concentration, (mg/L)
C_e	Concentration at equilibrium, (mg/g)
C_1	Concentration of X in solvent 1 (mole/L or mg/L)
C_2	Concentration of X in solvent 2 (mole/L or mg/L)
V	volume of solution (mL)
K_d	Partition coefficient (distribution constant).
q_m	maximum adsorbate capacity, (mg/g)
q_e	Amount of adsorbate per gram of adsorbent at equilibrium, (mg/g)
q_t	Amount of adsorbate per gram of adsorbent at any time t, (mg/g)
Kf	Pseudo-first-order rate constant (min^{-1})
Ks	Pseudo-second-order rate constant, (mg/g.min)
KF	Freundlich adsorption constant, (L/g)
K_d	The diffusion rate constant, (mg/g $min^{-1/2}$)
m	Amount of adsorbent added in mg
n	Freundlich constant
R^2	Linear regression coefficient
N_A	Avogadro's number
S_{total}	Specific surface area, (m^2/g)
$\Delta G°$	Gibbs free energy change, (kJ/mole)
$\Delta H°$	Enthalpy change, (kJ/mole)

ΔS°	Entropy change, (J/k mole)
COD	Chemical Oxygen Demand
BOD	Biological oxygen demand
BET	Brunauer-Emmett-Teller
XRD	X-ray diffraction
TGA	Thermogravimetric Analysis
UV-Vis	Ultraviolet-Visible
FTIR	Fourier Transform Infrared

ABSTRACT

The structural evolution of cost-effective Organo-Bentonite (Bentonite modified with different loadings of HDTMA (Hexadecyltrimethylammonium Bromide)) from 50 to 200% of the CEC with CMC (CarboxyMethyl Cellulose) in different percentages is investigated and linked to the adsorption uptake and mechanism of an important industrial dyes (Methylene Blue (MB), Bezathren Red (BzR) and Telon Blue (TB) in single and mixture system from the aqueous solution. The prepared materials were characterized by X-ray diffraction XRD, infrared spectroscopy measurements FT-IR and thermal analysis ATG/DTG. The intercalation of the surfactant cations (BAS) and the CarboxyMethyl Cellulose (BAS/CMC) in the interlayer spaces of bentonite (BA) was confirmed by the increase of the basal spacing from 1.13 to 1.78 nm and from 1.78 nm to 2.51 nm respectively.

The influence of several factors on the adsorption capacity such as contact time, dye solution pH, adsorbent dosage, initial dyes concentrations, and the temperature was investigated. The kinetic data were found to follow the pseudo second-order model for all dyes adsorption. The equilibrium data were analyzed using the Langmuir and Freundlich models. The Langmuir isotherm model is the most suitable to describe MB, BzR and TB dyes adsorption.

The calculated Langmuir maximum adsorption capacities for BAS adsorbent increased from 74 to 174.52 mg/g for MB and from zero to 107.87 and 306.74 mg/g, for BzR and TB respectively. Also for the BAS/CMC adsorbent, the maximum adsorption capacities increased from 74 to 161.81 mg/g for MB and from zero to 273.22 and 63.65 mg/g, for BzR and TB respectively. It is also important to note that, the formed particles at the end of the adsorption changes from powder in the case of BAS to a visible big flocs in BAS/CMC case. The adsorption process was found to be endothermic in nature in all cases (MB, TB, and BzR). It is also important to note that the particles formed at the end of adsorption change from powder in the case of BAS to large visible flocs in the case of BAS/CMC.

The prepared BAS/CMC composite were designed to decolorize and to reduce COD content in a mixture of three dyes, i.e., Methylene Blue (MB, cationic dye), Bezathren Red (BzR, vat dye), and Telon Blue (TB, anionic dye) using adsorption process. Optimum pH and the initial concentration of each dye were determined.

Adsorption experiments were performed on simulated effluent solutions containing equal and different concentrations of MB, BzR and TB dyes. Optimal adsorption conditions were found at pH 8 and a total concentration of 150 mg of dyes mix/L at 24 °C using 75 mg BAS/CMC

adsorbent, resulting in a COD reduction of more than 94% and decolorization of about 96%. It is also important to note that percentage of reduced COD is low in the case of the absence of Methylene Blue (43.73%) and very high in the other cases by approximately 88% due to the presence of a synergistic effect and strong electrostatic interactions between Methylene Blue and the two other dyestuffs.

Based on the obtained results in this thesis, we can conclude that the adsorbent BAS and BAS/CMC can be considered as a good material for the removal of MB, BzR and TB dyes in single and mixtures systems. Due to the availability, efficiency and low cost of these material, these results are encouraging to be tested and evaluated on an industrial scale with real and more complex wastewater.

General Introduction

One of the major future challenges facing humanity is to secure the supply of clean water to the world population. It is widely proven that population growth and pollution have a negative impact on water quality. Indeed, nowadays, dyes used in industrial activities are increasingly becoming a problematic class of pollutants to the environment. Due to the complex structure of dyes, their discharge to water bodies generates bad aesthetic and health problems (De Jesus da Silveira Neta et al., 2011). Over the last few years, several classes of dyes have been used in many industrial sectors such as rubber, textiles, cosmetics, plastics, leather, food and paper making (Kono, 2015). Wastewater discharged from these industries contains a variety of dyes and the majority of them are stable to light, heat and oxidizing agents and are usually non-biodegradable (Ngulube et al., 2017). Hence, the urgent need to remove them from the environment. Dyes can be classified as cationic, anionic, and nonionic (disperse/vat). These three kinds of dyes are the most widely used in many industries. Due to their complex structures, they are not easily biodegradable and they can therefore have destructive impacts on the environment (Kuppusamy et al., 2016). Today, adsorption is viewed as a viable procedure for the removal of dyes from the environment. It is a simple process that is economically feasible and it can help to recycle the adsorbents without any harmful residues. Indeed, a large number of studies have investigated the use of various adsorbents for the purpose of reducing dye concentrations in aqueous solutions. Materials like walnut husk (Çelekli et al., 2012), modified chitosan composite (Zhu et al., 2011), biochars from crop residues (Xu et al., 2011), natural zeolite (Akgül & Karabakan, 2011), cross-linked succinyl chitosan (Huang et al., 2011), modified bentonite (Ghemit et al., 2019), quaternized poly(4-vinylpyridine) copolymers (Medjahed et al., 2013), natural clinoptilolite (Ghaedi et al., 2011), activated carbon (Elmoubarki et al., 2015), and chromium-intercalated montmorillonite (Bouberka et al., 2006), have been used to remove dyes from aqueous solutions. Clays, such as bentonite, have shown high removal efficiency; it was found that their adsorption

capacities may exceed that of activated carbon under the same temperature and pH conditions (Ali et al., 2012). The adsorption and desorption of organic molecules on clays depend primarily on the surface properties of these materials and on the chemical properties of their molecules as well (Özcan et al., 2004). Note that the net negative charge on clays provides them with a high adsorption capacity toward positively charged cations such as cationic dyes, heavy metals, etc. However, clays have a poor affinity for negatively charged anionic dyes. It is worth indicating that a simple modification of clays can help to improve their adsorption capacities by the use of cationic polymers or surfactants through straightforward ion-exchange reactions which generate some interactions between the cationic species and the adsorbate (Kaya et al., 2013). Previous studies have shown that the removal of acid dyes can be better enhanced by the use of modified montmorillonite, in comparison with untreated montmorillonite. It is worth mentioning that modified montmorillonites have previously been prepared and used for Congo red dye adsorption. It was also found that the adsorption efficiency is influenced by the length of alkyl chains present in a series of alkyl ammonium bromides (Wang & Wang, 2008). Several authors have successfully modified montmorillonite using some unconventional modifiers (Açışlı et al., 2017), such as gemini surfactants, for the adsorption of organic contaminants (Yang et al., 2014). The results obtained showed that the adsorption capacity of surfactant-modified montmorillonites for organic contaminants was greatly improved in comparison with that of natural montmorillonite.

The overall objective of the present research is to synthesize a cost-effective, environmentally friendly and sustainable adsorbents based on clay and Biopolymers and to evaluate its effectiveness for the removal of three kinds of dyes, namely Methylene Blue (MB, cationic dye), Telon Blue (TB, anionic dye), and Bezathren Red (BzR, nonionic dye), from aqueous solutions by adsorption in single and mixture systems. Optimization of the adsorption conditions was possible by investigating the influence of different parameters. The

equilibrium data obtained were then assessed using various adsorption isotherm models. Some kinetic studies were also conducted in order to evaluate the adsorption mechanism of these dyes.

The thesis consists of 153 pages including table of contents, introduction, three chapters, conclusion, appendices, and reference lists included at the end of each chapter.

The First Chapter outlines a brief background of water sources, water pollutants and current methodologies used in the purification and treatment of wastewater containing organic dyes and inorganic heavy metal ions. It also describes the aim and the objectives of this research study as well as the organisation of this thesis

The Second Chapter is divided into four parts that present a literature review of the four main topics of this study.

The First Part presents a brief background of water sources, water pollutants and a detailed and up to date literature information about organic dyes, their classification, sources, applications, and their toxicity effects in the aquatic environment.

The Second Part is devoted to the bibliographical research on the properties and modifications of clays and their applications in different sectors.

The Third Part is intended for polysaccharides and biopolymers. It describes the latest and current state of art in modification and development of cost effective and environmentally friendly adsorbents, which are comparative to the high adsorption capacity commercial activated carbon in the removal of organic and inorganic pollutants.

In the Fourth Part, we outline the most current methodologies used in the purification and treatment of wastewater containing organic dyes and inorganic heavy metal ions. In addition, this part presents the classification of adsorption isotherms and kinetic models for batch and continuous adsorption processes. It also describes the aim and the specific objectives of this research study.

Chapter Three is devoted to the synthesis, characterization and application of synthesized materials in the adsorption of dyestuffs and is divided into three parts.

The First and Second Parts, present the synthesis and characterization of organo-bentonite (BAS) and organo-bentonite/Carboxymethyl Cellulose (BAS/CMC) materials and their adsorptive removal of three kinds of dyes, namely Methylene Blue, Telon Blue, and Bezathren Red from aqueous solutions by adsorption. It also provides the detailed experimental and data analysis results on the adsorption kinetics equilibrium, thermodynamics, and process design under various physio-chemical process parameters.

The Third Part evaluates the effectiveness of the prepared adsorbent (BAS / CMC) in the removal of organic dyes (MB, BzR and TB) in a mixed dye system from an aqueous solution under various conditions such as pH and the initial concentration of each dye by batch adsorption. The data analysis and mechanism of adsorption also presented here.

At the end, we close this thesis with a conclusion that gives an overview of the fruitful results of this research project. It also explains the gaps associated with this research and the future research direction and recommendations.

The main results of the thesis were published in one paper and communicated at six international conferences.

REFERENCES

Açışlı, Ö., Karaca, S., & Gürses, A. (2017). Investigation of the alkyl chain lengths of surfactants on their adsorption by montmorillonite (Mt) from aqueous solutions. *Applied Clay Science*, *142*, 90–99. https://doi.org/10.1016/j.clay.2016.12.009

Akgül, M., & Karabakan, A. (2011). Promoted dye adsorption performance over desilicated natural zeolite. *Microporous and Mesoporous Materials*, *145*(1–3), 157–164. https://doi.org/10.1016/j.micromeso.2011.05.012

Ali, I., Asim, M., & Khan, T. A. (2012). Low cost adsorbents for the removal of organic pollutants from wastewater. *Journal of Environmental Management*, *113*, 170–183. https://doi.org/10.1016/j.jenvman.2012.08.028

Bouberka, Z., Khenifi, A., Benderdouche, N., & Derriche, Z. (2006). Removal of Supranol

Yellow 4GL by adsorption onto Cr-intercalated montmorillonite. *Journal of Hazardous Materials*, *133*(1–3), 154–161. https://doi.org/10.1016/j.jhazmat.2005.10.003

Çelekli, A., Birecikligil, S. S., Geyik, F., & Bozkurt, H. (2012). Prediction of removal efficiency of Lanaset Red G on walnut husk using artificial neural network model. *Bioresource Technology*, *103*(1), 64–70. https://doi.org/10.1016/j.biortech.2011.09.106

De Jesus da Silveira Neta, J., Costa Moreira, G., da Silva, C. J., Reis, C., & Reis, E. L. (2011). Use of polyurethane foams for the removal of the Direct Red 80 and Reactive Blue 21 dyes in aqueous medium. *Desalination*, *281*(1), 55–60. https://doi.org/10.1016/j.desal.2011.07.041

Elmoubarki, R., Mahjoubi, F. Z., Tounsadi, H., Moustadraf, J., Abdennouri, M., Zouhri, A., El Albani, A., & Barka, N. (2015). Adsorption of textile dyes on raw and decanted Moroccan clays: Kinetics, equilibrium and thermodynamics. *Water Resources and Industry*, *9*, 16–29. https://doi.org/10.1016/j.wri.2014.11.001

Ghaedi, M., Hossainian, H., Montazerozohori, M., Shokrollahi, A., Shojaipour, F., Soylak, M., & Purkait, M. K. (2011). A novel acorn based adsorbent for the removal of brilliant green. *Desalination*, *281*(1), 226–233. https://doi.org/10.1016/j.desal.2011.07.068

Ghemit, R., Makhloufi, A., Djebri, N., Flilissa, A., Zerroual, L., & Boutahala, M. (2019). Adsorptive removal of diclofenac and ibuprofen from aqueous solution by organobentonites: Study in single and binary systems. *Groundwater for Sustainable Development*, *8*(February), 520–529. https://doi.org/10.1016/j.gsd.2019.02.004

Huang, X. Y., Bu, H. T., Jiang, G. B., & Zeng, M. H. (2011). Cross-linked succinyl chitosan as an adsorbent for the removal of Methylene Blue from aqueous solution. *International Journal of Biological Macromolecules*, *49*(4), 643–651. https://doi.org/10.1016/j.ijbiomac.2011.06.023

Kaya, E. M. Ö., Özcan, A. S., Gök, Ö., & Özcan, A. (2013). Adsorption kinetics and isotherm parameters of naphthalene onto natural- and chemically modified bentonite from aqueous solutions. *Adsorption*, *19*(2–4), 879–888. https://doi.org/10.1007/s10450-013-9542-3

Kono, H. (2015). Preparation and Characterization of Amphoteric Cellulose Hydrogels as Adsorbents for the Anionic Dyes in Aqueous Solutions. *Gels*, *1*(1), 94–116. https://doi.org/10.3390/gels1010094

Kuppusamy, S., Thavamani, P., Megharaj, M., Venkateswarlu, K., Lee, Y. B., & Naidu, R. (2016). Potential of Melaleuca diosmifolia as a novel, non-conventional and low-cost

coagulating adsorbent for removing both cationic and anionic dyes. *Journal of Industrial and Engineering Chemistry*, *37*, 198–207. https://doi.org/10.1016/j.jiec.2016.03.021

Medjahed, K., Tennouga, L., Mansri, A., Chetouani, A., Hammouti, B., & Desbrières, J. (2013). Interaction between poly(4-vinylpyridine-graft-bromodecane) and textile blue basic dye by spectrophotometric study. *Research on Chemical Intermediates*, *39*(7), 3199–3208. https://doi.org/10.1007/s11164-012-0832-2

Ngulube, T., Gumbo, J. R., Masindi, V., & Maity, A. (2017). An update on synthetic dyes adsorption onto clay based minerals: A state-of-art review. *Journal of Environmental Management*, *191*, 35–57. https://doi.org/10.1016/j.jenvman.2016.12.031

Özcan, A. S., Erdem, B., & Özcan, A. (2004). Adsorption of Acid Blue 193 from aqueous solutions onto Na-bentonite and DTMA-bentonite. *Journal of Colloid and Interface Science*, *280*(1), 44–54. https://doi.org/10.1016/j.jcis.2004.07.035

Wang, L., & Wang, A. (2008). Adsorption properties of Congo Red from aqueous solution onto surfactant-modified montmorillonite. *Journal of Hazardous Materials*, *160*(1), 173–180. https://doi.org/10.1016/j.jhazmat.2008.02.104

Xu, R. kou, Xiao, S. cheng, Yuan, J. hua, & Zhao, A. zhen. (2011). Adsorption of methyl violet from aqueous solutions by the biochars derived from crop residues. *Bioresource Technology*, *102*(22), 10293–10298. https://doi.org/10.1016/j.biortech.2011.08.089

Yang, S., Gao, M., & Luo, Z. (2014). Adsorption of 2-Naphthol on the organo-montmorillonites modified by Gemini surfactants with different spacers. *Chemical Engineering Journal*, *256*, 39–50. https://doi.org/10.1016/j.cej.2014.07.004

Zhu, H. Y., Jiang, R., Fu, Y. Q., Jiang, J. H., Xiao, L., & Zeng, G. M. (2011). Preparation, characterization and dye adsorption properties of γ-Fe 2 O 3 /SiO 2 /chitosan composite. *Applied Surface Science*, *258*(4), 1337–1344. https://doi.org/10.1016/j.apsusc.2011.09.045

CHAPTER II
LITERATURE REVIEW

PART I

1. DYE

1.1. Introduction

The art of color application to enhance our self appearance and the world around us has been known to man since time immemorial. Historical records of the use of natural dyes extracted from vegetables, fruits, flowers, certain insects and fish dating back to 3500 BC have been found. Color is the main attraction of any fabric. No matter how excellent its constitution, if unsuitably colored it is bound to be a failure as a commercial product. Fabric was earlier being dyed with natural dyes. These however gave a limited and a dull range of colors. Besides, they showed low color fastness when exposed to washing and sunlight (Kant, 2012).

Nowadays, dyes are becoming an important class of synthetic organic compounds used in many industries, especially textiles. Consequently, they have become common industrial environmental pollutants during their synthesis and later during fibre dyeing. The large-scale production and extensive application of synthetic dyes can cause considerable environmental pollution, making it a serious public concern. Legislation on the limits of colour discharge has become increasingly rigid. There is a considerable urgent need to develop treatment methods that are effective in eliminating dyes from their waste. Physicochemical and biological methods have been studied and applied, although each has its advantages and disadvantages, with the choice being based on the wastewater characteristics, available technology and economic factors. Some industrial scale wastewater treatment systems are now available; however, these are neither fully effective for complete colour removal nor do they address water recycling.

1.2. Dye sources, structure and their classifications

Dyes have been used as colour agents in textile, leather, paper, plastic, rubber, painting, cosmetic, food and pharmaceutical industries for centuries. The majority of natural dyes are extracted from plants and mineral sources (Shahid et al. 2013). Upon the introduction of industrial revolution, the industrial activities were increased dramatically and thus natural dyes production did not meet the industrial demand. Aniline purple was the first synthesised dye produced by W. H. Perkin back in 1856. Since then, synthetic dyes production have been increased significantly.

A dye can generally be described as a coloured substance that has an affinity for the substrate to which it is being applied. It is a coloured because it absorbs in the visible range of the spectrum at a certain wavelength (Table 1).

Table 1: Colours of the visible spectrum: wavelengths and frequencies intervals

Colour	Wavelength interval (nm)	Frequency interval (THz)
Red	~700 ~635	~430 ~480
Orange	~635 ~590	~480 ~510
Yellow	~590 ~560	~510 ~540
Green	~560 ~490	~540 ~610
Blue	~490 ~450	~610 ~670
Violet	~450 ~400	~670 ~750

In general, a small amount of dye in aqueous solution can produce a vivid colour, which is related with the high molar extinction coefficients. Colour can be quantified by spectrophotometry (visible spectra), chromatography (usually high performance liquid, HPLC) and high performance capillary electrophoresis (Figure. 1) (Rauf et al. 2010).
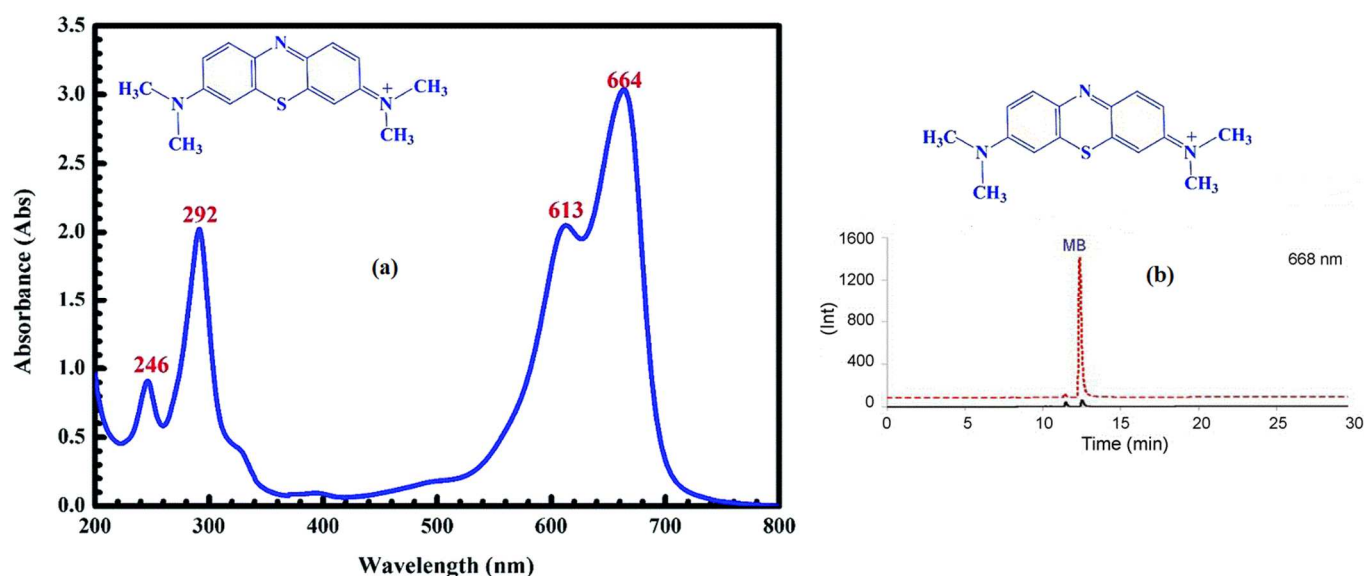
Figure 1: Visible spectra (a) and HPLC chromatogram (b) of Methylen Blue.

Synthetic dyes can be classified into acid dyes, reactive dyes, basic dyes, azo dyes, direct dyes, vat dyes and disperse dyes (Yagub et al. 2014a). Dye's classification and their chemical structure are presented in Table 2.

Table 2: Dye's classification and their chemical structure (Hernández et al. 2013, Yagub et al. 2014a).

Class	Examples of dyes	Chemical structure type
Anionic (Acid)	Congo Red, Methyl (orange and red) Acid (blue, black, violet, yellow)	Anthraquinone, xanthene, azo (including, nitroso, premetallised), nitro, and triphenylmethane.
Cationic (Basic)	Methylene Blue, Basic (red, brown, blue), Brilliant Green, Crystal Violet and Aniline Yellow	Hemicyanine, azo, cyanine, diazahemicyanine, azine diphenylmethane, xanthene, oxazine, triarylmethane, acridine and anthraquinone.
Direct	Martius Yellow, Direct (black, orange blue, violet, red	Phthalocyanine, azo, oxazine, and stilbene.
Reactive	Reactive (red, blue, yellow, black) Remazol (blue, yellow, red)	Anthraquinone, formazan, phthalocyanine, azo, oxazine and basic.
Disperse	Disperse (blue, red ,orange, yellow, brown)	Benzodifuranone, azo, anthraquinone, nitro, and styryl.
Vat	Indigo,Bezathren, Benzanthrone vat (blue and green)	Indigoids and anthraquinone.

The major structure element responsible for light absorption in dye molecules is the chromophore group, i.e., a delocalized electron system with conjugated double or simple bonds (Gomes, 2001). Chromophores frequently contain heteroatoms as N, O, and S, with non-bonding electrons. Common chromophores include -N=N- (azo), =C=O (carbonyl), =C=C=, C=NH, -CH=N-, NO or N-OH (nitroso), - NO_2 or NO-OH (nitro) and C=S (sulphur). As a complement to the electron acceptors action are the groups called auxochromes, which are electron donors generally on the opposite side of the molecule and their basic function is to increase colour. Indeed, the basic meaning of the word auxochrome is colour enhancer. Auxochromes can be classified as acidic (-COOH, -OH, $-SO_3H$) or basic (NHR, $-NR_2$, $-NH_2$). These groups also have the important property of giving a higher affinity to the fibre. The

chromogen, which is an aromatic structure (normally benzene, naphtalene or anthracene rings), is part of a chromogen-chromophore structure along with an auxochrome.

All dyes are water soluble except disperse dyes and vat dyes and they contain traces of metals such as copper, zinc, lead, chromium and cobalt in their aqueous solution. Synthetic dyes are generally classified into cationic dye, anionic dyes and non-ionic dyes based on the dye's particle charge in its aqueous solution. Cationic dyes is also known as basic dyes due to the presence of positive ions in the molecule's structure. Cationic dye interacts with the negative group presented on the fibre's molecules, thus colour can be attached firmly to the fibre. Anionic dyes contain acidic, direct and reactive dyes.

Anionic dyes have negative ions presence in their aqueous solution. Synthetic dyes exhibit characteristic differences in chemical bond structure such as azo, anthraquinone, triphenylmethane, phthalocyanine, formazin and oxazine. However they posse common features such as water solubility and ionic substituents (Hunger et al. 2007).

Reactive dyes contain reactive functional groups such as vinyl sulfone, chlorotriazine, trichloropyrimidine, and difluorochloropyrimidine that can undergo addition or substitution chemical reactions with the -OH, -SH, and -NH$_2$ groups present in textile fibers during the dyeing process (Demirbas, 2009; Labanda et al. 2009).

Disperse Vat dyes (of which indigo and woad are the most important examples) are water insoluble; however, under reducing conditions, they can be converted into a 'leuco' form (soluble in alkaline aqueous solutions), which penetrates the fibres during dyeing.

Metal-complex dyes exhibit higher light and wash fastness due to the presence of transition metals, such as chromium, copper, nickel or cobalt that modify the surface chemistry between the dye molecule and the fabric (Hao et al. 2000; Gomes 2001).

Azo dyes represent almost 60% of all the reactive dyes used in the textile industry followed by anthraquinone, indigoid, xanthene, arylmethane and phthalocyanine classes (Figure 2). (Wu et al. 2008). The color range obtained with this class of dyes is very wide (Gomes, 2001). More than one azo group can be present in the dye structure, dyes then being classified as azo, disazo, trisazo or poliazo as they have one, two, three or more groups. The anthraquinonic dyes are also widely used and comprise of a carbonyl group associated with a conjugated system of two benzene rings. As with the azo dyes, substitution groups in the aromatic rings are required to intensify the colour. The major difference is their need only of

electron donors once the carbonyl groups are in the uniquely possible position to act as electron acceptors.
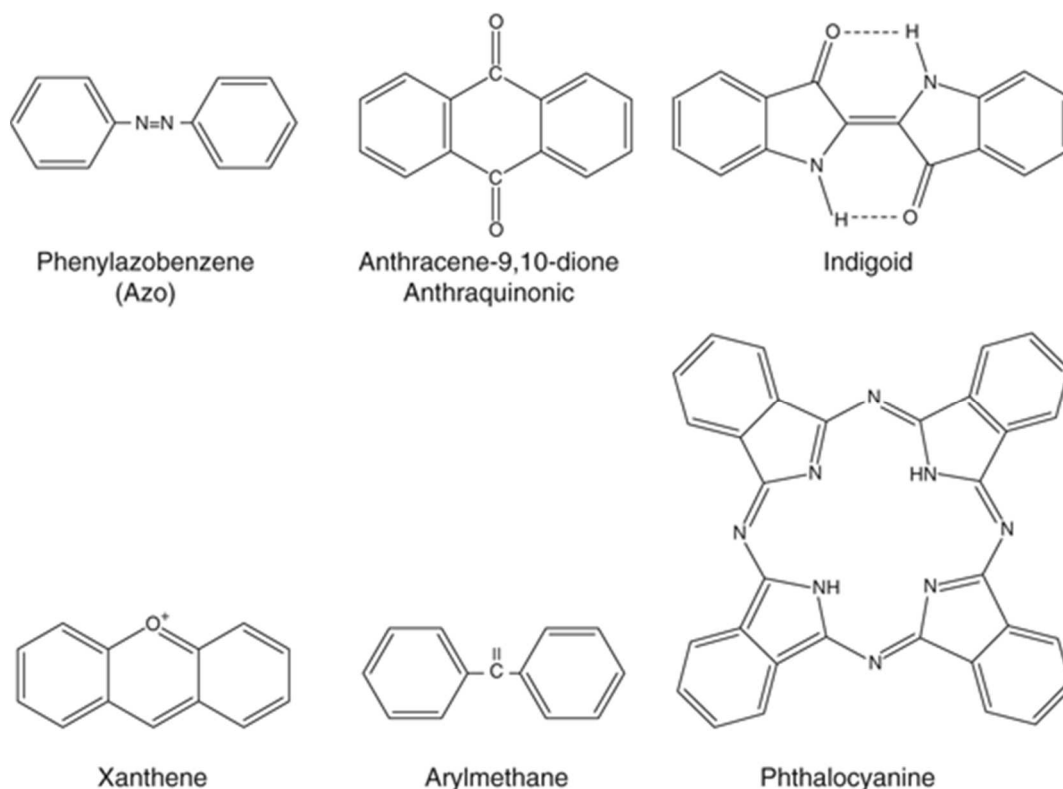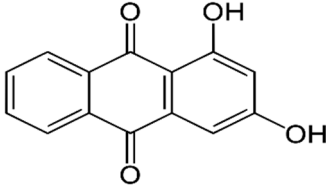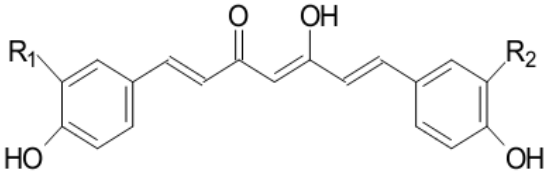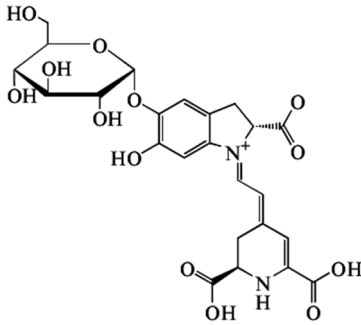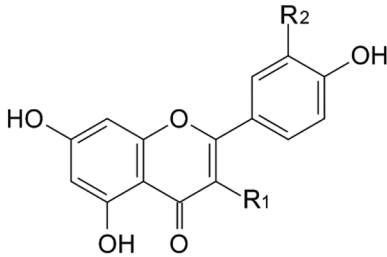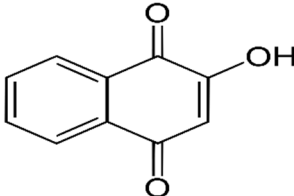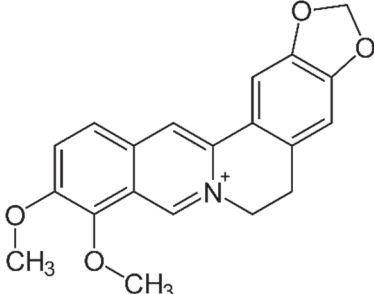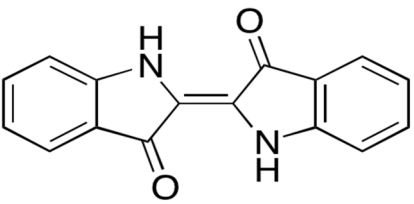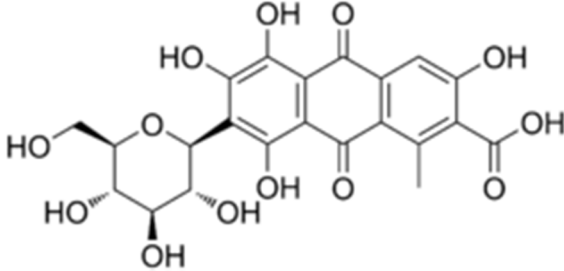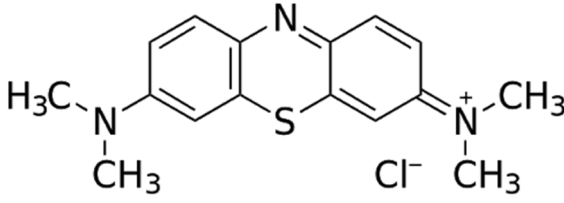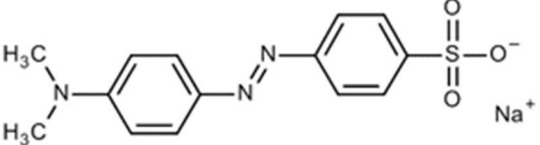
Figure 2. Different chromophores: Azo, anthraquinonic, indigoid, xanthene, arylmethane and phthalocyanine dye structures

Dyes are usually classified by their Colour Index (CI), developed by the Society of Dyes and Colourist (1984), which is edited every three months, It lists dyes firstly by a generic name based on its application and colour, then by assigning a 5-digit CI number based on its chemical structure, if known (O'Neill et al. 1999). Examples include Acid Blue 120 (26400), Reactive Red 4 (18105), and Mordant Yellow 10 (14010).

The most common natural and synthetic dyes used in textile industry are presented in Table 3 along with their scientific names and chemical structures.

Table 3: The common dyes used in textile industry (Samanta and Konar 2011, Shahid et al. 2013, Velho et al. 2017)

Dyes	Scientific names	Chemical structure
Indian madder	*Purpurin*	
Turmeric	*Curcuma Longa*	
Beetroot	*Betalain*	
Weld	*Reseda Luteola*	
Henna	*Lawsonia inermis*	

Berberry	*Berberis aristata*	
Indigo	*Indigofera tinctoria*	
Cochineal	*Dacylopius Coccus*	
Methylene blue	*methylthioninium chloride*	
Methyl orange	*Sodium 4-[4-(dimethylamino)phenyl]di azenylbenzene-1-sulfonate*	

Basic red 1	*Rhodamine 6G molbdosilicate*	
Congo red	*Lithium hydroxide 1H2O*	
Direct black 38	*Chlorazol black E*	
Bezathren Red FBB EPS	Disperse 11	
Telon Blue	Acid Blue 62	
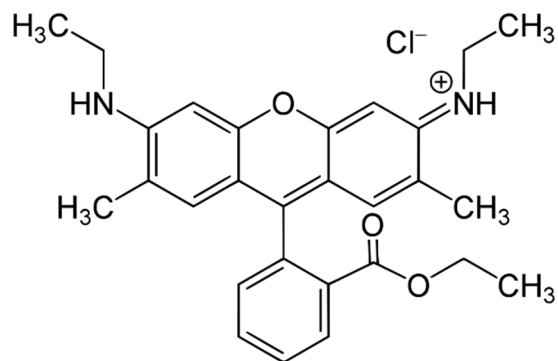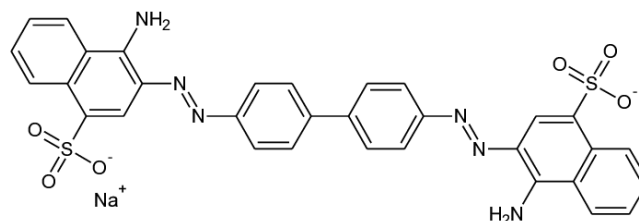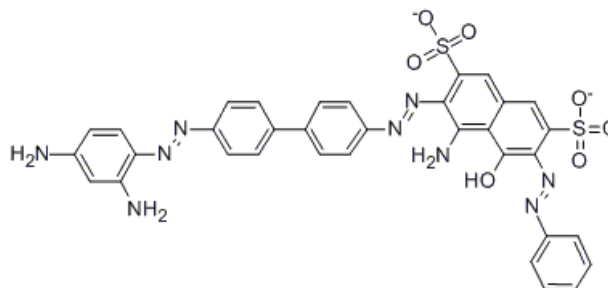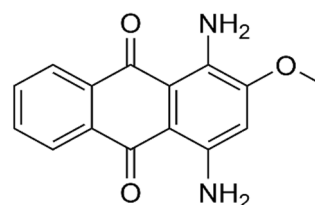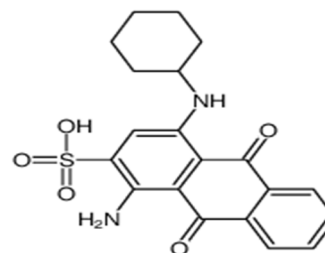
- **Examples of Dye-Fiber Interactions:**

The interaction with the fiber is partly based on ionic bonds between the sulfonate anions and the ammonium groups of the fiber, as shown below for wool:
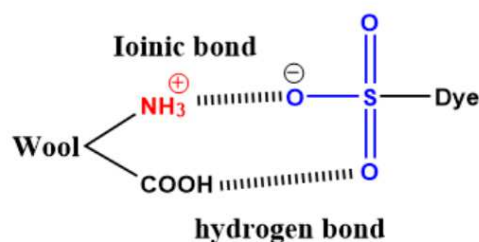
For polyamide, this is done under different pH conditions:
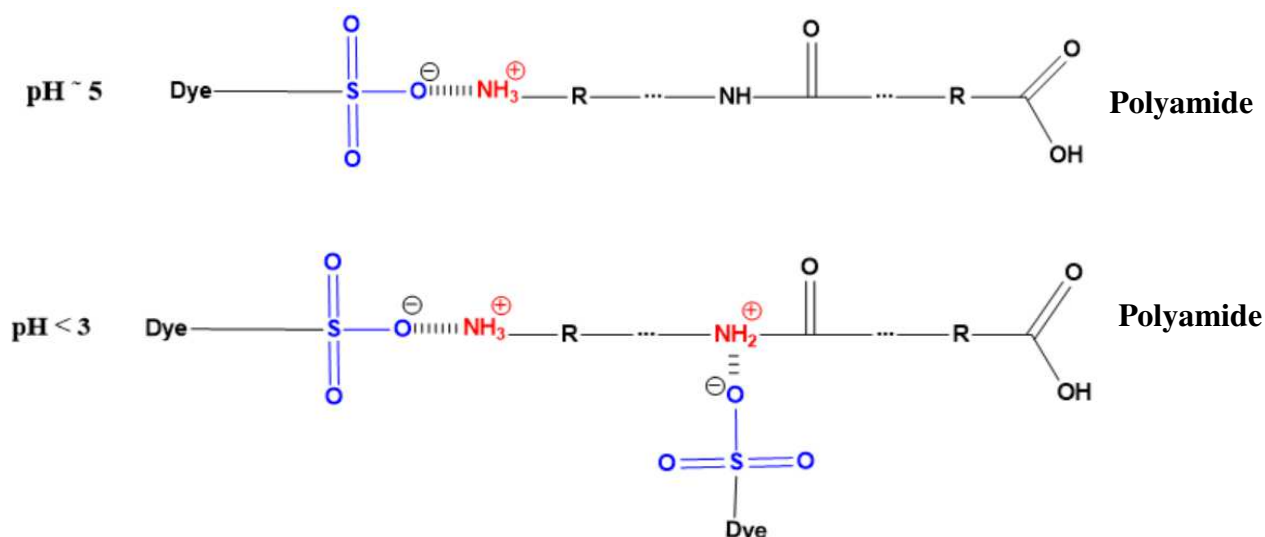
Figure. 3. The interactions Dye-Fiber by ionic bonds between sulfonate anions and ammonium groups in the case of polyamide under different pH conditions.

1.3. Health and Environmental Impact of dyes

Approximately 40 000 different synthetic dyes and pigments are used industrially, and about 450 000 tons of dyestuffs are produced worldwide. Azo dyes are the largest and more versatile class of dyes, accounting for up to 50% of the annual production (Malik & Grohmann, 2012).

Colour is usually the first contaminant to be recognized in a wastewater because a very small amount of synthetic dyes in water (< 1 ppm) are highly visible, affecting the aesthetic merit, transparency and gas solubility of water bodies. They have a complex structure and are photo-chemically stable, they adsorb and reflect the sunlight entering water, thereby interfering with the aquatic species growth and hindering photosynthesis. Additionally, they can have acute and/or chronic effects on organisms depending on their concentration and length of exposure, thus their effects on the environment have been a matter of concern for public and environmentalist (Quan et al. 2017).

Basic dyes are water soluble and they are highly visible in water even at very low concentration. Cationic dyes such as malachite green, aniline yellow, butter yellow, basic red, basic black, turquoise reactive, neutrichrome red and methylene blue are mainly used in textile and paper industries. Basic dye bearing effluents are toxic and can cause allergic dermatitis, skin irritation, mutations and even cancer (Eren, 2009). Also, cationic dyes can cause increased in heart rate, shock, vomiting, coronary vasoconstriction, decreased cardiac output, renal blood flow and mesenteric blood flow (Leyh et al. 2003; Mahmoud et al. 2012; Shakoor and Nasar 2016).
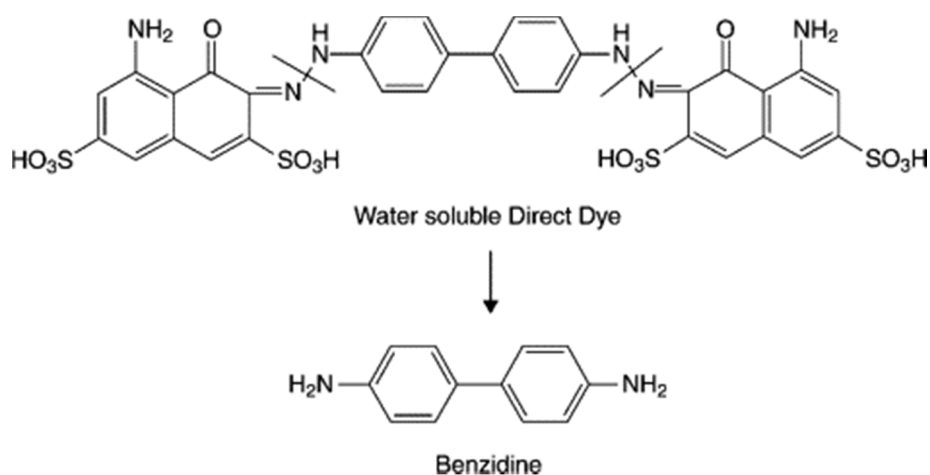
Figure. 4 shows a typical water-soluble dye that can generate carcinogenic benzidine metabolite upon reduction in the animal body (Chavan, 2011)

It is reported that more than 2000 structurally different azo dyes are currently in use and up to 130 azo dyes can form carcinogenic aromatic amines during anaerobic degradation process (Khan and Malik, 2014; Yaneva and Georgieva, 2012). Human expose to anionic and azo dyes and their by-products through the digestion, skin and lungs can cause disturbance in blood formation and even DNA damage which may lead to the genesis of malignant tumors (Khan and Malik, 2014). Further, the use of direct dyes is limited and it is generally used to colour the cellulosic and protein fibres through hydrogen bonds and Van der Waals force (Chakraborty, 2014). Some of direct dyes such as direct blue 6, direct brown 95 and direct black 38 can be metabolized to benzidine which is carcinogenic to humans.

The treatment of the effluents from the textile and dyestuff industries is challenging because the conventional wastewater treatment techniques are inadequate for the complete decolourization and removal of dye residues. This is due to the fact that dyes have complex aromatic molecular structures and thus they are stable and extremely resistant towards biological or chemical processing. (Tehrani-Bagha et al., 2010; Nguyen & Juang, 2013).

2. Wastewater Quality Assessment Parameters

A rapid development in science and technology and a vast usage of industrial processes are generating and releasing more and more pollutants into the environment. The number of pollutants and their concentrations in water are continuously increasing. Therefore, the analysis of chemical pollutants in water has become a serious concern to the professional world and to the authorities in charge of water quality (Chen et al., 2014). Some of the unique analytical parameter characteristics of the water pollution control industry are biochemical oxygen demand (BOD), chemical oxygen demand (COD), acidity, alkalinity, conductivity, hardness, metals, pH, and turbidity tests. Water quality depends on these parameters and their characterization tests (Henze, 2002).

2.1. Acidity

Acidity of water is determined when reacts with a strong base to a designated pH. Acidity indicates of how corrosive water is and the most common source of acidity in unpolluted water is carbon dioxide in the form of carbonic acid. Acidity is a measure of an aggregate property of water, and which can be interpreted in terms of specific substances only when the chemical composition of the sample is known (Brandi & Wilson-Wilde, 2013; Henze, 2002).

Acidity is classified by the pH value of a titration end point. Acidity caused by mineral acids contains a pH below 4.5 (Cheremisinoff & Davletshin, 2015). Industrial waste waters containing high mineral acidity must be neutralized before they are subjected to biological treatment or direct discharge to water sources. Standard methods for the examination of water and waste water recommends titration with sodium hydroxide to an end point pH of 3.7 to determine mineral acidity (Greenberg, 1984).

2.2. Alkalinity

Alkalinity is a measure of the capacity of water to neutralize acids. Alkalinity of water indicates the presence of bicarbonate, carbonate, and hydroxide ions. In waste water treatment, alkalinity is a quality parameter to determine the amenability of waste to the treatment process (Heze 2002). Waste water becomes alkaline when receiving alkalinity from the water supply, ground water, domestic use (detergents and soap-based products) and acid rain(Brandi & Wilson-Wilde, 2013).

Alkalinity is significant in the treatment processes for water and waste water. Alkalinity is expressed as phenolphthalein alkalinity or total alkalinity (Greenberg, 1984). Both types can be determined by titration with a standard sulfuric acid solution to an end point pH, evidenced by

the color change of a standard indicator solution. The pH also can be determined with a pH meter. Phenolphthalein alkalinity is determined by titration to a pH of 8.3 (the phenolphthalein end point) (Greenberg, 1984).

2.3. Conductivity

Conductivity is a measure of how well water can pass an electrical current. It is an indirect measure of the presence of inorganic dissolved solids. The presence of chloride, nitrate, sulfate, phosphate, sodium, magnesium, calcium, iron and aluminium increases conductivity of water. In addition, organic substances like oil, alcohol, and sugar conduct less electricity which indicates low conductivity of water (Murdoch et al., 1996).

The measurement of conductivity is generally expressed in S/cm (or mS/cm). The scale for conductivity starts at 0.05 µS/cm (at 25 °C) for ultra-pure water (Mike, 2005). The conductivity of natural waters, such as drinking water or surface water is typically in range of 100-1000 µS/cm.

2.4. Hardness

Hardness is frequently used as an assessment of the quality of water supplies. The hardness of a water is governed by the content of calcium and magnesium salts (temporary hardness), largely combined with bicarbonate and carbonate and with sulfates, chlorides, and other anions of mineral acids (permanent hardness).To distinguish the contributions of such anions from carbonates,hardness is sometimes termed as "carbonate hardnesss" or "noncarbonate hardness" and expressed as mg $CaCO_3$ (Wetzel, 2001). Hardness can be measured by calculation from the concentration of calcium and magnesium ions in the sample (Patnaik, 2010).

2.5. Metals

The effects of metals in water and wastewater range from beneficial through troublesome to dangerously toxic. Some metals are essential, others may adversely affect water consumers, wastewater treatment systems, and receiving waters. Some metals may be either beneficial or toxic, depending on concentration (Brandi & Wilson-Wilde, 2013).

2.6. Nitrogen

✓ Nitrogen as Ammonia

Ammonia (NH_3) is one of the most important pollutants in the aquatic environment because of its relatively highly toxic nature and its presence in surface water systems. It is discharged in large quantities in industrial, municipal and agricultural wastewaters. In aqueous solutions, ammonia assumes two chemical forms: NH_4^- ionized (less toxic/nontoxic) and NH_3 unionized (toxic). The relative concentration of ionized and unionized ammonia in an ammonia solution

are principally a function of pH, temperature and ionic strength of the aqueous solution (Rand & Petrocelli, 1985).

✓ **Nitrogen as Nitrate**

Nitrate (NO_3^-) generally occurs in trace quantities in surface water. It is the essential nutrient for many photosynthetic autotrophs and has been identified as the growth limit nutrient. It is only found in small amounts in fresh domestic wastewater. In effluent of nitrifying biological treatment plants, nitrate may be found in concentrations up to 30 mg nitrate as nitrogen/L (Brandi & Wilson-Wilde, 2013).

✓ **Nitrogen as Nitrite**

Nitrite (NO_2^-) is extremely toxic to aquatic life, however, is usually present only in trace amounts in most natural freshwater systems because it is rapidly oxidized to nitrate. In sewage treatment plants, nitrification process is used to convert ammonia to nitrate. The process may be impeded though causing discharge of nitrite at elevated concentrations into receiving waters (Revanasiddappa & Kiran Kumar, 2001).

2.7. pH

pH is an important limiting chemical factor for aquatic life. If the water in a stream is too acidic or basic, the H^+ or OH^- ion activity may disrupt aquatic organisms biochemical reactions by either harming or killing the stream organisms. pH is expressed in a scale with ranges from 1 to 14. A solution with a pH less than 7 has more H^+ activity than OH^- , and is considered acidic. A solution with a pH value greater than 7 has more OH^- activity than H^+, and is considered basic. The pH scale is logarithmic and making up and down the scale, the values change in factors of ten. A one-point pH change indicates the strength of the acid or base has increased or decreased tenfold (Patnaik, 2010).

Streams generally have a pH values ranging between 6 and 9, depending upon the presence of dissolved substances that come from bedrock, soils and other materials in the watershed. Changes in pH can change the aspects of water chemistry. For example, as pH increases, smaller amounts of ammonia are needed to reach a level that is toxic to fish. As pH decreases, the concentration of metal may increase because higher acidity increases their ability to be dissolved from sediments into the water (Murdoch et al., 1996).

2.8. Turbidity

Turbidity is a measure of the cloudiness of water (Schwartz et al., 2000). Cloudiness is caused by suspended solids (mainly soil particles) and plankton (microscopic plants and animals) that are suspended in the water (Davidson, 1994). Moderately low levels of turbidity

may indicate a healthy, well-functioning ecosystem, with moderate amounts of plankton present to balance the food chain. However, higher levels of turbidity pose several problems for water systems. Turbidity blocks out the light needed by submerged aquatic vegetation. It also can raise surface water temperatures above normal because suspended particles near the surface facilitate the absorption of heat from sunlight. Suspended soil particles may carry nutrients, pesticides, and other pollutants throughout a water system (Welsh, 1991). Turbid waters may also be low in dissolved oxygen. High turbidity may result from sediment bearing run-off, or nutrients inputs that cause plankton blooms (Murdoch et al., 1996).

2.9. Total Solids

Total Solids is a measure of the suspended and dissolved solids in a body of water. Thus, it is related to both conductivity and turbidity. To measure total suspended and dissolved solids, a sample of water is placed in a drying oven to evaporate the water, leaving the solids. To measure dissolved solids, the sample is filtered before it is dried and weighed. To calculate the suspended solids, the weight of the dissolved solids is subtracted from the total solids (Murdoch et al., 1996). Important components of the total solid load from the treatment plants include phosphorus, nitrogen, and organic matter. The amount of solids in wastewater is frequently used to describe the strength of the waste. The more solids present in a particular wastewater, the stronger that wastewater will be. If the solids in wastewater are mostly organic, the impact on a treatment plant is greater than if the solids are mostly inorganic. Gravimetric is the approved procedure total solids, total dissolved solids, total suspended solids, fixed and volatile solids and Volumetric is the method for measuring settleable solids (Greenberg, 1984).

3. Chemical Oxygen Demand (COD)

COD is defined as the amount of dissolved oxygen to oxidize and stabilize a sample when organic or inorganic matter of sample solution is responsive by a strong chemical oxidant. The COD value indicates the mass of oxygen consumed per liter of solution and expressed in milligrams per liter (mg/L). The higher the chemical oxygen demand, the higher the amount of pollution in the water sample. However, COD is considered one of the important quality control parameter of an effluent in wastewater treatment facility (Wu et al., 2011).

The complete oxidation of organic compounds under such strong oxidizing conditions produces carbon dioxide (CO_2) and water (H_2O). The COD for any organic compound can be theoretically calculated from writing a balanced equation (Bickerstaffe, 2006).

Using glucose as an example:

$$C_6H_{12}O_6 + 6\ O_2 \rightarrow 6\ CO_2 + 6\ H_2O$$
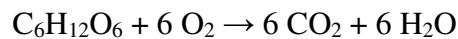
The theoretical COD of glucose can be calculated as :

$$\textbf{COD} = \frac{\text{grams of oxygen used}}{\text{grams of substrate used}} = \frac{(6\times32)}{(6\times12)+12+(6\times16)} = \frac{192}{180}$$

$$= \frac{1.067\ \text{g COD}}{\text{grams of substrate utilized}}$$

Glucose is converted to carbon dioxide and water by a stoichiometric amount of oxygen (1.067 mg of oxygen per mg of glucose).

In wastewater, if the concentration of glucose and the concentration of biomass is calculated before and after biological treatment, we can know how much oxygen was consumed during the conversion of glucose to biomass and end products. When this procedure for the COD test is strictly followed, the experimental result will not differ more than a few percent from the theoretical value. A list of the theoretical oxygen demand of a variety of other substances (Pitter & Chudoba, 1990), which can be contented in municipal and industrial wastewater is given in Table 4. It shows that 1 mg/L of oxalic acid has a theoretical COD of 0.18 mg/L where 1 mg/L of acetic acid has a theoretical COD of 1.07 mg/L.

Table 4: Theoretical COD values of 1 gm of variuos organic compounds.

COMPONENT	FORMULA	COD (mg/L)
Oxalic Acid	$C_2H_2O_4$	0.18
Formic Acid	CH_2O_2	0.35
Citric Acid	$C_6H_8O_7$	0.75
Acetic Acid	$C_2H_4O_2$	1.07
Glycerol	$C_3H_8O_3$	1.22
Phenol	C_6H_6O	2.38
Acetone	C_3H_6O	2.21
Ethanol	C_2H_6O	2.09
Methanol	CH_4O	1.50
Ethane	C_2H_5	3.73
Methane	CH_4	4.00

3.1 Methods to Measure COD

The dichromate method is the American Public Health Association (APHA) standard method for determining COD with the use of potassium dichromate. The amount of dichromate is determined by direct titration using Ferrous Ammonium Sulfate (FAS) as the titrant and ferroin (1, 10 phenanthroline ferrous sulfate) as the indicator (Bickerstaffe, 2006). During the course of the titration, the titrant (Fe^{2+}) reacts instantly with hexavalent chromium (Cr^{6+}) to form trivalent chromium (Cr^{3+}) and ferric ion (Fe^{3+}) which is shown below:

$$3Fe^{2+} + Cr^{6+} \rightarrow 3Fe^{3+} + Cr^{3+}$$
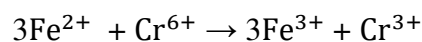
The final hexavalent chromium level is then subtracted from the initial level to determine the amount of hexavalent chromium reduced during the digestion. This difference is used to calculate the COD by following equation:

$$COD_{(mg/L)} = \frac{(A - B) \times N \times 8000}{V_{mL}\,(sample)}$$

Where, A is the mL FAS required for the titration of the blank, B is the mL FAS required for the titration of the sample, N is the normality of FAS.

In 1951, Medalaia presented the total pollution load of most wastewater discharges by this COD analysis. In 1990 the Association of Official Analytical Chemists described, the COD as a degree of pollution and one of the most important parameters to characterize pulping effluents (Horwitz, 1990). The conventional method for COD determination was then performed by adding a known amount of oxidant (such as potassium dichromate, potassium permanganate) to the sample to oxidize the organic matter in a digestion process at high temperature in open containers and then titrating the excess oxidant. The COD value was then calculated by subtracting the excess amount of oxidant from the initial. Figure. 4 shows the conventional method of measuring COD in wastewater.
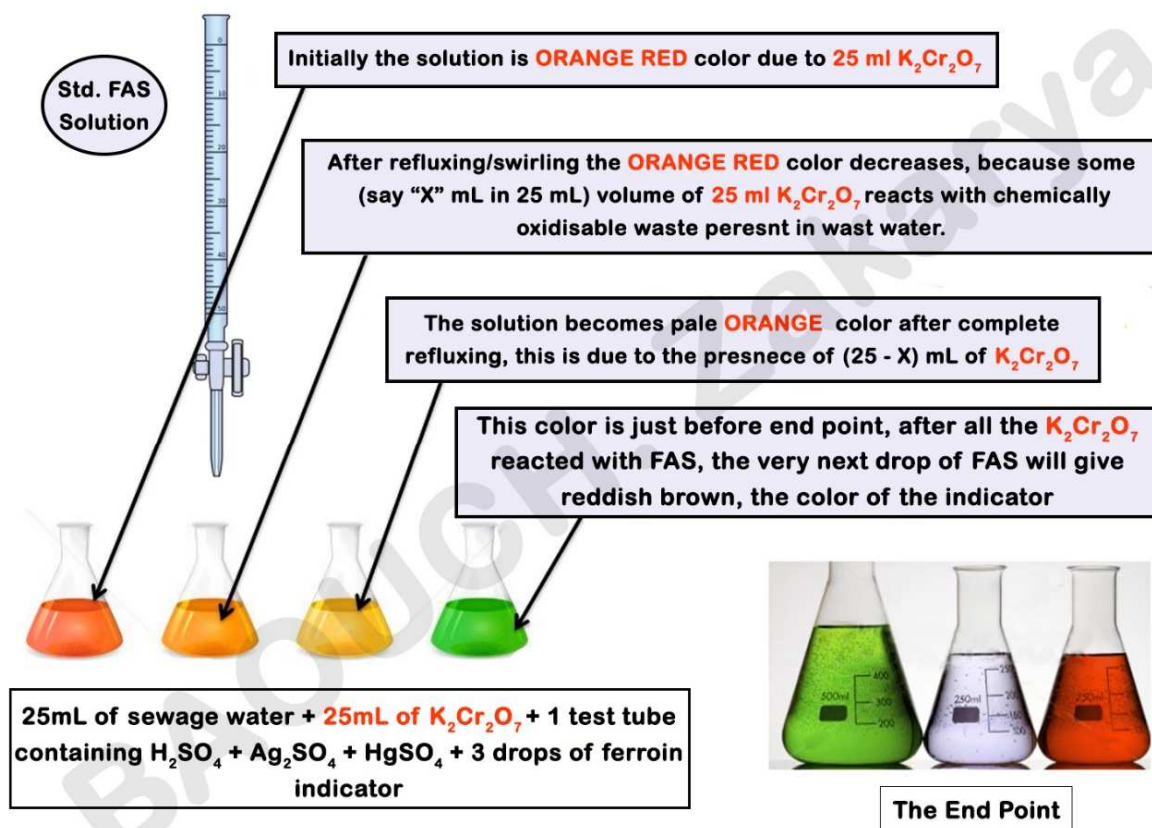
Figure 5: The conventional method of measuring COD in wastewater

The only interference in determining COD is the presence of Chloride (Dobbs & Williams, 1963). It can be eliminated by mixing mercuric sulfate ($HgSO_4$) in COD vials and diluting samples proper enough to reduce the chloride concentration. Also, titrimetric procedure requires a high degree of operator skill and take some time to perform. Colorimetric measurement of COD is considered to be a faster and easier method than titrimetric analysis. The sample is digested in an ampule, culture tube or vial under closed reflux conditions (Bickerstaffe, 2006). The following picture show the "COD Thermoreactor" instrument.

Figure 6: COD Thermoreactor instrument.

4. Objectives

Ensuring reliable access to clean and affordable water is a worldwide challenge that needs new water resource management approaches and technological improvements. It is extremely important to find low-cost water treatment methods especially in our country ALGERIA, where the economic benefits are usually more important than the environmental and health issues. Therefore, if a local low-cost material can be utilized in the water treatment, it will not only bring economic benefits but also decrease the environmental load and improve people's health and well-being. Therefore, this study has focused on synthesis and characterization of low-cost adsorbents based on local Bentonite and biopolymers for the removal of some industrial dyes from wastewater.

REFERENCES

Bickerstaffe, S. (2006). The science of 4×4. *Automotive Engineer (London)*, *31*(10), 37.

Brandi, J., & Wilson-Wilde, L. (2013). Standard Methods. In *Encyclopedia of Forensic Sciences: Second Edition*. https://doi.org/10.1016/B978-0-12-382165-2.00237-3

Chen, B., Wu, H., & Li, S. F. Y. (2014). Development of variable pathlength UV-vis spectroscopy combined with partial-least-squares regression for wastewater chemical oxygen demand (COD) monitoring. *Talanta*, *120*, 325–330. https://doi.org/10.1016/j.talanta.2013.12.026

Cheremisinoff, N. P., & Davletshin, A. (2015). Hydraulic Fracturing Operations. In *Hydraulic Fracturing Operations*. https://doi.org/10.1002/9781119099987

Davidson, W. S. (1994). Water quality monitoring. *Southcon Conference Record*, *2011*(5), 478–480. https://doi.org/10.1109/southc.1994.498151

Dobbs, R. A., & Williams, R. T. (1963). Elimination of Chloride Interference in the Chemical Oxygen Demand Test. *Analytical Chemistry*, *35*(8), 1064–1067. https://doi.org/10.1021/ac60201a043

David, J.D. (1991). Riparian forest buffers: function and design for protection and enhancement of water resources, volume 7. US Department of Agriculture, Forest Service, Northeastern Area, State & Private Forestry, Forest Resources Management.

Greenberg, A. E. (1984). Advances in Standard Methods for the Examination of Water and Wastewater. *Proceedings - AWWA Water Quality Technology Conference*, 11–13.

Malik, A., & Grohmann, E. (2012). Environmental protection strategies for sustainable development. In *Environmental Protection Strategies for Sustainable Development*. https://doi.org/10.1007/978-94-007-1591-2

Mogens.H. (2002). Wastewater treatment: biological and chemical processes. Springer Science & Business Media.

Revanasiddappa, H. D., & Kiran Kumar, T. N. (2001). New spectrophotometric method for the determination of nitrite in water. *Fresenius Environmental Bulletin*, *10*(10), 781–785. https://doi.org/10.1007/BF00388430

Schwartz, J., Levin, R., & Goldstein, R. (2000). Drinking water turbidity and gastrointestinal illness in the elderly of Philadelphia. *Journal of Epidemiology and Community Health*, *54*(1), 45–51. https://doi.org/10.1136/jech.54.1.45

Wu, G. Q., Bi, W. H., Lü, J. M., & Fu, G. W. (2011). Determination of chemical oxygen demand in water using near infrared transmission and UV absorbance method. *Guang Pu Xue Yu Guang Pu Fen Xi/Spectroscopy and Spectral Analysis*, *31*(6), 1486–1489. https://doi.org/10.3964/j.issn.1000-0593(2011)06-1486-04

Kant, R. (2012). Textile dyeing industry an environmental hazard. *Natural Science*, 04(01), 22–26. https://doi.org/10.4236/ns.2012.41004

Yagub, M.T., Sen, T.K., Afroze, S. and Ang, H.M. (2014a). Dye and its removal from aqueous solution by adsorption: A review. *Advances in Colloid and Interface Science*. 209(0), 172-184.

Shahid, M., Shahid ul, I. and Mohammad, F. (2013). Recent advancements in natural dye applications: a review. *Journal of Cleaner Production* 53(0), 310-331

Hernández-Montoya, V., Pérez-Cruz, M.A., Mendoza-Castillo, D.I., Moreno-Virgen, M.R. and Bonilla-Petriciolet, A. (2013). Competitive adsorption of dyes and heavy metals on zeolitic structures. *Journal of Environmental Management*, 116(0), 213-221.

Rauf, M. A., Meetani, M. A., Khaleel, A., & Ahmed, A. (2010). Photocatalytic degradation of Methylene Blue using a mixed catalyst and product analysis by LC/MS. *Chemical Engineering Journal*, *157*(2–3), 373–378. https://doi.org/10.1016/j.cej.2009.11.017

Robert, G.W. (2001). Limnology: lake and river ecosystems. Gulf Professional Publishing.

Gomes, J. R. (2001) Estrutura e Propriedades dos Corantes. Barbosa e Xavier Lda. Braga, Portugal

Hunger, K. (Ed.). (2007). Industrial dyes: chemistry, properties, applications. John Wiley & Sons.

Demirbas, A. (2009). Agricultural based activated carbons for the removal of dyes from aqueous solutions: A review. *Journal of Hazardous Materials,* 167(13), 1-9.

Labanda, J., Sabaté, J. and Llorens, J. (2009). Modeling of the dynamic adsorption of an anionic dye through ion-exchange membrane adsorber. *Journal of Membrane Science*. 340(1–2), 234-240

Wu, J.-S., Liu, C.-H., Chu, K.H. and Suen, S.-Y. (2008). Removal of cationic dye methyl violet 2B from water by cation exchange membranes. *Journal of Membrane Science,* 309(1–2), 239-245.

Hao, O. J., Kim, H., & Chiang, P.-C. (2000). Decolorization of Wastewater. Critical Reviews in Environmental Science and Technology, 30(4), 449–505. doi:10.1080/10643380091184237

Samanta, A.K. and Konar, A. (2011). Dyeing of textiles with natural dyes .Natural dyes, InTech

Tom, M., Martha, C. and Kate, O. (1996).The streamkeeper's field guide: watershed inventory and stream monitoring methods.

Velho, S.R.K., Brum, L.F.W., Petter, C.O., dos Santos, J.H.Z., Šimunić, Š. and Kappa, W.H. (2017). Development of structured natural dyes for use into plastics. *Dyes and Pigments,* 136, 248-254

Eugene, R.Weiner. (2010). Applications of environmental chemistry: a practical guide for environmental professionals. CRC press.

Bickerstaffe, S. (2006). The science of 4×4. *Automotive Engineer (London)*, *31*(10), 37.

Brandi, J., & Wilson-Wilde, L. (2013). Standard Methods. In *Encyclopedia of Forensic Sciences: Second Edition*. https://doi.org/10.1016/B978-0-12-382165-2.00237-3

Chen, B., Wu, H., & Li, S. F. Y. (2014). Development of variable pathlength UV-vis spectroscopy combined with partial-least-squares regression for wastewater chemical oxygen demand (COD) monitoring. *Talanta*, *120*, 325–330. https://doi.org/10.1016/j.talanta.2013.12.026

Cheremisinoff, N. P., & Davletshin, A. (2015). Hydraulic Fracturing Operations. In *Hydraulic Fracturing Operations*. https://doi.org/10.1002/9781119099987

Davidson, W. S. (1994). Water quality monitoring. *Southcon Conference Record*, *2011*(5), 478–480. https://doi.org/10.1109/southc.1994.498151

Dobbs, R. A., & Williams, R. T. (1963). Elimination of Chloride Interference in the Chemical Oxygen Demand Test. *Analytical Chemistry*, *35*(8), 1064–1067. https://doi.org/10.1021/ac60201a043

Greenberg, A. E. (1984). Advances in Standard Methods for the Examination of Water and Wastewater. *Proceedings - AWWA Water Quality Technology Conference*, 11–13.

Malik, A., & Grohmann, E. (2012). Environmental protection strategies for sustainable development. In *Environmental Protection Strategies for Sustainable Development*. https://doi.org/10.1007/978-94-007-1591-2

Mike, C. (2005). Calibration : A Technician's Guide. ISA.

Revanasiddappa, H. D., & Kiran Kumar, T. N. (2001). New spectrophotometric method for the determination of nitrite in water. *Fresenius Environmental Bulletin*, *10*(10), 781–785. https://doi.org/10.1007/BF00388430

Patnaik, P. (2010). Handbook of environmental analysis: chemical pollutants in air, water, soil, and solid wastes.

Pavel, P., & Jan. C. (1990). Biodegradability of organic substance in the aquatic environment.

Schwartz, J., Levin, R., & Goldstein, R. (2000). Drinking water turbidity and gastrointestinal illness in the elderly of Philadelphia. *Journal of Epidemiology and Community Health*, *54*(1), 45–51. https://doi.org/10.1136/jech.54.1.45

Horwitz, W. (1990). AOAC. Official methods of analysis of the association of official analytical chemists. Association of Official Analytical Chemists, Arlington, VA, USA.

Wu, G. Q., Bi, W. H., Lü, J. M., & Fu, G. W. (2011). Determination of chemical oxygen demand in water using near infrared transmission and UV absorbance method. *Guang Pu Xue Yu Guang Pu Fen Xi/Spectroscopy and Spectral Analysis*, *31*(6), 1486–1489. https://doi.org/10.3964/j.issn.1000-0593(2011)06-1486-04

For more information on DYES, please scan the QR code below:

PART II

2. CLAY

2.1 Introduction

By definition clays are naturally occurring alumino-silicate materials composed mainly of fine grained materials with colloid fraction of soils, rocks, sediments and water (Bhattacharyya & Gupta, 2008; Fouodjouo et al., 2017). The joint nomenclature committees (JNCs) of the Association Internationale pour I'Etude des Argiles (AIPEA) and the Clay Minerals Society (CMS) have recently defined clay as *"a naturally occurring material composed primarily of fine-grained minerals, which generally show plastic behavior at appropriate water contents and hardness upon drying or firing"*.

Clays have attracted wide interest for application in various sectors including process industries, agricultural sectors, engineering and construction sectors, environmental remediation and water treatment (Edi et al., 2015). In my research, Clay is chosen as starting material to develop wastewater sorbents for the textile industry. This choice is not only due to their abundance and inexpensiveness but also because of their physicochemical properties such as chemical and mechanical stability, larger specific surface area, higher charge density, layered structure, higher cation exchange capacity (Mukhopadhyay et al., 2017).

In this chapter, we present a review of the structural, mineralogical and chemical properties of clay and the effect of surface modification in their structures. We further looked at their applicability in wastewater removal in their raw and also in their modified form.

2.2 Composition and structure

The clay materials are basically composed of tiny crystalline substances of one or more members of a small group of minerals commonly known as clay minerals. Chemically, these minerals are hydrous alumina-silicate with other metallic ions. Their particles are very small in size, very flaky in shape and thus have considerable surface area. They can only be viewed with an electronic microscope. Clay minerals are formed from two basic structural units: tetrahedral and octahedral. (Mielenz, 1952; Dimitri & William, 2005).

The tetrahedral (T) sheet consist of cations coordinated to four oxygen atoms and linked to adjacent tetrahedral by sharing three corners to form two dimensional hexagonal mesh (Murray, 2007). The most common tetrahedral cations are Si^{4+}, Al^{3+} and Fe^{3+}.
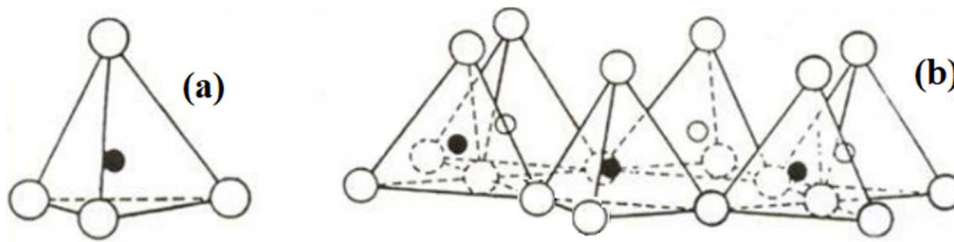
Figure 1. Single silica Tetrahedron unit (a) and sheet structure constructed from silica Tetrahedron units (b)

The second sheet is called octahedral sheet (O), which is comprised of six oxygen atoms which are closely parked together and hydroxyl ions in which cations are arranged to form octahedral coordination and linked to neighboring octahedral by sharing edge.
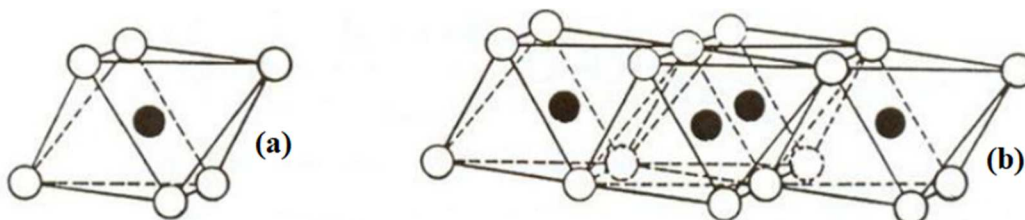
Figure 2. Single Octahedron unit (a) and a sheet structure constructed from Octahedron units (b)

The edge of shared octahedral forms sheet of hexagonal or pseudo hexagonal symmetry and shows different topologies depending on octahedral hydroxyl position (Jlassi et al., 2017). Cations in octahedral sheet are usually Al^{3+}, Fe^{3+}, Mg^{2+} or Fe^{2+}. When cation with positive valence of three (Al^{3+} or Fe^{3+}) is present in the octahedral sheet, only two-thirds of the possible positions are filled in order to balance the charges and the mineral is therefore termed dioctahedral.

Conversely, when cation with positive charge of two (e.g. Mg^{2+} and Fe^{2+}) is present, all three positions are filled to balance the structure and the mineral is termed trioctahedral. The phyllosilicate sheets are joined together by sharing the apical oxygen atom or hydroxyls to form hexagonal network with each sheet in a fundamental structure.

Based on the number and ratio of the sheets in the fundamental structural units, the existing cations substitutions in the octahedrons and tetrahedrons caused for resulting charge of the layers which can be descended into two main groups of clay mineral namely 1:1 (kaoline) and 2:1 (smectite and illite) (Moraes et al., 2017; Tournassat et al., 2015).

Type 1:1

This group of mineral is also called kaolin minerals, which is the basic mineral for kaolinite, dickite and hallocite (Brigatti et al., 2013). They consist of single tetrahedral sheet of SiO_4 and an octahedral sheet with Al^{3+} as octahedral cation. Both sheets combine to form a common a unit in such that the tip of silica tetrahedral points toward the octahedral sheet (Bhattacharyya & Gupta, 2008). The layer of the tetrahedral sheet is invented over the octahedral sheet with oxygen atoms and hydroxyls ions present to balance the charges being shared by the silica in the tetrahedral sheet and the aluminum in the octahedral sheet. With the layer charges close to zero, the kaolin mineral has essentially no interlayers and does not show interlayer expansion in the water because the contiguous layers within particles are strongly held together by Al-OH and O-Si-OH bonding supplemented by dipole–dipole and van der Waal interaction. **Figure 3** represents the typical structure of kaoline mineral (Schoonheydt, 2014).
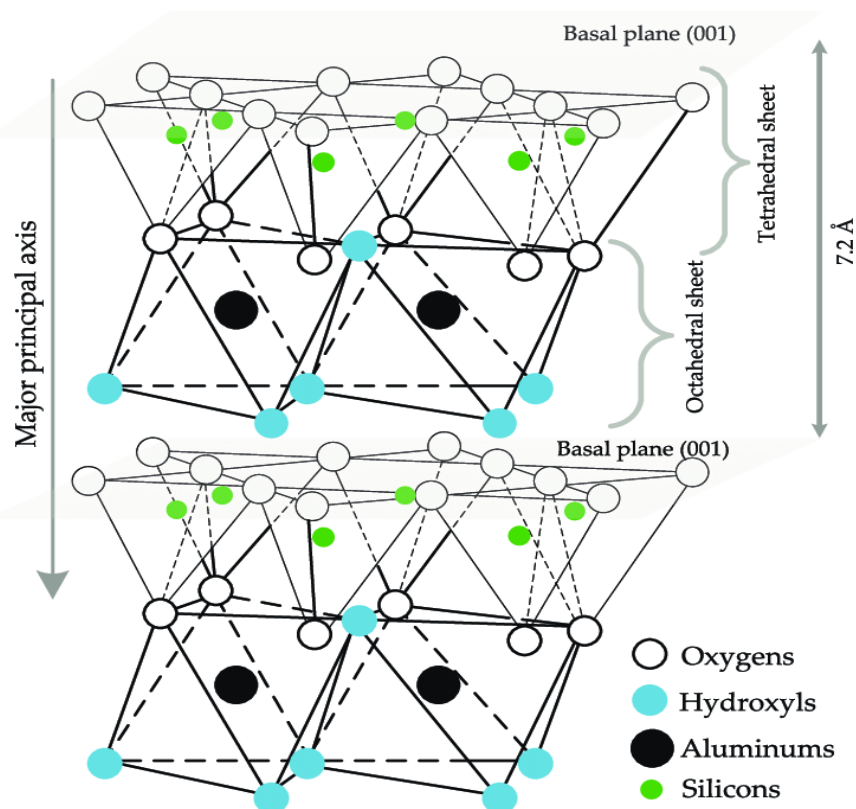
Figure. 3. Kaolinite lattice structure (Grim, 1968). Adapted and reprinted from Karam et al., 2017, Copyright 2017, with permission from Elsevier.

a) Type 2:1

Clay mineral groups such as smectite and vermiculite are part of 2:1 type and it constitutes minerals such as montmorillonite, saponite, nontronite and beidellite. The 2:1 minerals are composed of one octahedral sheet between two tetrahedral sheets. For which the interlayer thickness is 1 nm when the sheet is closed (Odom, 1984). Generally in this group of clay minerals isomorphic substitutions are observed, for example, possible substitutions of Si^{4+} in tetrahedron by Al^{3+} or those of Al^{3+} in octahedron by Fe^{2+} (Ummartyotin et al., 2016). Such substitution leads to permanent negative surface charge at the sheet by the presence of exchangeable cations (Rouquerol et al., 2013). The most common exchangeable cations in the interlayers are K^+, Na^+, Ca^{2+}, Mg^{2+} and H^+.

The 2:1 group minerals have higher charge density, higher surface area and higher swelling capacity (Bhattacharyya & Gupta, 2008). The swelling capacity of these type of clay arise from their structural features that enables water to overcome the electrostatic and van der Waals interactions keeping the layers together and penetrate into surface interlayers leading to hydrolization of Al and Si atoms to aluminol (AlOH) and silanol (SiOH) resulting in expansion. **Figure 4** presents the schematic diagram of 2:1 clay minerals.
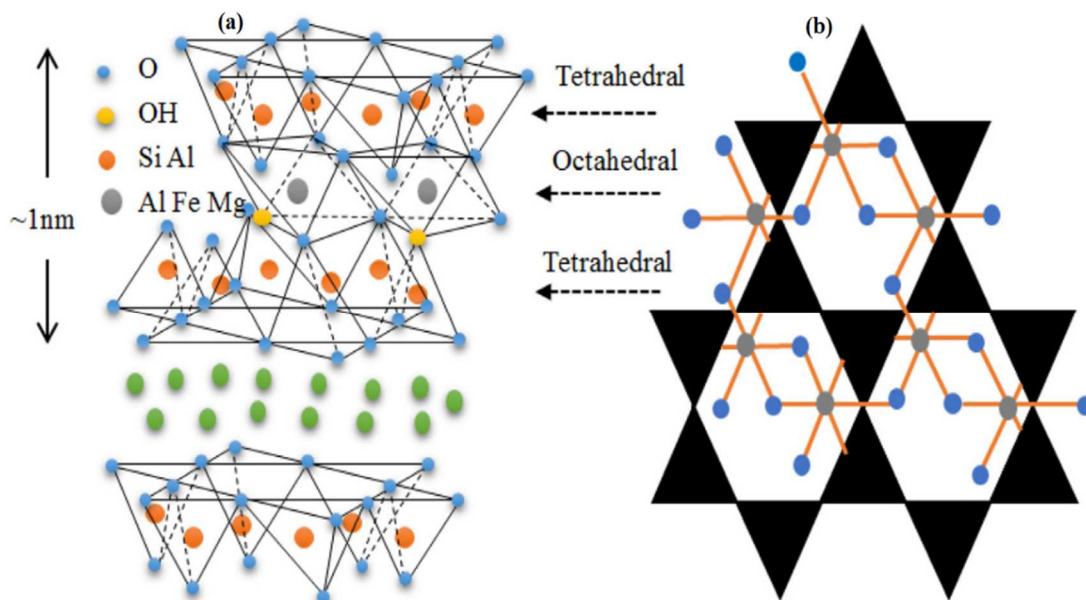
Figure. 4. Schematic representation of the 2:1 clay structure.

(A) Side view: tetrahedrons units of Mt assembled through weak van der Waals and electrostatic forces to form the primary particles, (B) Top view of Mt, hexagonal structure of oxygen and hydroxyl ligands of the octahedral layer. Adapted and reprinted from Swearingen et al., 2003, Copyright 2003, with permission from Elsevier.

Based on their crystalline arrangements, clay minerals are divided into three types namely, Kaolinites, Montmorillonite and Illite the properties of all three minerals are presented in Table 1

Table 1: Some Properties of Clay Minerals

Kaolinites	Montmorillonite	Illite
1:1 Layer	**2:1** Layer	**2:1** Layer
Hexagonal Flakes	Thin Flakes	Elongate
Low Base Exchange Capacity	High Base Exchange Capacity	Moderate Base Exchange Capacity
Minimal Layer Charge	High Layer Charge	Moderate Layer Charge
Low Surface Area	Very High Surface Area	High Surface Area
Largest Grain Size	Smallest Grain Size	Intermediate Grain Size
Lowest Dry Strength	Highest Dry Strength	Intermediate Dry Strength
Lowest Swelling and Shrinkage Behaviour	Largest Swelling and Shrinkage Behaviour	Intermediate Swelling and Shrinkage Behaviour

2.3 Cation exchange Capacity:

One of the important properties of the clay minerals is that contains cations that can be exchanged for any guest species of anion or cation by treating clay mineral with such clay mineral. The exchangeable cations are held on the outside of silica-alumina clay mineral structural units and the exchange does not affect the layout of the silica-alumina units (Grim, 1968). The ion exchange capacity phenomenon is measured in terms of milli-equivalents per gram or per 100 g. The commonly used cations used to evaluate the cation exchange capacity of the clay mineral includes; Mg^{2+}, Ca^{2+}, K^+, Na^+, H^+ and NH^{4+} (Odom, 1984)**.**

The total CEC consists of two parts namely the exchange capacity of the interlayer and that of the edges. The interlayer exchange capacity comes from isomorphic substitutions of aluminium by magnesium at octahedral and /or silicon by aluminium at tetrahedral leads to the net negative charge, the cations then balances this ionic deficiency. This part is independent of pH value, so gives almost constant value (Lagaly, 1981).

The CEC results from the edge are strongly pH dependent. At pH 7 about 20% of the CEC of smectite is located at the edges. In the acid pH range, the edges are positively charged; thus the edges do not contribute to the measured CEC. While in the basic pH range, the edges are negatively charged; therefore in this pH range all edges contribute to the CEC (Lagaly, 1981).

Different clay minerals portray different cation capacity depending on the substitution within the lattice structure (Grim, 1968)**.** Type 1:1 clay minerals such as kaolinite have limited substitution between their lattice structure compared to Type 2:1 clay minerals such as smectite, vermiculite and sepiolite and consequently they have lower cation exchange capacity (Murray, 2007)**.** Several studies have indicated that cation exchange capacity of the clay mineral decreases after modification by inorganic species (Gitari et al., 2015; Lenoble et al., 2002; Mukhopadhyay et al., 2017)**.** This is because modification involves the ion exchange reaction between the exchangeable cations in the clay interlayer and the guest species. Low CEC of modified clays suggests the irreversibility of cationic exchange and thus intercalated metallic polycations are hardly exchanged (Lenoble et al., 2002)**. Table 2** summarizes the cation exchange capacity of different clay minerals.

✓ **Method of CEC determination**

Operationally, CEC is defined as the sum of the ion amounts released when mixing a fixed mass of soil with a fixed volume of reactant solution. Methods for CEC determination consist in the complete saturation of soil exchange complex by a mono-ionic solution. The CEC is quantified by measuring the difference between initial and remaining added ion concentration. Alternatively, the added ion adsorbed to soil can be removed and subsequently quantified. Another way is to sum up the soil cations removed from exchange sites. Different methods have been already published for the determination of CEC. They differ by the reactant used, the variables measured, and the pH conditions during extraction. In all cases, the CEC is generally expressed as milliequivalent per 100 g of soil dried at 105 8C (meq. 100 g^{-1}).

(Orsini & Rémy, 1976) proposed to use $Co(NH_3)_6^{3+}$ as the exchange ion and to quantify the CEC through the measurement of the concentration of Co remaining in solution. This method applies to a large range of soils due to the use of a dilute reagent simulating field soil solution conditions. Furthermore, exchange takes place at similar pH to soil pH as the Hexaamminecobalt(III) chloride is a non-buffered reagent. This method is thus appropriate for soils with large amount of pH-dependent charges.

The Hexaamminecobalt(III) chloride method is frequently used due to its ability to measure CEC at soil pH. After exchange with $Co(NH_3)_6^{3+}$ ions, CEC is estimated via the measurement of the Co remaining in solution. This method allows a more rapid determination of CEC based on the measurement of the absorbance at 472 nm of the Hexaamminecobalt(III) chloride solution before and after exchange by the following Equation:

$$CEC = \frac{A_{initial} - A_{final}}{A_{initial}} \times 50 \times \frac{V}{m} \times 100 \qquad (1)$$

Where $A_{initial}$ (0.05 N) and A_{final} (assay) correspond respectively to the absorbencies at 472 nm of 0.05 N Hexaamminecobalt(III) chloride solution and of sample supernatant; V: volume in L of 0.05 N Hexaamminecobalt(III) chloride solution added to soil sample (0.04 L); m: soil dry mass used (2 g).

This method has been applied to various soil's horizons from four sites, selected to cover a wide range of CEC and pH values. The model obtained allows one to calculate CEC from absorbance at 472 nm with 95% confidence intervals. As CEC is of relevant meaning in agronomical and environmental purposes, and more recently in ecotoxicological studies, this modified method can be proposed as a rapid test for CEC evaluation.

2.4 Specific surface area

One of the essential properties of clay minerals is their larger surface area. This characteristic allows clay minerals to adsorb water and other environmental contaminants (Macht et al., 2011). Type 2:1 clay minerals such as smectite and vermiculite possess higher specific surface area as compared type 1:1 clay minerals such as kaolinite and halloysite because of their ability to swell (Murray, 2007). The total specific surface area of the clay is denoted by the sum of external surface area and the internal surface area corresponding to the interlayer spaces(Jlassi et al., 2017).

Table 2. Cation exchange capacity and specific surface area of clay minerals (Rowell, 1993).

Clay Mineral	Specific Surface (m²/g)	C.E.C (meq/100g)
Kaolinite	10 – 20	3 - 10
Illite	80 – 100	20 - 30
Montmorillonite	800	80 - 120
Chlorite	80	20 - 30

Several authors have indicated that total specific area of the clay mineral can be increased through modification to increase their functionality in different areas of application.

(Hua, 2015) reported an increase in surface area of Na-bentonite from 34.1 to 77.2 m^2/g after modification with Mn oxides. Bentonite modified with the combination of Mn oxides and poly(diallyldimethylammonium chloride) showed a sharp increase in surface area to 128.9 m^2/g. The increase in total specific area could be attributed to swelling of bentonite clay during modification.

(Mishra & Parida, 1997) also reported increased specific surface area for bentonite pillared with manganese oxides at temperature of 500°C. This was attributed to decomposition of the complex with increasing temperature to form the oxide pillar which generated the void micropores inside the clay layers. This phenomenon was also emphasized by (Bertella & Pergher, 2015) who also observed an increased in specific surface area of bentonite clay after pillaring using Al and Co from 58 to 304 m^2/g.

2.5 Swelling property

One of the most important property of smectite and corresponding bentonite is the uptake of water in the interlayer space and the resulting swelling of the mineral. Swelling is defined as the change in physical state of clay from an anhydrous solid to gel (Komine & Industry, 1994). It is due to this property that bentonite can be used as a disintegrate agent for tablets formulation, for preparation of oral and topical suspension (López-Galindo et al., 2007). There are two stages of swelling: one is the crystalline and the other is osmotic swelling. In former case the smectite can take water gradually from one to four layers (Norrish, 1954), controlled by balancing between strong electrostatic and hydration repulsive forces (Low, 1981). While in osmotic swelling complete dissociation of the smectite layers occur (Müller-Vonmoos & Løken, 1989), which is generally based on Defuse Double Layer Theory (Jellander et al., 1988). The increase in basal spacing by swelling depends on the bentonite mineralogy, types of exchangeable cation, magnitude of the layer charge and hydration of exchangeable cations (Onal, 2006). Usually sodium bentonite develop higher swelling than calcium ones, therefore for specific purposes the purification and conversion techniques are applied to improve the properties especially swelling of poor bentonite(Odom, 1984). According to European pharmacopoeia, the required swelling property of bentonite for pharmaceutical use is ≥22ml/2g (EPC, 2005).

2.6 Organo-Clays

As mentioned above, clay minerals consist of small crystalline particles with silicaoxygen tetrahedral sheets and aluminium or magnesium octahedral sheet, where an aluminium or magnesium ion is octahedrally coordinated to six oxygens or hydroxyls. Because of isomorphous substitution of silicon ion by aluminium ion in the tetrahedral layers or similar substitution of aluminium ion by magnesium ion, smectite minerals have a net negative charged. Thus, cations like sodium, potassium and calcium may be attracted to the mineral surface to neutralize the layer charge.

Organo-clays are synthesized by grafting cationic surfactants (Such as quaternary ammonium compounds $[(CH_3)_3NR]^+$ or $[(CH_3)_2NRR']^+$ where R and R' are alkyl or aromatic hydrocarbons etc.) onto clay minerals (S. Y. Lee & Kim, 2002). The interlaminar distance of the d_{001} plane of the clay which has not been organically modified, is relatively small, and the interlayer environment is hydrophilic. Intercalation of organic surfactant between layers of clays not only changes them from hydrophilic to hydrophobic, but also greatly increases the basal spacing of the layers. (Deng et al., 2003).

A number of studies have demonstrated that the d-spacings of the organoclays depend on the length of the alkyl chains and the packing density of the surfactants within the galleries of the clay minerals (Klapyta et al., 2001; Lagaly, 1981). In intercalated phyllosilicates with straight-chains alkylammonium, the organic cations are arranged with monolayer, bilayer, pseudobilayer or paraffin type configurations (S. Y. Lee & Kim, 2002). During the intercalation of the surfactants, the interlayer of the clay mineral is expanded, as shown by the XRD patterns (He et al., 2006).

The observed configuration will depend on the carbon chain lengths of alkylammonium cation (nc) and the layer charge of the clay mineral (J. F. Lee et al., 1989). Characteristic basal spacing, respectively of 13.6; 17.6 and 22Å distinguish the monolayer, bilayer and pseudolayer configurations; whereas basal spacing for samples with paraffin-type configurations increase linearly with nc.

When at least one of the nitrogen constituents is a long aliphatic chain, the interlayer space increases and the adsorption ion capacity is further increased (Andini et al., 2006). In addition, favorable interactions can arise with the R groups of the quaternary ammonium ions and organic molecules are more easily attracted into the expanded interlayer space of the clay. In this case, a number of Van der Waals and hydrophobic interactions can occur between alkyl chains. The

combination of the hydrophobic nature of the surfactant and the layered structure of the silicate layers leads to unique physico-chemical properties (He et al., 2006).

In such applications, the behavior and properties of organoclays strongly depend on the structure and the molecular arrangement of the organic molecules within the galleries of the clay minerals. Various arrangements have been proposed for the surfactant structural arrangement of the organic molecules within the clays based mainly on XRD and IR spectroscopy. The increased basal spacing together with hydrophobic surface makes organo-clays an effective material for adsorbing organic pollutants like pesticides and dyes in the treatment of drinking and wastewater contamination.

2.7. Applications of organo-clays as sorbents

Organo-clays have been used as sorbents in many applications. Some studies (Boyd et al., 1988; Jaynes & Boyd, 1991; Mortland et al., 1986) have showed that replacing the inorganic exchange cations of clay minerals with organic cations can result in greatly enhanced abilities to remove organic contaminants from water.

Previous studies have shown that the removal of acid dyes can be promoted by the use of sulfuric acid-activated MMT compared with untreated MMT (Özcan & Özcan, 2004). (Wang & Wang, 2008) prepared MMTs modified by a series of alkyl ammonium bromides with different alkyl chain lengths for the adsorption of Congo Red anionic dye in aqueous solutions. Other authors have successfully modified MMT using more unconventional modifiers (Açışlı et al., 2017), such as gemini surfactants, for the adsorption of organic contaminants (Liu et al., 2014; Yang et al., 2014). The results showed that the adsorption capacity of surfactant-modified MMTs for organic contaminants was greatly improved compared with that of pristine MMT. Some authors (Sheng et al., 1996) have used organo-clays to remove aromatic pollutants. hexadecyltrimethylammonium (HDTMA)-exchanged clays were shown to be able to adsorb benzene, nitrobenzene, chlorobenzene, trichloroethylene, and carbon tetrachloride. It was showed that organo-clays are effective sorbents for neutral organic contaminants (NOCs).

Besides using HDTMA clays, there are some studies(Kukkadapu & Boyd, 1995) which used tetramethylphosphonium-smectite (TMP-clay) and tetramethylammonium-smectite (TMA-clay) as adsorbents for a series of aromatic and chlorinated hydrocarbons. The sorption of benzene, alkylbenzenes, and carbon tetrachloride as vapours and as solutes from water was studied to evaluate the effect of water and adsorption efficiency. In this study, the Langmuir

isotherms were obtained which indicated that adsorption occurred predominantly in the interlayer micropores, apparently on mineral surfaces between the layers. It was found that TMP-clay is a better adsorbent than TMA-clay in presence of water.

REFERENCES

Açışlı, Ö., Karaca, S., & Gürses, A. (2017). Investigation of the alkyl chain lengths of surfactants on their adsorption by montmorillonite (Mt) from aqueous solutions. *Applied Clay Science*, *142*, 90–99. https://doi.org/10.1016/j.clay.2016.12.009

Andini, S., Cioffi, R., Montagnaro, F., Pisciotta, F., & Santoro, L. (2006). Simultaneous adsorption of chlorophenol and heavy metal ions on organophilic bentonite. *Applied Clay Science*, *31*(1–2), 126–133. https://doi.org/10.1016/j.clay.2005.09.004

Bertella, F., & Pergher, S. B. C. (2015). Pillaring of bentonite clay with Al and Co. *Microporous and Mesoporous Materials*, *201*(C), 116–123. https://doi.org/10.1016/j.micromeso.2014.09.013

Bhattacharyya, K. G., & Gupta, S. Sen. (2008). Adsorption of a few heavy metals on natural and modified kaolinite and montmorillonite: A review. *Advances in Colloid and Interface Science*, *140*(2), 114–131. https://doi.org/10.1016/j.cis.2007.12.008

Boyd, S. A., Sun, S., Lee, J. F., & Mortland, M. M. (1988). Pentachlorophenol Sorption By Organo-Clays. *Clays and Clay Minerals*, *36*(2), 125–130. https://doi.org/10.1346/CCMN.1988.0360204

Brigatti, M. F., Galán, E., & Theng, B. K. G. (2013). Structure and Mineralogy of Clay Minerals. In *Developments in Clay Science* (Vol. 5). https://doi.org/10.1016/B978-0-08-098258-8.00002-X

Deng, Y., Dixon, J. B., & White, G. N. (2003). Intercalation and surface modification of smectite by two non-ionic surfactants. *Clays and Clay Minerals*, *51*(2), 150–161. https://doi.org/10.1346/CCMN.2003.0510204

Edi, S. F., Ismadji, S., & Ayucitra, A. (2015). *SPRINGER BRIEFS IN MOLECULAR SCIENCE Clay Materials for Environmental Remediation*.

Fouodjouo, M., Fotouo-Nkaffo, H., Laminsi, S., Cassini, F. A., de Brito-Benetoli, L. O., & Debacher, N. A. (2017). Adsorption of copper (II) onto cameroonian clay modified by

non-thermal plasma: Characterization, chemical equilibrium and thermodynamic studies. *Applied Clay Science*, *142*, 136–144. https://doi.org/10.1016/j.clay.2016.09.028

Gitari, W. M., Ngulube, T., Masindi, V., & Gumbo, J. R. (2015). Defluoridation of groundwater using Fe3+-modified bentonite clay: optimization of adsorption conditions. *Desalination and Water Treatment*, *53*(6), 1578–1590. https://doi.org/10.1080/19443994.2013.855669

He, H., Frost, R. L., Bostrom, T., Yuan, P., Duong, L., Yang, D., Xi, Y., & Kloprogge, J. T. (2006). Changes in the morphology of organoclays with HDTMA+ surfactant loading. *Applied Clay Science*, *31*(3–4), 262–271. https://doi.org/10.1016/j.clay.2005.10.011

Hua, J. (2015). Synthesis and characterization of bentonite based inorgano-organo-composites and their performances for removing arsenic from water. *Applied Clay Science*, *114*, 239–246. https://doi.org/10.1016/j.clay.2015.06.005

Jaynes, W. F., & Boyd, S. A. (1991). Hydrophobicity of siloxane surfaces in smectites as revealed by aromatic hydrocarbon adsorption from water. *Clays and Clay Minerals*, *39*(4), 428–436. https://doi.org/10.1346/CCMN.1991.0390412

Jellander, R., Marčelja, S., & Quirk, J. P. (1988). Attractive double-layer interactions between calcium clay particles. *Journal of Colloid And Interface Science*, *126*(1), 194–211. https://doi.org/10.1016/0021-9797(88)90113-0

Jlassi, K., Krupa, I., & Chehimi, M. M. (2017). Overview: Clay Preparation, Properties, Modification. In *Clay-Polymer Nanocomposites*. Elsevier Inc. https://doi.org/10.1016/B978-0-323-46153-5.00001-X

Klapyta, Z., Fujita, T., & Iyi, N. (2001). Adsorption of dodecyl- and octadecyltrimethylammonium ions on a smectite and synthetic micas. *Applied Clay Science*, *19*(1–6), 5–10. https://doi.org/10.1016/S0169-1317(01)00059-X

Komine, H., & Industry, E. P. (1994). *I : o. 1*.

Kukkadapu, R. K., & Boyd, S. A. (1995). Tetramethylphosphonium- and tetramethylammonium-smectites as adsorbents of aromatic and chlorinated hydrocarbons: Effect of water on adsorption efficiency. *Clays and Clay Minerals*, *43*(3), 318–323. https://doi.org/10.1346/CCMN.1995.0430306

Lagaly, G. (1981). Characterization of clays by organic compounds. *Clay Minerals*, *16*(1), 1–21. https://doi.org/10.1180/claymin.1981.016.1.01

Lee, J. F., Crum, J. R., & Boyd, S. A. (1989). Enhanced Retention of Organic Contaminants by Soils Exchanged with Organic Cations. *Environmental Science and Technology*, *23*(11), 1365–1372. https://doi.org/10.1021/es00069a006

Lee, S. Y., & Kim, S. J. (2002). Transmission electron microscopy of hexadecyltrimethylammonium-exchanged smectite. *Clay Minerals*, *37*(3), 465–471. https://doi.org/10.1180/0009855023730044

Lenoble, V., Bouras, O., Deluchat, V., Serpaud, B., & Bollinger, J. C. (2002). Arsenic adsorption onto pillared clays and iron oxides. *Journal of Colloid and Interface Science*, *255*(1), 52–58. https://doi.org/10.1006/jcis.2002.8646

Liu, Y., Gao, M., Gu, Z., Luo, Z., Ye, Y., & Lu, L. (2014). Comparison between the removal of phenol and catechol by modified montmorillonite with two novel hydroxyl-containing Gemini surfactants. *Journal of Hazardous Materials*, *267*, 71–80. https://doi.org/10.1016/j.jhazmat.2013.12.039

López-Galindo, A., Viseras, C., & Cerezo, P. (2007). Compositional, technical and safety specifications of clays to be used as pharmaceutical and cosmetic products. *Applied Clay Science*, *36*(1–3), 51–63. https://doi.org/10.1016/j.clay.2006.06.016

Low, P. F. (1981). The Swelling of Clay: III. Dissociation of Exchangeable Cations. *Soil Science Society of America Journal*, *45*(6), 1074–1078. https://doi.org/10.2136/sssaj1981.03615995004500060013x

Macht, F., Eusterhues, K., Pronk, G. J., & Totsche, K. U. (2011). Specific surface area of clay minerals: Comparison between atomic force microscopy measurements and bulk-gas (N2) and -liquid (EGME) adsorption methods. *Applied Clay Science*, *53*(1), 20–26. https://doi.org/10.1016/j.clay.2011.04.006

Mielenz, R. C. (1952). Physical-Chemical Properties and Engineering Performance of Clays. *Clays and Clay Minerals*, *1*(1), 196–254. https://doi.org/10.1346/ccmn.1952.0010122

Mishra, T., & Parida, K. (1997). Transition-metal oxide pillared clays: Part 2 - A comparative study of textural and acidic properties of manganese(III) pillared montmorillonite and pillared acid-activated montmorillonite. *Journal of Materials Chemistry*, *7*(1), 147–152.

https://doi.org/10.1039/a603797f

Moraes, J. D. D., Bertolino, S. R. A., Cuffini, S. L., Ducart, D. F., Bretzke, P. E., & Leonardi, G. R. (2017). Clay minerals: Properties and applications to dermocosmetic products and perspectives of natural raw materials for therapeutic purposes—A review. *International Journal of Pharmaceutics*, *534*(1–2), 213–219. https://doi.org/10.1016/j.ijpharm.2017.10.031

Mortland, M. M., Shaobai, S., & Boyd, S. A. (1986). Clay-organic complexes as adsorbents for phenol and chlorophenols. *Clays & Clay Minerals*, *34*(5), 581–585. https://doi.org/10.1346/ccmn.1986.0340512

Mukhopadhyay, R., Manjaiah, K. M., Datta, S. C., Yadav, R. K., & Sarkar, B. (2017). Inorganically modified clay minerals: Preparation, characterization, and arsenic adsorption in contaminated water and soil. *Applied Clay Science*, *147*(February), 1–10. https://doi.org/10.1016/j.clay.2017.07.017

Müller-Vonmoos, M., & Løken, T. (1989). The shearing behaviour of clays. *Applied Clay Science*, *4*(2), 125–141. https://doi.org/10.1016/0169-1317(89)90004-5

Norrish, K. (1954). The swelling of montmorillonite. *Discussions of the Faraday Society*, *18*, 120–134. https://doi.org/10.1039/DF9541800120

Odom, I. E. (1984). Smectite clay minerals: properties and uses. *Philosophical Transactions of the Royal Society of London*, *A311*, 391–409. https://doi.org/10.1098/rsta.1984.0036

Özcan, A. S., & Özcan, A. (2004). Adsorption of acid dyes from aqueous solutions onto acid-activated bentonite. *Journal of Colloid and Interface Science*, *276*(1), 39–46. https://doi.org/10.1016/j.jcis.2004.03.043

Rouquerol, J., Llewellyn, P., & Sing, K. (2013). Adsorption by Clays, Pillared Clays, Zeolites and Aluminophosphates. In *Adsorption by Powders and Porous Solids: Principles, Methodology and Applications: Second Edition* (2nd ed.). Elsevier Ltd. https://doi.org/10.1016/B978-0-08-097035-6.00012-7

Sheng, G., Xu, S., & Boyd, S. A. (1996). Mechanism(s) controlling sorption of neutral organic contaminants by surfactant-derived and natural organic matter. *Environmental Science and Technology*, *30*(5), 1553–1557. https://doi.org/10.1021/es9505208

Ummartyotin, S., Bunnak, N., & Manuspiya, H. (2016). A comprehensive review on modified clay based composite for energy based materials. *Renewable and Sustainable Energy Reviews*, *61*, 466–472. https://doi.org/10.1016/j.rser.2016.04.022

Wang, L., & Wang, A. (2008). Adsorption properties of Congo Red from aqueous solution onto surfactant-modified montmorillonite. *Journal of Hazardous Materials*, *160*(1), 173–180. https://doi.org/10.1016/j.jhazmat.2008.02.104

Yang, S., Gao, M., & Luo, Z. (2014). Adsorption of 2-Naphthol on the organo-montmorillonites modified by Gemini surfactants with different spacers. *Chemical Engineering Journal*, *256*, 39–50. https://doi.org/10.1016/j.cej.2014.07.004

For more information on CLAYS, Please scan the QR code below:

PART III

3. BIOPOLYMERS

3.1 Introduction

Polymers are a class of "giant" molecules consisting of discrete building blocks linked together to form long chains. Simple building blocks are called monomers, while more complicated building blocks are sometimes referred to as "repeat units". The Rapid developments in the chemical industry have lead to the distribution of a wide variety of synthetic compounds into the environment (Esikova et al., 2012). Approximately 140 million tons of synthetic polymers are produced worldwide every year. Since polymers are extremely stable, their degradation cycles in the biosphere are unlimited. Environmental pollution by synthetic polymers, such as waste plastics and water soluble synthetic polymers in waste water has been recognized as a major problem. Plastics and polymers are an integrated part of our daily existence. However, because of stability and resistance to degradation, these are accumulated in the environment, at the rate of about 8% by weight and 20% by volume of the landfills (Premraj & Doble, 2005).

Biopolymers are defined as polymers formed under natural conditions during the growth cycles of all organisms. Therefore, they are also named natural polymers. They are formed within cells by complex metabolic processes. For materials applications, cellulose and starch are most interesting. However, there is an increasing attention in more complex hydrocarbon polymers produced by bacteria and fungi, particularly polysaccharides such as xanthan, curdlan, pullulan, chitin, chitosan and hyaluronic acid (Rhim & Ng, 2007).

In nature, there is no waste: all the products of living things are used as raw materials by others and the natural biopolymers have the advantage over synthetic polymers in that they are biodegradable and renewable as well as edible. However, relatively poor mechanical and water vapor barrier properties of those films are causing a major limitation for their industrial use. Research efforts have been focused on the property modification of natural biopolymer to improve their mechanical and water vapor barrier properties (Micard et al., 2000).

3.2 Polysaccharides, Composition and Structure

Polysaccharides are widely distributed in nature. These materials are important in different fields since they possess unique structures and characteristics that are different from those of typical synthetic polymers. Among the many kinds of polysaccharides, cellulose and chitin are the most important biomass resources. Cellulose is synthesized in plants, whereas

chitin is obtained from lower animals. They are the most abundant organic compounds on Earth. Chitin is structurally similar to cellulose, with acetamide groups at the C-2 positions in place of hydroxyl.
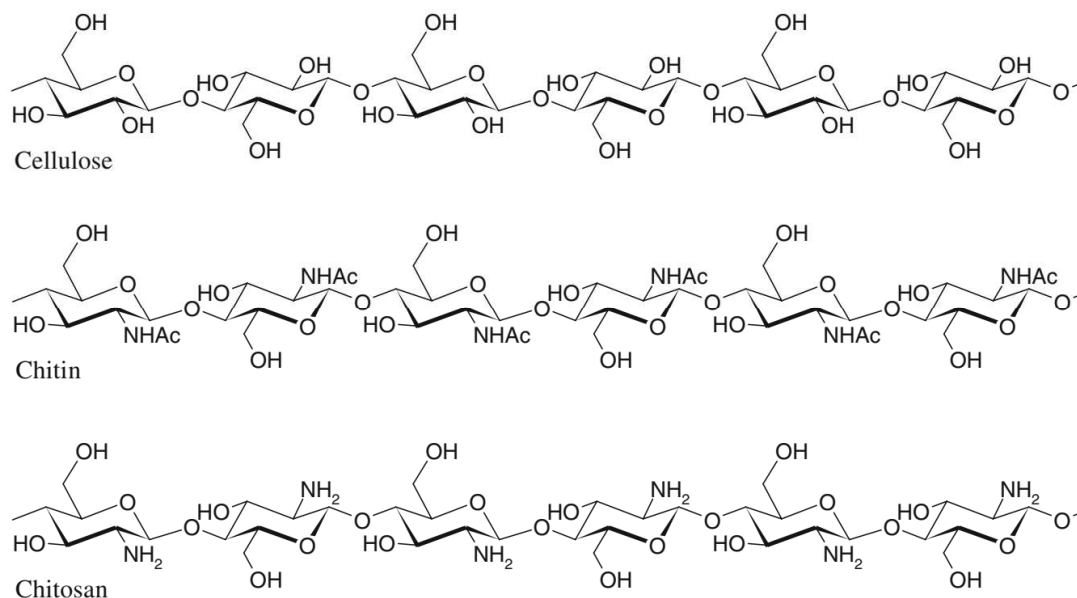
Figure. 1. Structures of polysaccharides: cellulose, chitin, and chitosan.

Chitin, poly(β-(1→4)-N-acetyl-D-glucosamine), is synthesized by an enormous number of living organisms and, depending on its source, occurs as two allomorphs, namely the α and β forms. It is extracted from crustaceans by acid treatment to dissolve calcium carbonate followed by alkaline extraction to solubilize proteins. In addition, a decolorization step is often added to remove leftover pigments and obtain a colorless product (Kurita, 2001).

Chitosan, the most important derivative of chitin, can be obtained by deacetylation of chitin under alkaline conditions. When the degree of deacetylation of chitin reaches about 50% (depending on the origin of the polymer), it becomes soluble in aqueous acidic media. The solubilization occurs by protonation of the NH_2 functional group on the C-2 position of the D-glucosamine repeating unit, whereby the polysaccharide is converted to a polyelectrolyte in acidic media. The presence of NH_2 groups in chitosan is the reason why it exhibits much greater potential compared with chitin for use in different applications. It is a special biopolymer having good properties including biodegradability, biocompatibility, and antibacterial activity so it is interesting as a novel type of functional material. Chitosan is the only pseudonatural cationic polymer and thus has many applications in different fields (Rinaudo, 2006).

Cellulose is argued to be the most abundant polymer in the nature and constitutes the main component of plant fibers, giving the plant rigidity. As early as 1838, Payen recognized cellulose as a definitive substance and coined the name "cellulose" (Payen, 1838). The origin of cellulose chemistry as a branch of polymer research dates back to 1920s and 1930s experiments on the acetylation and deacetylation of cellulose; these experiments resulted in the concept of polymer analogous reactions (Staudinger & Lohmann, 1933). It is a linear polysaccharide with long chains that consists of β-D-glucopyranose units joined by β-1.4 glycosidic linkages (Faruk et al., 2012; O'Connell et al., 2008) (Figure. 2). In one repeating unit of cellulose molecule, there are one methylol and two hydroxyl groups as functional groups.

Due to the absence of side chains or branching, cellulose chains can exist in an ordered structure. Therefore, cellulose is a semicrystalline polymer, and it contains both crystalline and amorphous phases. Although it is a linear polymer and contains two types of hydroxyl groups, primary hydroxyl in the methylol group ($-CH_2OH$) at C-6 and secondary hydroxyl groups (-OH) at C-3 and C-4, both of which are hydrophilic, it does not dissolve in water and in common solvents due to strong hydrogen bonds between the cellulose chains. As a result, the hydrogen bonds between the cellulose chains and van der Waals forces between the glucose units lead to the formation of crystalline regions in cellulose (O'Connell et al., 2008).
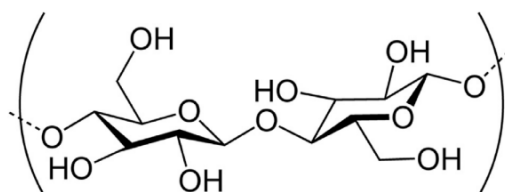
Figure. 2. The structure of repeating unit of cellulose molecule.

In addition to cellulose, these materials also contain hemicelluloses, and a small amount of lignin. Wood and cotton are the raw materials for the commercial production of cellulose. Cellulose in its natural state serves as a structural material within the complex architecture of plant cell walls with variation in its content. In wood, it constitutes about 40-50% in leaf fibers, in canes: bamboo 40-55%, in cereal straw: barley 48%, oat 44-53%, rice 43-49%, wheat 49-54%, and Cottonseed hairs are the purest source, it contains 90-99% of cellulose (Klemm et al., 1999).

Currently, the isolation, characterization, and applications of various forms of cellulose, including crystallites, nanocrystals, whiskers, nanofibrils, and nanofibers, are gaining much attention in various fields (Siró & Plackett, 2010). Novel methods for their production range

from top-down methods involving enzymatic/chemical/physical methodologies for their isolation from wood; from wood pulp, pulp industry wastes, native cellulose in the form of cotton, cellulosic agricultural residues (e.g., sugar beet pulp) or microcrystalline cellulose (MCC) by acid hydrolysis and forest/agricultural residues to the bottom-up production of cellulose nanofibrils from glucose by bacteria.

3.3 Chemically Modified Cellulose

Unmodified cellulose has a low adsorption capacity as well as variable physical stability. However, a chemical modification of cellulose can be executed to achieve adequate structural durability and an efficient adsorption capacity for pollutants (Güçlü et al., 2003). The properties of cellulose, such as its hydrophilic or hydrophobic character, elasticity, water sorbency, adsorptive or ion exchange capability, resistance to microbiological attack and thermal resistance, are usually modified by chemical treatments. The β-D glucopyranose on the cellulose chain contains one primary hydroxyl group and two secondary hydroxyl groups. Functional groups may be attached to these hydroxyl groups through a variety of reactions. The main routes of direct cellulose modification in the preparation of adsorbent materials are esterification, etherification, graft polymerization, halogenations, oxidation and alkali treatment.

- **Esterification**

The esterification reaction of cellulose relies on the reaction between the hydroxyl group and an acid, acid anhydride and acid halide under acid catalysis. A novel type of adsorbent (CM) was synthesized by (Y. Zhou et al., 2012). Cellulose was modified with maleic anhydride to remove heavy metal ions and organic dyes. The adsorption of Hg(II) ions as heavy metal ions by CM was examined, while the adsorption of basic fuchsine, methylene blue and crystal violet as organic dyes by CM was investigated. The maximum adsorption capacity of Hg(II) was found to be 172.5 mg g^{-1}, and the fraction of removal of those organic dyes was 88.10, 98.47 and 92.85 % under the optimum conditions, respectively. The esterification process increases the carboxylic content of the wood fibre surface, leading to a corresponding increase in the sorption of divalent metal ions.

- **Etherification**

The alcoholic hydroxyl groups of the cellulose can react with the alkyl halide or other etherifying reagents under basic conditions and generate a corresponding cellulose ether. Common etherification reagents are haloalkoxy, alkyl epoxides, glycidyl, silane, and isocyanate

(Habibi et al., 2010). The etherification reaction is carried out under homogeneous conditions, pyridine, sodium hydroxide, triethylamine, etc. as a catalyst in accordance with the following steps: (1) dispersing and wetting; (2) etherifying reagent was added into dispersant; (3) termination of the etherification reaction; (4) Separation and Purification.

(Bradl, 2004) chemically modified sawdust with amidoxime groups by reacting acrylonitrile with the sawdust through an etherification reaction to add cyano groups to the cellulose structure. These cyano groups were then amidoximated by reaction with hydroxylamine. This amidoximated sawdust had a high adsorption capacity for Cu (II) of 246 mg g-1 and for Ni(II) of 188 mg.g^{-1}. Silane treatment can reduce the quantity of the surface hydroxyl groups and the hydrophilic of cellulose.

- **Graft polymerization**

The graft copolymerization reaction of cellulose can be divided into three categories: Free radical polymerization, ionic polymerization and condensation or addition polymerization. Graft copolymerization only happens on the surface of the cellulose in the amorphous region and the crystalline region, and the length of the branched chain may be far more than the main chain. The inherent advantages of the cellulose are not destroyed and at the same time the cellulose is given new performance, such as the adsorption of heavy metals and dye.

(Hashem, 2006) has prepared a sunflower stalk graft copolymer by the reaction of ground sunflower stalks (SFS) with acrylonitrile (AN) in aqueous solution initiated by KMnO$_4^-$ citric acid (CA) system. Amidoximation of the grafted stalks was performed by the reaction of grafted SFS with hydroxylamine hydrochloride in alkaline medium to obtain amidoximated sunflower stalks (ASFS). The study of adsorption of Cu (II) shows that the ASFS was effectively used in adsorption of Cu (II) ions from aqueous solution.

- **Halogenation, oxidation, etc...**

Halogenation represents another cellulose modification technique. (Aoki et al., 1999) prepared 6-Deoxy-6-mercaptocellulose and its S-substituted derivatives from 6-bromo- 6-deoxycellulose and their sorption behavior for metal ions was examined. Carboxyl, amino, isothiouronium, mercapto and additional hydroxyl groups were introduced to cellulose. The first two groups were effective for the sorption of many kinds of metal ions. Ag(I) was sorbed strongly by all the derivatives studied. Many derivatives sorbed large amounts of Hg(II).

The oxidation of cellulose introduces new functional groups, such as the aldehyde group, the ketone group, the carboxyl group, or the enol group, and generates the different nature of

the water-soluble or insoluble oxides named oxidized cellulose. Depending on the difference of oxidation conditions, the oxidation products of cellulose will have an acidic effect and restore features. (Ma et al., 2012) prepared Ultrafine cellulose nanofibers, 5-10 nm in diameter. They were prepared from oxidation of wood pulp using the (2,2,6,6- tetramethylpiperidin-1-yl) oxyl (TEMPO)/NaBr/NaClO process followed by mechanical treatment. Carboxylate groups on the surface of these nanofibers provide negative charges, which are very effective to adsorb radioactive UO_2^{2+} in water. The UO_2^{2+} adsorption capability of ultrafine cellulose nanofibers was about 167 mg/g, which is 2-3 times higher than those of typical adsorbents such as montmorillonite, ion imprinted polymer particles, modified silica particles/fibrous membranes, and hydrogels. The Table 1 summarises some methods for direct modification of cellulose leading to dyes and heavy metals adsorbent materials.

3.4 Polymer - Clay Nanocomposites

Polymer-clay nanocomposites are a class of hybrid materials composed of organic polymer materials and nano scale clay fillers (Giannelis, 1996). Recently, polymer-clay nanocomposites have received significant attention as an alternative to conventional filled polymers. Because of their nanometer-size dispersion, the polymer-clay nanocomposites exhibit the large scale improvement in the mechanical and physical properties compared with pure polymer or conventional composites. These include increased modulus and strength, decreased gas permeability, increased solvent and heat resistance, and decreased flammability (Giannelis, 1998). Montmorillonite (MMT), hectrite, and saponite are frequently used pristine layered silicates, which are combined with polymeric materials to form nanocomposites (Sinha Ray & Okamoto, 2003). Among the nano-scale clays, MMT is of particular interest and has been studied widely. As mentioned above (in clay session), MMT is a clay mineral consisting of stacked silicate sheets with a high aspect ratio and a plate-like morphology. This high aspect ratio (ratio of length to thickness) plays an important role for the enhancement of mechanical and physical properties of composite materials. Chemically, MMT consists of two fused silicate tetrahedral sheets sandwiching an edge-shared octahedral sheet of either magnesium or aluminum hydroxide (Alexandre & Dubois, 2000; Giannelis, 1996; Sinha Ray & Okamoto, 2003). Its distinctive advantages of high surface area, large aspect ratio (50–1000), and platelet thickness of 1 nm make it suitable for reinforcement purposes (Uyama et al., 2003).

These clays usually contain hydrated sodium or potassium ions (Giannelis, 1998) and in this state these silicates are miscible only with hydrophilic polymers such as poly(ethylene oxide) (PEO), poly(vinyl alcohol) (PVOH), and natural biopolymers such as starches and

proteins (Pandey et al., 2005; Sinha Ray & Okamoto, 2003). However, the hydrophilic nature of the MMT surface impedes its homogeneous dispersion in an organic polymer phase (Alexandre & Dubois, 2000; Sinha Ray & Okamoto, 2003). Therefore, it is very crucial to induce the organophilicity of MMT to make it compatible with the organic polymer.

In the interlayer region of MMT there exists Na$^+$ and Ca^{2+}, which can be replaced by the alkylammonium and alkylphosphonium ions, rendering the clay into an organophilic nature. The organic modifier plays an important role for producing the nanocomposite. It may either enhance the interaction between the clay and the polymer, making it more suitably mixed, or it may favor the intercalation of the polymer chain by dictating the gallery spacing (Kumar et al., 2003; Su & Wilkie, 2003).

When these organoclays are mixed with a polymer, three types of composites are commonly obtained: tactoid, intercalated, and exfoliated structures (Figure. 3).
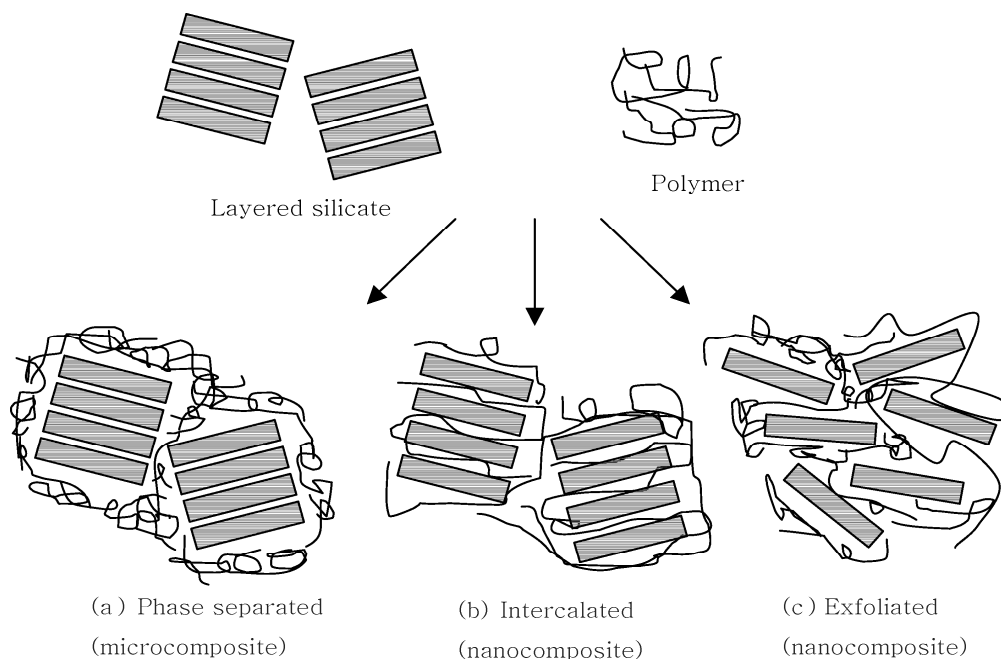
Figure. 3. Types of composite structure of polymer-layered silicate clay materials (Adapted from (McGlashan & Halley, 2003))

In tactoids, complete clay particles are dispersed within the clay matrix and the layers do not separate. The mixture of polymer and organoclays are microscale composites, and the clay only serves as a conventional filler. Intercalation and exfoliation produce two ideal nanoscale composites. In an intercalated nanocomposite often a single polymer chain will be driven between the clay silicate layers, but the system still remains quite well ordered in a stacked type of arrangement. In an exfoliated nanocomposite the silicate layers are completely

delaminated from each other and are well-dispersed. It is this second type, the exfoliated nanocomposite, which has been shown to exhibit the most significant improvements in physical properties (O. et al., 1993). The formation of intercalation or exfoliation depends on the type of the organoclay and upon the processing conditions (Li & Ha, 2003).

The degree of intercalation and exfoliation of layered silicates in polymer nanocomposites can be quantified using X-ray diffraction (XRD) and transmission electron microscopy (TEM). Generally, the intercalated layered silicate has a defined interlayer spacing basal reflection corresponding to the d_{001} spacing in a XRD diffractogram. Conversely, there is no coherent X-ray diffraction from the exfoliated silicates. TEM is a complementary technique to XRD wherein an image of the dispersion of the silicate within a polymer matrix can be quantified and analyzed(Lebaron et al., 1999; Sinha Ray & Okamoto, 2003).

- **Synthesis of Nanocomposites**

Various methods have been used to synthesize polymer-clay nanocomposites, and their properties have been found to be dependent on the preparation procedure (Artzi et al., 2002; Suh et al., 2000; Wan et al., 2003). In situ polymerization, solvent intercalation/exfoliation and melt intercalation/exfoliation are the three major pathways for the formation of nanocomposites

− **In situ polymerization,** involves the combination of clay and monomer, followed by the polymerization of the monomer, which ideally locks the exfoliated clay particles in the resulting polymer matrix.

− **In solution intercalation,** the clay is first swollen in a solvent and the polymer (intercalant) is dissolved in the solvent. Both solutions are then combined, and the polymer chains intercalate and displace the solvent within the interlayer of the clay (Shen et al., 2002). The solution intercalation method is good for the intercalation of polymers with little or no polarity into the layered structure, and facilitates the production of thin films with polymer-oriented clay intercalated layers. This technique has been widely used with water-soluble polymers to produce intercalated nanocomposites such as poly(ethylene oxide) (PEO) (Choi et al., 2001).

− **In melt intercalation,** the clay and polymer are added together above the melting temperature of the polymer; they may be held at this temperature for a period of time, put under shear, or other conditions to encourage the intercalation and the exfoliation of the clay. Of these, melt intercalation is the most appealing approach because of its versatility, its compatibility

with current polymer processing equipment such as extrusion and injection molding, and its environmentally benign character due to the absence of solvents (Shen et al., 2002).

3.5 Application in water treatment :

Adsorbents based on naturally occurring support materials gained increasing emphasis due to their availability in large quantities, their relatively low cost, and their facile chemical modification to introduce specific functional groups for enhanced metal binding ability (Kang et al., 2015), while of the various biological adsorbents, cellulose-based materials were believed to be a potential alternative for the removal of various contaminants.

Cellulose is an ideal raw material for the fabrication of absorbents for the removal of toxic pollutants. Nevertheless, there still exist some drawbacks in the applications of these cellulose-based adsorbents. For instance, desorption of contaminants from adsorbents is difficult and usually strong acids are needed, producing new pollutants. In addition, the adsorption behavior is uncontrollable. Recently, surface graft modifications have been considered as a convenient route for introducing new chemical and physical properties to cellulose.

Table. 1. Comparison of adsorption capacities of raw and modified cellulose-based adsorbents for different pollutants.

Modification Method	Adsorbate	Maximum adsorption capacity (mmol/g) of untreated adsorbent	Maximum adsorption capacity (mmol/g) of modified adsorbent	Reference
Esterification	Methyl violet	0.11	0.26	(C. H. Zhou et al., 2012)
Alkaline treatment	Cd(II)	0.16	0.65	(Memon et al., 2007)
Silynation	Cu(II)	0.26	3.15	(Hokkanen et al., 2014)
	Cd(II)	0.07	4.20	
	Ni(II)	0.26	2.73	
Oxidation	Methylene blue	0.37	2.40	(Batmaz et al., 2014)
Esterification	Cu(II)	0.03	1.64	(Geay et al., 2000)
	Ni(II)	0.05	1.66	

	Cd(II)	0.04	1.50	
Alkaline treatment	Cu(II)	0.04	0.11	(Šćiban et al., 2006)
	Zn(II)	0.01	0.24	
Esterification	Methylene blue	0.06	0.18	(Janoš et al., 2009)
	Egacid orange	0.03	0.21	

Various cellulose-based adsorbents have been investigated extensively in order to minimize the usage of costly activated carbon or avoiding the use of other expensive and complex treatment technologies such as chemical precipitation, ion exchange, membrane filtration etc.

The adsorbents mainly depends on the characteristics of the wastewater. In particular, uptake is strongly pH dependent, which may be a limiting factor for the use of adsorbent. In many cases, the removed pollutants are weak electrolytes, for which the adsorption equilibrium depends on the solution pH. For example, different amino-modified cellulose-based materials are considered to be potential adsorbents for metals and other pollutants. Limiting factors for these adsorbents might be the amino groups which have low efficiency in pollutants uptake under low pH range, present in acidic waste waters, because of the protonation of the amino groups. In addition to pH, more than one factors such as contact time, initial influent concentration, temperature, adsorbent dosage etc. can also significantly affect the adsorption process.

REFERENCES

Alexandre, M., & Dubois, P. (2000). Polymer-layered silicate nanocomposites: Preparation, properties and uses of a new class of materials. *Materials Science and Engineering R: Reports*, *28*(1), 1–63. https://doi.org/10.1016/S0927-796X(00)00012-7

Aoki, N., Fukushima, K., Kurakata, H., Sakamoto, M., & Furuhata, K. I. (1999). 6-Deoxy-6-mercaptocellulose and its S-substituted derivatives as sorbents for metal ions. *Reactive and Functional Polymers*, *42*(3), 223–233. https://doi.org/10.1016/S1381-5148(98)00076-5

Artzi, N., Nir, Y., Narkis, M., & Siegmann, A. (2002). Melt blending of ethylene-vinyl alcohol copolymer/clay nanocomposites: Effect of the clay type and processing conditions. *Journal of Polymer Science, Part B: Polymer Physics*, *40*(16), 1741–1753. https://doi.org/10.1002/polb.10236

Batmaz, R., Mohammed, N., Zaman, M., Minhas, G., Berry, R. M., & Tam, K. C. (2014). Cellulose nanocrystals as promising adsorbents for the removal of cationic dyes. *Cellulose*, *21*(3), 1655–1665. https://doi.org/10.1007/s10570-014-0168-8

Bradl, H. B. (2004). Adsorption of heavy metal ions on soils and soils constituents. *Journal of Colloid and Interface Science*, *277*(1), 1–18. https://doi.org/10.1016/j.jcis.2004.04.005

Choi, H. J., Kim, S. G., Hyun, Y. H., & Jhon, M. S. (2001). Preparation and rheological characteristics of solvent-cast poly(ethylene oxide)/montmorillonite nanocomposites. *Macromolecular Rapid Communications*, *22*(5), 320–325. https://doi.org/10.1002/1521-3927(20010301)22:5<320::AID-MARC320>3.0.CO;2-3

Esikova, T., Ponamoreva, O., Baskunov, B., Taran, S., & Boronin, A. (2012). Transformation of low-molecular linear caprolactam oligomers by caprolactam-degrading bacteria. *Journal of Chemical Technology and Biotechnology*, *87*(9), 1284–1290. https://doi.org/10.1002/jctb.3789

Faruk, O., Bledzki, A. K., Fink, H. P., & Sain, M. (2012). Biocomposites reinforced with natural fibers: 2000-2010. *Progress in Polymer Science*, *37*(11), 1552–1596. https://doi.org/10.1016/j.progpolymsci.2012.04.003

Geay, M., Marchetti, V., Clément, A., Loubinoux, B., & Gérardin, P. (2000). Decontamination of synthetic solutions containing heavy metals using chemically modified sawdusts bearing polyacrylic acid chains. *Journal of Wood Science*, *46*(4), 331–333.

https://doi.org/10.1007/BF00766226

Giannelis, E. P. (1996). Polymer layered silicate nanocomposites. *Advanced Materials*, *8*(1), 29–35. https://doi.org/10.1002/adma.19960080104

Giannelis, E. P. (1998). Polymer-Layered Silicate Nanocomposites: Synthesis, Properties and Applications. *Applied Organometallic Chemistry*, *12*(10–11), 675–680. https://doi.org/10.1002/(SICI)1099-0739(199810/11)12:10/11<675::AID-AOC779>3.0.CO;2-V

Güçlü, G., Gürdağ, G., & Özgümüş, S. (2003). Competitive Removal of Heavy Metal Ions by Cellulose Graft Copolymers. *Journal of Applied Polymer Science*, *90*(8), 2034–2039. https://doi.org/10.1002/app.12728

Habibi, Y., Lucia, L. A., & Rojas, O. J. (2010). Cellulose nanocrystals: Chemistry, self-assembly, and applications. *Chemical Reviews*, *110*(6), 3479–3500. https://doi.org/10.1021/cr900339w

Hashem, A. (2006). Amidoximated sunflower stalks (ASFS) as a new adsorbent for removal of Cu (II) from aqueous solution. *Polymer - Plastics Technology and Engineering*, *45*(1), 35–42. https://doi.org/10.1080/03602550500371620

Hokkanen, S., Repo, E., Suopajärvi, T., Liimatainen, H., Niinimaa, J., & Sillanpää, M. (2014). Adsorption of Ni(II), Cu(II) and Cd(II) from aqueous solutions by amino modified nanostructured microfibrillated cellulose. *Cellulose*, *21*(3), 1471–1487. https://doi.org/10.1007/s10570-014-0240-4

Janoš, P., Coskun, S., Pilařová, V., & Rejnek, J. (2009). Removal of basic (Methylene Blue) and acid (Egacid Orange) dyes from waters by sorption on chemically treated wood shavings. *Bioresource Technology*, *100*(3), 1450–1453. https://doi.org/10.1016/j.biortech.2008.06.069

Kang, H., Liu, R., & Huang, Y. (2015). Graft modification of cellulose: Methods, properties and applications. *Polymer*, *70*, A1–A16. https://doi.org/10.1016/j.polymer.2015.05.041

Klemm, D., Philipp, B., & Mischnick, P. (1999). Comprehensive Cellulose Chemistry. Vols 1 & 2. *Angewandte Chemie-International Edition*, *38*(12), 1824.

Kumar, S., Jog, J. P., & Natarajan, U. (2003). Preparation and characterization of poly(methyl methacrylate)-clay nanocomposites via melt intercalation: The effect of organoclay on the

structure and thermal properties. *Journal of Applied Polymer Science*, *89*(5), 1186–1194. https://doi.org/10.1002/app.12050

Kurita, K. (2001). *20090305_cc360dd02e430800e96apRsjRjvBbmlq.attach.pdf*. *26*.

Lebaron, P. C., Wang, Z., & Pinnavaia, T. J. (1999). Polymer-layered silicate nanocomposites: An overview. *Applied Clay Science*, *15*(1–2), 11–29. https://doi.org/10.1016/S0169-1317(99)00017-4

Li, X., & Ha, C. S. (2003). Nanostructure of EVA/organoclay nanocomposites: Effects of kinds of organoclays and grafting of maleic anhydride onto EVA. *Journal of Applied Polymer Science*, *87*(12), 1901–1909. https://doi.org/10.1002/app.11922

Ma, H., Hsiao, B. S., & Chu, B. (2012). Ultrafine cellulose nanofibers as efficient adsorbents for removal of UO 22+ in water. *ACS Macro Letters*, *1*(1), 213–216. https://doi.org/10.1021/mz200047q

McGlashan, S. A., & Halley, P. J. (2003). Preparation and characterisation of biodegradable starch-based nanocomposite materials. *Polymer International*, *52*(11), 1767–1773. https://doi.org/10.1002/pi.1287

Memon, S. Q., Memon, N., Shah, S. W., Khuhawar, M. Y., & Bhanger, M. I. (2007). Sawdust-A green and economical sorbent for the removal of cadmium (II) ions. *Journal of Hazardous Materials*, *139*(1), 116–121. https://doi.org/10.1016/j.jhazmat.2006.06.013

Micard, V., Belamri, R., Morel, M. H., & Guilbert, S. (2000). Properties of chemically and physically treated wheat gluten films. *Journal of Agricultural and Food Chemistry*, *48*(7), 2948–2953. https://doi.org/10.1021/jf0001785

O., K., Usuki, A., Kojima, Y., Kawasumi, M., Okada, A., Fukushima, Y., Kurauchi, T., & Kamigaito, O. (1993). Synthesis of nylon 6-clay hybrid. *Journal of Materials Research*, *8*(05), 1179.

O'Connell, D. W., Birkinshaw, C., & O'Dwyer, T. F. (2008). Heavy metal adsorbents prepared from the modification of cellulose: A review. *Bioresource Technology*, *99*(15), 6709–6724. https://doi.org/10.1016/j.biortech.2008.01.036

Pandey, J. K., Pratheep Kumar, A., Misra, M., Mohanty, A. K., Drzal, L. T., & Singh, R. P. (2005). Recent advances in biodegradable nanocomposites. *Journal of Nanoscience and Nanotechnology*, *5*(4), 497–526. https://doi.org/10.1166/jnn.2005.111

Premraj, R., & Doble, M. (2005). Biodegradation of polymers. *Indian Journal of Biotechnology*, *4*(2), 186–193. https://doi.org/10.17516/1997-1389-2015-8-2-113-130

Payen, A. (1838) Mémoire sur la composition du tissu propre des plantes et du ligneux (Memoir on the composition of the tissue of plants and of woody material). *Comptes Rendus* 7:1052–1056

Rhim, J. W., & Ng, P. K. W. (2007). Natural biopolymer-based nanocomposite films for packaging applications. *Critical Reviews in Food Science and Nutrition*, *47*(4), 411–433. https://doi.org/10.1080/10408390600846366

Rinaudo, M. (2006). Chitin and chitosan: Properties and applications. *Progress in Polymer Science (Oxford)*, *31*(7), 603–632. https://doi.org/10.1016/j.progpolymsci.2006.06.001

Šćiban, M., Klašnja, M., & Škrbić, B. (2006). Modified softwood sawdust as adsorbent of heavy metal ions from water. *Journal of Hazardous Materials*, *136*(2), 266–271. https://doi.org/10.1016/j.jhazmat.2005.12.009

Shen, Z., Simon, G. P., & Cheng, Y. B. (2002). Comparison of solution intercalation and melt intercalation of polymer-clay nanocomposites. *Polymer*, *43*(15), 4251–4260. https://doi.org/10.1016/S0032-3861(02)00230-6

Sinha Ray, S., & Okamoto, M. (2003). Polymer/layered silicate nanocomposites: A review from preparation to processing. *Progress in Polymer Science (Oxford)*, *28*(11), 1539–1641. https://doi.org/10.1016/j.progpolymsci.2003.08.002

Siró, I., & Plackett, D. (2010). Microfibrillated cellulose and new nanocomposite materials: A review. *Cellulose*, *17*(3), 459–494. https://doi.org/10.1007/s10570-010-9405-y

Staudinger, H., & Lohmann, H. (1933). uber hochpolymere Verbindungen. 81. *Justus Liebigs Ann. Chem.*, *505*(1), 41–51.

Su, S., & Wilkie, C. A. (2003). Exfoliated poly(methyl methacrylate) and polystyrene nanocomposites occur when the clay cation contains a vinyl monomer. *Journal of Polymer Science, Part A: Polymer Chemistry*, *41*(8), 1124–1135. https://doi.org/10.1002/pola.10659

Suh, D. J., Lim, Y. T., & Park, O. O. (2000). The property and formation mechanism of unsaturated polyester-layered silicate nanocomposite depending on the fabrication methods. *Polymer*, *41*(24), 8557–8563. https://doi.org/10.1016/S0032-3861(00)00216-0

Uyama, H., Kuwabara, M., Tsujimoto, T., Nakano, M., Usuki, A., & Kobayashi, S. (2003). Green nanocomposites from renewable resources: Plant oil-clay hybrid materials. *Chemistry of Materials*, *15*(13), 2492–2494. https://doi.org/10.1021/cm0340227

Wan, C., Qiao, X., Zhang, Y., & Zhang, Y. (2003). Effect of different clay treatment on morphology and mechanical properties of PVC-clay nanocomposites. *Polymer Testing*, *22*(4), 453–461. https://doi.org/10.1016/S0142-9418(02)00126-5

Zhou, C. H., Zhang, D., Tong, D. S., Wu, L. M., Yu, W. H., & Ismadji, S. (2012). Paper-like composites of cellulose acetate-organo-montmorillonite for removal of hazardous anionic dye in water. *Chemical Engineering Journal*, *209*, 223–234. https://doi.org/10.1016/j.cej.2012.07.107

Zhou, Y., Jin, Q., Hu, X., Zhang, Q., & Ma, T. (2012). Heavy metal ions and organic dyes removal from water by cellulose modified with maleic anhydride. *Journal of Materials Science*, *47*(12), 5019–5029. https://doi.org/10.1007/s10853-012-6378-2

For more information on BIOPOLYMERS, Please scan the QR code below:

PART IV

4. SORPTION

4.1 Introduction

The term sorption is generally used for describing the combined process of absorption and adsorption. These processes involve a substance (adsorbate and absorbate) to be adsorbed onto and/or absorbed within a substrate, as shown in Figure 1, While the absorption involves the uptake of adsorbates from the bulk phase into the network of the adsorbent (phase transfer) (Al-Asheh et al., 2009), adsorption is the attraction of the adsorbate from the bulk phase onto the surface of the adsorbent (Yamamoto et al., 2012). Whereas, absorption is a volume-driven phenomenon, adsorption is a surface-driven phenomenon.
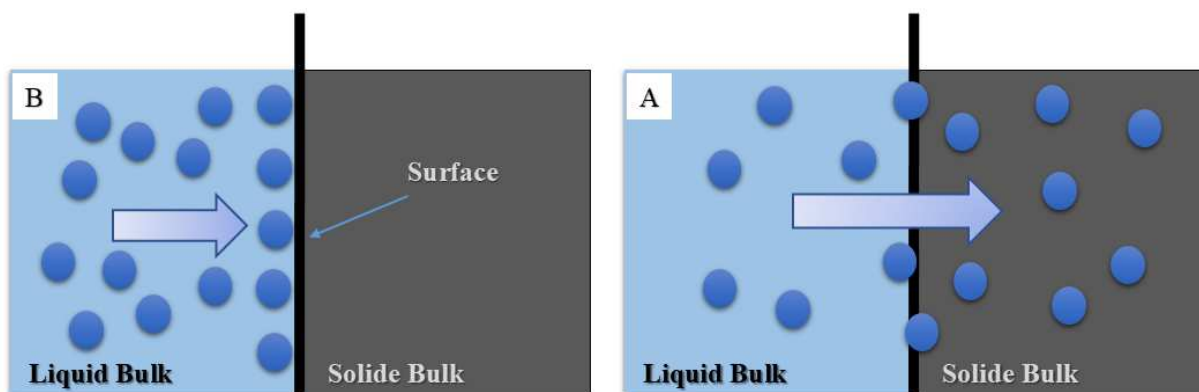
Figure. 1. A) Gas-Solid Absorption and B) Liquid Solid Adsorption process. Solid line denotes the solid-medium phase boundary.

4.2 Absorption vs Adsorption processes

Sorption is an accepted term that represents a combination of two phenomena, absorption and adsorption. During adsorption process, the adsorbate species from the bulk phase binds to the surface of adsorbent while absorption takes place within the interior phase of the sorbent.

Absorption as a physical process can be estimated according to the "Nernst distribution law" since the absorbed substance is uniformly distributed in the bulk of the other (Negi, 2007). This law suggests distribution of a solute (solid or liquid) in non-miscible solvents. This law can be represented using following Equation 1, where C_1 is concentration of X in solvent 1, C_2 is concentration of X in solvent 2, and K_d is a constant called the partition coefficient (distribution constant).

$$\frac{C_1}{C_2} = k_d \qquad (1)$$

In general, the adsorption process is categorized by: (i) physisorption, and (ii) chemisorption.

- **Physisorption** involves non-covalent interactions between the adsorbate and the adsorbent by physical forces such as van der Waals interactions, surface charge interaction (e.g., electrostatic forces), dipolar (e.g., hydrogen bonding), and π-π interactions.

- **Chemisorption** describes covalent bonding interactions, Metal-ligand binding, ion-ion interactions between the adsorbate and adsorbent. The interaction between the adsorbate and adsorbent is driven by multiple intermolecular forces such as van der Waals and/or hydrogen bonding. These interactions that result in physical adsorption are weak and reversible, where the process has an enthalpy of desorption ca. 20-40 kJ/mol.

The nature of the physical adsorption can be understood according to the polarity of the interacting species. Indeed, polarity of the interacting species plays an important role in physisorption as a driving force. Physisorption also occurs via solvent driven association such as the hydrophobic effect, where the apolar adsorbate resides on the surface of the sorbent leading to an overall increase in the entropy of the solvent (water) medium (Blokzijl & Engberts, 1993).

By contrast, chemisorption occurs via strong interactions that result in irreversible adsorption between the adsorbate-adsorbent system. The driving force for chemical adsorption is valence force that is similar to processes related to covalent bond formation, where sharing of electrons occurs for the adsorbate-adsorbent system.

Chemisorption is characterized by large exothermic heats of adsorption in the range 100-400 kJ/mol. By contrast, physisorption is often characterized by heats of adsorption that lie below 100 kJ/mol.

4.3 Solution-Phase Adsorption

Liquid-phase adsorption on solid adsorbents occurs via equilibrium or dynamic processes. As briefly mentioned before, an adsorption process can be carried out using batch and column methods. The focus of this discussion will concentrate on the batch technique. Batch studies at equilibrium have some benefits, such as easy access to sorption sites at the interior of the adsorbent. In this method, the solid adsorbents are placed in the solution phase, which consists of the adsorbate/solvent, adsorbate species, and the solvent medium, where the adsorbent surface interacts with the ensemble until equilibrium occurs between the bound and unbound sites of the adsorbent. At equilibrium, the maximum sorption capacity (q_m) can be

determined graphically via a plot of sorption capacity (q_e) vs. equilibrium or total concentration and analyzed using a suitable isotherm model (Foo & Hameed, 2010). For liquid-phase adsorption process, q_e is a function of the mole fraction of the solute relative to the specific surface area of the adsorbent. Assuming that the ideal-dilute solution condition governs the adsorption process, q_e can be estimated using mass-balance considerations, the initial concentration of adsorbate (C_0), equilibrium concentration of adsorbate (C_e), mass of the adsorbent (m) and volume of solution (V) according to Equation 2.

$$q_e = \frac{(C_0 - C_e)}{m} \times V_{solution} \qquad (2)$$

The sorptive uptake (*%P*) of PNP from aqueous solution was calculated using Equation 3:

$$P_\% = \frac{(C_0 - C_e)}{C_0} \times 100\% \qquad (3)$$

4.4 Dye-based adsorption method

At equilibrium conditions, the uptake of an adsorbate by an adsorbent system can be determined using mass-balance considerations provided that the fraction of free or bound adsorbate can be determined. In the case of adsorbates that contain chromophores, the decrease in the concentration of the unbound species (C_e) can be measured using the optical absorbance properties of the adsorbate, according to the Beer-Lambert law.

For dyes such as *p*-nitrophenol (PNP) and phenolphthalein (PHP), the observed colour can be induced by hydrogen bonding with water (as solvent) that reduces the energy gap for the $\pi \rightarrow \pi^*$ electronic transition. When adsorption of dyes takes place in the bonding sites of the adsorbent, the adsorbate is no longer dispersed in the bulk solvent but exists in a bound state by interaction with the adsorbent. PNP will exhibit a distinct yellow colour in the presence of the solvent; therefore, this dye-based technique can be coupled with batch equilibrium and/or kinetic studies for studying the adsorption process since the optical density can be related to the concentration of unbound dye in solution (B. Liu et al., 2014).
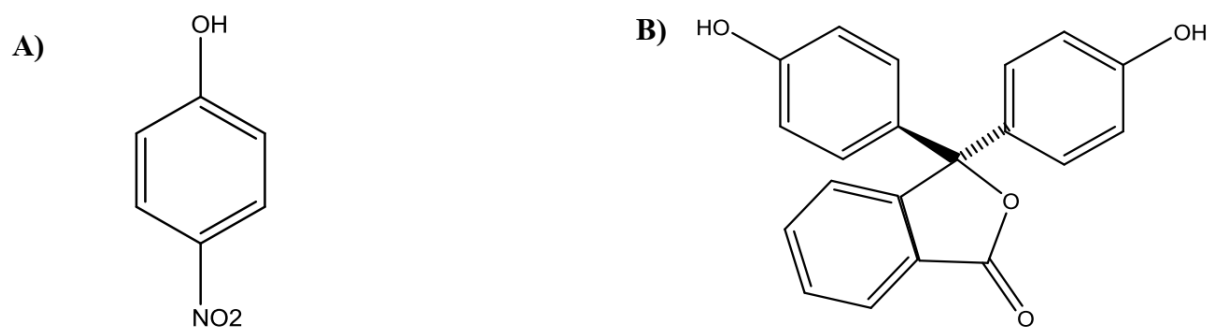
Figure. 2. The molecular structure of A) p-nitrophenol (PNP) and B) phenolphthalein (PHP) in their non-ionized forms.

Based on the assumption of large molar absorptivity coefficients for various dyes, the UV-Vis method is considered sensitive to dye concentration over the μM to mM range. In addition, these dyes can be employed to estimate the sorption capacity of adsorbent materials to estimate textural properties, analogous to the use of the nitrogen adsorption method. Thus, the ability to measure free or bound dye in a heterogeneous sorption process enables evaluation of the binding affinity, sorption site accessibility, and even surface area of the adsorbent (Voudrias et al., 2018). Furthermore, it is well established that dyes can exist in various ionization states (cationic, anionic, or neutral forms) depending on the pH and nature of the dye. In the case of solvent (water and ethanol) adsorption, the major reason for adsorption studies that employ model dyes such as *p*-nitrophenol (PNP) and phenolphthalein (PHP) relate to the insight provided on the textural and surface chemical properties of adsorbents.

The properties are dependent on the nature of the dye-adsorbent system according to the type of adsorbent-adsorbate interactions. PNP is an aromatic dye with a pKa of 7.14. The pH of the PNP solution can be adjusted using a buffer, depending on adsorption conditions required. It should be noted that some ionization occurs near the pKa value so the pH conditions need to be adjusted to control the degree of ionization of such adsorbate species, according to the Henderson-Hasselbalch equation (Po & Senozan, 2001).

At pH conditions well below the pKa, the dye exists in its non-ionized form; whereas, the dye will exist as an anion species above its pKa. The sorption properties of phenolphthalein (PHP) were reported by Bertau and Jorg using amylose-based polysaccharides. The degree of decolorization is related to the relative accessibility of the –OH groups of the polysaccharide to afford decolorization of PHP. The sorption process resulted in variable decolourization of phenolphthalein (PHP) because of the formation of noncovalent complexes (Bertau & Jörg,

2004).A noticeable change in the molar absorptivity of PHP is evidenced by complex formation according to a decolourization from pink to transparent in alkaline solution, especially for adsorption onto β-cyclodextrin and its polymer forms (Y. Liu & You, 2001). PHP is a special category of dye since the binding with -OH groups, especially in the case of β-cyclodextrin, leads to a shift in pKa of the dye to result in optical transparency vs. a strong absorbance ca. 500 nm above its pKa value. In some ways, the shift in pKa above is analogous to the colour change observed in acid-base titrations on going from colourless to pink upon titration with a base as PHP goes from below to above its pKa of the dianion species. PHP is considered as a reporter dye with "on-off" properties according to its bound and unbound states, especially in the case of adsorption by polysaccharides for the reasons of pKa shift described above. In summary, the application of the dyeadsorption method using adsorbents provides more detailed information about structural and surface chemical properties of the adsorbents by accounting for the role of surface chemistry and textural properties in the overall mechanism of adsorption (Wilson et al., 2011).

The adsorption process can be studied through graphs referred to as adsorption isotherms, defined as a graph with the amounts of adsorbate bound onto the surface of an adsorbent (ordinate) and concentration of the adsorbate (abscissa) at constant temperature and pressure. The adsorption isotherm profiles are categorized according to the nature of the adsorption process. The shape of the adsorption isotherm is an informative tool for understanding the size of the pores on the surface of the adsorbents. The following discussion outlines the various categories of adsorption isotherm in more detail.

4.5 Adsorption isotherms

According to the International Union of Pure and Applied Chemistry (IUPAC), there are six general types of adsorption isotherms (Kumar et al., 2015). Each isotherm type is governed by the surface area and the pore diameter of the adsorbent material. Pore sizes can be classified according to their relative diameter:

✓ **Macropores**: Possess pore diameters larger than 50 nm.
✓ **Mesopores**: Possess pores within the range of 2-50 nm.

The hysteresis loop is associated with the secondary pore filling process of capillary condensation. For this range, the pores are large enough to fit more than gas molecules and capillary condensation may occur.

✓ **Micropores**: Possess pore diameters of 2 nm and less. Typically, pores of such small dimensions afford adsorption of one gas molecule within the cross-sectional area to accommodate the gas that lead to formation of adsorbed monolayers similar to the Type I isotherm.
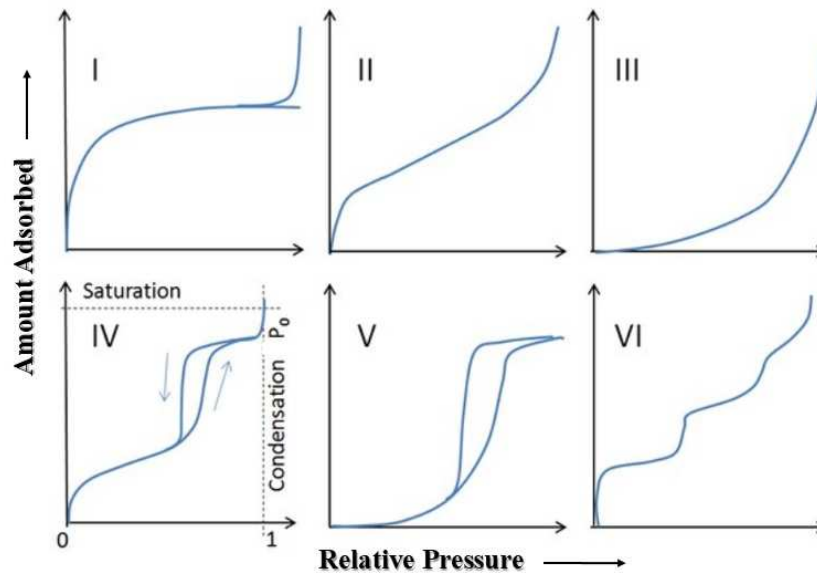
Figure. 3. Variable types of sorption isotherms (IUPAC report) for gas adsorption.
(Copyright 2016, with permission from Elsevier).

Type I

This isotherm type shows a monotonic increase in uptake, which reaches a specific sorption capacity at the plateau region. Adsorbents in this category are usually microporous materials with a very small cross-sectional area such as activated carbon or zeolites (Kumar et al., 2015).

Type II

This isotherm type shows two extremes in terms of pore size dimensions representative of large macropores. The surface area of the pores is large enough to allow formation of multilayer adsorption with no limitations.

Type III

This isotherm type is observed when strong adsorbate-adsorbate interactions exist and the binding of adsorbate molecules with one another exceeds the interaction between the adsorbate and adsorbent.

Type IV

Mesoporous materials tend to follow the Type IV isotherm profile, which describes multilayer adsorption processes. This isotherm suggests the occurrence of capillary condensation in the case where a hysteresis loop for the adsorption-desorption profile is observed.

Type V

This type isotherm curve is analogous to Type III but the interactions between the adsorbates are weaker in this case. This isotherm type shows finite sorption sites by a plateau. The presence of a hysteresis loop suggests that the agglomerated particles desorb cooperatively as a collective group.

Type VI

This type of curve represents a step-wise multilayer adsorption profile. Initially, one sorption site is filled and another site will be occupied thereafter. This type of isotherm reveals that the required energy to adsorb at one site should differ sufficiently from other sites for preferential filling to take place.

4.6 Classification of adsorption isotherm models

a) Langmuir isotherm

Irving Langmuir developed this isotherm a century ago to explain the adsorption behaviour of hydrogen gas on a palladium surface using a simple kinetic mode (Langmuir & al., 1957). He applied several assumptions to create this model. The first assumption dealt with the nature of the materials. He assumed a homogeneous surface that results in sorption sites on the material surface with similar energy of adsorption if each site can be treated independently. Secondly, he supposed monolayer coverage for adsorption, which means one layer of adsorbates on the surface. Lastly, he assumed that the adsorbate gas should behave like an ideal gas so that interaction between the gases within the monolayer could be neglected.
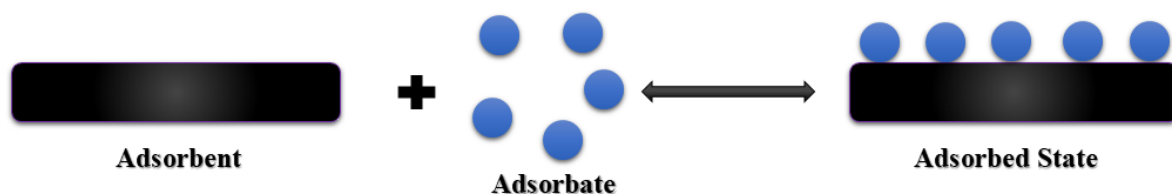
Figure. 4. Langmuir model of gas adsorption onto a solid adsorbent.

$$\frac{C_e}{q_e} = \frac{C_e}{q_{max}} + \frac{1}{(q_{max}.K_L)} \qquad (4)$$

q_e (mmol/g or mg/g) is the sorption capacity or amount of material adsorbed per gram of substrate. q_{max} (mmol/g or mg/g) is defined as the maximum adsorption capacity of the material at saturation and K_L is the equilibrium adsorption constant for the adsorbent/adsorbate system.

b) Freundlich isotherm

According to the Freundlich isotherm model, the heat of adsorption for all sorption sites is not absolutely uniform to account for surface heterogeneities.
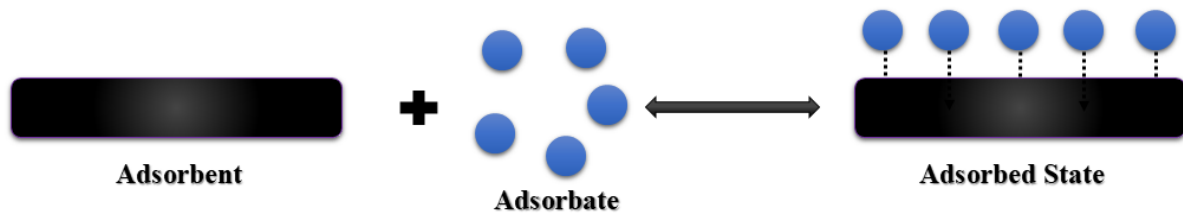
Figure. 5. The Sips and Freundlich isotherm model of gas, where surface heterogeneity is included.

$$\mathbf{lnq_e = ln(K_f) + \frac{1}{n}ln(C_e)} \qquad (5)$$

This model can be described using Equation 5, where the surface heterogeneity is the parameter 1/n. The major difference between the two models is that the Freundlich model assumes that an infinite amount of adsorbate can be taken up by the adsorbent. On the other hand, the Langmuir model assumes monolayer adsorption that undergoes saturation as soon as each site binds with an adsorbate (D'Arcy et al., 2014).

c) Sips isotherm

The Langmuir and Freundlich isotherm models have common assumptions for considering monolayer coverage. However, Freundlich isotherms can account for surface heterogeneity while the Langmuir model assumes monolayer adsorption. By considering the occurrence of surface heterogeneity, the Langmuir isotherm does not account for variable enthalpy of adsorption at the sorption sites and is no longer valid. Thus, application of a general Langmuir-Freundlich isotherm is a great advantage, where the sorption capacity at saturation can be described as a function of the energy distribution for the sorption sites. For cases with distribution of heat of adsorption close to unity, the Langmuir isotherm (unitary heat of adsorption) is preferred, especially if the distribution follows Gaussian behaviour. Based on these rules for combination of the Langmuir and Freundlich isotherm models, the Sips isotherm model was developed (Sips, 1948).

$$ln\left(\frac{q_e}{q_{max}-q_e}\right) = \frac{1}{n}ln(C_e) + ln(K_s) \qquad (6)$$

In the case where the n_s parameter is not close to the unity, the equation represents the Freundlich isotherm model and reflects surface heterogeneity. Equilibrium constant K_s represents binding affinity of the adsorbate to the sorption sites. A large value of K_s indicates that the sites are readily accessible and adsorption is favoured at the adsorption sites.

When the exponent value (n_s) approaches unity, the model converges to the Langmuir isotherm model, where the energy of the sorption site has a singular value. At dilute concentration, the model converges to the Freundlich isotherm. It is important to note that this model assumes monolayer coverage when ns is equal to unity.

The Sips model is very useful for the study of solution-phase adsorption, due to its ability to account for both Langmuir and Freundlich adsorption behaviour. However, the assumptions of the Sips isotherm are not generally applicable under two limiting conditions. Firstly, when there is a strong lateral adsorbate-adsorbate interaction, all previous isotherms assume ideal solutions with zero enthalpy of mixing. One weakness related to the Freundlich and Sips isotherms indicates that the "n_s" parameter enables one to infer the possibility of heterogeneous sites, while lateral interactions between adsorbates can contribute surface heterogeneities. Thus, the assumptions of the Sips isotherm can be violated when the lateral adsorbate-adsorbate interaction dominates (e.g. Type III isotherm). Secondly, assumptions of the Sips isotherm are violated when multilayer formation occurs.

d) Brunauer-Emmett-Teller (BET) isotherm model

All three previous isotherms (Langmuir, Freundlich, and Sips) primarily considered monolayer coverage; whereas, the BET model takes into account multilayer adsorption. Multilayer adsorption occurs after formation of a monolayer, where the next adsorbed layers are stacked on top of one another through adsorbate-adsorbate interactions (Brunauer et al., 1938). Depending on the strength of the interaction between layers, Type II-V isotherms may be obtained. Specifically, this model can be employed as a useful tool for providing thermodynamic information such as the enthalpy of adsorption/desorption. Determination of the sorption capacity of the substrate at the first monolayer is possible if the BET model follows a Type II or IV isotherm.
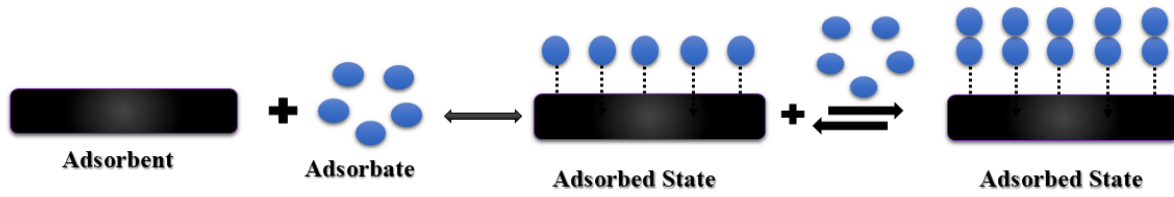
Figure. 6. BET model of physical adsorption for gas. The dashed lines represent bonding between the adsorbate and the adsorbent surface.

In this model, the constant term C (cf. Equation 7) is considered a function of the enthalpy for adsorption on the first layer and enthalpy of condensation for the gas. A larger value of C suggests a large enthalpy for adsorption of adsorbates with the adsorbent, and this implies that adsorption of a species onto the adsorbent surface does not occur favourably. This leads to adsorption of molecules on the surface of the adsorbent, where additional species are able to adsorb onto the existing bound layer of adsorbate instead of the adsorbent surface directly. Unlike the other isotherms, the initial concentration (C_0) of the adsorbate is required. The BET isotherm model predicts the saturation accurately when an amount of adsorbate is bound to the surface of the adsorbent. The BET model assumes that the formation of multiple layers of adsorbate continues until the adsorbate is completely adsorbed onto the adsorbent surface and condensation occurs.

$$\frac{n_{ads}}{n_m} = \frac{C\left(P/P_0\right)}{\left(1-P/P_0\right)\left(1+(C-1)\,P/P_0\right)} \qquad (7)$$

Where P and P_0 are equilibrium and the saturation pressure of adsorbates, respectively, n_{ads} is adsorbed gas quantity, the n_m represents the monolayer capacity, and C is BET constant.

The use of the BET method as a static technique employs a sorption isotherm for calculating the surface area of adsorbents (ISO [International Organization for Standardization]. (2010)). A derivate equation of the BET expression can be used to calculate the surface area of adsorbents according to the Equation 8.

$$\frac{P}{(P_0-P)n_{ads}} = \frac{1}{n_m C} + \frac{(C-1)}{n_m C} \times \frac{P}{P_0} \qquad (8)$$

The parameters (n_m and C) of the BET equation can be obtained by plotting the adsorption isotherm typically at a relative pressure (P/P_0) range of 0.05-0.35 due to existence of a linear relationship. Through the n_m value, the surface area can be calculated using molecular cross-sectional area (A) through Equation 9.

$$S_{total} = \frac{n_m N_A}{V} \qquad \textbf{(9)}$$

Where N_A is Avogadro's number and V is the molar volume of the adsorbate. Then, the specific surface area (m^2/g) can be calculated by dividing the total surface area by the sample weight (g).

$$S_{total} = \frac{S_{BET}}{Sample\ mass} \qquad \textbf{(10)}$$

The method of Barrett, Joyner, and Halenda (BJH) is a well-known procedure for calculating the pore size distribution of a material from experimental isotherms according to the Kelvin model of pore filling. The BJH equation can be expressed by Equation 11 (Barrett et al., 1951) :

$$V_{ads}(x_k) = \sum_{i=1}^{k} \Delta V_i \big(r_i \leq r_c(x_k)\big) + \sum_{i=k+1}^{n} \Delta S_i t_i \big(r_i > r_s(x_k)\big) \qquad \textbf{(11)}$$

V_{ads} (x_k) is the volume of adsorbate at relative pressure (x_k), V_i is pore volume, S_i represents the pore surface area of pores, and t is the thickness of the adsorption layer.

As briefly outlined above, the adsorption isotherm can be used for calculation of surface area and pore size distribution. Furthermore, the shape of an obtained isotherm using these models can be employed as a tool for the interpretation of an adsorption process. The following section will provide useful information on types and application of the hysteresis of adsorption/desorption curves for characterization of the textural properties (e.g porosity and surface area) of a material.

- **Hysteresis in solid-gas adsorption/desorption curves**

A typical nitrogen gas-adsorption isotherm can be obtained by plotting q_e vs. the relative pressure (P/P$_0$). For instance, depending on the pore shape, cylindrical pores often display type H1 profiles, while ink-bottle pores have type H2 profiles (Kumar et al., 2015). Gas absorbed into the structure of the adsorbent undergoes condensation. The desorption process takes place after the condensation step and occur in the solution state. Therefore, the amount of heat (enthalpy of adsorption) evolved during this processes are different. The desorption branch generally differs from the isotherm branch of adsorption due to the difference for the enthalpy of adsorption vs. desorption. Based on this difference, hysteresis loops have been described based on gas adsorption results, where this technique can provide useful information on the adsorption-desorption process. (cf. Figure 7)

Type H1

The H1 type of hysteresis is possible when nitrogen gas adsorbs onto the walls of the pores prior to formation of multilayers until the pore volume is fully occupied. Cylindrical pores are associated with this type of hysteresis as the filling of the pores occurs uniformly within the pore and allows a steep asymptote profile when condensation occurs.

Type H2

The H2 hysteresis is related to ink-bottle pores due to difficulties in the filling for some of the pores. Although the adsorption into the pores is similar to H1, attenuation of capillary condensation is the reason behind this hysteresis loop. The IUPAC types of profiles note that desorption isotherms are governed by other factors that can also affect the isotherm shape, such as the presence of network pores within a material. However, the desorption curve does not follow the original/initial desorption branch of the hysteresis profile.

Type H3

The H3 hysteresis loop exists in the isotherm due to adsorbate-adsorbate interaction following the completion of the monolayer coverage. For example, thin slit-like capillaries can promote this type of hysteresis (Yoshida & Ruthven, 1983).

Type H4

This type of isotherm is distinguished by the high adsorption affinity of the adsorbent, which indicates microporosity that allows for strong adsorbent-adsorbate interactions (Kumar et al., 2015). The desorption-isotherm branch looks like the H3 type and the pore structure is almost slit-shaped.
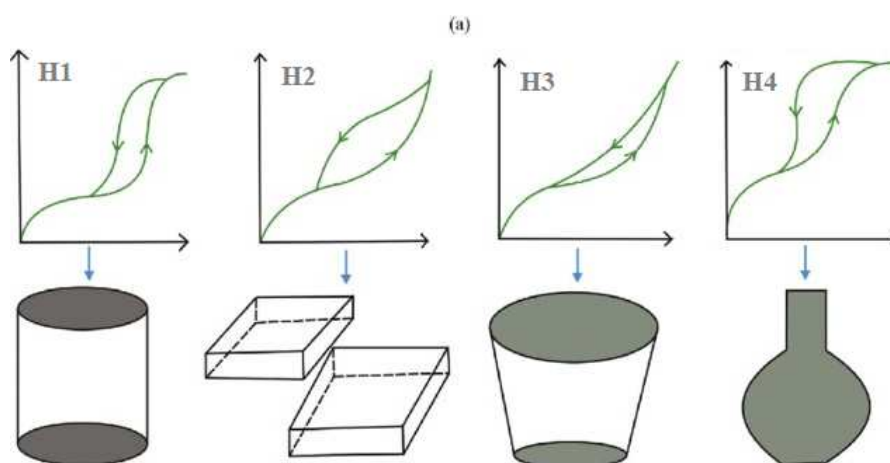
Figure. 7. The four general hysteresis loops detected for nitrogen adsorption and desorption as defined by IUPAC. (Copyright 2016, with permission from Elsevier).

Isotherm types and models are useful analyzing tools for understanding of the adsorption process under variable conditions. One of the main factors governing the adsorption process is the adsorbent itself. Adsorbents with different structural and chemical properties and even different shapes behave differently toward adsorbates. To gain a better grasp of the adsorption process, familiarity with the physicochemical properties of various types of adsorbents is essential.

4.7 Adsorption Kinetic models

The adsorption kinetics can be tested by three common types of models: the pseudo-firstorder (PFO), pseudo-second-order (PSO) and pore diffusion models (PDM).

PFO and PSO models are used to evaluate the adsorption mechanism. The non-linear Equation 12 and linear Equation13 pseudo first-order kinetic models (Lagergren, 1898) are expressed as:

$$q_e = q_t(1 - e^{-k_1 t}) \qquad (12)$$

$$ln(q_e - q_t) = lnq_e - k_1 t \qquad (13)$$

k_1 (min^{-1}) is the rate constant of the PFO kinetic equation and where q_e (mg/g) and q_t (mg/g) are the uptake amounts of adsorbate at equilibrium and variable time (t). The PFO kinetic model for adsorption is expressed as plots of q_t vs t and $ln(q_e - q_t)$ vs t for non-linear and linear PFO models, respectively. The values of K_1 and q_e can be obtained from the slope and intercept of plots of $ln(q_e - q_t)$ vs t.

The non-linear Equation 12 and linear Equation 13 second-order kinetic models are defined by the following equations (Borah et al., 2011; Ho & McKay, 1998).

$$\frac{1}{(q_e - q_t)} = \frac{1}{q_e} + k_2 t \qquad (14)$$

$$\frac{t}{q_t} = \frac{1}{k_2 q_e^2} + \frac{t}{q_e} \qquad (15)$$

The parameter k_2 is the adsorption rate constant (g.mg^{-1} .min^{-1}) according to the PSO model. The PFO kinetic model for adsorption is expressed as a plot of q_t vs t and t/q_t vs t for non-linear and linear analyses, respectively. The k_2 and q_e parameters can be obtained from the slope and intercept from plots of t/q_t vs t.

The pore diffusion equation is described by the following Equation 16:

$$k_t = k_d t^{0.5} \qquad (16)$$

Kd (mg/g min$^{-1/2}$) is the diffusion rate constant, and q_t is the amount of adsorbate adsorbed at time (t). A plot of q_t against $t^{1/2}$ yields a slope equal to the K_d term.

REFERENCES

Al-Asheh, S., Banat, F., & Fara, A. A. (2009). Dehydration of ethanol-water azeotropic mixture by adsorption through phillipsite packed-column. *Separation Science and Technology*, *44*(13), 3170–3188. https://doi.org/10.1080/01496390903182479

Barrett, E. P., Joyner, L. G., & Halenda, P. P. (1951). The Determination of Pore Volume and Area Distributions in Porous Substances. I. Computations from Nitrogen Isotherms. *Journal of the American Chemical Society*, *73*(1), 373–380. https://doi.org/10.1021/ja01145a126

Bertau, M., & Jörg, G. (2004). Saccharides as efficacious solubilisers for highly lipophilic compounds in aqueous media. *Bioorganic and Medicinal Chemistry*, *12*(11), 2973–2983. https://doi.org/10.1016/j.bmc.2004.03.041

Blokzijl, W., & Engberts, J. B. F. N. (1993). Hydrophobic Effects. Opinions and Facts. *Angewandte Chemie International Edition in English*, *32*(11), 1545–1579. https://doi.org/10.1002/anie.199315451

Borah, J. M., Sarma, J., & Mahiuddin, S. (2011). Adsorption comparison at the α-alumina/water interface: 3,4-Dihydroxybenzoic acid vs. catechol. *Colloids and Surfaces A: Physicochemical and Engineering Aspects*, *387*(1–3), 50–56. https://doi.org/10.1016/j.colsurfa.2011.07.024

Brunauer, S., Emmett, P. H., & Teller, E. (1938). Adsorption of Gases in Multimolecular Layers. *Journal of the American Chemical Society*, *60*(2), 309–319. https://doi.org/10.1021/ja01269a023

D'Arcy, M., Bullough, F., Moffat, C., Borgomeo, E., Teh, M., Vilar, R., & Weiss, D. J. (2014). Adsorption of oxy-anions in the teaching laboratory: An experiment to study a fundamental environmental engineering problem. *Journal of Chemical Education*, *91*(4), 505–510. https://doi.org/10.1021/ed300220d

Foo, K. Y., & Hameed, B. H. (2010). Insights into the modeling of adsorption isotherm systems. *Chemical Engineering Journal*, *156*(1), 2–10. https://doi.org/10.1016/j.cej.2009.09.013

Ho, Y. S., & McKay, G. (1998). Sorption of dye from aqueous solution by peat. *Chemical Engineering Journal*, *70*(2), 115–124. https://doi.org/10.1016/S1385-8947(98)00076-X

ISO [International Organization for Standardization]. (2010). Determination of the specific surface area of solids by gas adsorption - BET method (ISO 9277:2010(E)). *Reference Number ISO*, *9277*(9277), 30 pp. https://doi.org/10.1007/s11367-011-0297-3

Kumar, P., Kim, K. H., Kwon, E. E., & Szulejko, J. E. (2015). Metal-organic frameworks for the control and management of air quality: Advances and future direction. *Journal of Materials Chemistry A*, *4*(2), 345–361. https://doi.org/10.1039/c5ta07068f

Lagergren, S. (1898). Zur Theorie der Sogenannten Adsorption Gelöster Stoffe. *K. Sven. Vetenskapsakad. Handl.*, 24, 1–39

Liu, B., Yang, F., Zou, Y., & Peng, Y. (2014). Adsorption of phenol and p -nitrophenol from aqueous solutions on metal-organic frameworks: Effect of hydrogen bonding. *Journal of Chemical and Engineering Data*, *59*(5), 1476–1482. https://doi.org/10.1021/je4010239

Liu, Y., & You, C. C. (2001). Inclusion complexation of β-cyclodextrin and 6-O-α-maltosyl- and 2-O-(2-hydroxypropyl)-β-cyclodextrins with some fluorescent dyes. *Journal of Physical Organic Chemistry*, *14*(1), 11–16. https://doi.org/10.1002/1099-1395(200101)14:1<11::AID-POC329>3.0.CO;2-7

Negi, A. S. (2007). A Textbook of Physical Chemistry. New Age International, New Delhi,1-1008.

Po, H. N., & Senozan, N. M. (2001). The Henderson-Hasselbalch equation: Its history and limitations. *Journal of Chemical Education*, *78*(11), 1499–1503. https://doi.org/10.1021/ed078p1499

Sips, R. (1948). On the structure of a catalyst surface. *The Journal of Chemical Physics*, *16*(5), 490–495. https://doi.org/10.1063/1.1746922

Suits, C. G.; Miles, J. M. Irving Langmuir. (1881-1957). A Biographical Memoir, National Academy of Sciences Biographical Memoir. 1974, 214-47

Voudrias, E., Fytianos, K., & Bozani, E. (2018). Sorption-desorption isotherms of dyes from aqueous solutions and wastewaters with different sorbent meterials. *Global NEST JournalGlobal NEST: The International Journal*, *4*(1), 75–83. https://doi.org/10.30955/gnj.000233

Wilson, L. D., Mohamed, M. H., & Headley, J. V. (2011). Surface area and pore structure properties of urethane-based copolymers containing β-cyclodextrin. *Journal of Colloid and Interface Science*, *357*(1), 215–222. https://doi.org/10.1016/j.jcis.2011.01.081

Yamamoto, T., Kim, Y. H., Kim, B. C., Endo, A., Thongprachan, N., & Ohmori, T. (2012). Adsorption characteristics of zeolites for dehydration of ethanol: Evaluation of diffusivity of water in porous structure. *Chemical Engineering Journal*, *181–182*, 443–448. https://doi.org/10.1016/j.cej.2011.11.110

Yoshida, H., & Ruthven, D. M. (1983). Dynamic behaviour of an adiabatic adsorption column-I Analytic solution for irreversible adsorption. *Chemical Engineering Science*, *38*(6), 877–884. https://doi.org/10.1016/0009-2509(83)80009-8

For more information on SORPTION and wastewater treatment methods, please scan the QR code below:

CHAPTER III
MATERIALS, CHARACTERISATION AND EXPERIMENT METHODS.

INTRODUCTION

The overall objectives of this research are focused on the preparation and characterization of hybrid composite materials based on Biopolymer (CMC) and Clay (Bentonite) for the application of the adsorption of dyes from water in single and mixture systems.

The objectives proposed in this thesis research can be further organized by dividing it into various parts:

- Part One: is dedicated to the purification of raw bentonite and to study the possibility of interposing HDTMA-Br molecules in it with the aim of obtaining OrganoBentonite materials (BAS) and using them as an adsorbent to remove three types of dyes namely Methylene Blue (cationic dye), Telon Blue (anionic dye), and Bezathren Red (nonionic dye), from aqueous solutions. The equilibrium data obtained were then assessed using various adsorption isotherm models. Some kinetic studies were also conducted in order to evaluate the adsorption mechanism.

- In the Part Two, a simple method was employed for intercalation of CarboxyMethyl Cellulose (CMC) into the OrganoBentonites (BAS), for this, a series of BAS/CMC nanocomposites with different percentage of Carboxymethyl Cellulose were synthesized under different conditions. The nanocomposites were characterized by the Fourier transform infrared (FT-IR) spectrophotometer, X-ray diffraction (XRD) method, and thermal gravimetric (TG) analysis. The effects of different reaction conditions on the intercalation of the CMC in the Organobentonite sheets were investigated by controlling the amount of Hexadecyl trimethyl ammonium bromide (HDTMA) in the Bentonite (BA) and the weight ratios of CMC added to the organic bentonite (BAS). The obtained materials (BAS/CMC) are then used as adsorbents for the last three dyes, Methylene Blue, Telon Blue, and Bezathren Red.

- The Part Three has been designed to study the efficiency of the synthesized adsorbents (BAS and BAS / CMC) to decolorize and reduce the COD content in the mixture system of the three previous dyes using the adsorption process. The effect of operational parameters such as initial dye concentration of each dye were evaluated.
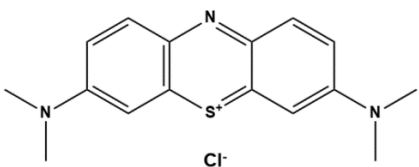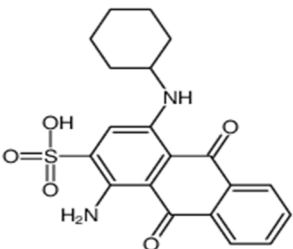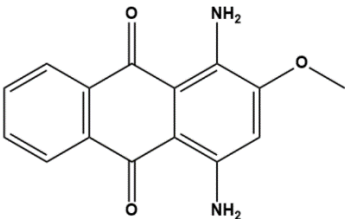
PART I
ORGANO-BENTONITE

1. EXPERIMENT METHOD

1.1 Materials

The hexadecyltrimethylammonium bromide (HDTMA-Br) was purchased from Sigma Aldrich (99% purity) and used as received. Sodium chloride (NaCl) was provided by Aldrich and was used without further purification. Likewise, Methylene Blue (MB), and Telon Blue (TB) were purchased from Sigma-Aldrich and Bezathren Red (BzR) were taken from the company E.A.T.I.T, Sebdou, Tlemcen and utilized without further purification. Some specific characteristics of these three dyes are summarized in Table 1.

Table 1. Physicochemical characteristics of dyes used in this study

Name	Molecular Structure	Nature	M_w (g/mol)	λ_{max} (nm)
Methylene Blue (Basic Blue 9)		Cationic	319.851	664
Telon Blue (Acid Blue 62)		Anionic	400.44	640
Bezathren Red FBB EPS (Disperse 11)		Disperse	268.272	505

a) Bentonite sample

The starting material used in this study was natural bentonite (NB), provided by the National Company of Non-Ferrous Mining Products and Useful Substances (ENOF - Algeria). Natural bentonite, which is essentially composed of montmorillonite (80%), contains a large

number of impurities. The chemical composition of natural bentonite (NB) was determined by X-ray fluorescence (XRF) spectrometry, and the data obtained are reported in Table 2.

Table 2. Chemical composition of natural bentonite.

Species	SiO_2	Al_2O_3	Fe_2O_3	CaO	MgO	Na_2O	K_2O	TiO_2	LOI
% (w/w)	65.2	17.25	2.10	1.20	3.10	2.15	0.60	0.20	8.20

Raw bentonite was purified under laboratory conditions (Makhoukhi et al., 2015). In order to remove impurities, such as carbonates, quartz, and organic matter, the bentonite was dispersed in bidistilled water, and the clay fraction (< 2 μm) was recovered through sedimentation. In order to obtain sodium bentonite, the solid phase was then saturated with sodium ions in a 1 M sodium chloride solution and stirred; this operation was repeated three times. When saturation was achieved, the resulting solid was washed with bidistilled water several times in order to remove excess salt; the final product was sodium bentonite (BA). Then, the hexamminecobalt (III) chloride was used to determine the cation exchange capacity (CEC) which was found equal to 85 meq g/100 g.

b) Preparation of OrganoBentonite (BAS)

The amount of 2 g of sodium bentonite (BA) was dispersed into 50 mL of distilled water. Then, 200 mL of the HDTMA-Br solution were added dropwise to this suspension, and the mixture was shaken using a mechanical shaker for 4 hours at 80 °C. Note that the initial amounts of HDTMA-Br in the aqueous phase were equivalent to various percentages of CEC (from 50 to 200 meq g /100 g BA). The resulting material was centrifuged at 4000 rpm, for 30 min, to yield a clear supernatant. Afterwards, the solid was washed several times with warm distilled water, until complete disappearance of bromide anions, as indicated by the silver nitrate ($AgNO_3$) test. Next, the ensuing OrganoBentonite was dried at 60 °C, then crushed and sieved for particles less than 100 μm. The OrganoBentonites obtained were labeled as BAS 0.5, BAS 1, BAS 1.2, BAS 1.5 and BAS 2, according to the percentage of CEC.

c) Batch adsorption studies

The adsorption capacities of the prepared composites for MB, TB and BzR dyes were evaluated using a batch equilibrium procedure. For this, the stock dyes solutions (1000 mg.L^{-1}) were first prepared by dissolving MB and TB in deionized water. For the vat dye BzR, a sodium hydroxide solution and hydrosulfite salts were used for the preparation of the aqueous solution. The stock solutions were then diluted in deionized water to achieve the desired concentration

ranges. Subsequently, the dried sample (25 mg) was immersed in each dye solution (40 mL). The dye solutions containing the adsorbents were then shaken at 400 rpm. Finally, each solution was centrifuged a 4000 rpm for a period of 15 mn, and the ensuing supernatant was analyzed using a UV-Visible spectrophotometer (OPTIZEN 1412 UV/VIS) at their maximum wavelengths (664, 495 and 505 nm for MB, TB, and BzR, respectively).

Furthermore, adsorption experiments were conducted in conical flasks, at a constant agitation speed of 400 rpm, while varying the pH of the solution from 2 to 11, the adsorbent dosage from 10 to 100 mg, the contact time from 2 to 180 min, the initial dye concentration from 5 to 200 mg/L and the temperature from 25 to 50 °C.

The adsorption capacity and removal efficiency of the prepared composite were calculated based on the initial and final concentrations of dyes present in the solution, using the following Equation. (1):

$$q_e = \frac{(C_0 - C_e).V}{m} \qquad (1)$$

Where C_0 and C_e are the initial and equilibrium dye concentrations, respectively, V is the volume of dye aqueous solution (L) and m is the mass of adsorbent (g).

1.2 Characterization

The XRD patterns of the samples were obtained with X-ray diffractometer ULTIMA IV (Rigaku, Tokyo, Japan), operating with Copper Kα radiation (λ=1.54 Å) at 40 kV and 30 mA. All experiments were carried out at ambient temperature with 2θ varying between 2 and 40°, a scan speed of 2°/min and a step size of 0.02°.

Infrared (IR) spectra of the samples were obtained using an Agilent Cary 600 Series FTIR Spectrometer equipped with DRIFT (Diffuse Reflectance Infra-red Fourier Transform) accessories. Spectra over the 4,000 –500 cm^{-1} range were obtained by the co-addition of 64 scans with a resolution of 4 cm^{-1} and a mirror velocity of 0.6329 cm.s^{-1}.

Thermogravimetric analyses of the samples were obtained using High-resolution TGA (TA Instruments Q Series Q600 SDT). 10 mg of finely ground sample was heated in an open platinum crucible with a heating rate of 10 °C/min and temperature from 50 to 800 °C under a nitrogen atmosphere flow rate of 100 mL/min.

2. RESULTS AND DISCUSSION

2.1 X-Ray Diffraction

The X-ray diffraction pattern of purified Bentonite (BA) was compared to that of the natural bentonite (NB), as illustrated by (Figure. 1). It clearly appears that the clay mineral crystallinity of BA was not diminished upon purification.
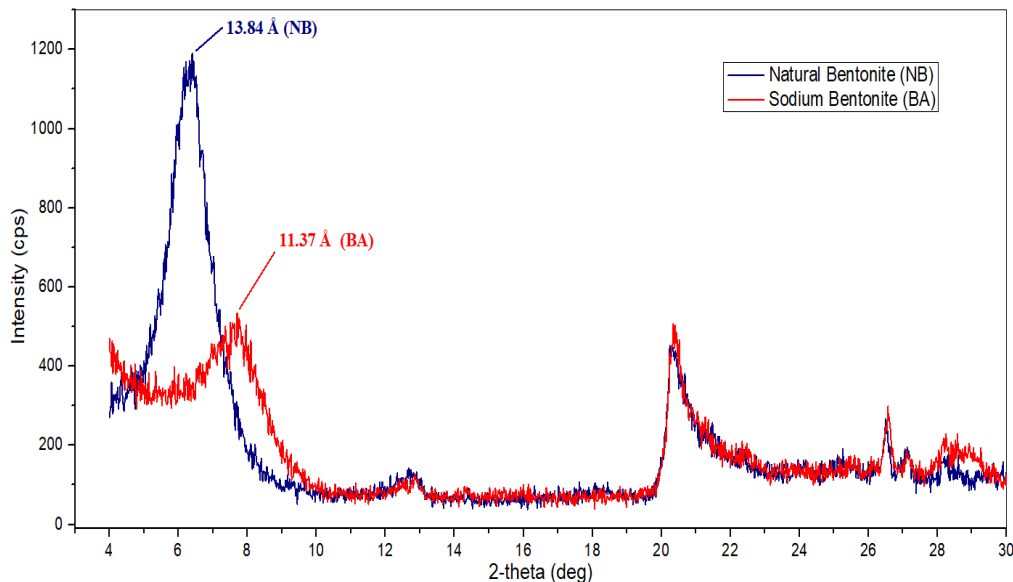
Figure. 1. XRD patterns for bentonites before and after purification.

Figure.1 shows the XRD pattern of natural bentonite (NB) and BA was exhibiting the reflection peak occurred at 6.4° and 7.7°, respectively. The interlayer spacing distance of the bentonites was found to be 13.84 Å and 11.37 Å respectively.

The decrease in the interlayer spacing of NB was due to cationic exchange of Ca^{2+}, Mg^{2+} and K^+ cations, replaced by Na^+ cations which have a smaller atomic radius.

The X-ray diffraction patterns of the absorbents BA and BAS are presented in Figure. 2a, while the variation of the interlamellar distance (Δd) as a function of the amount of intercalated surfactant molecules is depicted in Figure.2b.
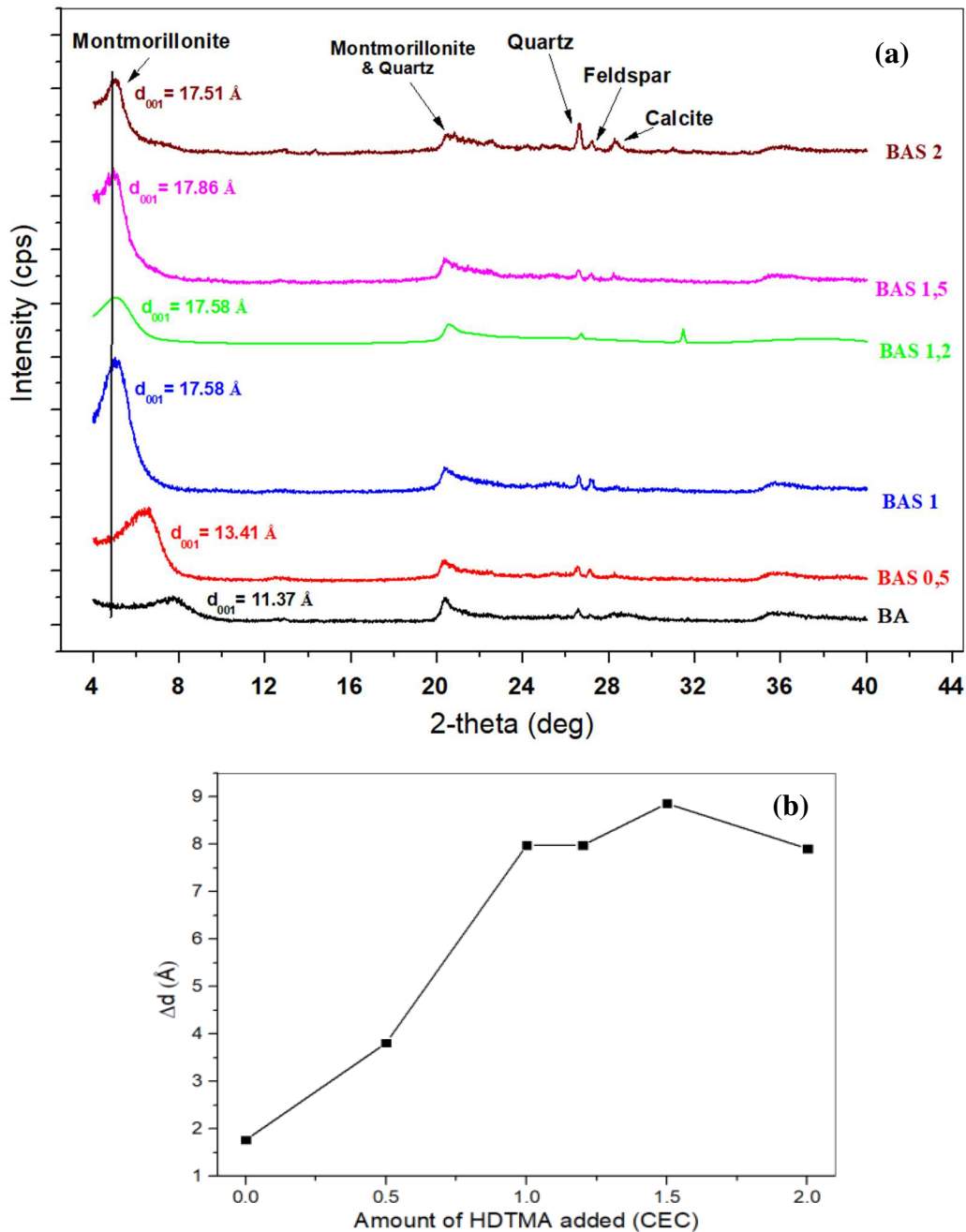
Figure. 2. XRD analysis of BA and BAS samples and values of their interlamellar distances $d_{(001)}$ at different surfactant concentrations (a), and Δd (b).

The interlayer spacing values $d_{(001)}$, of the parent BA and of BAS clay samples, were determined using low-angle XRD. For BA, as can be seen in Figure. 2a, a broad peak was observed at $2\theta = 7.76°$ which corresponds to montmorillonite. This result suggests an interlamellar distance $d_{(001)}$ of 11.37 Å. For BAS 0.5 sample (Figure. 2a), corresponding to 0.5 CEC of BA, a sharp peak was observed at $2\theta = 6.58°$, which corresponds to $d_{(001)} = 13.41$ Å. Upon the addition of HDTMA molecules, the peak positions shifted to lower angles, in accordance with the HDTMA loading. A displacement of the angle 2θ was observed from 7.76° to 5.04° with an increase in $d_{(001)}$ values from 11.37 Å for BA to 17.86 Å for the organophilic

clay BAS 1.5, which confirms the intercalation of ammonium ions in the interlayer space (Huang et al., 2017). However, for higher HDTMA loadings, the peak position remained nearly constant, which means that a saturation limit was reached for the intercalation of the HDTMA molecules inside the BA material. These findings are in accordance with the FTIR and TGA results.

A cation exchange process was used to compensate for the excess negative charges, and the sodium ions were replaced by the positively charged surfactant molecules. The thickness of a layer in a single unmodified montmorillonite structural unit was considered to be equal to 9.6 Å (Darder et al., 2003). By subtracting the thickness of the single montmorillonite unit (9.6 Å) from the $d_{(001)}$ spacing of the surfactant-modified clay, the interlamellar spacing Δd, occupied by the HDTMA molecules, can be deduced. It is worth noting that the Δd values increased from 3.81 Å in the case of BAS 0.5 to reach 8.26 Å in the case of BAS 1.5; it then remained almost unchanged with greater HDTMA loadings (Figure. 2b).

According to (Zhu et al., 2013) The theoretical length of the HDTMA cation is 25 Å, and the height of alkyl chain is 4.0 Å and the nail-head is 5.1 Å since HDTMA cation lies flat between the bentonite layers. Based on this study, we can conclude that in the case of BAS 1.5 and 2 CEC the HDTMA molecules are adopting a bilayer arrangement in bentonite sheets.
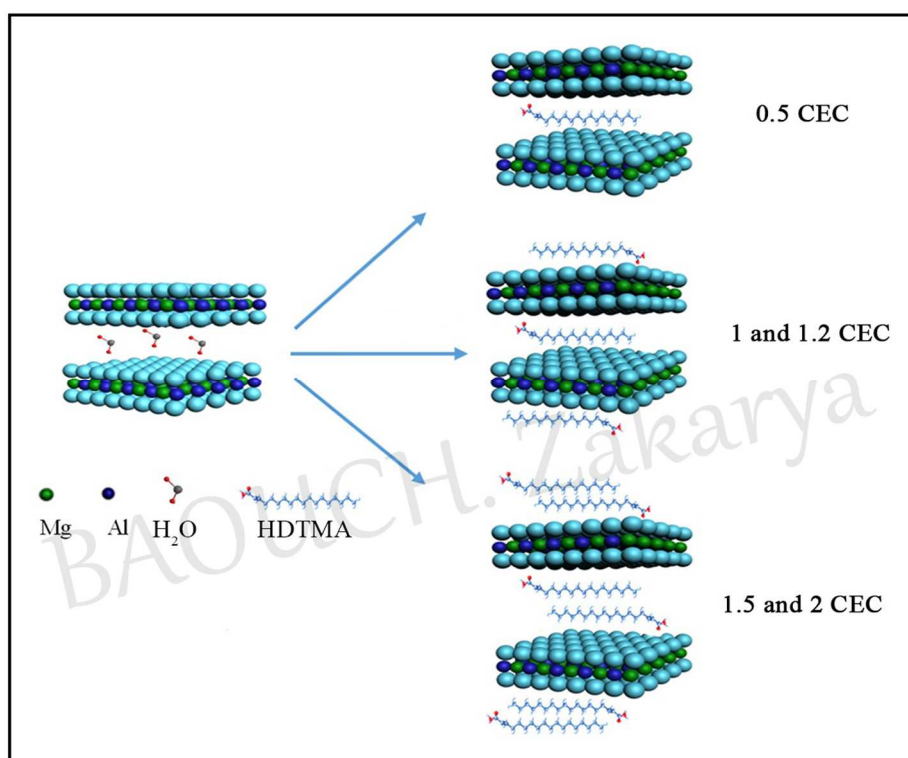
Figure 3. An illustration of the HDTMA arrangement in the bentonite layers at different ratios

2.2 Infrared Spectroscopy

The IR spectra of BA and BAS, depicted in Figure 3a, indicate that modification of clay was successfully achieved. It should be noted that the FTIR spectra were characterized by an important absorption band reduction, between 3300 and 3750 cm^{-1}, indicating the new hydrophobic behavior of the BAS samples. The bands corresponding to hydroxyl groups indicated the progressive replacement of water molecules by those of the cationic surfactant. (Parolo et al., 2014).

The presence of cationic surfactant molecules in BAS composites was confirmed by the appearance of new absorption bands. The spectra (Figure.4a) showed additional absorption bands, at 2927 cm^{-1} and 2854 cm^{-1}, which are assigned to the asymmetric and symmetric stretching vibrations of $-CH_2$ groups, respectively.

Another new band that appeared at 1464 cm^{-1} was attributed to the bending vibrations of methyl group C-H in the ammonium groups.
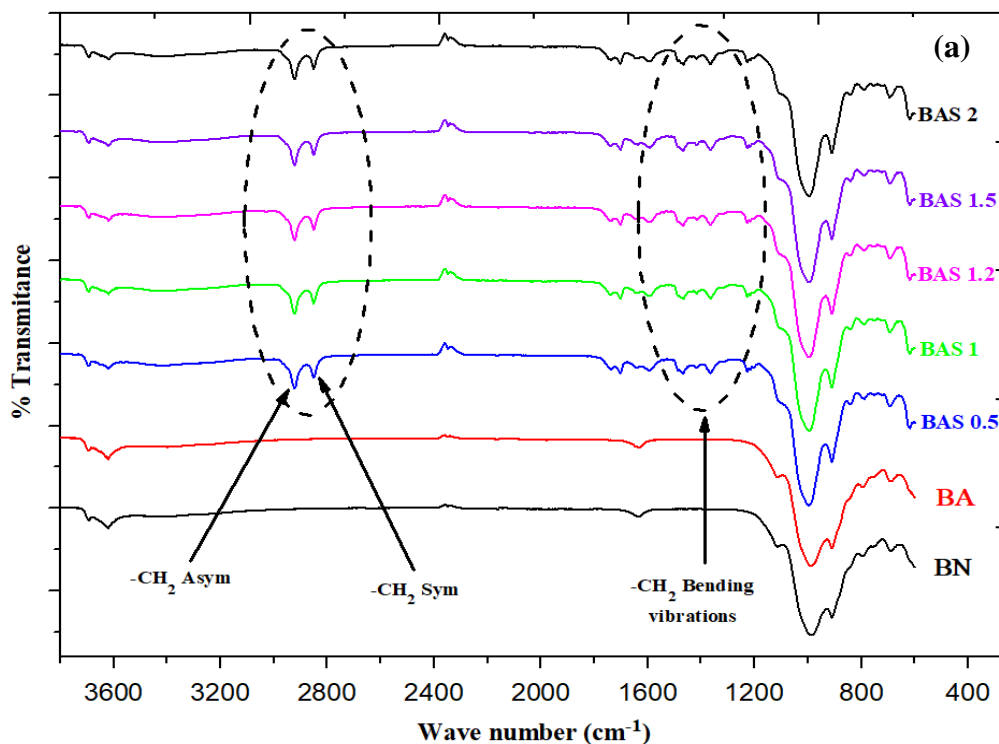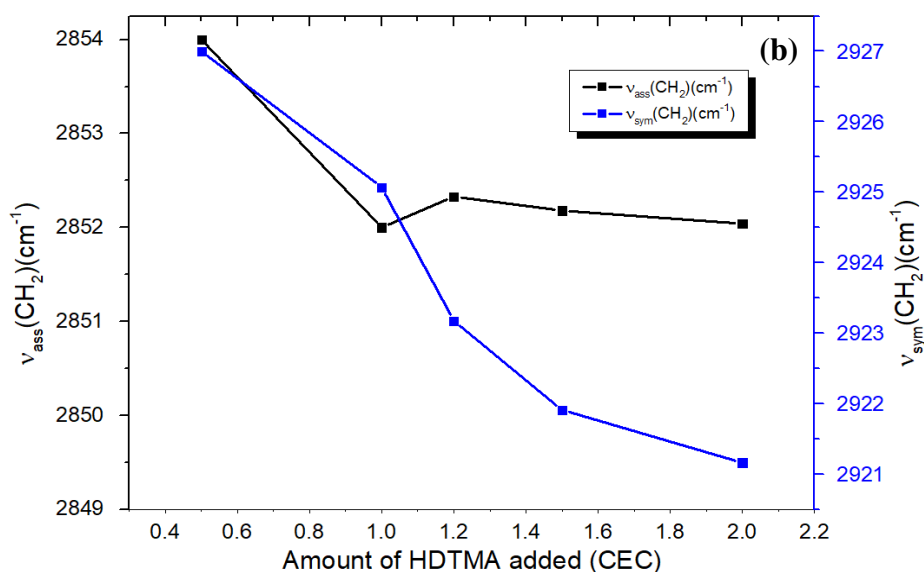
Figure 4. IR spectra of BN, BA and of BAS samples (a); Variation of vas(-CH₂-) and vs (-CH₂-) as a function of HDTMA loading (b).

When the surfactant loadings were increased, the peak intensity and peak area of the absorption bands at 2927 cm⁻¹ and 2854 cm⁻¹ for BAS samples became stronger and sharper, exhibiting a sudden initial increase in the incorporation of HDTMA molecules. By increasing the amount of HDTMA loading, these bands shifted towards lower frequencies (Figure. 4b), suggesting a transition from a disordered liquid-linke conformation of alkyl chains at low HDTMA loadings to a more ordered state at higher loadings where the modifier alkyl chains exhibited highly ordered all-trans conformations (Vaia et al., 1994).

2.3 Thermogravimetric Analysis

In order to investigate the structural properties of modified clays and to estimate the surfactant adsorbed onto sodium bentonite, some thermogravimetric analysis (TGA) experiments were conducted under a nitrogen atmosphere. The TGA and DTG results obtained, which are presented in Figures 5a and 5b, indicate that unmodified sodium bentonite (BA) exhibited a mass loss of 5.31 % at 64 °C, which corresponds to the loss of the interlayer water. A second mass loss of 5.26 %, between 170 °C and 800 °C, was related to the dehydration of the BA layers, including condensation of both the intralamellar Al(OH) and structural Al(OH) in clay (Xie et al., 2001). The TGA and DTG data of all BAS samples showed a similar degradation profile (Figure. 5a), indicating the presence of both surface bound and intercalated organic modifiers. However, for BAS 0.5 sample, only one peak at around 407 °C was observed, suggesting that, at low modifier loadings, intercalation occurs only within the BA interlayers. For BAS samples, the resulting thermograms suggested the occurrence of additional

weight losses within the temperature range between 170 and 460 °C. The corresponding degradations could not be observed in the thermogram of the BA sample.

These findings indicate that HDTMA surfactant molecules intercalated in the interlayer spaces are more thermally stable due to the barrier effect of clay sheets (Zhu et al., 2001). Note also that the DTG curves of surfactant-modified sodium bentonite samples (BAS 0.5, BAS 1, BAS 1.2, BAS 1.5 and BAS 2) presented four kinds of weight losses (Table 3). The first phase of degradation between 50 and 170 °C was attributed to the vaporization of free water. It is worth indicating that in this phase when the HDTMA loading goes up, these weight losses get smaller. Moreover, the presence of Alkylammonium leads to the conversion of hydrophilic surfaces to hydrophobic and organophilic ones. These findings confirm the hydrophilicity loss of BAS samples (Xi et al., 2010).
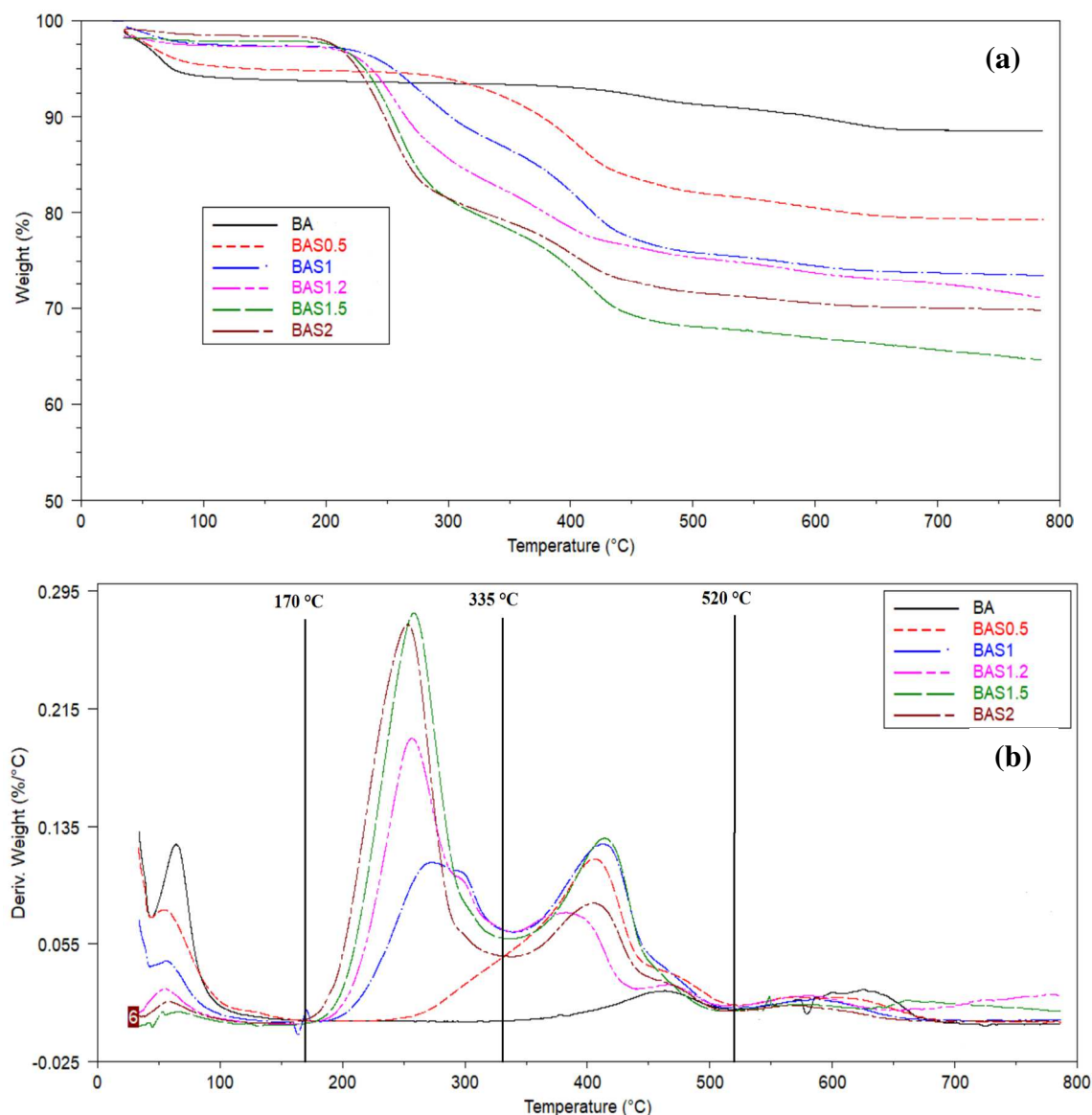
Figure 5. TGA (a) and DTG (b) thermograms of BA and BAS samples.

The second greatest mass loss, which was observed within the range from 170 and 335 °C, turned out to be more pronounced in BAS than in BA. Since pure HDTMA bromide decomposes at about 250 °C (Erdem et al., 2010), then the peak observed corresponds to the decomposition of some cationic surfactant molecules adsorbed on the external surface of clay. The third most important weight loss occurred between 335 and 520 °C; it is certainly due to the decomposition of cationic surfactants intercalated within the BA layers (Majdan et al., 2010). The last weight loss occurred between 520 and 800 °C; it corresponds to the dehydroxylation of the aluminosilicates (Xi et al., 2010).

Table 3. Summary of TGA analysis of BA and BAS samples, at different surfactant concentrations.

Samples	Dehydratation (water adsorbed by metal cations)	Adsorbed surfactant Decomposition	Intercalated surfactant Decomposition	Dehydroxylation	% Surfactant
	Before 170 °C % mass- loss	From [170 to 335 °C] % mass- loss	From [335 to 520°C] % mass- loss	After 520 °C % mass- loss	
BA	5.31	0.41	2.3	2.55	-
BAS 0.5	4.45	2.27 - 0.41 = 1.86	10.74 - 2.3 = 8.44	2.6	10.3
BAS 1	2.26	9.8 - 0.41 = 9.39	11.88 - 2.3 = 9.58	2.2	18.97
BAS 1.2	1.05	14.25-0.41 = 13.84	7.98 -2.3 = 5.68	4	19.52
BAS 1.5	**0.35**	**18.75 - 0.41 = 18.34**	**11.23 - 2.3 = 8.51**	**1.68**	**26.85**
BAS 2	0.78	18.68 -0.41 = 18.27	8.3 - 2.3 = 6.0	1.62	24.27

2.4 The point of zero charge (pH$_{ZPC}$)

pH$_{pzc}$ is the pH for which the net surface charge of the adsorbent is equal to zero. This is an important parameter in determining the adsorption capacity of the surface and the type of surface active centers. In the present work, the pH$_{ZPC}$ of the adsorbent (BA and BAS 1.5) was determined using a batch equilibrium method, following the procedures previously outlined by Monvisade et al. (Monvisade & Siriphannon, 2009).

For this, 100 ml of a solution of known initial pH (goes from 1 to 12 by adding HCL / NaOH) of KCl (0.1 mol / L) was mixed with 30 mg of the adsorbent (BAS) in conical flasks of 150 mL and stirred for 24 hours, then the final pH is measured and noted (pH$_f$). The difference between the initial and final pH (pH$_f$ - pH$_i$) was plotted against the initial pH (pH$_i$) and the point of intersection of the resulting curve with the pH$_i$ axis corresponds to pH$_{ZPC}$. The results are shown in the Figure 6.
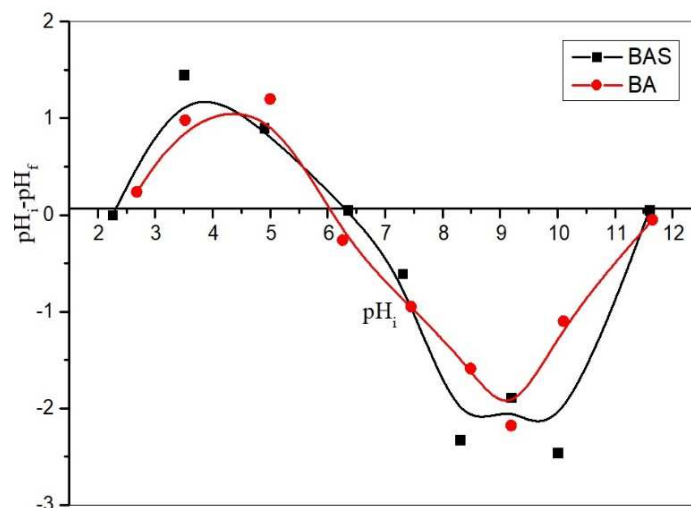
Figure 6. Determination of the pH of zero point of charge (pH$_{ZPC}$) for BA and BAS.

The pH of zero point charge (pH$_{ZPC}$) of Organobentonites was about 6.34. At pH values below and above the ZPC, the BAS composites exhibited a positive and negative charge, respectively. It was found that for a pH value of about 11, the BAS surface was less negative. Moreover, for a pH less than the PZC, BAS composites exhibited a net positive surface charge that was attributed to the presence of ammonium groups $N^+(CH_3)_3$.

2.5 Dyes Adsorption Studies

Before starting the adsorption studies, we had first chose the right adsorbent that gives good adsorption results with all three dyes. For this purpose, we tested all the previously prepared composites in a free pH medium at constant concentration (50mg/L), mass (25mg) and temperature (24°C ± 1°C) for 24 hours.

Table 4. The adsorption tests of the three dyes with the prepared composites

Samples	% of Adsorption Methylene Blue	% of Adsorption Telon Blue	% of Adsorption Bezathren Red
BA	97	3.5	0
BAS 0.5	97	14.2	6.4
BAS 1	97.7	42.1	34.5
BAS 1.2	98.1	86.5	64.1
BAS 1.5	**98**	**99.9**	**96.8**
BAS 2	88.1	98.3	98.1

Based on the results in Table 4 and taking into consideration the adsorption yield, the economic aspect. We have selected the adsorbent BAS 1.5 to carry out a complete adsorption study for the three dyestuffs (Methylene Blue, Telon Blue, and Bezathren Red).

a) Effect of pH

The pH of the aqueous solution is an important parameter in the adsorption process. It is important to identify the effect of pH on adsorption, as it helps to determine the optimized operational parameters and consequently establish the most appropriate adsorption mechanism. Adsorption experiments of three different dyes onto BAS 1.5 were carried out to examine the effect of pH (in a range from 2 to 11) on the removal efficiency of these three dyes from an aqueous solution. The results obtained are given in Figure 7.

It was found that the pH has no significant effect on the adsorption efficiency of methylene blue (BM). In addition, the absorption capacity at equilibrium (q_e) increased slightly (about 1 mg/g) as the pH value rose from 2 to 11. These results are in good agreement with those described in a previous study (Jourvand et al., 2015).
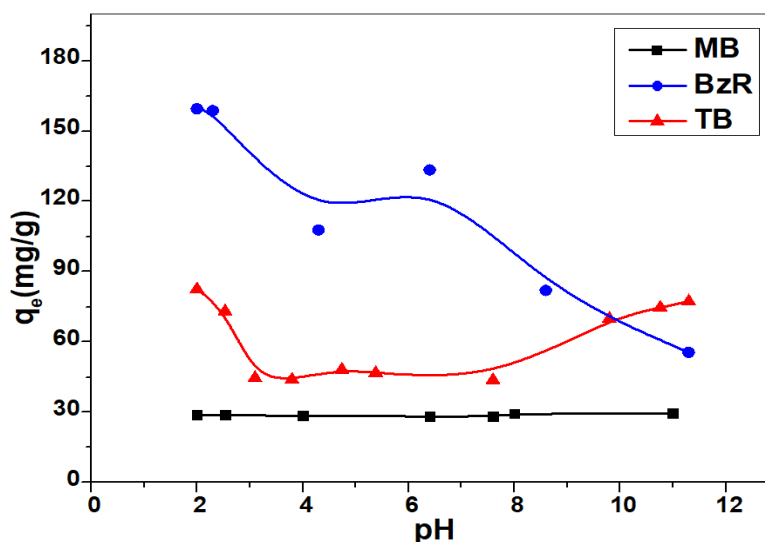
Figure 7. Effect of pH effect on the adsorption of dyes onto BAS 1.5 composite.

Moreover, non-ionic dyes, like BzR, are generally water-insoluble dyes which are generally encountered in the form of colloidal particles (Gupta & Suhas, 2009); they are slightly negatively charged in solution (Kim et al., 2004). The pH of zero point charge (pH$_{ZPC}$) of BAS 1.5 was about 6.34. At pH values below and above the ZPC, the Organobentonite exhibited a positive and negative charge, respectively. It was found that for a pH value of about 11, the BAS 1.5 surface was less negative. Moreover, for a pH less than the ZPC, BAS 1.5 composite exhibited a net positive surface charge that was attributed to the presence of ammonium groups $N^+(CH_3)_3$. For lower pH values, the removal efficiency was enhanced because of the electrostatic attraction between the negative charges of dye molecules and the positively charged surface of the adsorbent. Obviously, functional groups exhibited different degrees of ionization at different pH values. For pH values greater than the ZPC, the BAS surface charge tended to be negative. When the pH value rose from 2 to 11, the adsorption of Bezathren Red

(BzR) dropped. In this case, adsorption is favored by weak interactions such as Van der Waals interactions, hydrogen bonds and hydrophobic bonds.

However, Telon Blue (TB) dye exhibited a different adsorption behavior. It can clearly be observed on the representative curve that the adsorption capacity q_e reached two maximum values of 82.5 and 77.25 mg/g, corresponding to two pH values of 2 and 11, respectively. At pH = 2, protons were available, which engendered an increased electrostatic attraction between the negatively charged TB dye anions and the positively charged BAS 1.5 adsorption sites. The noted high adsorption capacity was certainly due to the strong electrostatic interaction between the ammonium cations of composite BAS 1.5 and the dye anions. It is important to note that the adsorption capacity decreased as the pH value augmented. Moreover, the positive charge on the composite decreased gradually and consequently the surface became negatively charged (Zohra et al., 2008). Note also that for pH values greater than 8, the adsorption capacity went up. It is worth mentioning that the surface charge of composite BAS 1.5 was less negative at pH =11, which favored the adsorption of anionic dye molecules, probably due to hydrophobic interactions.

b) Effect of Contact Time

The effect of contact time on the adsorption of MB, BzR, and TB dyes, at various time points, onto the composite BAS 1.5 were investigated using a fixed adsorbent dose of 25 mg. As shown in Figure 8, the adsorption of dyes onto the Organobentonite increased for longer contact time.
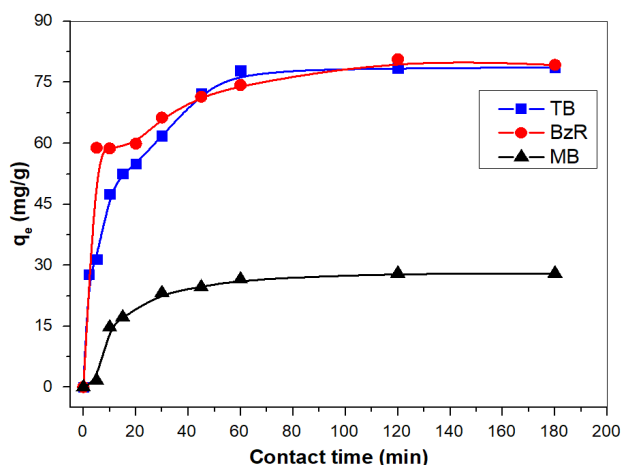
Figure 8. Effect of time on the adsorption of dyes onto BAS 1.5 composite.

The result obtained is consistent with those reported in previous studies (Bhatt et al., 2012; Rajabi et al., 2016). It is clearly noted that at the beginning, the adsorption rate of dyes was fast. After this rapid dye adsorption, the adsorbent surface became saturated and this adsorption rate dropped. The adsorption efficiency reached 80 % in less than 20 min. Saturation of the BAS 1.5 composite substrate was observed at 60 min, which suggests that the aggregation

of dye molecules took place around the BAS 1.5 particles. After 60 min, no significant increase in the adsorption efficiency was detected. Therefore, the contact time of 60 minutes was selected for all subsequent measurements.

➢ **Adsorption kinetic models**

A kinetic study was carried out with the pseudo-first order and pseudo-second order kinetic models for the purpose of studying the adsorption process of dyes onto BAS 1.5 composite. These models are represented by Equations (2) and (3).

$$\ln(q_e - q_t) = \ln q_e - k_1 t \qquad (2)$$

$$\frac{t}{q_t} = \frac{1}{k_2 q_e^2} + \frac{t}{q_e} \qquad (3)$$

Where q_e is the adsorption capacity at equilibrium (mg/g), q_t (mg/g) is the amount of dye adsorbed at time t; k_1 (min^{-1}) and k_2 (g mg^{-1}min^{-1}) are the pseudo-first and pseudo-second order rate constants, respectively.

The adsorption kinetic plots are shown in Figure. 9a and Figure. 9b. The kinetic parameters and correlation coefficient (R^2) of the two models are given in Table 5. Regarding the pseudo-first order model, it was noted that R^2 increased from 0.781 to 0.985, and the equilibrium capacity (q_e, cal), calculated by the equation of the model, was much smaller than the experimental value (q_e, exp) for both dyes MB and TB but not for BzR. Thereby, the pseudo-first order kinetic model was not suitable to model the sorption process of MB and TB dyes onto the BAS 1.5 composite. However, the pseudo-second order kinetic model described better the adsorption processes of MB and TB based on the correlation coefficient values which were found above 0.99 and greater than those of the pseudo-first order model, except for BzR (Table 5).

With regard to the adsorption of MB and BT dyes, the suggested mechanism involved valence forces through the exchange of electrons between dye molecules and BAS 1.5 composite (Orucoglu & Haciyakupoglu, 2015).

The adsorption mechanism of BzR which behaved as an anionic dye was probably due to the electrostatic attractions between the charged surface and charged dye molecules, considering the chemical characteristics of the surfactant-modified clay and dye molecules (Keyhanian et al., 2016; Muthukumaran et al., 2016).
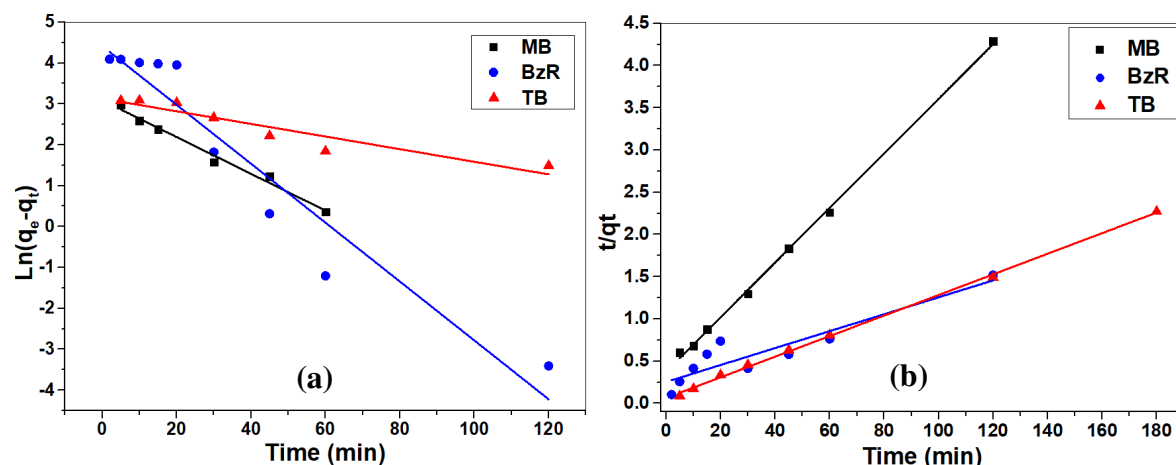
Figure 9. a) Pseudo-first-order kinetics model (a) and pseudo-second-order kinetics model (b) for the adsorption of different dyes on BAS 1.5 composite.

Table 5. Pseudo-first and Pseudo-second order kinetic parameters for the adsorption of dyes onto BAS 1.5 composite

Dye	q_e (exp) (mg.g^{-1})	Pseudo-first order			Pseudo-second order		
		k_1 (min^{-1})	q_e(cal) (mg.g^{-1})	R^2	k_2 (min^{-1})	q_e(cal) (mg.g^{-1})	R^2
BM	28	0.044	21.86	0.985	0.0034	31.25	0.998
BzR	79.73	0.072	82.59	0.923	0.00039	100	0.852
TB	80.64	0.015	22.78	0.781	0.00235	81.96	0.999

c) Effect of Adsorbent Dosage

The effect of the adsorbent dose on the adsorption of MB, TB and BzR dyes was studied by varying the amount of BAS 1.5 composite adsorbent. Figure.10 presents the adsorption of dyes by BAS 1.5 composite, at different adsorbent doses (10 -100 mg) for the dye solution volume of 40 mL, at dye concentrations of 20, 50 and 100 mg/L, for MB, TB, and BzR, respectively.
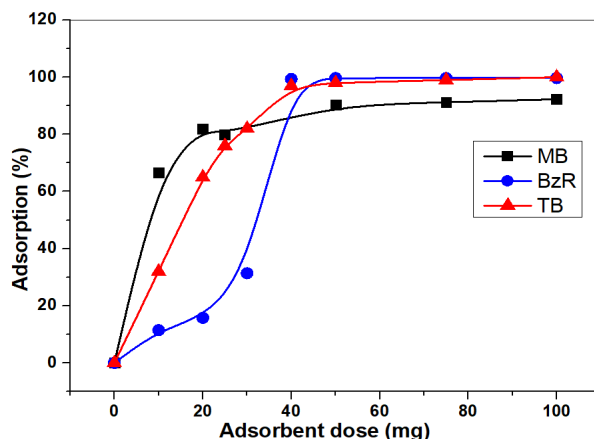
Figure 10. Effect of adsorbent dose on the adsorption of dyes onto BAS 1.5 composite.

The results presented in Figure.10 indicate clearly that the adsorption efficiency started increasing with the adsorbent dosage at the beginning, which suggests that a greater surface area and more adsorption sites were available. The optimal BAS composite adsorbent dose for the adsorption of TB and BzR dyes was found to be 40 mg; however, a better dose (25 mg) was needed for the adsorption of MB. Moreover, for m > 25 mg, no significant variation in the adsorption efficiency was observed for MB. Therefore, the dose of 25 mg of BAS 1.5 composite was selected for all subsequent measurements.

d) Adsorption Isotherm Studies

The adsorption isotherms were studied by mixing 25 mg of the composite with a series of MB, TB, and BzR solutions, at different initial concentrations (from 5 to 200 mg/L); the mixtures thus obtained were stirred for 60 min. Figure.11 indicates that at low equilibrium concentrations, the adsorption capacities increased quickly. Note that the values of q_e increased slowly when C_e was within the range [10 - 20 mg/L] for all the adsorption of all dyes. However, when C_e increased beyond 60 mg/L, the q_e values remained nearly unchanged. These findings suggest that the initial dye concentration is an important parameter in the adsorption process.
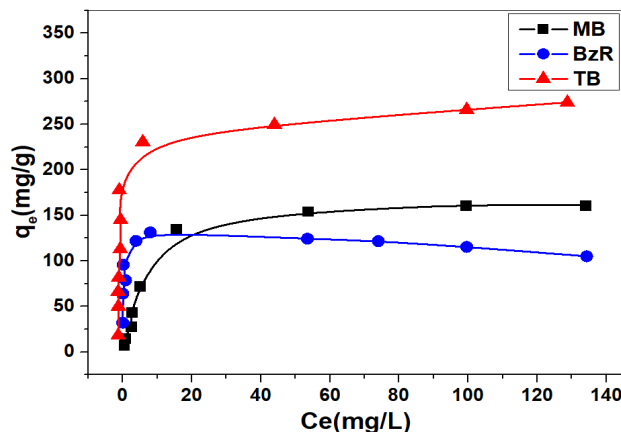
Figure. 11. Effect of initial dye concentration on the adsorption of dyes onto BAS 1.5 composite.

Langmuir and Freundlich isotherms are represented by Equations (4) and (5):

$$\frac{C_e}{q_e} = \frac{C_e}{q_{max}} + \frac{1}{q_{max}.\,K_L} \qquad (4)$$

$$\ln q_e = \ln K_F + \frac{1}{n}\ln C_e \qquad (5)$$

Where C_e is the equilibrium concentration of dye (mg/L), q_e is the amount of dye adsorbed on BAS 1.5 composite (mg/g), K_L is the Langmuir adsorption constant (L/mg), q_{max} is the maximum monolayer adsorption capacity of the adsorbent (mg/g), K_F is the Freundlich adsorption constant, which is related to the adsorption capacity, and n is the heterogeneity factor. The Langmuir and Freundlich adsorption isotherms for dyes adsorbed onto BAS 1.5 composite are presented in Figure 12. The isotherm parameters obtained from these models are summarized in Table 6. The equilibrium data obtained fit better to the Langmuir model than to the Freundlich model, as can be seen in Figure 12. This is indicative of the homogeneity of the adsorption sites on the BAS 1.5 composite particles. In addition, as clearly indicated in Table 6, all 1/n values are below 1, which is suggestive of a normal Langmuir isotherm. However, when the 1/n value is above unity, it is indicative of the cooperative adsorption (Jović-Jovičić et al., 2008). Moreover, when the values of 1/n are between 0.103 and 0.542, it means that there is a favorable adsorption (Hameed et al., 2007).
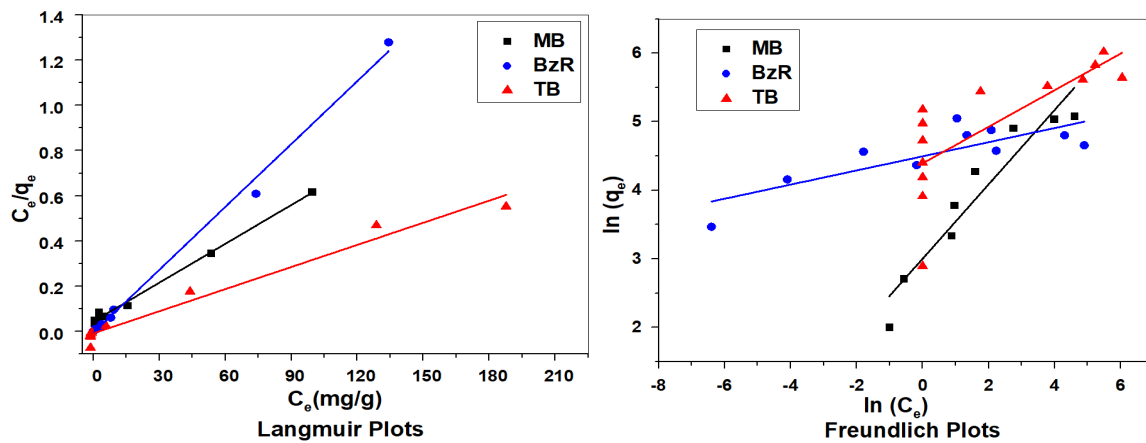
Figure. 12. Isotherm plots for the adsorption of dyes onto BAS1.5.

Table 6. Langmuir and Freundlich isotherm parameters for the adsorption of MB, TB and BzR dyes onto BAS1.5 composite

Dye	pH	Langmuir			Freundlich		
		K_L (L/mg)	q_m (mg.g^{-1})	R^2	K_F (L/g)	1/n	R^2
MB	6.4	0.130	174.52	0.997	20.122	0.542	0.895
TB	11	0.382	306.74	0.971	80.868	0.210	0.537
BzR	2.5	0.163	107.87	0.994	89.59	0.103	0.614

e) Thermodynamic Studies

The influence of temperature on the adsorption behavior of different dyes onto BAS 1.5 composite was also investigated under optimized conditions, at the temperatures of 298, 303, 313 and 323 K. A thermodynamic analysis was conducted to understand the characteristics and mechanisms of adsorption. The thermodynamic parameters $\Delta G°$, $\Delta H°$, and $\Delta S°$ were calculated using Equations (6), (7) and (8).

$$K_d = q_e/C_e \tag{6}$$

$$\Delta G° = -RT \ln K_d \tag{7}$$

$$\ln K_d = \frac{\Delta S^0}{R} - \frac{\Delta H^0}{RT} \tag{8}$$

Where K_d is the distribution coefficient (L/g), T is the temperature (K), and R is the gas constant (8.314 J/mol K). The enthalpy change ($\Delta H°$/ kJ.mol^{-1}) and the entropy change ($\Delta S°$/ J.mol^{-1}.K^{-1}) were computed from the slope and intercept of the linear plot of ln K_d versus 1/T, as presented in Figure 13.
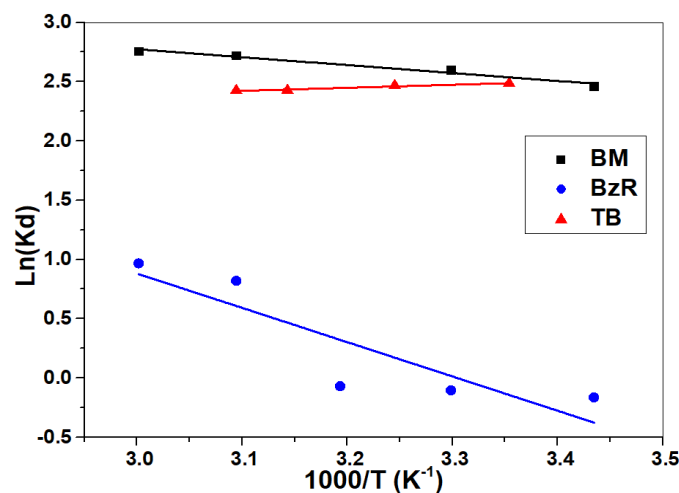
Figure 13. The Van't Hoff plots for the adsorption of dyes onto BAS1.5 composite.

The previously calculated thermodynamic parameters $\Delta G°$, $\Delta H°$, and $\Delta S°$ are summarized in Table 7. Generally, the absolute magnitude of free energy change for physisorption is between -20 and 0 kJ.mol^{-1} (Yu et al., 2001).

The results relating to the adsorption process of BM, BT and BzR dyes, at 298, 303, 313, 323 K, show that the free energy values were negative, which is indicative of a spontaneous and favorable adsorption process onto BAS 1.5 composite, except for BzR at 298 K, where the $\Delta G°$ value was positive, suggesting that the adsorption was non-spontaneous and less favorable at that temperature. It is worth recalling that positive values of $\Delta H°$ imply an endothermic reaction. The positive values of $\Delta S°$ indicated an increase in entropy and the solid-liquid interface became more random during the adsorption process of dyes.

Table 7. Thermodynamic parameters for the adsorption process of dyes onto BAS1.5 composite at various temperatures

Dye	$\Delta H°$ (kJ.mol^{-1})	$\Delta S°$ (J.mol^{-1}.K^{-1})	$\Delta G°$ (kJ.mol^{-1})			
			298 K	303 K	313 K	323 K
MB	12.11	58.6	-5.36	-5.65	-6.24	-6.83
TB	2.09	13.64	-1.98	-2.04	-2.18	-2.32
BzR	24.04	79.46	0.36	-0.048	-0.84	-1.64

2.6 Proposed adsorption mechanism

The composite under study consists of bentonite clay and surfactant. According to previous literatures (Errais et al., 2012; Mahmoodi et al., 2019), and based on the composite structure, the hydrophilic adsorption occurs between the composite and different dyes, as shown in Figure 14. It is worth mentioning that the quaternary ammonium cationic surfactant turns the composite hydrophilic. It is widely acknowledged that cationic surfactants can produce strong electrostatic adsorption of anionic dyes. This process leads to ultrahigh adsorption capacities of the composite for BzR and TB molecules. Moreover, hydrogen bonding may occur between the oxygen silanol groups of bentonite and both of nitrogen and oxygen atoms of dyes. Therefore, the excellent adsorption properties of BAS composite can be attributed to the synergistic effect of hydrogen bonding as well as to the electrostatic interactions between the adsorbent and MB, TB and BzR dyes.

Adsorption of Telon Blue, Bezathren Red, and Methylene Blue.
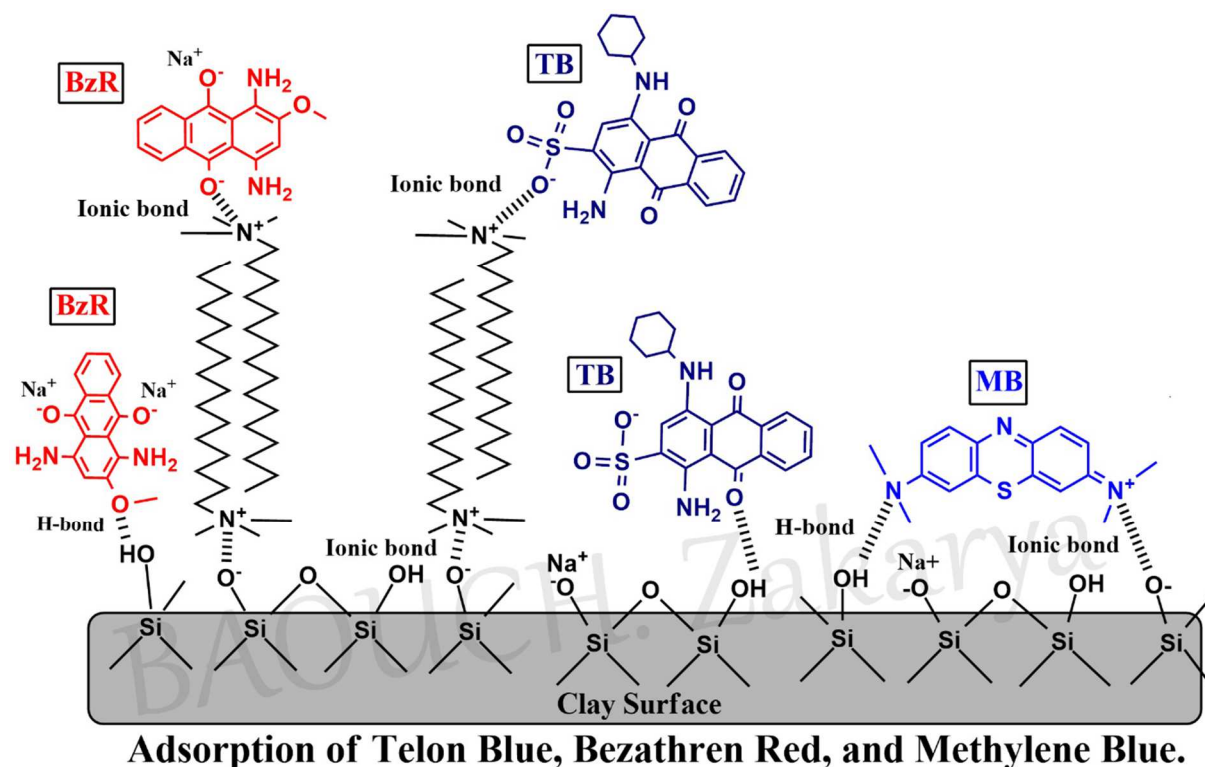
Figure 14. Proposed mechanism for the adsorption of Telon Blue, Bezathren Red and Methylene Blue onto BAS1.5 composite.

2.7 Explanation and Comparisons

You might be wondering why we didn't use the raw material as adsorbent (purified bentonite), I would like to tell you that at any pH and for Telon Blue (TB) and Bezathrene Red (BzR) the adsorption capacity is zero, and for Methylene Blue is equal to 74 mg/g but the separation of the supernatant from the adsorbent requires centrifugation which is not practical on an industrial scale (figure. 15).
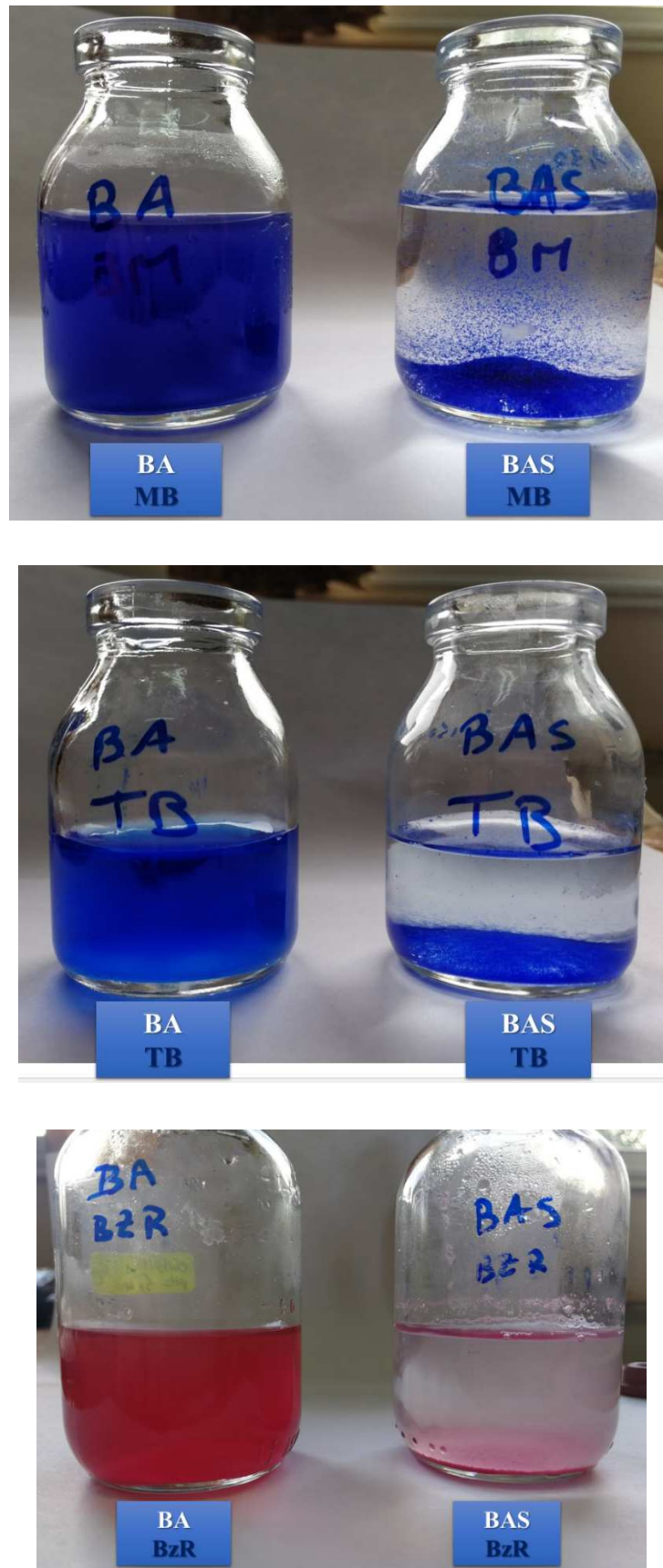
Figure. 15. The natural dyes decantation after adsorption onto BA and BAS.

In conclusion, the adsorption capacity of BM, BzR and TB dyes at 298K obtained in this study is compared with those determined by other authors (Auta & Hameed, 2013; Belbachir & Makhoukhi, 2017; Torabinejad et al., 2017; Zhou et al., 2014). These results are given in Table 8.

Table 8. Comparison of the maximum adsorption capacities for BM, BzR and TB adsorption on BAS 1.5 with those of other adsorbents

Dyes	Adsorbent	Maximum adsorption capacity (mg/g)	Ref
MB	Montmorillonite	74	(Yu et al., 2001)
	Acid modified clay beads	223.19	(Zhou et al., 2014)
	BAS 1.5	**174.52**	**Present study**
TB	Mesoporous silicate/polypyrrole	55.55	(Auta & Hameed, 2013)
	BAS 1.5	**306.74**	**Present study**
BzR	Sodic Montmorillonite	48.52	(Belbachir & Makhoukhi, 2017)
	BAS 1.5	**107.87**	**Present study**

REFERENCES

Auta, M., & Hameed, B. H. (2013). Acid modified local clay beads as effective low-cost adsorbent for dynamic adsorption of methylene blue. *Journal of Industrial and Engineering Chemistry*, *19*(4), 1153–1161. https://doi.org/10.1016/j.jiec.2012.12.012

Belbachir, I., & Makhoukhi, B. (2017). Adsorption of Bezathren dyes onto sodic bentonite from aqueous solutions. *Journal of the Taiwan Institute of Chemical Engineers*, *75*, 105–111. https://doi.org/10.1016/j.jtice.2016.09.042

Bhatt, A. S., Sakaria, P. L., Vasudevan, M., Pawar, R. R., Sudheesh, N., Bajaj, H. C., & Mody, H. M. (2012). Adsorption of an anionic dye from aqueous medium by organoclays: Equilibrium modeling, kinetic and thermodynamic exploration. *RSC Advances*, *2*(23), 8663–8671. https://doi.org/10.1039/c2ra20347b

Binaeian, E., Seghatoleslami, N., & Chaichi, M. J. (2016). Synthesis of oak gall tannin-immobilized hexagonal mesoporous silicate (OGT-HMS) as a new super adsorbent for the removal of anionic dye from aqueous solution. *Desalination and Water Treatment*, *57*(18), 8420–8436. https://doi.org/10.1080/19443994.2015.1020513

Darder, M., Colilla, M., & Ruiz-Hitzky, E. (2003). Biopolymer-clay nanocomposites based on chitosan intercalated in montmorillonite. *Chemistry of Materials*, *15*(20), 3774–3780. https://doi.org/10.1021/cm0343047

Erdem, B., Özcan, A. S., & Özcan, A. (2010). Preparation of HDTMA-bentonite: Characterization studies and its adsorption behavior toward dibenzofuran. *Surface and Interface Analysis*, *42*(6–7), 1351–1356. https://doi.org/10.1002/sia.3230

Errais, E., Duplay, J., Elhabiri, M., Khodja, M., Ocampo, R., Baltenweck-Guyot, R., & Darragi, F. (2012). Anionic RR120 dye adsorption onto raw clay: Surface properties and adsorption mechanism. *Colloids and Surfaces A: Physicochemical and Engineering Aspects*, *403*, 69–78. https://doi.org/10.1016/j.colsurfa.2012.03.057

Gupta, V. K., & Suhas. (2009). Application of low-cost adsorbents for dye removal - A review. *Journal of Environmental Management*, *90*(8), 2313–2342. https://doi.org/10.1016/j.jenvman.2008.11.017

Hameed, B. H., Din, A. T. M., & Ahmad, A. L. (2007). Adsorption of methylene blue onto

bamboo-based activated carbon: Kinetics and equilibrium studies. *Journal of Hazardous Materials*, *141*(3), 819–825. https://doi.org/10.1016/j.jhazmat.2006.07.049

Huang, P., Kazlauciunas, A., Menzel, R., & Lin, L. (2017). Determining the Mechanism and Efficiency of Industrial Dye Adsorption through Facile Structural Control of Organo-montmorillonite Adsorbents. *ACS Applied Materials and Interfaces*, *9*(31), 26383–26391. https://doi.org/10.1021/acsami.7b08406

Jourvand, M., Shams Khorramabadi, G., Omidi Khaniabadi, Y., Godini, H., & Nourmoradi, H. (2015). Removal of methylene blue from aqueous solutions using modified clay. *Journal of Basic Research in Medical Sciences*, *2*(1), 32–41. http://jbrms.medilam.ac.ir/article-1-120-en.html

Jović-Jovičić, N., Milutinović-Nikolić, A., Gržetic, I., & Jovanović, D. (2008). Organobentonite as efficient textile dye sorbent. *Chemical Engineering and Technology*, *31*(4), 567–574. https://doi.org/10.1002/ceat.200700421

Keyhanian, F., Shariati, S., Faraji, M., & Hesabi, M. (2016). Magnetite nanoparticles with surface modification for removal of methyl violet from aqueous solutions. *Arabian Journal of Chemistry*, *9*, S348–S354. https://doi.org/10.1016/j.arabjc.2011.04.012

Kim, T. H., Park, C., Shin, E. B., & Kim, S. (2004). Decolorization of disperse and reactive dye solutions using ferric chloride. *Desalination*, *161*(1), 49–58. https://doi.org/10.1016/S0011-9164(04)90039-2

Mahmoodi, N. M., Abdi, J., Taghizadeh, M., Taghizadeh, A., Hayati, B., Shekarchi, A. A., & Vossoughi, M. (2019). Activated carbon/metal-organic framework nanocomposite: Preparation and photocatalytic dye degradation mathematical modeling from wastewater by least squares support vector machine. *Journal of Environmental Management*, *233*(August 2018), 660–672. https://doi.org/10.1016/j.jenvman.2018.12.026

Majdan, M., Pikus, S., Gajowiak, A., Sternik, D., & Zieba, E. (2010). Uranium sorption on bentonite modified by octadecyltrimethylammonium bromide. *Journal of Hazardous Materials*, *184*(1–3), 662–670. https://doi.org/10.1016/j.jhazmat.2010.08.089

Makhoukhi, B., Djab, M., & Amine Didi, M. (2015). Adsorption of Telon dyes onto bis-imidazolium modified bentonite in aqueous solutions. *Journal of Environmental Chemical*

Engineering, *3*(2), 1384–1392. https://doi.org/10.1016/j.jece.2014.12.012

Monvisade, P., & Siriphannon, P. (2009). Chitosan intercalated montmorillonite: Preparation, characterization and cationic dye adsorption. *Applied Clay Science*, *42*(3–4), 427–431. https://doi.org/10.1016/j.clay.2008.04.013

Muthukumaran, C., Sivakumar, V. M., & Thirumarimurugan, M. (2016). Adsorption isotherms and kinetic studies of crystal violet dye removal from aqueous solution using surfactant modified magnetic nanoadsorbent. *Journal of the Taiwan Institute of Chemical Engineers*, *63*, 354–362. https://doi.org/10.1016/j.jtice.2016.03.034

Orucoglu, E., & Haciyakupoglu, S. (2015). Bentonite modification with hexadecylpyridinium and aluminum polyoxy cations and its effectiveness in Se(IV) removal. *Journal of Environmental Management*, *160*, 30–38. https://doi.org/10.1016/j.jenvman.2015.06.005

Parolo, M. E., Pettinari, G. R., Musso, T. B., Sánchez-Izquierdo, M. P., & Fernández, L. G. (2014). Characterization of organo-modified bentonite sorbents: The effect of modification conditions on adsorption performance. *Applied Surface Science*, *320*, 356–363. https://doi.org/10.1016/j.apsusc.2014.09.105

Rajabi, M., Mirza, B., Mahanpoor, K., Mirjalili, M., Najafi, F., Moradi, O., Sadegh, H., Shahryari-ghoshekandi, R., Asif, M., Tyagi, I., Agarwal, S., & Gupta, V. K. (2016). Adsorption of malachite green from aqueous solution by carboxylate group functionalized multi-walled carbon nanotubes: Determination of equilibrium and kinetics parameters. *Journal of Industrial and Engineering Chemistry*, *34*, 130–138. https://doi.org/10.1016/j.jiec.2015.11.001

Torabinejad, A., Nasirizadeh, N., Yazdanshenas, M. E., & Tayebi, H.-A. (2017). Synthesis of conductive polymer-coated mesoporous MCM-41 for textile dye removal from aqueous media. *Journal of Nanostructure in Chemistry*, *7*(3), 217–229. https://doi.org/10.1007/s40097-017-0232-7

Vaia, R. A., Teukolsky, R. K., & Giannelis, E. P. (1994). Interlayer Structure and Molecular Environment of Alkylammonium Layered Silicates. *Chemistry of Materials*, *6*(7), 1017–1022. https://doi.org/10.1021/cm00043a025

Xi, Y., Mallavarapu, M., & Naidu, R. (2010). Preparation, characterization of surfactants

modified clay minerals and nitrate adsorption. *Applied Clay Science*, *48*(1–2), 92–96. https://doi.org/10.1016/j.clay.2009.11.047

Xie, W., Gao, Z., Pan, W. P., Hunter, D., Singh, A., & Vaia, R. (2001). Thermal degradation chemistry of alkyl quaternary ammonium Montmorillonite. *Chemistry of Materials*, *13*(9), 2979–2990. https://doi.org/10.1021/cm010305s

Yu, Y., Zhuang, Y. Y., & Wang, Z. H. (2001). Adsorption of water-soluble dye onto functionalized resin. *Journal of Colloid and Interface Science*, *242*(2), 288–293. https://doi.org/10.1006/jcis.2001.7780

Zhou, K., Zhang, Q., Wang, B., Liu, J., Wen, P., Gui, Z., & Hu, Y. (2014). The integrated utilization of typical clays in removal of organic dyes and polymer nanocomposites. *Journal of Cleaner Production*, *81*, 281–289. https://doi.org/10.1016/j.jclepro.2014.06.038

Zhu, J., Morgan, A. B., Lamelas, F. J., & Wilkie, C. A. (2001). Fire properties of polystyrene-clay nanocomposites. *Chemistry of Materials*, *13*(10), 3774–3780. https://doi.org/10.1021/cm000984r

Zohra, B., Aicha, K., Fatima, S., Nourredine, B., & Zoubir, D. (2008). Adsorption of Direct Red 2 on bentonite modified by cetyltrimethylammonium bromide. *Chemical Engineering Journal*, *136*(2–3), 295–305. https://doi.org/10.1016/j.cej.2007.03.086

CHAPTER III

PART II.

INTRODUCTION

In this part, a simple method was employed for intercalation of Carboxymethyl Cellulose (CMC) into the Organobentonite (BAS), for this, a series of BAS/CMC nanocomposites with different percentage of Carboxymethyl Cellulose was synthesized under different conditions. The composites was characterized by the Fourier transform infrared (FT-IR) spectrophotometer, X-ray diffraction (XRD) method, and thermal gravimetric (TG) analysis. The effects of different reaction conditions on the intercalation of the CMC in the Organobentonite sheets was investigated by controlling the amount of Hexadecyl trimethyl ammonium bromide (HDTMA) in the Bentonite (BA) and the weight ratios of CMC added to the organic bentonite (BAS). The obtained materials (BAS/CMC) are then used as adsorbents to remove three types of dyes namely Methylene Blue (cationic dye), Telon Blue (anionic dye), and Bezathren Red (nonionic dye), from aqueous solutions. The equilibrium data obtained were then assessed using various adsorption isotherm models. Some kinetic studies were also conducted in order to evaluate the adsorption mechanism.

PART II

ORGANO-BENTONITE/CARBOXYMETHYL CELLULOSE

(BAS/CMC)

1. EXPERIMENT METHOD

1.1 Materials

a) Carboxymethyl Cellulose (CMC)

CMC is an anionic, water-soluble cellulose derivative obtained by introducing –CH$_2$COOH groups into cellulose molecular chain (Figure.1). (Chakraborty et al., 2006).
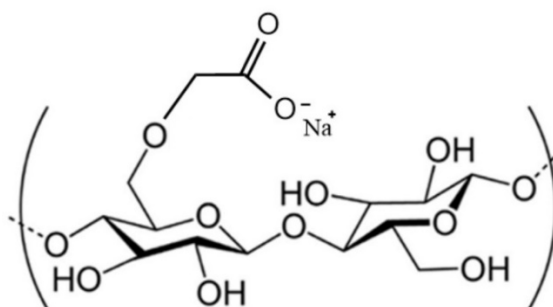
Figure. 1. Idealized unite structure of Carboxymethyl Cellulose (DS 1.0).

✓ **Information on the CMC used in this study**

The Carboxymethyl Cellulose Sodium salt used in our study was purchased from Prolabo and used as received.

Some important specific characteristics of this powder are as follows:

CAS No.	9004-32-4
pH value, 1% aqueous solution	6.5-8.5
Loss on drying	8.0 % Max
Sodium content	6.5-9.5 %
Degree of substitution DS	0.82-0.95
Viscosity, Brookfield LVT, SP 4; 30 RPM	3000-4000 cps

b) Bentonite samples:

The starting material used in this study was OranoBentonite (BAS) synthesized according to the same method mentioned in part I. The obtained composites BAS/CMC were also characterized using the same instruments mentioned in Part I.

c) Preparation of CMC/BAS Composites

Aliquots (0.5 g) of various samples of BAS (0.5, 1, 1.2, 1.5, and 2.0 CEC) was dispersed into 50 mL of distilled water for 1 hours. In parallel, different amounts of CMC equal to (0.025, 0.05, 0.125, 0, 25, and 0.5) g were dissolved in 50mL of distilled water at 60 ° C. Then, the CMC solution was added drop-by-drop and shaken using a mechanical shaker for 4 hours at 80 °C to obtain the nanocomposites.

✓ **In the first step**, the nanocomposites was synthesized by fixing the organophilic of BAS in 1.5 CEC and changing the weight ratios of CMC/BAS to be (0.025/0.5, 0.05/0.5, 0.125/0.5, 0.25/0.5, and 0.5/0.5).

✓ **In the second step**, we have fixed the weight of both CMC and BAS in 0.5g and we changed the organophilic inside Bentonite (0.5, 1, 1.2, 1.5, and 2.0 CEC).

The formed composites were centrifuged at 4000 rpm for 30 min and washed several times with warm distilled water until the pH value of the supernatant reached 7.0. The obtained solid was then dried at 105 °C for 12 h, ground and sifted with a 100-mesh sieve.

d) Batch adsorption studies:

The adsorption capacities of the prepared composites (BAS/CMC) for MB, TB and BzR dyes were evaluated using the same batch equilibrium procedure mentioned in Part I. The adsorption capacity and removal efficiency of the prepared composite were calculated based on the initial and final concentrations of dyes present in the solution, using the following Equation. (1):

$$q_e = \frac{(C_0 - C_e).V}{m} \qquad (1)$$

where C_0 and C_e are the initial and equilibrium dye concentrations, respectively, V is the volume of dye aqueous solution (L) and m is the mass of adsorbent (g).

2. RESULTS AND DISCUSSION

2.1 X-Ray Diffraction

XRD is an effective method for the investigation of the intercalation existence of Bentonite. The XRD patterns of BA, BAS, and BAS/CMC nanocomposite are shown in Figure. 2 and 3. The d-spacing of the inter-gallery spacing was determined using Bragg's law, $n\lambda = 2d \sin\theta$; where n is an integer, λ the wavelength, and θ the scattering angle.

The first step: The nanocomposites was synthesized by fixing the type of BAS in 1.5 CEC and changing the weight ratios of CMC/BAS to be (0.025/0.5, 0.05/0.5, 0.125/0.5, 0.25/0.5, and 0.5/0.5). The XRD patterns and variation of the interlayer space are shown in Figure.2 and Table. 1.
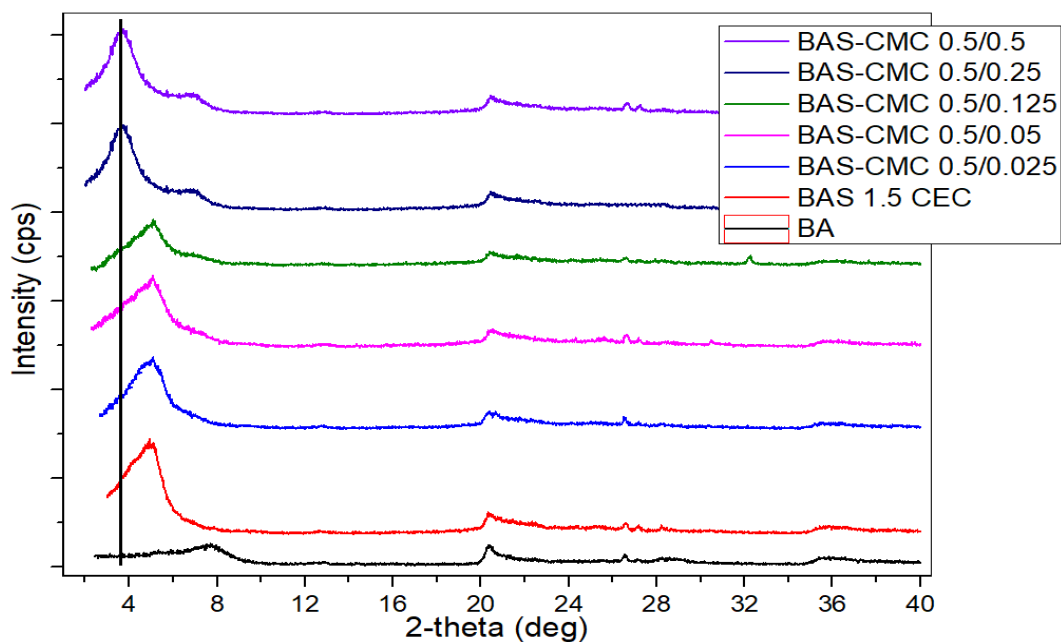
Figure. 2. XRD patterns of BA, BAS 1.5, and BAS 1.5/CMC samples at different amounts of CMC

The following table summarizes the variation of the interlamellar distance as a function of the amounts of CMC added in comparison with BA and BAS where there is no CMC.

Table 1. Variation of interfoliar distance as a function of the amount of CMC added

Composite	d_{001} (Å)	Δd (Å)
BA	11.37	-
BAS 1.5	**17.86**	**-**
BAS/CMC, 0.5/0.025	17.30	0.56
BAS/CMC, 0.5/0.05	17.34	0.52
BAS/CMC, 0.5/0.125	17.37	0.49
BAS/CMC, 0.5/0.25	**25.18**	**7.32**
BAS/CMC, 0.5/0.5	**24.11**	**6.25**

According to Bragg's law, it can be noted that the Organobentonite (BAS) shows a typical diffraction peak at $2\theta = 7.76°$, corresponding to a basal spacing of 17.86 Å (the interlayer distance of BA is 11.37 Å). Upon the addition of CMC from 0.025 to 0.125g, the d_{001} peak positions had not changed to lower angles which means that the CMC chains had not intercalated yet in the BAS sheets and they are still on the surface of bentonite.

The increase in the quantity of CMC from 0.25 to 0.5, generate a decrease in the value of 2θ from 7.76 ° to 3.65 ° which is reflected by an increase in the interlamellar distance d_{001} from 11. 37 Å to 25.18 Å. This increase in the d spacing confirms the intercalation of the CMC molecules in the BAS sheets.

The variation of the interlayer distance (Δd) of the obtained nanocomposites was estimated to be about 7.32 and 6.25 Å for BAS/CMC, 0.5/0.25 and BAS/CMC, 0.5/0.5 nanocomposites, respectively. Considering the size of glucose ring in cellulose crystal (5 Å) (Meyer & Misch, 1937), and comparing the obtained results with the BAS, we can conclude that the CMC molecules are successfully intercalated and the interlayer gallery could be considered in this case as a monolayer arrangement in BAS sheets.

The second step: The nanocomposites in this case was synthesized by fixing the weight of both CMC and BAS at 0.5 g and changing the organophilic inside BAS to be, (0.5, 1, 1.2, 1.5, 2 CEC). The XRD patterns and variation of the interlayer space d_{001} are shown in Figure.3 and Table. 2.
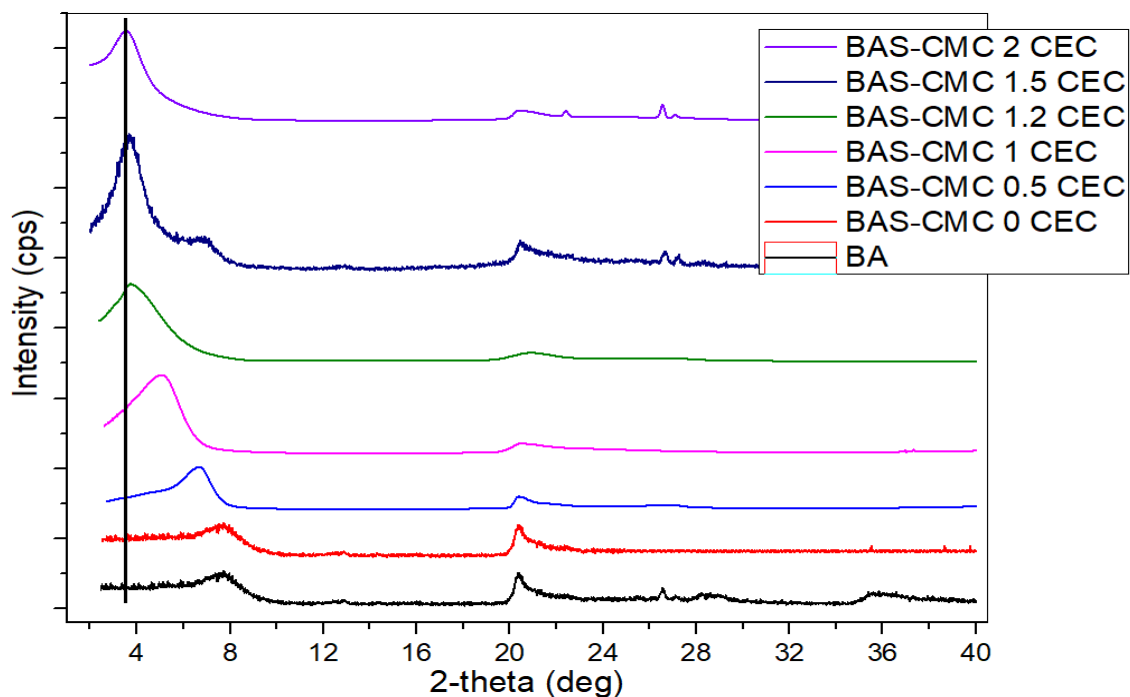
Figure 3. XRD diffractograms of BA and BAS / CMC samples in different organophilic percentages.

The interlayer spacing, $d_{(001)}$, of the different patterns are summarized in the following table.

Table 2. Variation of interfoliar distance as a function of the organophilic of bentonite.

Composite	d_{001} (Å)	Composite	d_{001} (Å)	Δd (Å)
BA	11.37	BA/CMC 0 CEC	11.86	+ 0.46
BAS 0.5	13.41	BAS/CMC 0.5 CEC	13.25	- 0.16
BAS 1	17.58	BAS/CMC 1 CEC	17.44	- 0.14
BAS 1.2	17.58	BAS/CMC 1.2 CEC	23.59	+ 6.01
BAS 1.5	17.86	**BAS/CMC 1.5 CEC**	**24.85**	**+ 7.00**
BAS 2	17.51	BAS/CMC 2 CEC	24.11	+ 6.6

From Table 2, we notice that the interlayer spacing increases with the increasing of the organophilic (HDTMA inside the bentonite) from **11.86** Å to **24.85** Å.

105

From a Non-Organopilic bentonite (BAS/CMC 0 CEC) to an organophilic bentonite with a loadings of HDTMA equal to 1 CEC (BAS/CMC 1 CEC), the position of the interlayer distance peaks d_{001} remained almost constant. This could be explained by the insufficiency of the HDTMA molecules inside bentonite (low organophilic) to intercalate the CMC rings within its sheets. However, with a greater HDTMA loadings (from 1.2 to 2 CEC), we notice a jump in the interlayer distance from **17.86** to **24.85** Å with a gap Δd of + 7 Å between (BAS 1.5) and (BAS/CMC 1.5 CEC). The position of the peaks remained almost constant with a variation of the interlayer distance (Δd) around 6 Å. These results suggest that there were a saturation limit for the intercalation of the CMC molecules inside the BAS, and considering the size of glucose ring in cellulose crystal (5 Å) (Meyer & Misch, 1937), we can say that the CMC molecules are successfully intercalated and the interlayer gallery could be considered in this case as a monolayer arrangement in BAS sheets.

The reason why CMC chains cannot adopt a multilayer arrangement in BAS sheets can be explained by the presence of the $-CH_2COO^-$ groups in cellulosic backbones causing a loss of the possibility of parallel association of CMC chains in sheet-like structures due to both a steric hindrance and electrostatic repulsion. (Meyer & Misch, 1937)

2.2 Infrared Spectroscopy

The FTIR spectra of BA, BAS, and BAS/CMC samples in the wavenumber range of 4000-500 cm^{-1} were shown in Figure. 4. to obtain clear information about their chemical structures.

The spectrum of bentonite (BA) exhibited absorption bands at 3400 and 1640 cm^{-1} this was assigned to the stretching and bending vibrations of the OH groups for the water molecules adsorbed on bentonite surface, and a band at 3620 cm^{-1} which represented the stretching vibration of the hydroxyl groups coordinated to octahedral Al^{3+} cations (Sdiri et al., 2011). The bentonite spectrum also contained a band between 695 and 794 cm^{-1} which were attributed to Feldspar and Quartz respectively (Sdiri et al., 2011). The intensive band at 1000 cm^{-1} was assigned to the Si-O stretching vibration, whereas the bands around 622 and 694 cm^{-1} were ascribed to Si-O-Al (where Al was the octahedral cation) and Si-O-Si bending vibrations, respectively.

The spectrum of Organobentonite (BAS) showed additional absorption bands, at 2927 cm^{-1} and 2854 cm^{-1}, which are assigned to the asymmetric and symmetric stretching vibrations of -CH₂ groups, respectively. In addition, another new band that appeared at 1464 cm^{-1} was attributed to the bending vibrations of methyl group C-H in the ammonium groups.
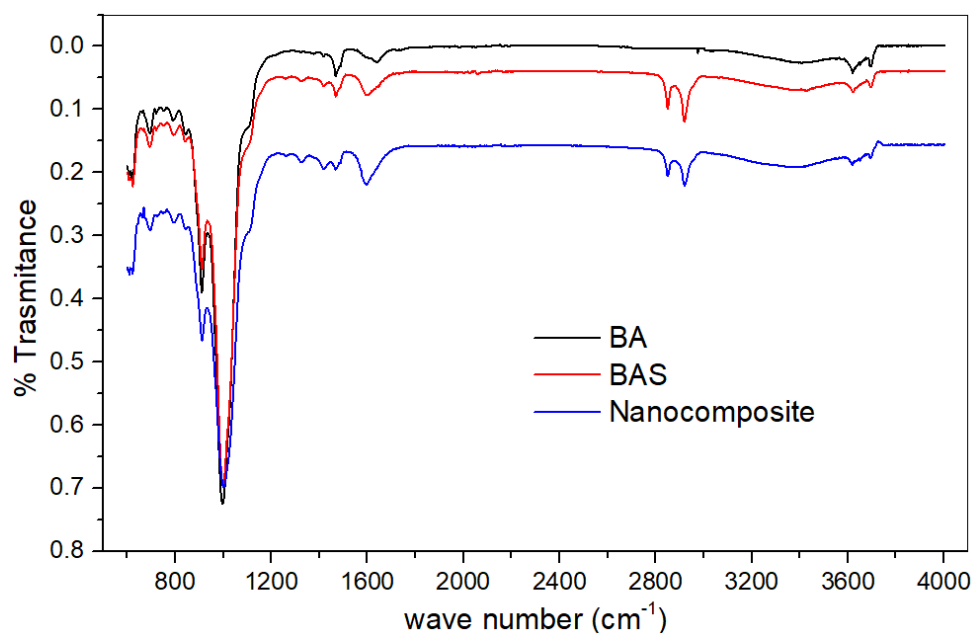
Figure. 4. IR spectra of BA, BAS, and BAS/CMC samples.

The FTIR spectra of BAS/CMC exhibited the broad band centred at 3400 cm^{-1}, attributed to the stretching of –OH groups and intermolecular and intramolecular hydrogen bonds. In addition, the peak about C–H stretching associated with the ring methane hydrogen atoms appeared at 2913 cm^{-1}. Moreover, the peaks at 1420 and 1602 cm^{-1} were related to the symmetric and asymmetric stretching vibrations of the carboxylate groups. The absorption bands between 1000 and 1200 cm^{-1} were ascribed to characteristic of the –C–O– stretching on polysaccharide skeleton (Luna-Martínez et al., 2011; Wu et al., 2011).

2.3 Thermogravimetric Analysis

In order to investigate the structural properties of the prepared BAS/CMC composites and to estimate the surfactant and CMC adsorbed and/or absorbed onto bentonite (BA), some thermogravimetric analysis (TGA) experiments were conducted under Nitrogen atmosphere. The TGA and DTG results obtained, which are presented in Figures 5 and 6.

For CMC, a four-step degradation behavior is observed in the range [50 - 800 °C]. The first weight loss below 200 °C is attributed to the evaporation of adsorbed moister. The second weight loss from 200 to 600 C, with a maximum degradation peak at 292 °C followed by a smooth degradation (third step), is attributed to decarboxylation and decomposition of CMC and formation of carbonaceous char. The final weight loss (above 600°C) is related to the rapid volatilization and oxidation of char and formation of Na_2CO_3 (Basta & El-Saied, 2000).

– **The first step**: BAS were fixed at 0.5g and the organophilic at 1.5 CEC
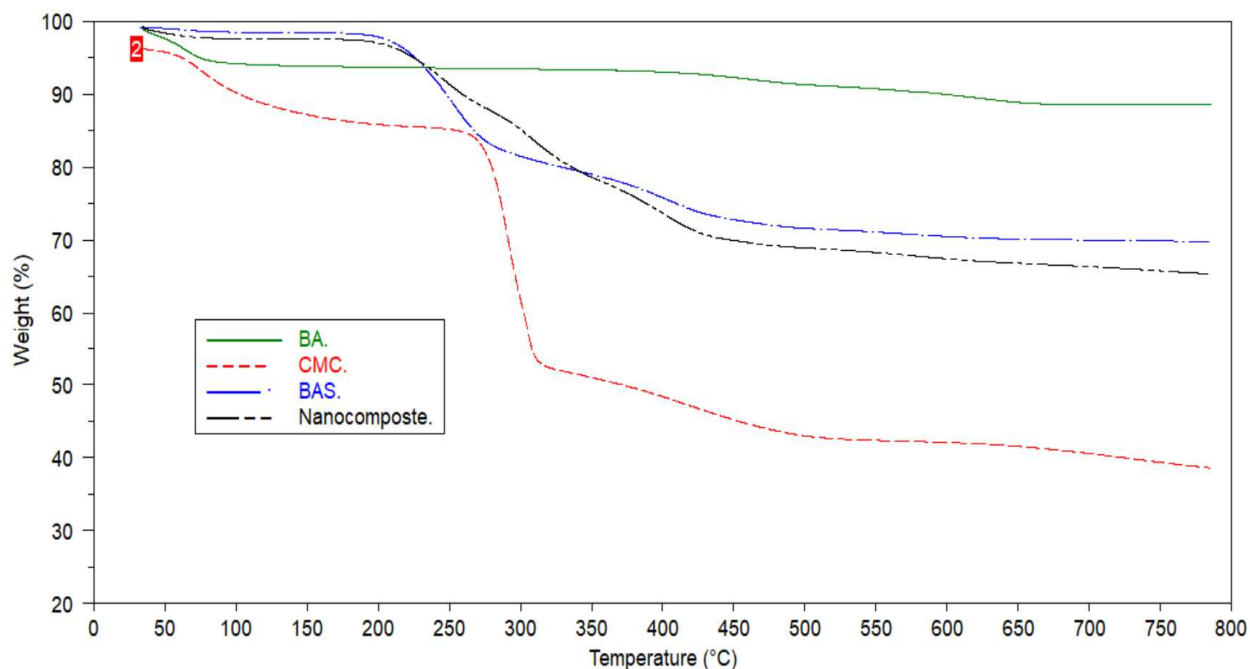
Figure. 5. TGA thermograms of BA, BAS and BAS/CMC samples at different
CMC ratios (BAS = 0.5 g)

As it can be seen in Figure 5, thermal behavior of the CMC is changed significantly in BAS/CMC nanocomposites. A three-step degradation behaviour is observed for all BAS/CMC nanocomposites studies. The first weight loss under 170 ° is observed, which is related to the physically adsorbed water. The second weight loss step appears in the range of 170–350 °C it corresponds to the degradation of the adsorbed CMC and HDTMA on the surface of BA. The following degradation step from 350 to 520 °C is related to degradation of HDTMA and intercalated CMC rings between the bentonite sheets. The last degradation occurs between 520 and 800 °C corresponds certainly to the dehydroxylation of aluminosilicates.
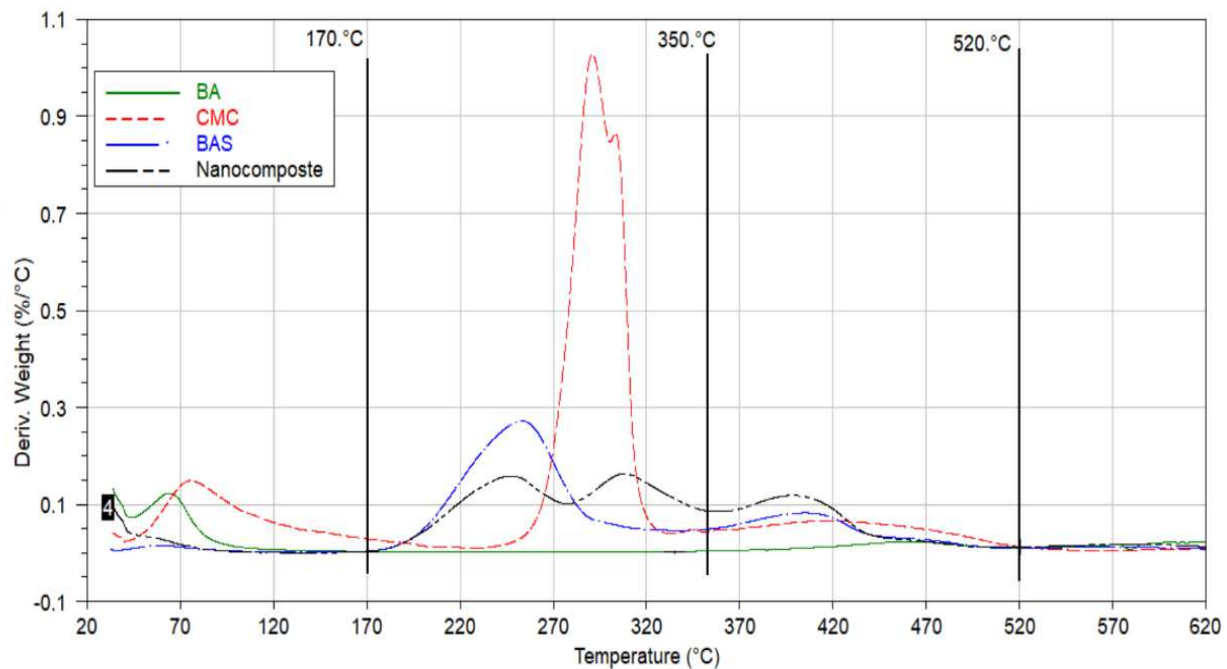
Figure. 6. DTGA thermograms of BA, BAS and BAS/CMC samples at different CMC ratios (BAS = 0.5 g).

As it can be seen in Figure 6, the apparent weight loss from all studied samples was assigned at the first degradation stage (50 - 170 °C). This could be attributed to the loss of moisture content as hydrogen-bond water to the polysaccharide structure (i.e. CMC) as well as dehydration of Bentonite at the ambient temperature (170 °C). With increasing temperature, the rate of weight loss increased and both second and third degradation stages took place between 170 and 350 °C. The observed weigh loss could be related to the degradation of the adsorbed CMC and HDTMA on the surface of BA. The following degradation step from 350 to 520 °C it's related to degradation of HDTMA and intercalated CMC between the bentonite sheets. The last degradation occurs between 520 and 800 °C it corresponds certainly to the dehydroxylation of aluminosilicates. On the other hand, the developed BAS/CMC composites were found more thermally stable with increasing temperature than the native polymer (CMC). When the temperature required for CMC polymer to loss it half weight ($T_{50\%}$) at 445.89 °C, the prepared composites BAS/CMC are still stable at this temperature and lose only 22% of their weights. These observations could be related to the stability of Bentonite at higher temperatures, since the dehydroxylation of the aluminosilicates within the Bentonite layers occurs at temperatures beyond 520 °C. As a result, Bentonite enhanced the stability of the developed composites. The obtained results are consistent with other studies which focused on studying the effect of clays encapsulation on the thermal behavior of beads prepared from other natural polysaccharides (Belhouchat et al., 2017; Ely et al., 2009).

Table 3 summarizes the different percentages of weight loss in the three stages of decomposition.

Table 3. The summary of TGA analysis of BA, BAS 1.5, and Nanocomposites samples at different CMC concentrations.

Samples	Dehydratation (water adsorbed)	Adsorbed Molecules Decomposition	Intercalted molecules decomposition	Dehydroxylation	% ORG MATTER
	Before 170 °C % weight- loss	From [170 to 350 °C] % weight- loss	From [350 to 520°C] % weight- loss	After 520 °C % weight - loss	
BA	5.31	0.41	2.30	2.55	-
BAS 1.5	0.35	19.6 - 0.41 = 19.21	10.36 - 2.3 = 08.06	1.68	28.14
BAS/CMC 0.5/0.025	0.61	21.97 - 0.41 = 21.56	10.04 - 2.3 = 7.74	2.03	29.30
BAS/CMC 0.5/0.05	1.50	24.41 - 0.41 = 24.00	9.37 - 2.3 = 7.07	3.27	31.07
BAS/CMC 0.5/0.125	2.10	26.55 - 0.41 = 26.14	8.1 - 2.3 = 5.80	3.10	31.94
BAS/CMC 0.5/0.25	1.40	15.46 - 0.41 = 15.05	10.24 - 2.3 = 7.94	3.12	22.99
BAS/CMC 0.5/0.5	1.77	18.91 - 0.41 = 16.50	9.94 – 2.3 = 7.64	3.38	24.14

The following table shows the percentages of CMC present in the BAS/CMC composites.

Table 4. The percentage of CMC in the nanocomposites samples at different CMC concentrations.

Samples	% of ORG MATTER	% CMC	State
BAS 1.5	**28.14**	-	-
BAS/CMC 0.5/0.025	29.30	1.16	on the surface
BAS/CMC 0.5/0.05	31.07	2.93	on the surface
BAS/CMC 0.5/0.125	31.94	3.8	on the surface
BAS/CMC 0.5/0.25	**22.99**	- 5.15	**Intercalation**
BAS/CMC 0.5/0.5	**24.14**	- 4	**Intercalation**

From Table 4, it can be seen that for the composites BAS/CMC (**0.5/0.025, 0.5/0.05, 0.5/0125),** the percentage of CMC adsorbed on the BAS surface (related to XRD analyses) increases with by increasing the amount of added CMC. However, in cases where the CMC rings are intercalated (BAS/CMC (**0.5/0.25** and **0.5/0.5**) related to XRD analyses)) in BAS sheets, we notice that there is a sudden drop in the percentage of overall organic matter compared to the starting material (**BAS 1.5)**. These results can be explained by the fact that there is an intercalation of CMC in the interfoliar space, these generates an elimination of HDTMA molecules adopting a bilayer arrangement linked by weak interactions.

- **The second step**: Figure 7 shows the TGA thermograms in the case where the amount of BAS and CMC are fixed at 0.5g and we changed the organophilic of bentonite (0.5, 1, 1.2, 1.5, 2 CEC).
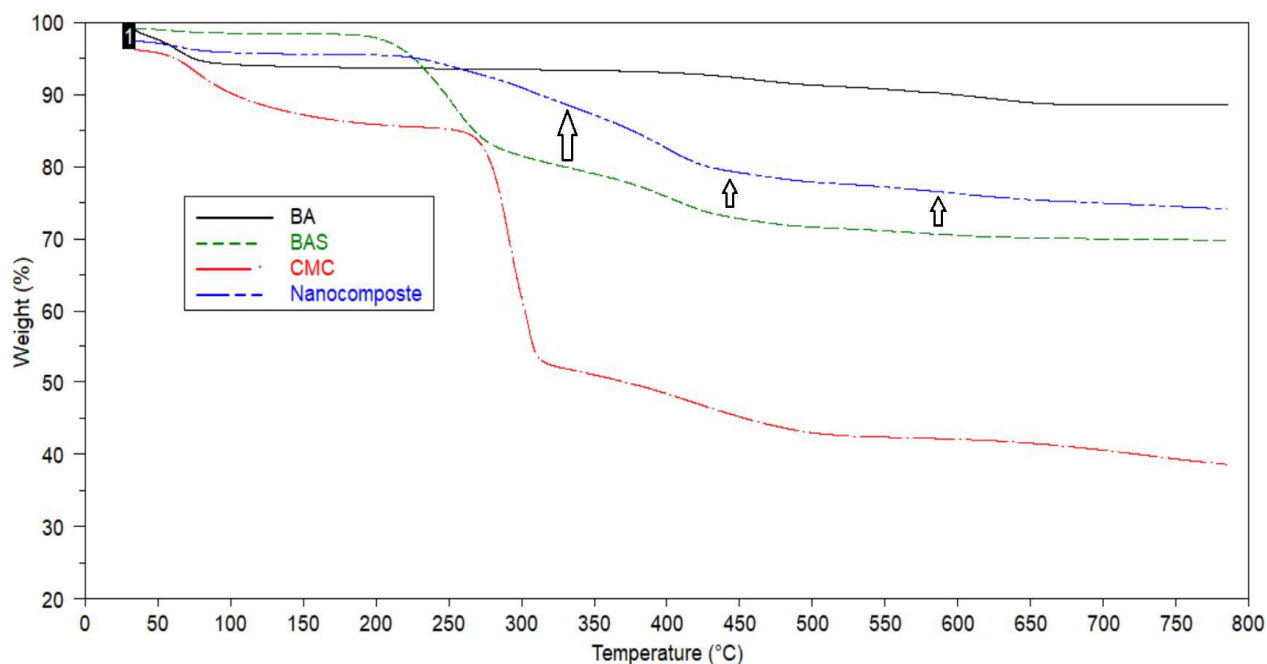
Figure 7. TGA thermograms of BA, BAS and BAS/CMC samples at different organophilic ratios (BAS and CMC = 0.5 g)

Table 5 summarizes the different percentages of weight loss in the three stages of decomposition.

Table 5. The summary of TGA analysis of BA, BAS/CMC, and Nanocomposites samples at different organophilic rates.

Samples	Dehydratation (water adsorbed)	Adsorbed Molecules Decomposition	Intercalted molecules decomposition	Dehydroxylation	% ORG MATTER
	Before 170 °C	From [170 to 350 °C]	From [350 to 520 °C]	After 520 °C	
	% weight- loss	% weight- loss	% weight- loss	% weight - loss	
BA/CMC 0 CEC	2.25	2.5 - 0.41 = 2.09	4.6 - 2.3 =2.3	2.8	**4.39**
BAS/CMC 0.5 CEC	1.72	3.87 - 0.41 = 3.46	8.60 - 2.3 = 6.30	3.58	**9.76**
BAS/CMC 1 CEC	1.91	8.41 - 0.41 = 8.00	9.56 - 2.3 = 7.26	3.49	**15.26**
BAS/CMC 1.2 CEC	2.10	9.80 - 0.41 = 10.21	10.1 - 2.3 = 7.80	3.10	**18.01**
BAS/CMC 1.5 CEC	1.40	15.46 - 0.41 = 15.05	10.24 - 2.3 = 7.94	3.12	**22.99**
BAS/CMC 2 CEC	1.77	14.91 - 0.41 = 14.50	9.94 – 2.3 = 7.64	3.38	**22.14**

From Table 5, it is clear that the more the organophilic increases (from 0 CEC to 2 CEC), the more the percentage of overall organic matter increases from 4.39 to 22.99%.

The following table shows the change in the percentage of overall organic matter before and after the addition of CMC.

Table 6. Comparison of the percentages of organic matter before and after the reactions

Samples (Before)	% of ORG MATTER	Samples (After)	% of ORG MATTER
BA	2.7	BA/CMC 0 CEC	4.39
BAS 0.5	10.3	BAS/CMC 0.5 CEC	9.76
BAS 1	18.97	BAS/CMC 1 CEC	15.26
BAS 1.2	19.52	BAS/CMC 1.2 CEC	18.01
BAS 1.5	26.85	BAS/CMC 1.5 CEC	22.99
BAS 2	24.27	BAS/CMC 2 CEC	22.14

Based on the results described in Table 6, we found that the percentage of overall organic matter in the case of BA (non-organophilic bentonite) and BA/CMC 0 CEC increases by 1.69%,

however, in all other cases, BAS (before) and BAS/CMC (after), the percentage of overall organic matter decreases. From this result, we confirm the latest findings and we claim that the addition of CMC generates an elimination of HDTMA molecules bound by weak interactions or those molecules adopting a bilayer arrangement.

HDTMA molecules act as an intermediate that promotes the adsorption and/or intercalation (depending on the quantity) of CMC chains in bentonite.

✓ Thermal Stability

The TGA analysis also gives us information on the thermal stability of the prepared composts. By comparing the percentage changes in weight loss at 800 °C, it is evident that the thermal stability of CMC in composites has increased, and as can be seen in Figure 7, the BAS/CMC had higher thermal stability (25.88% loss at 800 °C) than the BAS (31.21% loss at 800°C) and CMC (61.42% loss at 800°C). This improvement in the thermal stability of the prepared composites could be attributed to the insulating and barrier effect of the BAS layers (Ding et al., 2006). The residuals obtained at 800 °C are approximately 38.6, 69.8 and 74.2% for CMC, BAS and the BAS/CMC composite, respectively.

✓ Stability in Acidic and Alkaline media

The study of the stability of composites in acid and basic media is a very important factor, especially for the adsorption of dyes in the textile industry where the pH can be very high and variable (depending on the type of dyes and their use). For this, we had put 30 mg of the prepared composites in reaction with 100 ml of a strongly acidic (HCl, pH=1) and basic (NaOH, pH=12) solution for 24 hours. Figure 8 shows the percentage weight loss in the range [50 to 800 °C] of the composite before and after treatment.
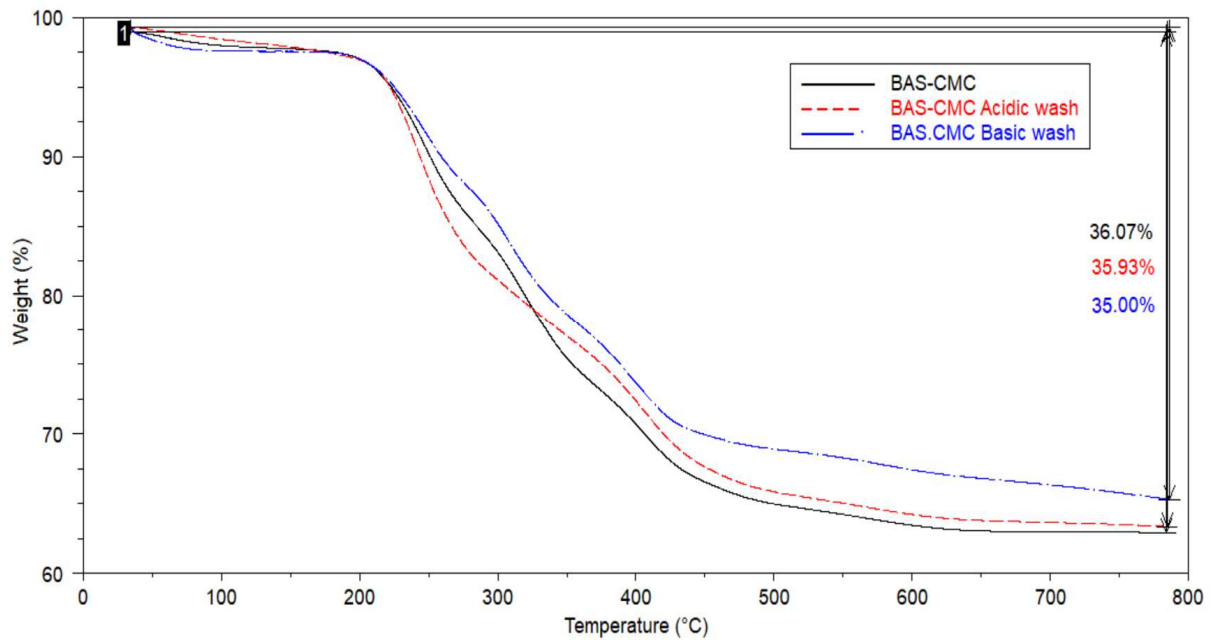
Figure 8. TGA thermograms of BAS/CMC before and after acidic and basic treatments.

Figure 8 shows that the percentage change in weight loss is about 1%, which means that the composite is stable in both acid and basic media. This suggests that the biopolymer (CMC) and HDTMA molecules in the composite do not deteriorate and remain stable in similar environments.

2.4 The point of zero charge (pH$_{ZPC}$)
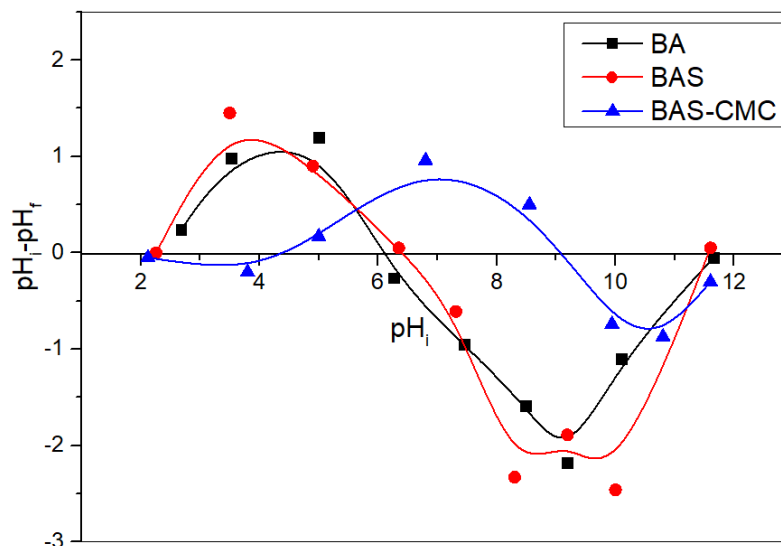
Figure 9. Determination of the pH of zero point of charge (pH$_{ZPC}$) for BAS/CMC.

The pH of zero point charge (pH$_{ZPC}$) of BAS/CMC composite was about 9.2. At pH values below and above the ZPC, the BAS composites exhibited a positive and negative charge, respectively. It was found that for a pH values below 4.5, the BAS/CMC surface was slightly negative due to the presence of carboxylic groups of CMC. Moreover, for a pH less than the

PZC and above 4.5, the composite exhibited a net positive surface charge that was attributed to the presence of ammonium groups $N^+(CH_3)_3$ of HDTMA. for a pH value higher than PZC, the BAS/CMC surface was more negative.

2.5 Dyes Adsorption Studies

Before starting the adsorption studies, we had first chose the right adsorbent that gives good adsorption results with all three dyes. For this purpose, we tested all the previously prepared composites in a free pH medium at constant concentration (100mg/L), mass (25mg) and temperature (24°C ± 1°C) for 24 hours in order to have results comparable to those of the first study.

Table 7. The adsorption tests of the three dyes with the prepared composites

Samples	% of Adsorption Methylene Blue	% of Adsorption Telon Blue	% of Adsorption Bezathren Red
BA	97	3.5	0
BAS 1.5	93	56.1	99.6
BAS/CMC 0.5/0.025	**97.24**	**99.7**	**56.88**
BAS/CMC 0.5/0.05	91.31	98.51	20
BAS/CMC 0.5/0.125	90.44	92.69	5.4
BAS/CMC 0.5/0.25	89.79	98.31	17.46
BAS/CMC 0.5/0.5	91.95	97.71	18.09

Based on the results in Table 7 and taking into consideration the adsorption yield, the economic aspect, and the nature of the flocs formed. We have selected the adsorbent (BAS/CMC 0.5/0.025) to carry out a complete adsorption study for the three dyestuffs (Methylene Blue, Telon Blue, and Bezathren Red).

a) pH Effect

First of all, we had started by studying the pH of the aqueous solution because of its importance on the adsorption process. This allows us to determine the optimized operational parameters and thus to establish the most appropriate adsorption mechanism.

Adsorption experiments of three different dyes onto BAS/CMC 0.5/0.025 were carried out to examine the effect of pH (in a range from 2 to 11) on the removal efficiency of these three dyes from an aqueous solution. The results obtained are shown in Figure 10. It was found that the pH has no significant effect on the adsorption efficiency of methylene blue (BM). In

addition, the absorption capacity at equilibrium (q_e) increased slightly (about 1mg/g) as the pH value rose from 2 to 11. These results are in good agreement with those described in a previous study (Jourvand et al., 2015).
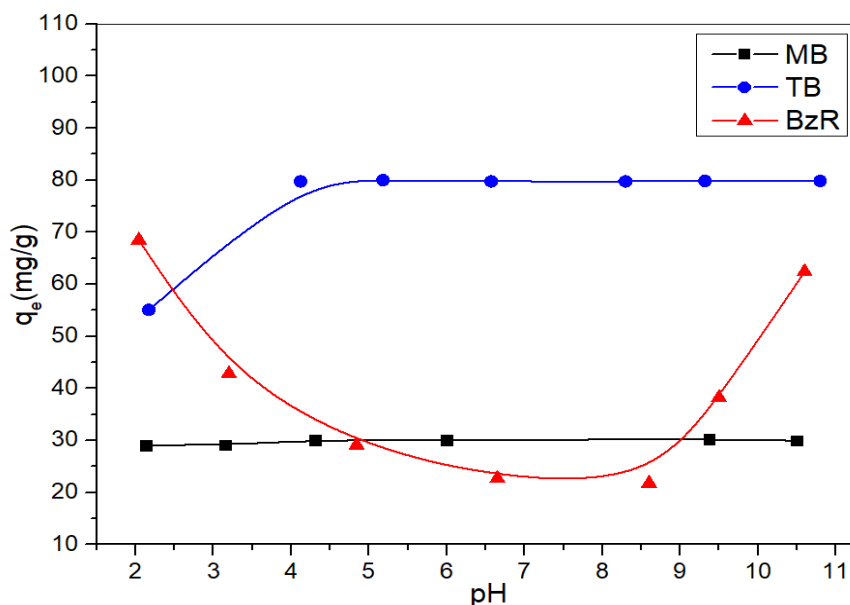
Figure. 10. Effect of pH effect on the adsorption of dyes onto BAS/CMC 0.5/0.025.

The Telon Blue (TB) dye exhibited a different adsorption behavior. It can clearly be observed on the representative curve that the adsorption capacity q_e reached two maximum values of 55.1 and 80.7 mg/g, corresponding to two pH intervals of less than 4 and from 4 to 11, respectively.

The observed high adsorption capacity in the pH range of [4 to 9.2] was certainly due to the strong electrostatic interaction between the ammonium cations of composite BAS/CMC and the dye anions. It is important to note that the adsorption capacity is stabilized as the pH value augmented. Moreover, the positive charge in the composite decrease gradually and consequently the surface becomes negatively charged (Zohra et al., 2008). Note also that for pH values greater than 9.2, the adsorption capacity remained the same. It is worth mentioning that the surface charge of composite BAS/CMC was less negative at pH values above 9.2, which it favored the adsorption of anionic dye molecules, probably due to hydrophobic and hydrogen interactions.

At pH less than 4, the adsorption capacity decrease from 80.7 to 55.1 mg/g. This decrease can be explained by the fact that, in acidic media, protons are available in excess, which generated an increased electrostatic attraction between the negatively charged carboxylate groups in the CMC rings and the H^+ protons, resulting a decrease of the overall positive charge in the composite to become slightly negative (Figure 9), which generated an

electrostatic repulsion between TB dye molecules and negatively charged BAS/CMC adsorption sites.

Moreover, for non-ionic dyes, like BzR, are generally water-insoluble dyes which are generally encountered in the form of colloidal particles (Gupta & Suhas, 2009); they are slightly negatively charged in solution (Kim et al., 2004). In general, the adsorption of these types of dyes is not promoted by electrostatic bonds, they are generally adsorbed by Van der Waals interactions, hydrogen linkages, and hydrophobic bonds. The highest adsorption capacity (68 mg/g) was observed at pH=2, which is certainly due to the fact that at this pH, there is more chance of such interactions forming than at other pH's where the composite is positively and/or negatively charged. As it can be seen from figure 10, the adsorption capacity decreases as the pH increases up to point 9.2 (PZC) and then it started increasing again to reach 62 mg/g at pH 11 where the composite was less electrically charged (figure 9).

b) Effect of Contact Time

The effect of contact time on the adsorption of MB, BzR, and TB dyes, at various time points, onto the composite BAS/CMC were investigated using a fixed adsorbent dose of 25 mg. As shown in Figure 6, the adsorption of dyes onto the composite increased for longer contact time.
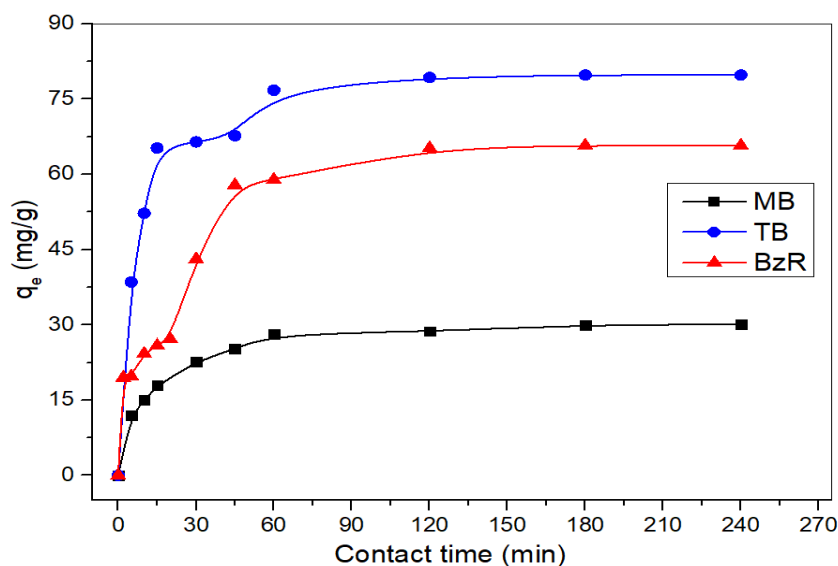
Figure. 11. Effect of time on the adsorption of dyes onto BAS/CMC composite.

The result obtained is in line with previous studies (Bhatt et al., 2012; Rajabi et al., 2016). It is clearly noted that at the beginning, the adsorption rate of dyes was fast. After this rapid dye adsorption, the adsorbent surface became saturated and this adsorption rate dropped. The adsorption efficiency reached 80 % in less than 20 min. Saturation of the composite substrate was observed at 60 min, which suggests that the aggregation of dye molecules took place around the adsorbent particles. After 60 min, no significant increase in the adsorption

efficiency was detected. Therefore, the contact time of 60 minutes was selected for all subsequent measurements.

➢ **Adsorption Kinetic Models**

Kinetic modeling not only allows estimation of sorption rates but also leads to suitable rate expressions characteristic of possible reaction mechanisms. In this respect, the pseudo-first-order and pseudo-second-order kinetics models (four linear forms) were investigated.

The adsorption kinetic plots are shown in Figure. 12a and Figure. 12b. The kinetic parameters and correlation coefficient (R^2) of the two models are given in Table 8.
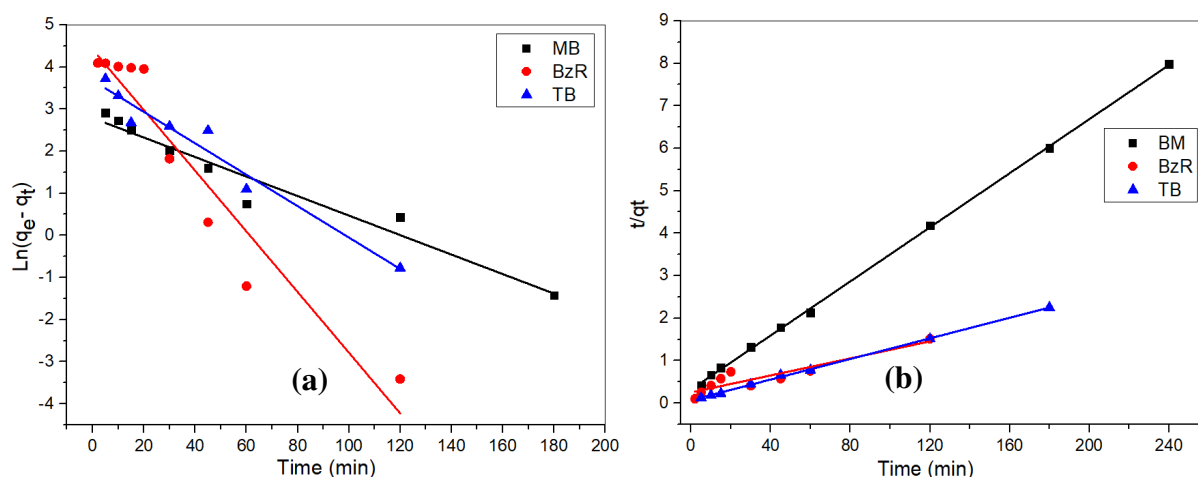
Figure. 12. Pseudo-first-order kinetics model (a) and pseudo-second-order kinetics model (b) for the adsorption of different dyes on BAS 1.5 composite.

From the pseudo-first order model, it was noted that R^2 increased from 0.91 to 0.94 and the equilibrium capacity (q_e, cal), calculated using the equation of the model, was much smaller than the experimental value (q_e, exp) for both dyes MB and TB but not for BzR. Thereby, the pseudo-first order kinetic model was not suitable to model the sorption process of MB and TB dyes onto the BAS/CMC composite. However, the pseudo-second order kinetic model described better the adsorption processes of MB and TB based on the correlation coefficient values which were found above 0.99 and greater than those of the pseudo-first order model, except for BzR (Table 8).

Table 8. Pseudo-first and Pseudo-second order kinetic parameters for the adsorption of dyes onto BAS 1.5 composite

Dye	q_e (exp) (mg.g^{-1})	Pseudo-first order			Pseudo-second order		
		k_1 (min^{-1})	q_e(cal) (mg.g^{-1})	R^2	k_2 (min^{-1})	q_e(cal) (mg.g^{-1})	R^2
BM	30.07	0.023	16.22	0.944	0.0031	31.44	0.999
BzR	79.73	0.071	82.63	0.912	0.00039	100	0.831
TB	79.76	0.037	39.56	0.948	0.00194	82.64	0.998

With regard to the adsorption of MB and BT dyes, the suggested mechanism involved that the rate-limiting step may be chemical sorption or chemisorption involving valence forces through sharing or exchange of electrons between dye molecules and BAS/CMC composite (Y S Ho & Mckay, 1999).

The adsorption mechanism of BzR that behaved as a non-ionic dye was probably due to the physical attractions (hydrogen, hydrophobic, and Van der Waals interactions) bonds between the surface of the adsorbent and dye molecules. The name physisorption was given since the rate-limiting step in this kind of mechanism is diffusion and it's not dependent on the concentrations of both reactant (physical exchange) (Yuh Shan Ho, 2006).

c) Effect of Adsorbent Dosage

The effect of the adsorbent dose on the adsorption of MB, TB and BzR dyes was studied by varying the amount of the adsorbent from 10 to 50 mg.
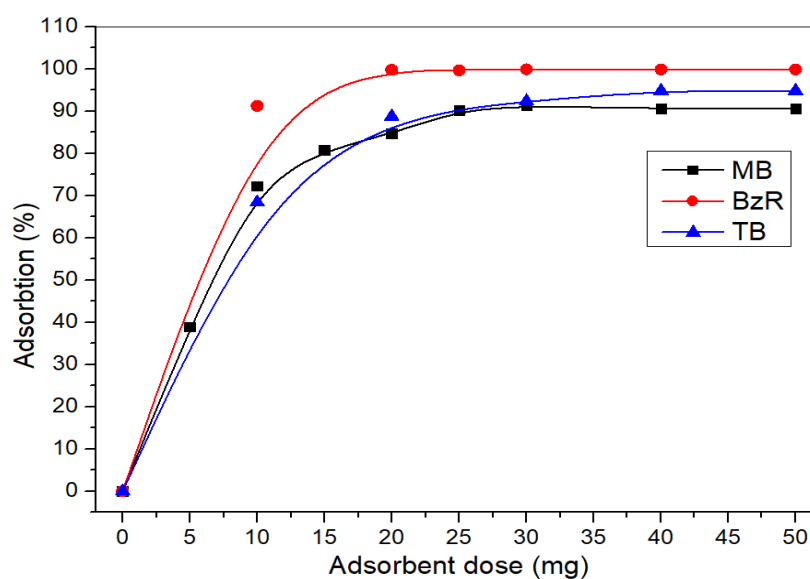
Figure. 13. Effect of adsorbent dose on the adsorption of dyes onto BAS/CMC composite.

The results presented in Figure.13 indicate clearly that the adsorption efficiency started increasing by the increasing of the amount of the adsorbent at the beginning, which suggests that a greater surface area and more adsorption sites were available. The optimal adsorbent dose for the adsorption of TB and BzR dyes was found to be 20 mg. However, a better dose (25 mg) was needed for the adsorption of MB. Moreover, for m > 25 mg, no significant variation in the adsorption efficiency was observed for MB. Therefore, the dose of 25 mg of the adsorbent was selected for all subsequent measurements.

d) Adsorption Isotherm Studies

The adsorption isotherms were studied by mixing 25 mg of the composite with a series of MB, TB, and BzR solutions, at different initial concentrations (from 5 to 300 mg/L). Thus, the mixtures thus obtained were stirred for 60 min. Figure.14 indicates that at low equilibrium concentrations, the adsorption capacities increased quickly. Note that the values of q_e increased slowly when C_e was within the range [10 - 20 mg/L] for all the adsorption of all dyes. However, when C_e increased beyond 50 mg/L, the q_e values remained nearly unchanged. These findings suggest that the initial dye concentration is an important parameter in the adsorption process.
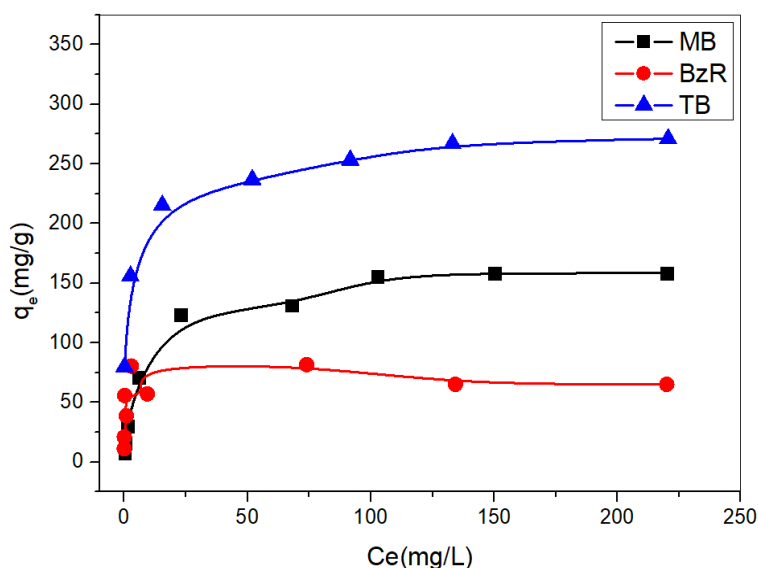
Figure. 14. Effect of initial dye concentration on the adsorption of dyes onto BAS/CMC composite.

The Langmuir and Freundlich adsorption isotherms are presented in Figure. 15. The isotherm parameters obtained from these models are summarized in Table 9. The equilibrium data obtained fit better to the Langmuir model than to the Freundlich model, as it can be seen from Figure. 15. This is indicative of the homogeneity of the adsorption sites on the BAS/CMC composite particles. In addition, as clearly indicated in Table 9, all 1/n values are below 1, which is suggestive of a normal Langmuir isotherm. However, when the 1/n value is above

unity, it is indicative of the cooperative adsorption (Jović-Jovičić et al., 2008). Moreover, when the values of 1/n are between 0.103 and 0.542, it means that there is a favorable adsorption (Hameed et al., 2007).
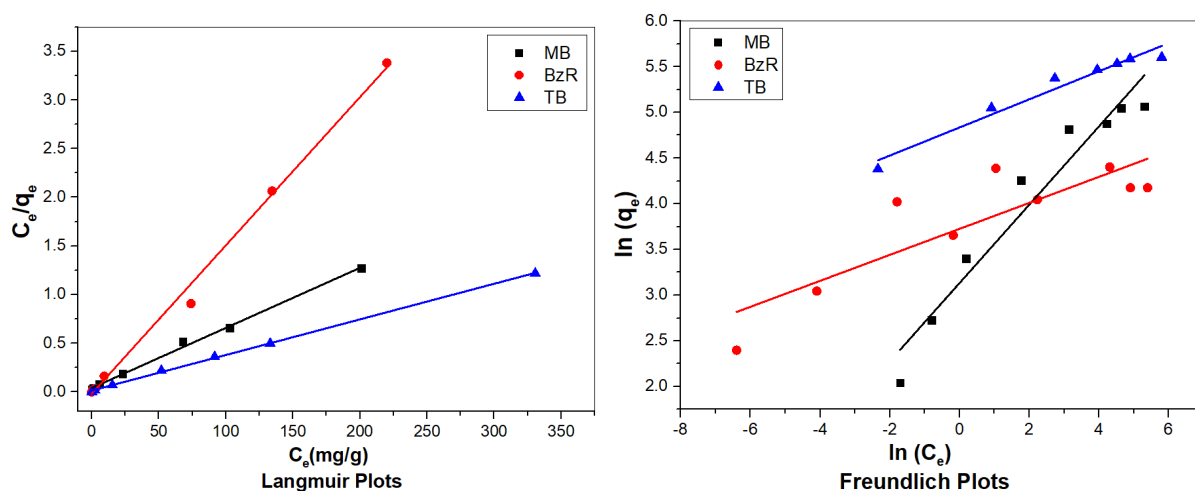
Figure. 15. Langmuir and Freundlich Isotherm plots for dyes adsorption.

Table 9. Langmuir and Freundlich isotherm parameters for dyes adsorption onto BAS/CMC composite

Dye	pH	Langmuir			Freundlich		
		K_L (L/mg)	q_m (mg.g^{-1})	R^2	K_F (L/g)	1/n	R^2
MB	6.4	0.152	161.81	0.996	22.94	0.428	0.933
BzR	2.1	0.901	65.63	0.995	41.48	0.142	0. 712
TB	6.5	0.258	273.22	0.999	125.83	0.153	0.954

e) Thermodynamic Studies

The influence of temperature on the adsorption behavior of different dyes onto BAS/CMC composite was also investigated under optimized conditions, at the temperatures of 298, 303, 313 and 323 K. A thermodynamic analysis was conducted to understand the characteristics and mechanisms of adsorption.

The previously calculated thermodynamic parameters $\Delta G°$, $\Delta H°$, and $\Delta S°$ are summarized in Table 10. Generally, the absolute magnitude of free energy change for physisorption is between -20 and 0 kJ.mol^{-1} (Yu et al., 2001).
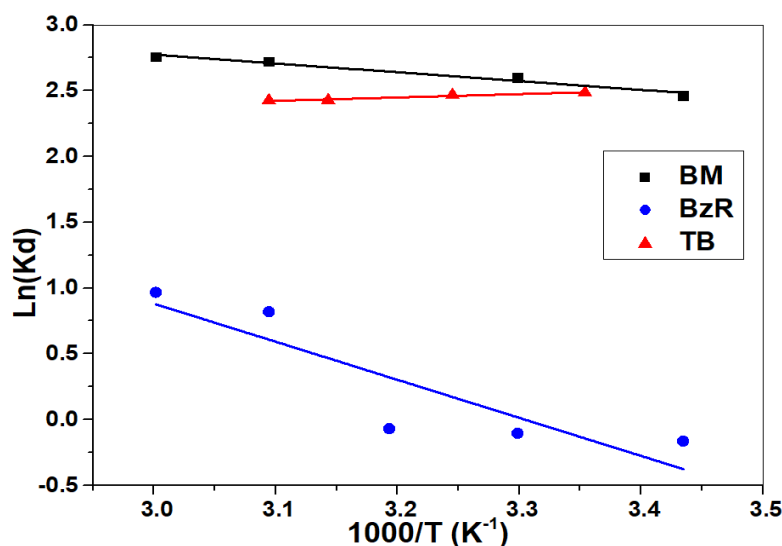
Figure. 16. The Van't Hoff plots for the adsorption of dyes onto BAS/CMC composite.

The results relating to the adsorption process of BM, BT and BzR dyes, at 298, 303, 313, 323 K, show that the free energy values were negative, which is indicative of a spontaneous and favorable adsorption process onto BAS/CMC composite, except for TB and (BzR at 298 K), where the $\Delta G°$ value was positive, suggesting that the adsorption was non-spontaneous and less favorable at these temperatures. It is worth recalling that positive values of $\Delta H°$ imply an endothermic reaction. The positive values of $\Delta S°$ indicated an increase in entropy and the solid-liquid interface became more random during the adsorption process of dyes.

Table 10. Thermodynamic parameters for the adsorption process of dyes onto BAS1.5 composite at various temperatures

Dye	$\Delta H°$ (kJ.mol^{-1})	$\Delta S°$ (J.mol^{-1}.K^{-1})	$\Delta G°$ (kJ.mol^{-1})			
			298 K	303 K	313 K	323 K
MB	5.34	34.37	-4.90	-5.07	-5.41	-5.76
BzR	24.44	81.55	0.13	-0.26	-1.085	-1.90
TB	30.71	90.01	3.88	3.43	2.53	1.63

2.6 Proposed Adsorption Mechanism

The composite under study consists of bentonite clay and surfactant. According to previous literatures (Errais et al., 2012; Mahmoodi et al., 2019), and based on the composite structure, the hydrophilic adsorption occurs between the composite and different dyes, as shown in Figure. 17. It is worth mentioning that the quaternary ammonium cationic surfactant turns the composite hydrophilic. It is widely acknowledged that cationic surfactants can produce strong electrostatic adsorption of anionic dyes. This process leads to ultrahigh adsorption capacities of

the composite for BzR and TB molecules. Moreover, hydrogen bonding may occur between the oxygen silanol groups of bentonite and both of nitrogen and oxygen atoms of dyes. Therefore, the excellent adsorption properties of BAS/CMC composite can be attributed to the synergistic effect of hydrogen bonding as well as to the electrostatic interactions between the adsorbent and MB, TB and BzR dyes.

The presence of 5% of CMC in the composite, change the physical appearance of the adsorbent obtained at the end of adsorption. The CMC in this case play the role of a binding agent between BAS particles that cause an increasing in the particle size from microfloc (in the BAS case) to large visible particles in suspension (Figure 17).
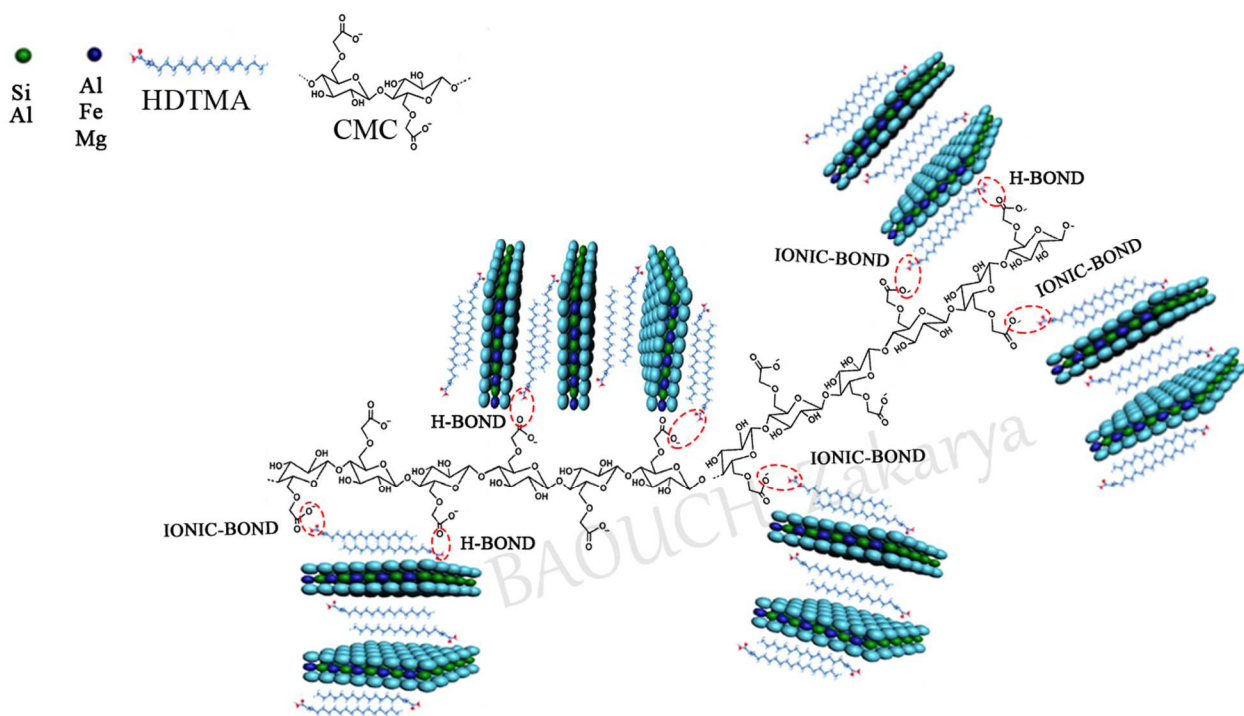
Figure. 17. An illustration of the composite BAS/CMC 0.5/0.025 formed using 5% of CMC

2.7 Explanation and Comparisons

You may wonder why we have added CMC to the BAS composite if it gives good results. We would like to tell you that the main reason we add CMC to BAS composite is for practical reasons on an industrial scale.

As mentioned before, the presence of only 5% of CMC in the composite, change the physical appearance of the adsorbent obtained at the end of adsorption. It increase the adsorbent particle size from microfloc (in the BAS case) to large visible particles in suspension (Figure 17). The presence of CMC in the BAS composite further speeds up sedimentation and ensures efficient solid/liquid separation once the floc has reached its optimum size and strength.

Large volumes of wastewater can be treated quickly, which minimizes the environmental impact in terms of the surface area required for wastewater storage facilities, and solid waste can also be discharged with appropriate characteristics.

In conclusion, the adsorption capacity of BM, BzR and TB dyes at 298K obtained in this study is compared with those determined in the previous study and by other authors (Auta & Hameed, 2013; Belbachir & Makhoukhi, 2017; Torabinejad et al., 2017; Zhou et al., 2014). These results are given in Table 11.

Table 11. Comparison of the maximum adsorption capacities for BM, BzR and TB adsorption on BAS 1.5 with those of other adsorbents

Dyes	Adsorbent	Maximum adsorption capacity (mg/g)	Ref
MB	Montmorillonite	74	(Yu et al., 2001)
	Acid modified clay beads	223.19	(Zhou et al., 2014)
	BAS 1.5	174.52	Present study
	BAS/CMC 0.5/0.025	**161.81**	**Present study**
TB	Mesoporous silicate/polypyrrole	55.55	(Auta & Hameed, 2013)
	BAS 1.5	306.74	Present study
	BAS/CMC 0.5/0.025	**273.22**	**Present study**
BzR	Sodic Montmorillonite	48.52	(Belbachir & Makhoukhi, 2017)
	BAS 1.5	107.87	Present study
	BAS/CMC 0.5/0.025	**65.63**	**Present study**

Figure. 18. The physical state of the macro-flocs formed at the end of adsorption.

REFERENCES

Auta, M., & Hameed, B. H. (2013). Acid modified local clay beads as effective low-cost adsorbent for dynamic adsorption of methylene blue. *Journal of Industrial and Engineering Chemistry*, *19*(4), 1153–1161. https://doi.org/10.1016/j.jiec.2012.12.012

Basta, A. H., & El-Saied, H. (2000). Characterization of polymer complexes by thermal and IR spectral analyses. *Polymer - Plastics Technology and Engineering*, *39*(5), 887–904. https://doi.org/10.1081/PPT-100101411

Belbachir, I., & Makhoukhi, B. (2017). Adsorption of Bezathren dyes onto sodic bentonite from aqueous solutions. *Journal of the Taiwan Institute of Chemical Engineers*, *75*, 105–111. https://doi.org/10.1016/j.jtice.2016.09.042

Belhouchat, N., Zaghouane-Boudiaf, H., & Viseras, C. (2017). Removal of anionic and cationic dyes from aqueous solution with activated organo-bentonite/sodium alginate encapsulated beads. *Applied Clay Science*, *135*, 9–15. https://doi.org/10.1016/j.clay.2016.08.031

Bhatt, A. S., Sakaria, P. L., Vasudevan, M., Pawar, R. R., Sudheesh, N., Bajaj, H. C., & Mody, H. M. (2012). Adsorption of an anionic dye from aqueous medium by organoclays: Equilibrium modeling, kinetic and thermodynamic exploration. *RSC Advances*, *2*(23), 8663–8671. https://doi.org/10.1039/c2ra20347b

Chakraborty, T., Chakraborty, I., & Ghosh, S. (2006). *Sodium Carboxymethylcellulose - CTAB Interaction: A Detailed Thermodynamic Study of Polymer - Surfactant Interaction with Opposite Charges*. *3*(9), 9905–9913.

Ding, P., Chen, W., & Qu, B. (2006). Recent progress in polymer layered double hydroxide nanocomposites. *Progress in Natural Science: Materials International*, *16*(6), 573–579. https://doi.org/10.1080/10020070612330037

Ely, A., Baudu, M., Basly, J. P., & Kankou, M. O. S. A. O. (2009). Copper and nitrophenol pollutants removal by Na-montmorillonite/alginate microcapsules. *Journal of Hazardous Materials*, *171*(1–3), 405–409. https://doi.org/10.1016/j.jhazmat.2009.06.015

Errais, E., Duplay, J., Elhabiri, M., Khodja, M., Ocampo, R., Baltenweck-Guyot, R., & Darragi, F. (2012). Anionic RR120 dye adsorption onto raw clay: Surface properties and adsorption mechanism. *Colloids and Surfaces A: Physicochemical and Engineering Aspects*, *403*, 69–78. https://doi.org/10.1016/j.colsurfa.2012.03.057

Gupta, V. K., & Suhas. (2009). Application of low-cost adsorbents for dye removal - A review. *Journal of Environmental Management*, *90*(8), 2313–2342. https://doi.org/10.1016/j.jenvman.2008.11.017

Hameed, B. H., Din, A. T. M., & Ahmad, A. L. (2007). Adsorption of methylene blue onto

bamboo-based activated carbon: Kinetics and equilibrium studies. *Journal of Hazardous Materials*, *141*(3), 819–825. https://doi.org/10.1016/j.jhazmat.2006.07.049

Ho, Y S, & Mckay, G. (1999). *Pseudo-second order model for sorption processes. 34*, 451–465.

Ho, Yuh Shan. (2006). Review of second-order models for adsorption systems. *Journal of Hazardous Materials*, *136*(3), 681–689. https://doi.org/10.1016/j.jhazmat.2005.12.043

Jourvand, M., Shams Khorramabadi, G., Omidi Khaniabadi, Y., Godini, H., & Nourmoradi, H. (2015). Removal of methylene blue from aqueous solutions using modified clay. *Journal of Basic Research in Medical Sciences*, *2*(1), 32–41. http://jbrms.medilam.ac.ir/article-1-120-en.html

Jović-Jovičić, N., Milutinović-Nikolić, A., Gržetic, I., & Jovanović, D. (2008). Organobentonite as efficient textile dye sorbent. *Chemical Engineering and Technology*, *31*(4), 567–574. https://doi.org/10.1002/ceat.200700421

Kim, T. H., Park, C., Shin, E. B., & Kim, S. (2004). Decolorization of disperse and reactive dye solutions using ferric chloride. *Desalination*, *161*(1), 49–58. https://doi.org/10.1016/S0011-9164(04)90039-2

Luna-Martínez, J. F., Hernández-Uresti, D. B., Reyes-Melo, M. E., Guerrero-Salazar, C. A., González-González, V. A., & Sepúlveda-Guzmán, S. (2011). Synthesis and optical characterization of ZnS-sodium carboxymethyl cellulose nanocomposite films. *Carbohydrate Polymers*, *84*(1), 566–570. https://doi.org/10.1016/j.carbpol.2010.12.021

Mahmoodi, N. M., Abdi, J., Taghizadeh, M., Taghizadeh, A., Hayati, B., Shekarchi, A. A., & Vossoughi, M. (2019). Activated carbon/metal-organic framework nanocomposite: Preparation and photocatalytic dye degradation mathematical modeling from wastewater by least squares support vector machine. *Journal of Environmental Management*, *233*(August 2018), 660–672. https://doi.org/10.1016/j.jenvman.2018.12.026

Meyer, K. H., & Misch, L. (1937). Positions des atomes dans le nouveau modèle spatial de la cellulose. *Helvetica Chimica Acta*, *20*(1), 232–244. https://doi.org/10.1002/hlca.19370200134

Rajabi, M., Mirza, B., Mahanpoor, K., Mirjalili, M., Najafi, F., Moradi, O., Sadegh, H., Shahryari-ghoshekandi, R., Asif, M., Tyagi, I., Agarwal, S., & Gupta, V. K. (2016). Adsorption of malachite green from aqueous solution by carboxylate group functionalized multi-walled carbon nanotubes: Determination of equilibrium and kinetics parameters. *Journal of Industrial and Engineering Chemistry*, *34*, 130–138. https://doi.org/10.1016/j.jiec.2015.11.001

Sdiri, A., Higashi, T., Hatta, T., Jamoussi, F., & Tase, N. (2011). Evaluating the adsorptive capacity of montmorillonitic and calcareous clays on the removal of several heavy metals in aqueous systems. *Chemical Engineering Journal*, *172*(1), 37–46. https://doi.org/10.1016/j.cej.2011.05.015

Torabinejad, A., Nasirizadeh, N., Yazdanshenas, M. E., & Tayebi, H.-A. (2017). Synthesis of conductive polymer-coated mesoporous MCM-41 for textile dye removal from aqueous media. *Journal of Nanostructure in Chemistry*, *7*(3), 217–229. https://doi.org/10.1007/s40097-017-0232-7

Wu, D., Chang, P. R., & Ma, X. (2011). Preparation and properties of layered double hydroxide-carboxymethylcellulose sodium/glycerol plasticized starch nanocomposites. *Carbohydrate Polymers*, *86*(2), 877–882. https://doi.org/10.1016/j.carbpol.2011.05.030

Yu, Y., Zhuang, Y. Y., & Wang, Z. H. (2001). Adsorption of water-soluble dye onto functionalized resin. *Journal of Colloid and Interface Science*, *242*(2), 288–293. https://doi.org/10.1006/jcis.2001.7780

Zhou, K., Zhang, Q., Wang, B., Liu, J., Wen, P., Gui, Z., & Hu, Y. (2014). The integrated utilization of typical clays in removal of organic dyes and polymer nanocomposites. *Journal of Cleaner Production*, *81*, 281–289. https://doi.org/10.1016/j.jclepro.2014.06.038

Zohra, B., Aicha, K., Fatima, S., Nourredine, B., & Zoubir, D. (2008). Adsorption of Direct Red 2 on bentonite modified by cetyltrimethylammonium bromide. *Chemical Engineering Journal*, *136*(2–3), 295–305. https://doi.org/10.1016/j.cej.2007.03.086

CHAPTER III

PART III.

PART III
STUDY OF THE DECOLORIZATION AND COD REDUCTION EFFICIENCY OF THE MIXTURE OF THE THREE DYES (MB, BZR, AND TB).

INTRODUCTION

The detection of dyes is a difficult process because of the large variety of functional groups in different dyes and their diverse properties. In addition, the effluents are usually very complex mixtures due to the process of coloration, which may require various kinds of additives to enhance the color of the dye. Analytical procedures for the determination of dyes at parts per million (ppm) levels are very limited. Most of the dyes are non-volatile hence gas chromatography cannot be used. HPLC & Mass spectrometry have been used for some dyes (Tincher & Robertson, 1982) but the direct determination of dyes in effluents and environmental samples is expensive and requires special procedures that are not readily available.

The presence of organic substances in the water affects dissolved oxygen (DO). The reduction of dissolved oxygen levels not only affects aquatic microorganisms and the ecological balance but also causes environmental problems by reducing the population of beneficial microorganisms that naturally degrade harmful organic substances. This gives an idea of the organic load of the effluent. DO depletion is often thought of as an increase in chemical oxygen demand (COD) and biological oxygen demand (BOD), which refers to the amount of oxygen needed to completely oxidize organic substances in water, chemically and biologically, respectively. In wastewater treatment plant, chemical oxygen demand is needed to be measured. The amount of chemical oxygen demand determines the degree of water pollution by organic material

Our main objective is to use our support as an effective adsorbent to treat textile effluents, which contains different types of dyes namely cationic, anionic, and neutral (vat dye). In this context, we have tested the effectiveness of our material (BAS/CMC 0.5/0.025) that has several advantages such as its availability, easy made, and low cost, in mixing dyes in binary and ternary systems. For this purpose, we have chosen three dyes as models of Cationic (Methylene Blue), Anionic (Telon Blue), and Vat (Bezathrene Red) dyes because of their wide use in the textile industry and their adverse effects on health and the environment.

1. EXPERIMENTAL METHOD

1.1 Batch adsorption studies:

The adsorption capacities of the prepared composite (BAS/CMC 0.5/0.025) for MB, TB and BzR dyes were evaluated using the same batch equilibrium procedure mentioned in Part I with an amount of adsorbent equal to 75 mg and a volume of 120 mL at different pH and concentrations. The adsorption capacity and removal efficiency of the prepared composite were evaluated using UV-visible spectrums and COD analysis.

1.2 Determination of COD (open system reflux method)

Under defined conditions, certain substances contained in water are oxidized at boiling point (150 °C) by an excess of potassium dichromate, in an acid medium and in the presence of silver sulphate acting as an oxidation catalyst and mercury (II) sulphate allowing chloride ions to be complexed. Excess potassium dichromate is dosed with iron ammonium sulphate.

Oxidizable materials (especially organic materials) in the sample are oxidized by the potassium dichromate under the above-mentioned conditions.

The potassium dichromate is reduced:

$$Cr_2O_7^{2-} + 14\ H^+ + 6\ e^- \rightarrow\ 2\ Cr^{3+} + 7\ H_2O \qquad (1)$$
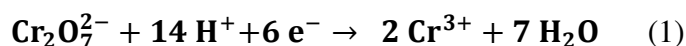
The residual potassium dichromate is dosed with a solution of iron (II) and ammonium sulphate (i.e. Fe^{2+}), in the presence of ferroin (oxidation-reduction indicator):

$$Fe^{2+} \rightarrow\ Fe^{3+} +\ e^- \qquad (2)$$
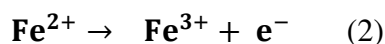
The overall reaction of the dosage is as follows:

$$Cr_2O_7^{2-} + 14\ H^+ + 6\ Fe^{2+} \rightarrow\ 2\ Cr^{3+} + 6\ Fe^{3+} + 7\ H_2O \qquad (3)$$

It is then possible to determine the amount of potassium dichromate consumed during the test and to deduce the equivalent amount of oxygen.

It will be possible to determine:

- The total COD (dissolved and suspended solids) of the sample (total COD).

- The dissolved COD, after the sample has been decanted for 2 hours (COD_{ad2}).

To limit the interference of chlorides, mercury sulfate is added, which leads to the formation of chloromercurate (II), soluble and little oxidizable:

$$Hg^{2+} + 2Cl^- \rightarrow HgCl_2 \qquad (4)$$
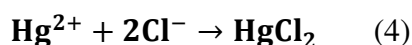
1.2.1 Special Equipment

- COD Analysis Thermoreactor that allows us to control temperature and time.

- Reflux apparatus composed of a 250 mL flat-bottomed tube or flask with a ground neck and an adaptable refrigerator.

The device is cleaned by boiling under reflux a mixture of 5 mL potassium dichromate solution, 15 mL sulfuric acid/silver sulfate solution, and 10 mL water.

✓ **Reagents**

- **Sulphuric acid solution at 4 mol/L:**

Sulphuric acid (d = 1.84)	220 mL
Deionized water	q.s.f. 1 L

Pour sulphuric acid into water. After cooling, make up to 1 L.

- **Silver sulfate solution at 10 g/L in sulfuric acid :**

Crystallized silver sulfate	(Ag_2SO_4) 10 g
Sulphuric acid (d = 1.84)	q.s.f. 1 L

Dissolve silver sulfate in 40 mL deionized water, add 960 mL sulfuric acid carefully.

- **Ferrous Ammonium Sulfate (Mohr Salt) solution at 0.12 mol/L:**

Ammonium Iron (II) sulfate hexahydrate $FeSO_4(NH_4)_2SO_4, 6H_2O$	47.0 g
Sulphuric acid (d = 1.84)	20 mL
Deionized water	q.s.f. 1 L

Dissolve iron ammonium sulfate in water, add sulfuric acid. After cooling, adjust the volume to 1 L.The concentration of this solution should be checked daily.

- **Ferroin solution**

1, 10-phenanthroline	1.5 g
Iron (II) sulphate $FeSO_4, 7H_2O$	0.7 g
Deionized water	q.s.f. 100 mL

Dissolve phenanthroline and iron sulfate in water and complete the volume. A commercial solution can also be used.

- Potassium dichromate standard solution at 0.04 mol/L, containing mercury (II) sulfate:

Mercury sulphate (II)	80 g
Sulphuric acid (d = 1.84)	100 mL
Potassium dichromate $K_2Cr_2O_7$	11.767 g
Deionized water	q.s.f. 1 L

Dissolve 80 g of mercury (II) sulfate in about 800 mL of deionized water. Carefully add 100 mL of sulfuric acid. Let it to cool and then add 11.767 g potassium dichromate, (previously dried at 105 °C for 2 hours). Transfer the solution quantitatively to a 1 L volumetric flask and make up to volume. This solution is stable for about 1 month.

- **Reference solution: Copper**(II) **phthalocyanine tetrasulfonic acid tetrasodium salt with a COD of 100 mg/L of oxygen:**

$(C_{32}H_{12}CuN_8Na_4O_{12}S_4)$ 0.666 g

Deionized water   q.s.f. 1 L

Dilute this solution 1/10^e with deionized water.

This solution at 0.066 g/L has a theoretical COD of 100 mg/L. Stored at 4 °C, it remains stable for about 3 months.

- **Verification of the concentration of the Ammonium iron (II) sulfate (Mohr's Salt)**

In a beaker, put 5 mL of potassium dichromate standard solution (at 4 mol/L). Then add approx. 100 mL of sulfuric acid (at 4 mol/L).

Titrate with Ammonium iron (II) sulfate using a few drops of ferroin solution as a color indicator and determine the volume (V_{Eq}) of Ammonium iron (II) sulfate required to turn red.

The concentration C (in mol/L) of the Ammonium iron (II) sulphate solution is given by the formula below where the volumes are expressed in mL:

$$C_{mol/L} = \frac{V_{dichromate} \times 0.04}{V_{Eq}} \times 6 = \frac{1.2}{V_{Eq}} \qquad (5)$$

1.2.2 Sample Analysis

Operators must be informed of the risks involved in handling concentrated sulfuric acid solutions and oxidizing reagents at high temperatures (boiling of the mixture, approx. 150 °C). All necessary precautions must therefore be taken.

Place 10.0 mL of sample in a reaction tube. If the COD of the sample is higher than 800 mg/L O2, an appropriate dilution should be performed.

Add 5.00 mL of potassium dichromate solution (0.040 mol/L).

Slowly and carefully, add 15 mL of the sulfuric acid solution containing silver sulfate, stirring the tube thoroughly.

Apply 1 to 2 drops of sulfuric acid to the ground neck of the tube to lubricate it and connect the coolant to the reaction tube. Make sure that the coolant rotates easily in the tube run-in (otherwise add an additional drop of acid).

Place the tube in the heating block and boil (150 °C ± 5 °C) for 2 hours.

Turn off the heating and remove the tubes with their refrigerants. Allow them to cool down and then carefully rinse the coolant by collecting the wash water in the reaction tube.

Transfer the contents of the tube to a 250 mL Erlenmeyer flask, rinse and dilute with approximately 75 mL of distilled water.

Add 2 to 3 drops of Ferroin and titrate with the Ammonium iron (II) sulphate solution.

- **Blank Trial**

Proceed in the same way by replacing the sample with 10.0 mL deionized water. The consumption of potassium dichromate in this assay should be very low and not exceed 0.5 mL.

Higher values may be due to insufficient cleanliness of the glassware or errors in reagent concentrations.

- **Control Test With The Reference Solution**

Proceed in the same way, replacing the sample with 10.0 mL of the 0.066 g/L reference solution. This solution should have a COD of 100 ± 18 mg/L oxygen.

1.2.3 Results Expression

The chemical oxygen demand (COD) expressed in milligrams of oxygen per liter is equal to:

$$\frac{8\ 000\ (V_0 - V_1)\ C}{V} \qquad (6)$$

V_0: Volume of Ammonium iron (II) sulphate required for the dosage (mL).

V_1: Volume of Ammonium iron (II) sulphate required for the blank trial (mL).

C: Concentration of the Ammonium iron (II) sulphate solution (in mol/L).

V: Volume of the test sample (in mL).

- **Remarks**

- The method is very satisfactory for COD higher than 50 mg/L and chloride contents (expressed as Cl) lower than 1.5 g/L.

- In the presence of large amounts of chlorides, the sample can be diluted 1/10 or 1/100 if the amount of reducing material allows it.

- If the COD is greater than 700 mg/L, dilute with permuted water.

- Take all necessary precautions to eliminate the introduction of organic matter from glassware, permuted water, and the atmosphere.

- If the chloride content is higher than 1.5 g/L, increase the amount of mercury sulphate to maintain an $HgSO_4/Cl$ ratio close to 10.

- If nitrites interfere with the dosage, add 10 mg sulfamic acid per mg nitrite.

- This method uses concentrated acid solutions at high temperature, which requires the implementation of specific precautions and particular vigilance.

- The effluents resulting from this dosage must be stored for detoxification, as they contain toxic compounds (Cr, Ag, and Hg) in an acid environment.

Reference Method : *NF T90-101 (février 2001). Qualité de l'eau – Détermination de la demande chimique en oxygène (DCO) (Indice de classement : T90-101).*

2. RESULTS AND DISCUSSION

In this part, we studied the decolourization and COD reduction of a solution containing a mixture of dyes (MB, BzR, and TB), using the adsorbent (BAS/CMC 0.5/0.025) to evaluate its adsorption efficiency in dye mixtures as a Simulated Effluent. Some parameters influencing the adsorption of these dyes in mixture system were studied such as the initial pH of the solution and the concentration of each dye in the medium.

2.1 pH Effect

a. Preparation of the Simulated Effluent

A dye stock solution was prepared by taking 40 mL of each dye at fixed concentration ($C_{MB}=C_{BzR}=C_{TB}=$ 20 mg/L), resulting in a total volume of 120 mL and a concentration of 80 mg of dyes mix/L. The adsorption of the simulated effluent was carried out in room temperature, by adding 75 mg of our adsorbent in the pH range of 2 to 10 for a duration of 120 min. After a suitable time, the dye solution was separated from the adsorbent by centrifugation for 10 minutes at 4000 rpm. The UV-visible decolourization spectra and COD reduction results are shown in Figures 1 and 2 in the Table 1.

As shown in figure 1, the Absorbance of the simulated effluent before adsorption was abruptly decreased from 0.63 (at pH 8.35) to 0.06 and 0.007 for pH 2 to pH 10 respectively. The percentage of the decolourization was 89.5 and 98.8 % for pH 2 to pH 10 respectively (Table 1).
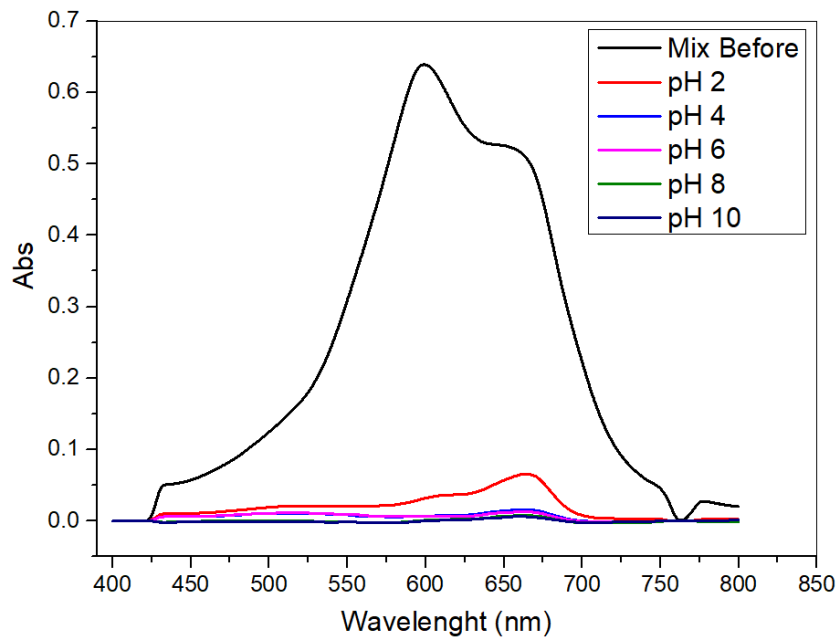
Figure 1: The UV-visible decolourization spectra of the simulated effluent at different pH values

The results and percentages of COD removal before and after adsorption as a function of pH are shown in Figure 2 and Table 1.
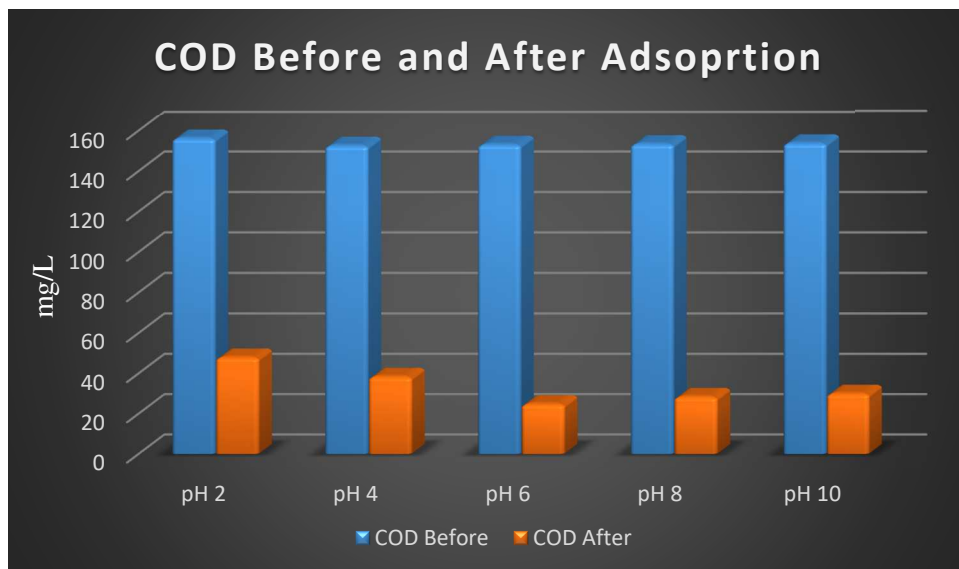
Figure 2. The variation in COD before and after adsorption of the simulated effluent at different pH values.

According to figures 1 and 2 and from the Table 1, we can clearly see that the percentage of decolourization and COD reduction are very high and they are about 98% and 80% respectively. The highest percentages of decolourization and COD reduction were obtained at pH 6, with values of 98.09 and 83.8% respectively.

Table 1: summary of decolorization and COD results BEFORE and AFTER adsorption of the simulated effluent at different pH values.

pH	Absorbance		% of Decolorization	COD (mg/L)		% of COD removal
	Before	After		Before	After	
2	0.63	0.066	89.52	156.2	48	69.27
4	0.63	0.015	97.61	152.6	38.4	74.83
6	0.63	0.012	98.09	153.1	24.8	83.80
8	0.63	0.077	98.77	153.4	28.4	81.48
10	0.63	0.0086	98.63	153.8	30	80.49

2.2 Concentration Effects

2.2.1. Adsorption in Equal Concentrations

a. Preparation of Simulated Effluent

A dye stock solution was prepared by taking 40 mL of each dye at equal concentrations ($C_{(MB=BzR=TB)}$ = 10, 20, 30, 40, 50, 100 mg/L), resulting in a total volume of 120 mL and a concentrations of 30, 60, 90, 120, 150, 300 mg of dyes mix/L. The adsorption of the simulated effluent was carried out in room temperature, by adding 75 mg of our adsorbent without pH adjustment (The pH of the mixed dyestuff solution was 8.35) for a duration of 120 min. After a suitable time, the dye solution was separated from the adsorbent by centrifugation for 10 minutes at 4000 rpm. The UV-visible decolourization spectra and COD reduction results are shown in Figures 3 and 4 and in the Table 2.
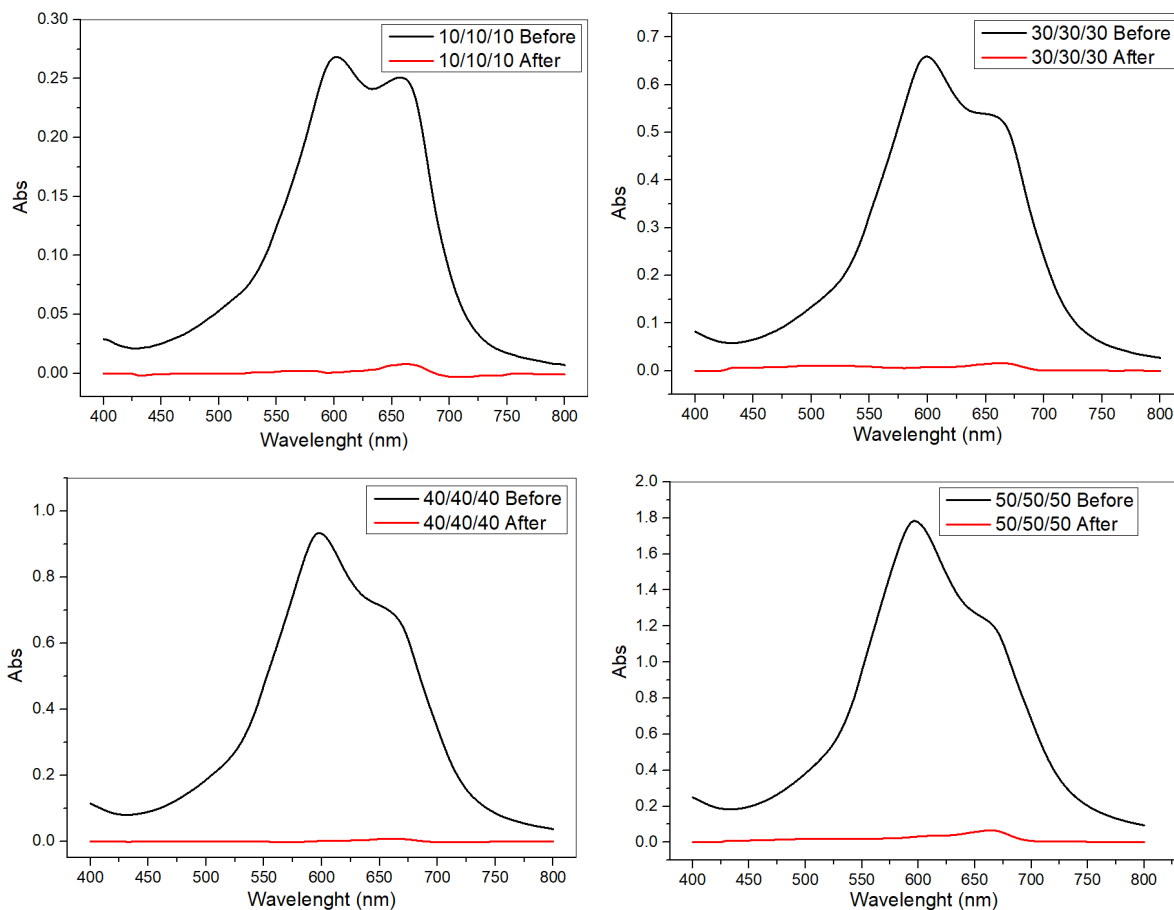
Figure 3: The UV-visible decolourization spectra of the simulated effluent at equal concentrations.

From Figure 3 and the percentages presented in Table 2, it is quite obvious that the Absorbances of the solutions have considerably decreased, which means that the intensity of the color in the solutions has been considerably reduced, by approximately 98%.
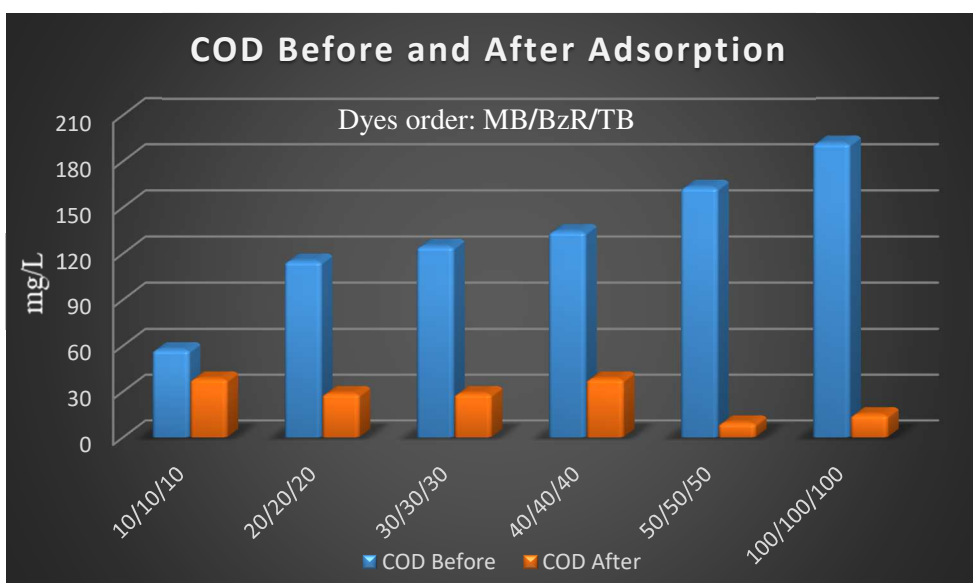
Figure 4. The variation in COD before and after adsorption of the simulated effluent at equal concentrations.

The following table summarizes the different results of the decolorization and COD reduction BEFORE and AFTER adsorption of the simulated effluent at equal concentrations.

Table 2: summary of decolorization and COD results BEFORE and AFTER adsorption of the simulated effluent at equal concentrations.

C (mg/L) MB/BzR/TB	Absorbance		% of Decolorization	COD (mg/L)		% of COD removal
	Before	After		Before	After	
10/10/10	0.251	0.0084	96.65	57.60	38.40	33.33
20/20/20	0.63	0.012	98.09	115.20	28.80	75.00
30/30/30	0.68	0.016	97.64	124.80	28.80	76.92
40/40/40	0.934	0.001	99.89	134.40	38.40	71.42
50/50/50	1.786	0.071	96.02	163.20	09.60	94.11
100/100/100	-	-	-	326.40	48.00	85.29

From Figure 2 and the percentages of COD reduction shown in Table 2, it can be seen that the percentage of reduced COD increases with increasing concentration. This result is the opposite of the usual, where the percentage of COD reduction decreases with increasing concentration(Jung & Pandit, 2018; Martin et al., 2010; Saha et al., 2014).

At very high concentrations of about 150 mg of dyes mix/L, the COD reached its optimum of 9.6 mg/L, equivalent to 94.11% of reduction, while at a low concentration of 30 mg of dyes mix/L, the COD was 38.40 mg/L, which is equivalent to a very low percentage reduction of around 33.33%.

This led us to ask more questions and to make further experiments by varying the concentration of each dye and taking into account the precipitation phenomenon to understand why the COD is higher in low concentrations and lower in high concentrations.

2.2.2. Adsorption in Different Concentrations
a. Preparation of Simulated Effluent
A dye stock solution was prepared by taking 40 ml of each dye in equal concentrations and in the absence of one of the dyes. (C $_{(MB, BzR, TB)}$ = 100 mg/L), resulting in a total volume of 80 mL and a concentration of 200 mg of dyes mix/L. The adsorption of the simulated effluent

was carried out in room temperature, by adding 75 mg of our adsorbent without pH adjustment (The pH of the mixed dyestuff solution was 8.35) for a duration of 120 min. After a suitable time, the dye solution was separated from the adsorbent by centrifugation for 10 minutes at 4000 rpm. The COD reduction results are shown in Figures 5 and Table 3.
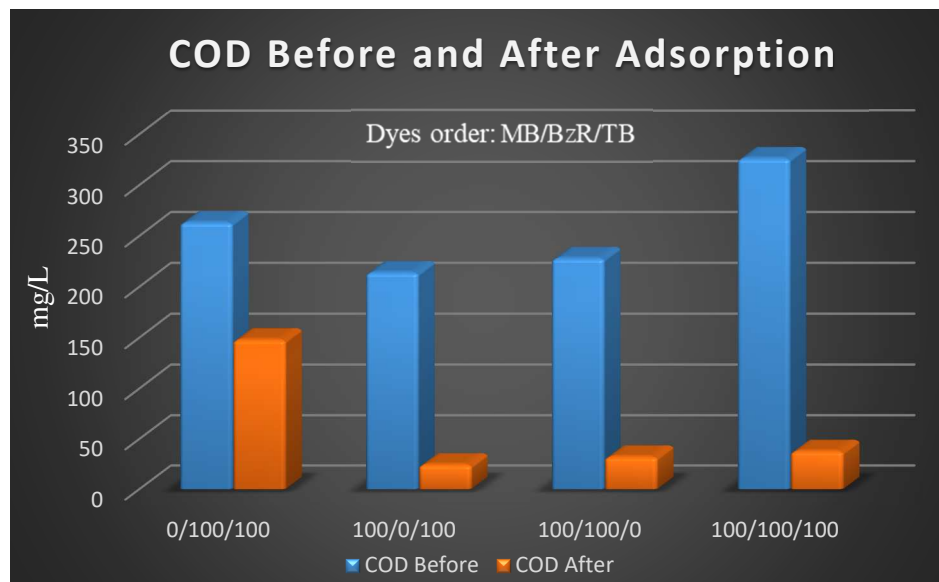
Figure 5. The variation in COD before and after adsorption of the simulated effluent in the absence of one of the dyes.

From Figure 5 and the percentages of COD reduction shown in Table 3, it can be seen that the percentage of reduced COD is low only in the case of the absence of Methylene Blue (43.73%) and very high in the other cases by approximately 88%. This is due to the presence of strong electrostatic interactions between the cationic dye (MB), the anionic (TB) and vat (BzR) dye (synergism effect).

Table 3: Summary of COD results BEFORE and AFTER adsorption of the simulated effluent in the absence of one of the dyes.

C (mg/L) MB/BzR/TB)	COD (mg/L)		% of COD removal
	Before	After	
0/100/100	263.40	148.20	43.73
100/0/100	214.20	24.60	88.51
100/100/0	228.20	32.40	85.80
100/100/100	326.40	38.00	88.35

To confirm this result, we add another experiment where we set the concentration of BzR and TB at 50 mg/L and we increase the concentration of MB from 0 to 100 mg/L.
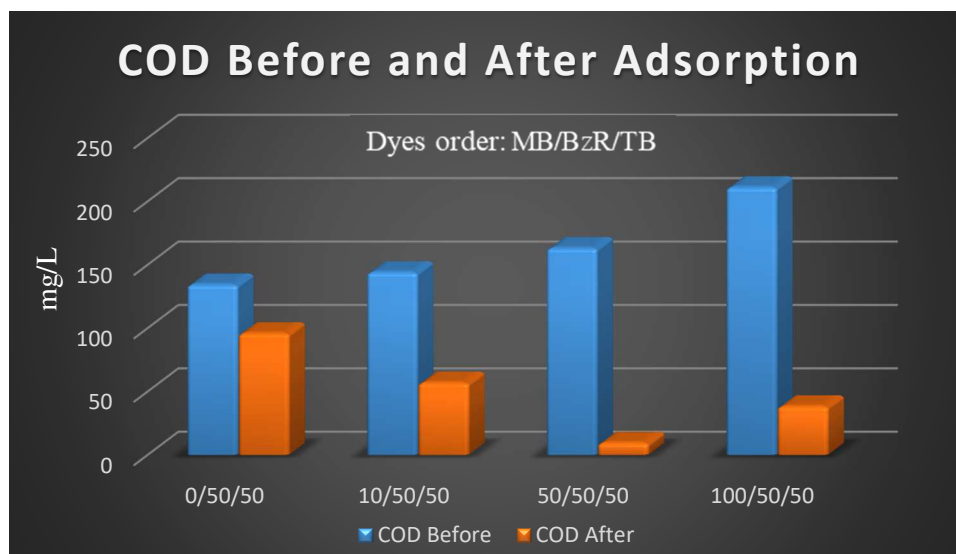
Figure 6. The variation in COD before and after adsorption of the simulated effluent in the presence and absence of Methylene Blue at different concentrations.

As can be seen in Figure 6 and the percentages of reduced COD presented in Table 4, the adsorption is too low in the case of the absence of Methylene Blue, and it increases with the increase of its concentration to reach a maximum at a concentration of 100 mg/L. The adsorption rate increases from 28.57% (in the absence of MB) to 81.81% (in the presence of 100mg/L MB). This confirms the previous result that Methylene Blue acts as an agent that improves adsorption and assists in the fixation of the other two dyes in the substrate.

Table 4: Summary of COD results BEFORE and AFTER adsorption of the simulated effluent in the absence of Methylene Blue at different concentrations.

C (mg/L) MB/BzR/TB	COD (mg/L)		% of COD removal
	Before	**After**	
0/50/50	134.40	96.00	28.57
10/50/50	144.20	57.00	60.47
50/50/50	163.20	9.60	94.11
100/50/50	211.20	38.40	81.81

Figure 7. The solutions obtained after adsorption at different concentrations of Methylene Blue.

As mentioned before, the presence of only 5% of CMC in the BAS composite can remove the three type of dyes MB (cationic), BzR (Vat) and TB (Anionic) in a single system or in a mixture. It also change the physical appearance of the adsorbent obtained at the end of adsorption. It increase the adsorbent particle size from microfloc (in the BAS case) to large visible particles in suspension. The presence of CMC in the BAS composite further accelerates sedimentation and ensures efficient solid/liquid separation once the floc has reached its optimum size and strength. Large volumes of wastewater can be treated quickly, which minimizes the environmental impact in terms of the surface area required for wastewater storage facilities, and solid waste can also be discharged with appropriate characteristics.

Based on the obtained results in this work, we can conclude that the adsorbent BAS/CMC 0,5/0.025 can be considered as a good material for the removal of MB, BzR and TB dyes in single and mixtures systems. Due to the availability, efficiency and low cost of these material, these results are encouraging to be tested and evaluated on an industrial scale with real and more complex wastewater.
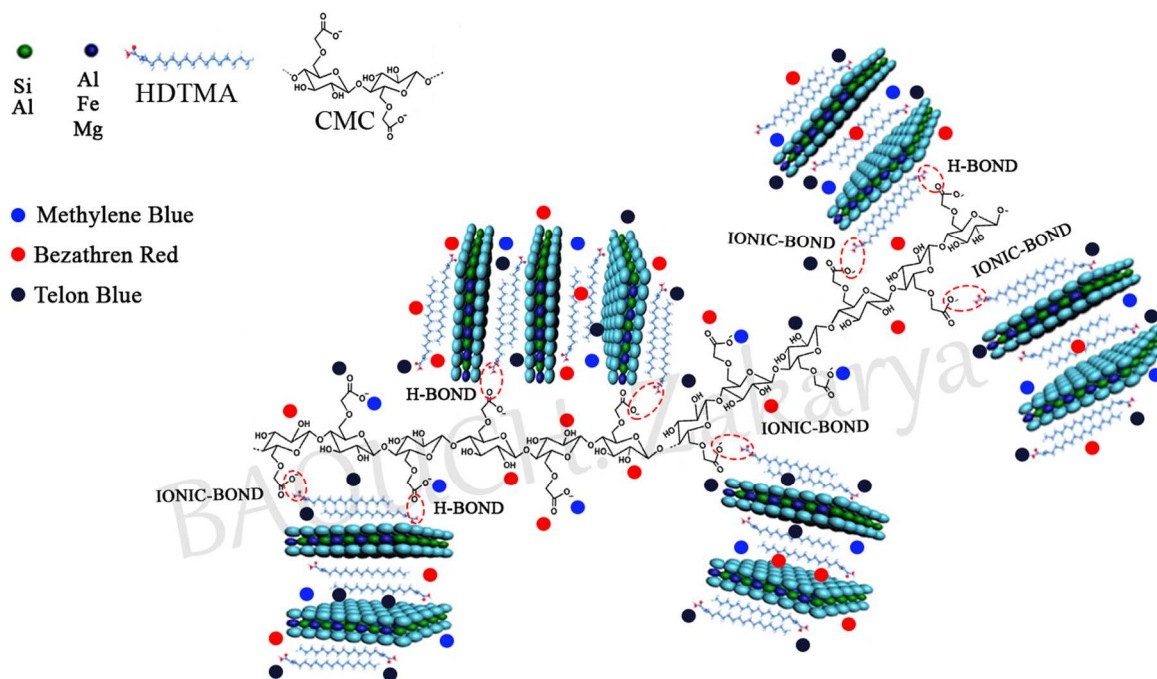
Figure. 8. An illustration for the adsorption of Telon Blue, Bezathren Red and Methylene Blue onto BAS/CMC 0.5/0.025 composite.

REFERENCES

Jung, S. P., & Pandit, S. (2018). Important factors influencing microbial fuel cell performance. In *Biomass, Biofuels, Biochemicals: Microbial Electrochemical Technology: Sustainable Platform for Fuels, Chemicals and Remediation*. Elsevier B.V. https://doi.org/10.1016/B978-0-444-64052-9.00015-7

Martin, E., Savadogo, O., Guiot, S. R., & Tartakovsky, B. (2010). The influence of operational conditions on the performance of a microbial fuel cell seeded with mesophilic anaerobic sludge. *Biochemical Engineering Journal*, *51*(3), 132–139. https://doi.org/10.1016/j.bej.2010.06.006

Saha, P., Khan, M., Deb, T., Sony, S., & Baishnab, A. (2014). Treatment of Textile Dyes by Bio-chemical Process in Stirred Tank Sequencing Batch Bioreactor (STSBBR). *Journal of Chemical Engineering*, *27*(2), 83–87. https://doi.org/10.3329/jce.v27i2.17808

Tincher, W.C. and Robertson, J.R., (1982). Analysis of Dyes in Textile Dyeing Wastewater. *Textile Chemist & Colorist*, *14*(12).

For More information on Wastewater Treatment Methods and COD reduction, Please Scan the QR code below.

General Conclusion

GENERAL CONCLUSION

Wastewater effluents resulted from various industrial activities contain large volume of organic and inorganic pollutants. Their presence pose a serious risk to the ecosystem and human health. Therefore, their removal is of the utmost importance. It has been estimated that the total amount of organic dye consumption in textile industry alone worldwide is more than 10,000 tonnes per year and approximately 2- 20 % of these dyes are discharged into water streams.

Various physical, chemical and biological separation methods are used to treat these aqueous phase pollutants. However, adsorption process is widely used in the removal of organic dyes and inorganic heavy metal ions pollutants from wastewater due to its simple design, ease of operation, cost effective and insensitive to toxic substances. The effects of different physiochemical process parameters such as initial adsorbate concentration, adsorbent dose, solution pH, solution temperature and contact time on adsorption process have been reviewed in Chapter III of this thesis. In addition, Chapter II highlights wide range of adsorbents used in the removal of these pollutants such as agricultural solid waste, modified biomass waste, and activated carbon as well as inorganic clay mineral materials.

This thesis investigates the feasibility of an Algerian Bentonite-based Bio-adsorbent as a cost-effective alternative adsorbent for the removal of industrial dyes. The structural evolution of an Organo-Bentonite (Bentonite modified with different loadings of HDTMA (Hexadecyltrimethylammonium Bromide)) from 50 to 200% of the CEC with CMC (CarboxyMethyl Cellulose) in different percentages is investigated and linked to the adsorption uptake and mechanism of an important industrial dyes called (Methylene Blue (MB), Bezathren Red (BzR) and Telon Blue (TB) in single and mixture system from the aqueous solution. The prepared materials were characterized by X-ray diffraction XRD, infrared spectroscopy measurements FT-IR and thermal analysis ATG/DTG. The intercalation of the surfactant cations (BAS) and the CarboxyMethyl Cellulose (BAS/CMC) in the interlayer spaces of bentonite (BA) was confirmed by the increase of the basal spacing from 1.13 to 1.78 nm and from 1.78 nm to 2.51 nm respectively.

The influence of several factors on the adsorption capacity such as contact time, dye solution pH, adsorbent dosage, initial dyes concentrations, and the temperature was investigated. The kinetic data were found to follow the pseudo second-order model for all dyes adsorption. The equilibrium data were analyzed using the Langmuir and Freundlich models. The Langmuir

isotherm model is the most suitable to describe MB, BzR and TB dyes adsorption. The calculated Langmuir maximum adsorption capacities for BAS adsorbent increased from 74 to 174.52 mg/g for MB and from zero to 107.87 and 306.74 mg/g, for BzR and TB respectively. Also for the BAS/CMC adsorbent, the maximum adsorption capacities increased from 74 to 161.81 mg/g for MB and from zero to 273.22 and 63.65 mg/g, for BzR and TB respectively. The adsorption process was found to be endothermic in all cases (MB, TB, and BzR). It is also important to note that, the particles formed at the end of adsorption changes from powder in the case of BAS to large visible flocs in the case of BAS/CMC.

The prepared BAS/CMC composite were designed to decolorize and to reduce COD content in a mixture of three dyes, i.e., Methylene Blue (MB, cationic dye), Bezathren Red (BzR, vat dye), and Telon Blue (TB, anionic dye) using adsorption process. Optimum pH and the initial concentration of each dye were determined.

The Adsorption experiments were performed on simulated effluent solutions containing equal and different concentrations of MB, BzR and TB dyes. Optimal adsorption conditions were found at pH 8 and a total concentration of 150 mg of dyes mix/L at 24 °C using 75 mg BAS/CMC adsorbent, resulting in a COD reduction of more than 94% and decolorization of about 96%. It is also important to note that percentage of reduced COD is low in the case of the absence of Methylene Blue (43.73%) and very high in the other cases by approximately 88% due to the presence of a synergistic effect and strong electrostatic interactions between Methylene Blue and the two other dyestuffs.

Finally, it can be concluded from this research study, that the adsorbents BAS and BAS/CMC can be considered as a good material for the removal of MB, BzR and TB dyes in single and mixtures systems. Due to the availability, efficiency and low cost of these material, these results are encouraging to be tested and evaluated on an industrial scale with real and more complex wastewater.

▪ RECOMMENDATIONS AND FUTURE RESEARCH DIRECTION

The feasibility of the of Bentonite clay and the synthesized Organo-Bentonite and Organo-Bentonite/Carboxymethyl Cellulose based Bio-adsorbents in the removal of organic MB, BzR, and TB dyes were thoroughly examined in this research study. However, future study should be carried out to improve and examine other process conditions in order to evaluate the use of these adsorbents in real industrial applications. The list as shown below is not meant to

be complete. It only indicates selected aspects and future research directions that currently considered to be important.

✓ First of all, we regret that we have not been able to perform BET analyses since July 2018 to date on January 2021 due to numerous obstacles, and unfortunately, we cannot see the evolution of the pore volumes and the specific surface of the prepared composites. This analysis will be performed when operational equipment is found and the results will be published in a new paper.

✓ The applicability of these adsorbents should be extended to the removal of heavy metals and a mixture of dyes and heavy metals as well.

✓ Real industrial effluents contain wide range of organic and inorganic pollutants simultaneously therefore, it is recommended to use real wastewater sample as adsorbates.

✓ It is very important to produce effective and low-cost bio-adsorbents which can work effectively under natural conditions such as neutral pH, normal temperature with fast reaction time (less than 1 hour). Therefore, more experiments should be performed in this direction.

✓ The final waste disposal or reuse of the adsorbents and the captured dyes and valuable compounds has to be studied, i.e. there needs to be a methodology applied regarding what to do with the used adsorbent and the captured compounds attached to it.

✓ Naturally, the regeneration of the adsorption materials needs to be studied. However, if the material is easy to produce at relatively low cost, regeneration might not be reasonable, but instead, if the pollutants are held strongly by the material, it could be used for other purposes such as in construction materials e.g. when building roads.

✓ The final challenge, after gaining knowledge of the adsorption process and the importance of photocatalysis in the field of water treatments, a collaboration is needed to study the possibility of combining adsorption and photocatalysis in a hybrid technique. Some of the drawbacks of the individual techniques can be overcome by some characteristics of other techniques, and the benefits of each process can be consolidated, and thus the sustainability and process efficiency can be improved by hybrid methods.

- **TGA and DTGA Thermograms of BA, BAS, and BAS-CMC composites at different CMC percentages**

APPENDIX

- **TGA and DTGA Thermograms of BA, CMC, and BAS-CMC composites at different organophilic ratios.**
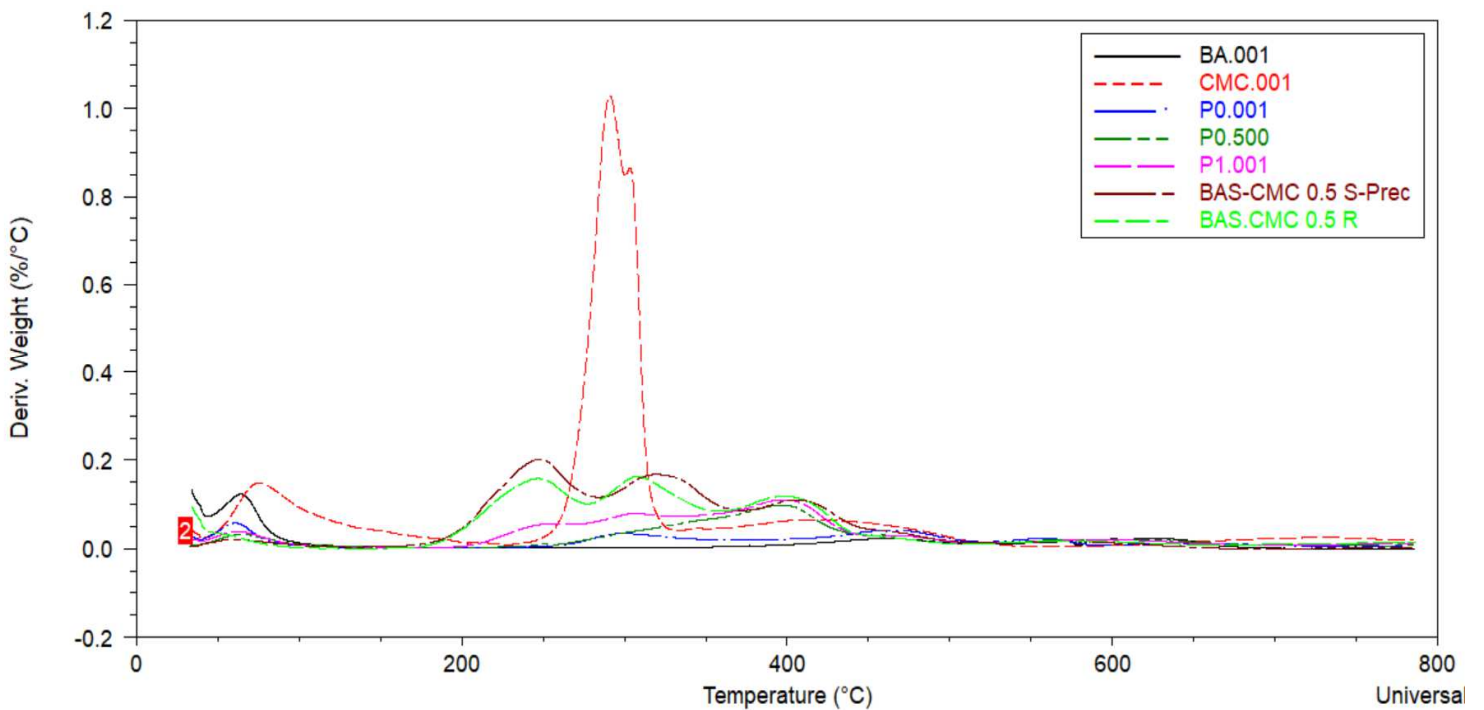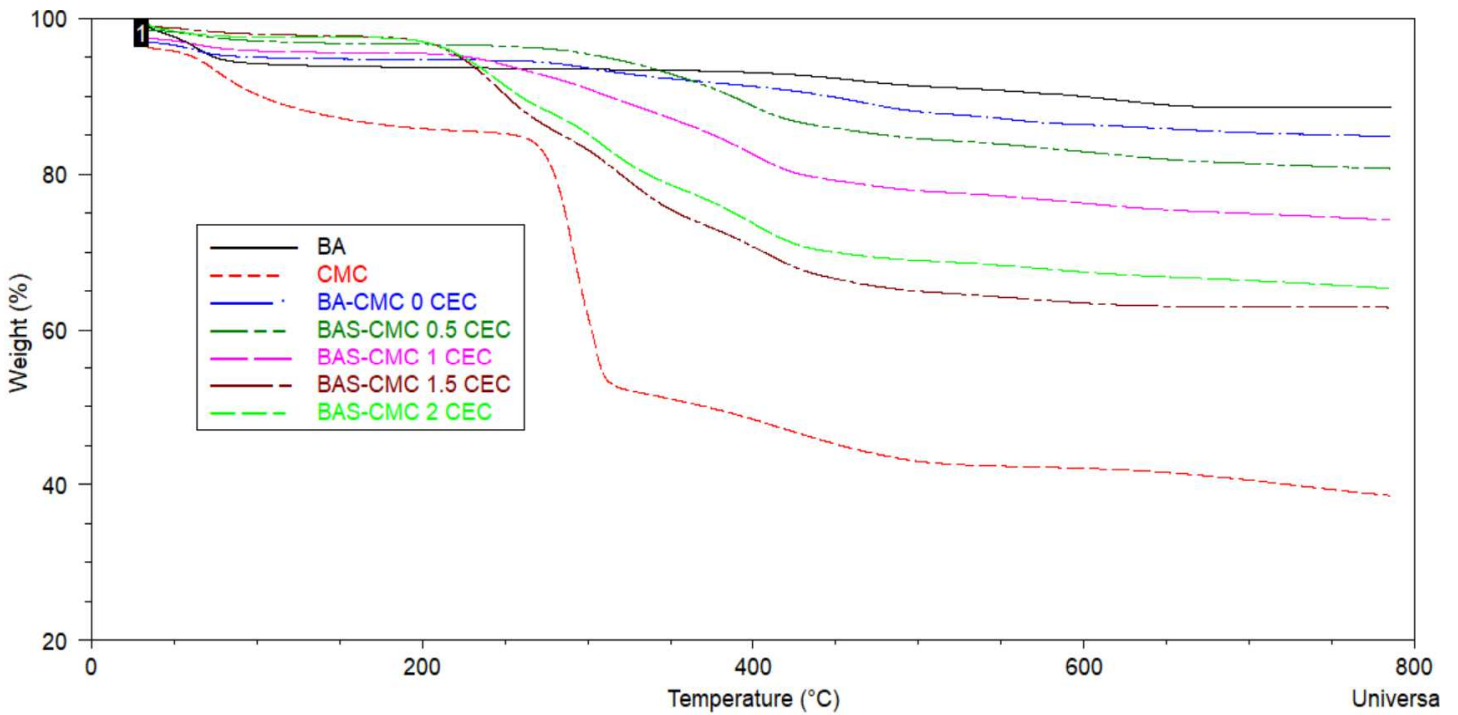
APPENDIX

- **FTIR spectrums of BA, BAS, and BAS-CMC composites at different CMC percentages**
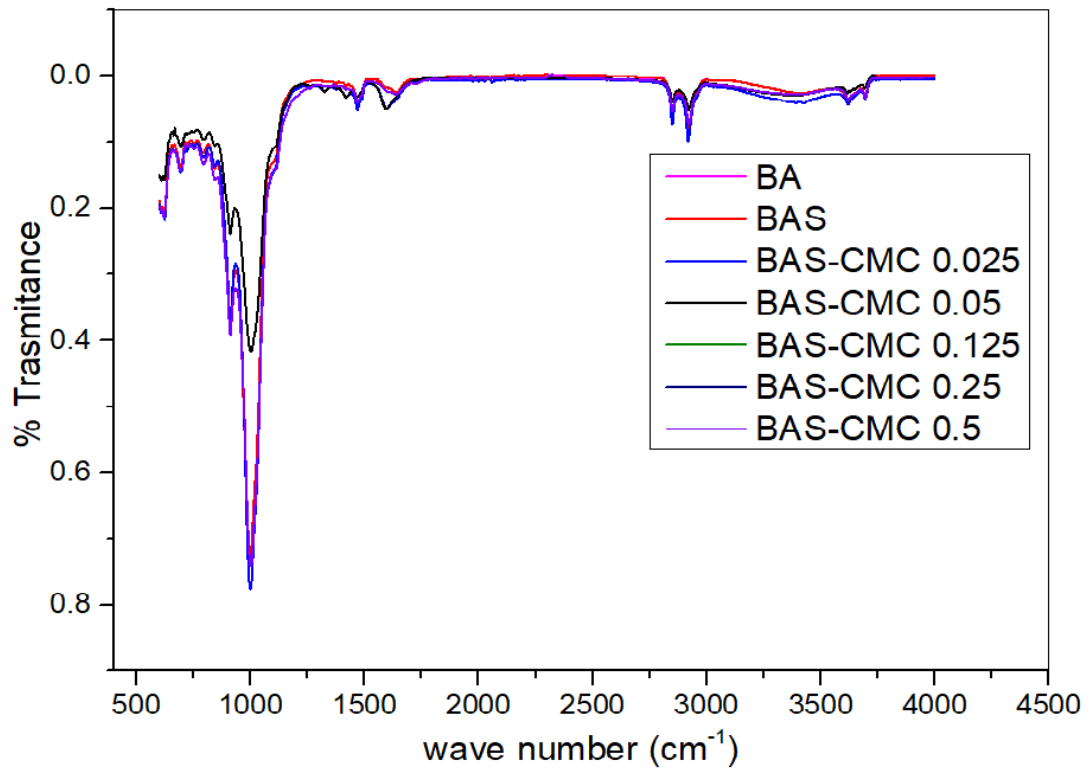
- **The calibration curve of Methylene Blue (MB)**
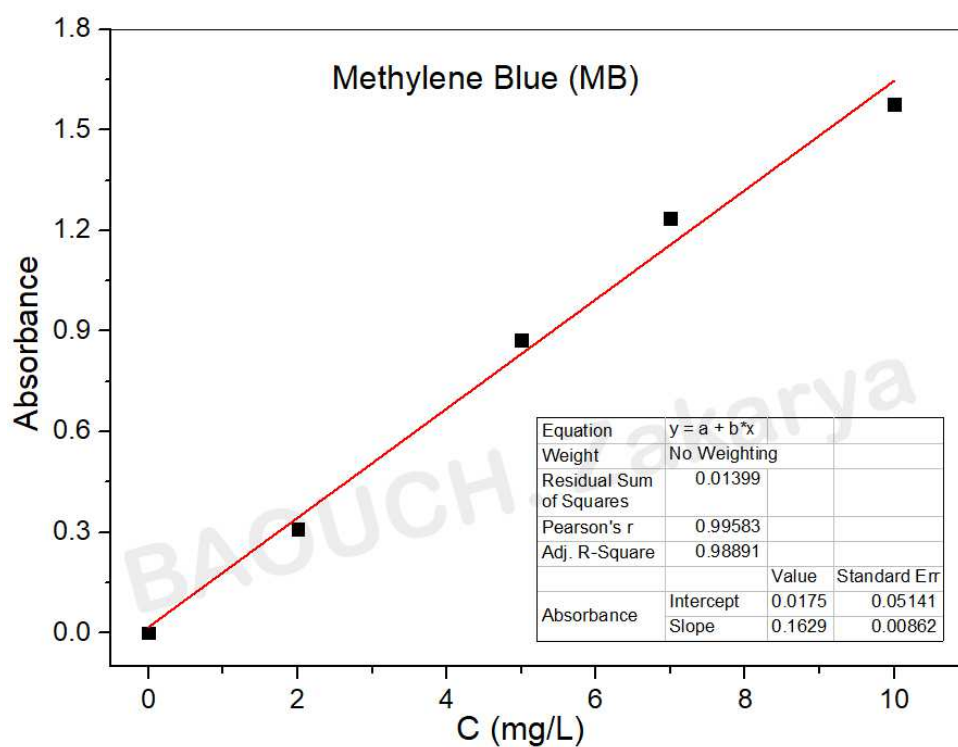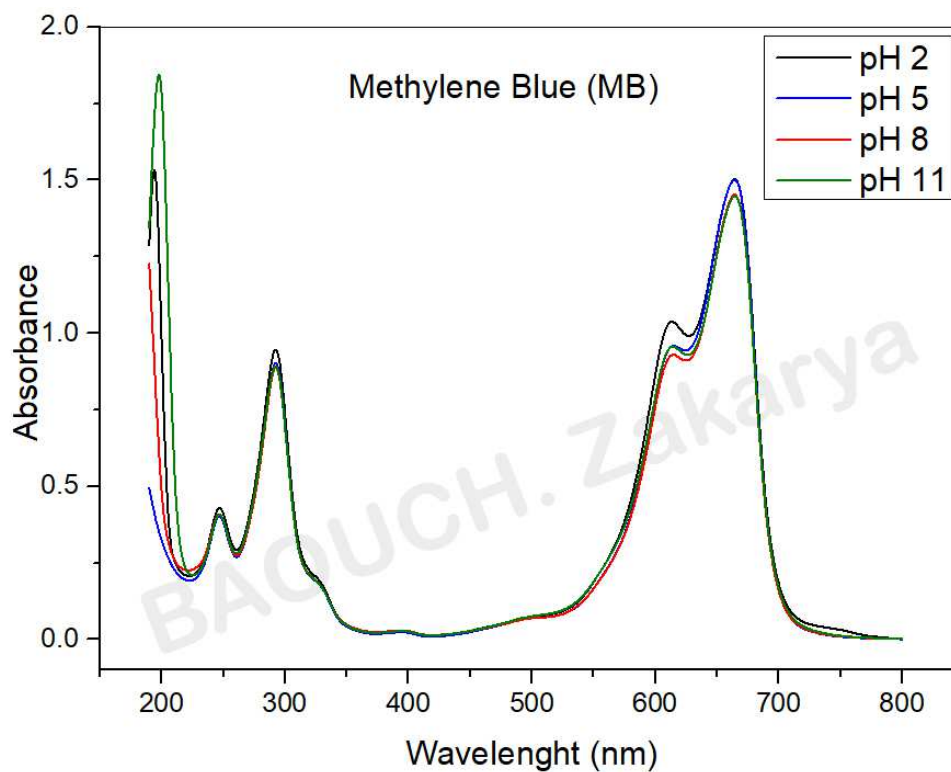
- **The calibration curve of Bezathren Red (BzR)**

Bezathren Red (BzR)

Bezathren Red (BzR)

Equation	y = a + b*x		
Weight	No Weighting		
Residual Sum of Squares	9.1E-6		
Pearson's r	0.99997		
Adj. R-Square	0.99992		
		Value	Standard Error
Absorbance	Intercept	-0.0019	0.00183
	Slope	0.00605	2.75379E-5
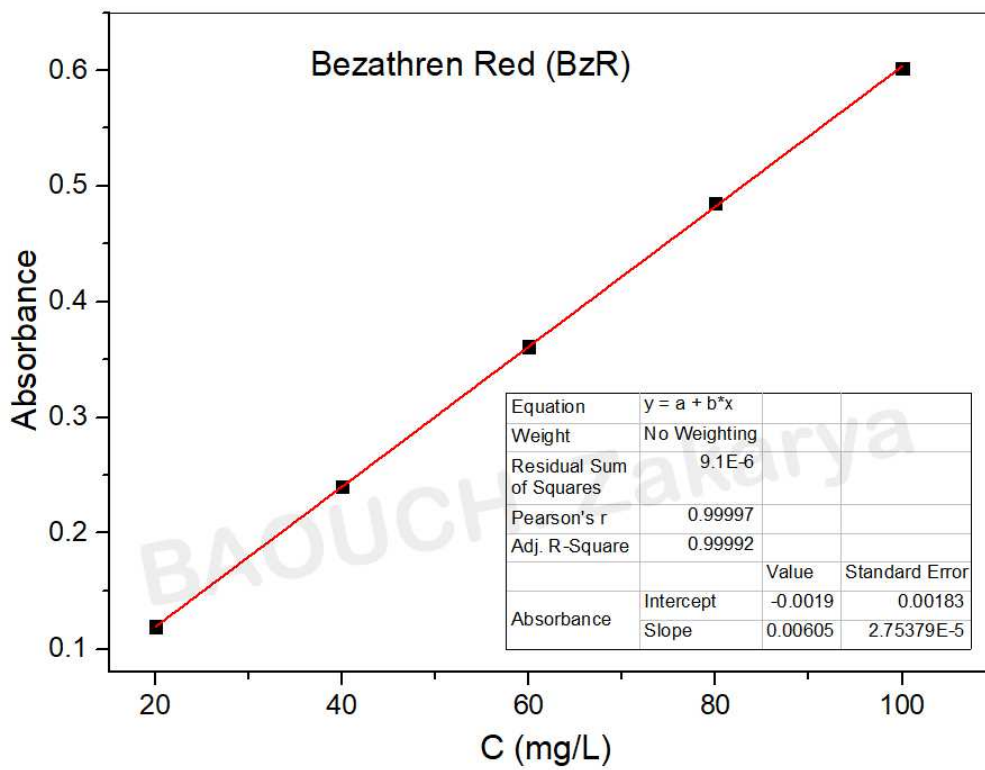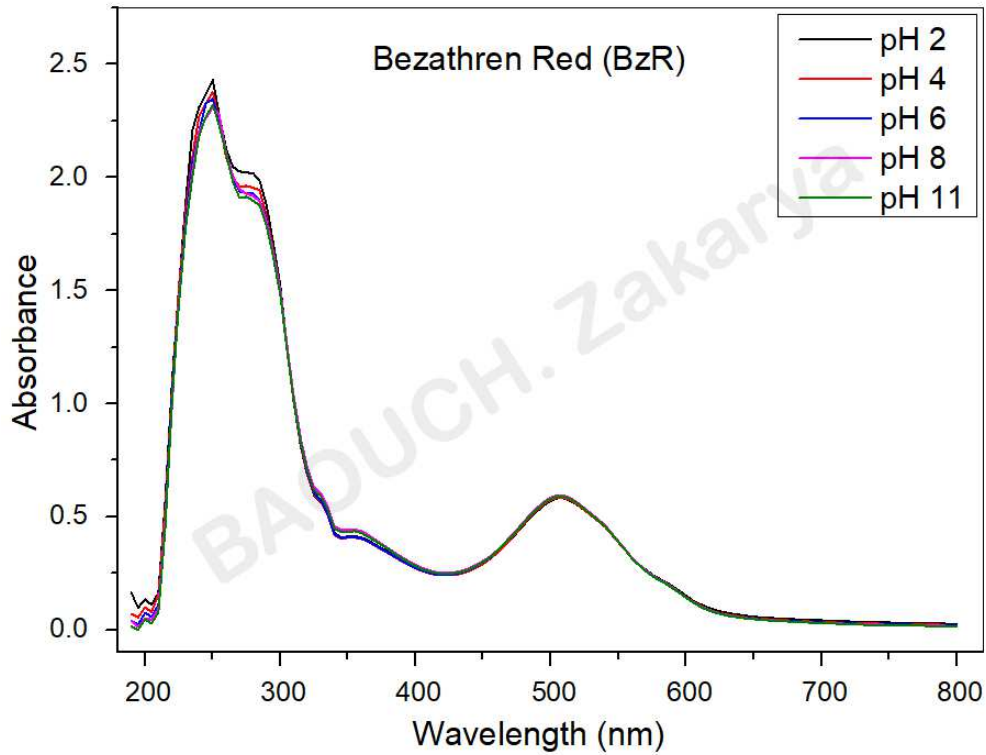
- **The calibration curve of Telon Blue (TB)**

TELON BLUE (TB)

TELON BLUE (TB)

Equation	y = a + b*x		
Weight	No Weighting		
Residual Sum of Squares	0.00741		
Pearson's r	0.99904		
Adj. R-Square	0.99783		
		Value	Standard Erro
Absorbance	Intercept	0.0293	0.01962
	Slope	0.0203	3.16621E-4
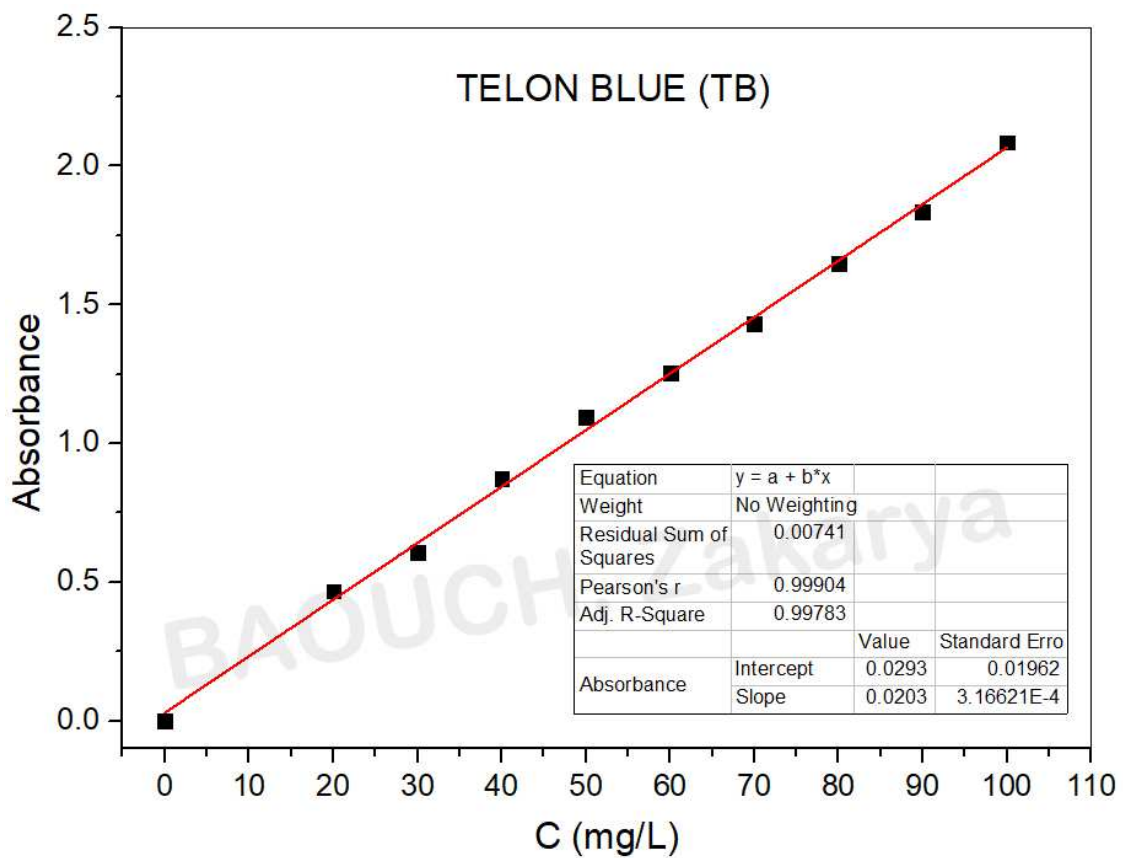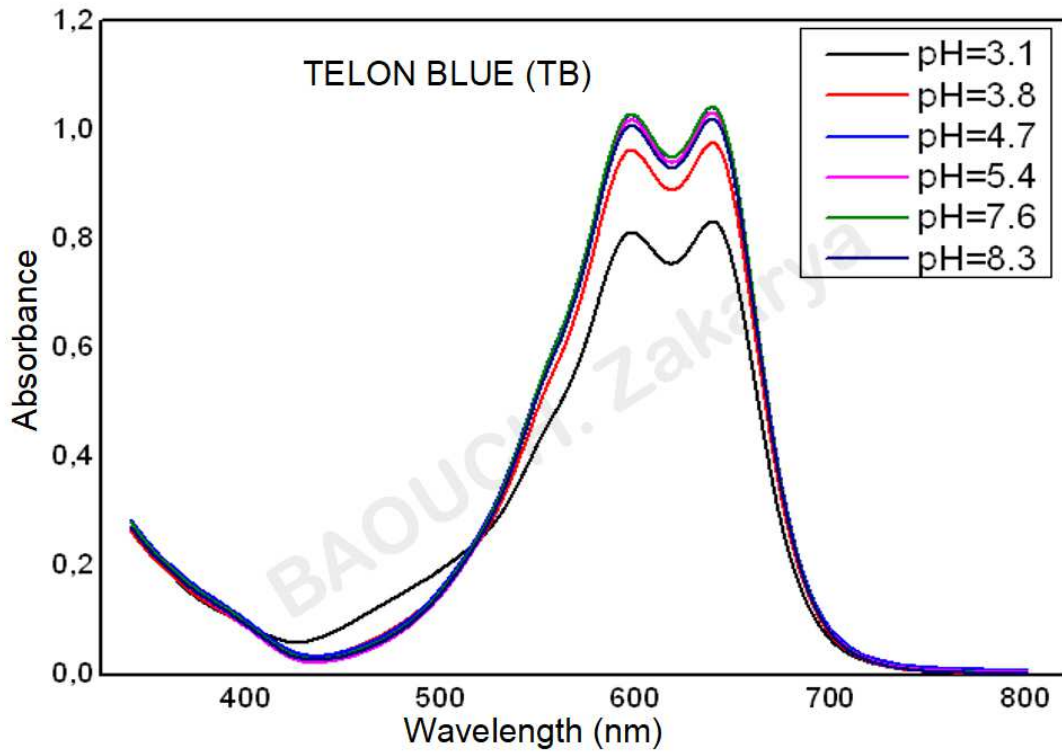
APPENDIX

The Copyrights of the images used in the bibliography section:

Thank you for your order!

Dear Mr. Baouch Zakarya,

Thank you for placing your order through Copyright Clearance Center's RightsLink® service.

Order Summary

Licensee:	Algeria, Tlemcen
Order Date:	Mar 17, 2020
Order Number:	4791290138266
Publication:	Applied Clay Science
Title:	Exfoliation of montmorillonite and related properties of clay/polymer nanocomposites
Type of Use:	reuse in a thesis/dissertation
Order Ref:	Fig. 1. Schematic representation of the Mt structure
Order Total:	0.00 USD

View or print complete details of your order and the publisher's terms and conditions.

Sincerely,

Copyright Clearance Center

Tel: +1-855-239-3415 / +1-978-646-2777
customercare@copyright.com
https://myaccount.copyright.com

Thank you for your order!

Dear Mr. Baouch Zakarya,

Thank you for placing your order through Copyright Clearance Center's RightsLink® service.

Order Summary

Licensee:	Algeria, Tlemcen
Order Date:	Nov 5, 2020
Order Number:	4942551372558
Publication:	Applied Clay Science
Title:	Heating-freezing effects on the orientation of kaolin clay particles
Type of Use:	reuse in a thesis/dissertation
Order Ref:	DOI: 10.1016/j.clay.2017.09.028
Order Total:	0.00 USD

View or print complete details of your order and the publisher's terms and conditions.

Sincerely,

Copyright Clearance Center

Tel: +1-855-239-3415 / +1-978-646-2777
customercare@copyright.com
https://myaccount.copyright.com

Baouch Zakarya — Jul 15, 2020

Hello Dr.Matthieu, I am Mr. BAOUCH Zakarya from Algeria, I am a Ph.D. Student in chemistry, I came here to ask you the permission to use one of your figures in my thesis named " Figure II.1.1. Isothermes d'adsorption-désorption classiques observés dans la littérature".
Cordialement.

Matthieu Lépinay to you — Aug 10, 2020

Hello Zakarya,

Sorry for the delay, I don't spend much time on ResearchGate...
No problem for me, you can use these figures.
A reference would be nice of course :)

Good luck with your thesis !
Best regards,
Matthieu

APPENDIX

Should you need any further information about my thesis or related work, please do not hesitate to contact me. You can find as below…

E-MAIL

zakarya.baouch@univ-tlemcen.dz

RESEARCHGATE:

https://www.researchgate.net/profile/Baouch_Zakarya

LINKEDIN:

https://www.linkedin.com/in/zakarya-baouch-a2632b115/

INSTAGRAM:

https://www.instagram.com/baouch.zakarya/

FACEBOOK:

https://www.facebook.com/baouch.zakarya

Or you can just scan the QR code below

Adsorption of Different Dyes from Aqueous Solutions Using Organo-clay Compposites

Z. Baouch, K.I. Benabadji* and B. Bouras

Laboratory of Organic Electrolytes and Polyelectrolytes Application (LAEPO). Department of Chemistry, Faculty of Sciences, Tlemcen University, B. P. 119 13000 Tlemcen, Algeria

(Received 10 June 2020, Accepted 19 August 2020)

The structural evolution of cost-effective organo-clays; _i.e._, bentonite modified with various loadings of hexadecyltrimethylammonium bromide (HDTMA-Br), from 50 to 200% of the cationic exchange capacity, labeled as BAS 0.5, BAS 1, BAS 1.2, BAS 1.5 and BAS 2, was investigated. The materials BAS were prepared and then characterized by X-ray diffraction (XRD), infrared spectroscopy (FTIR), and thermal analysis (ATG/DTG). The increase in the basal spacing, from 1.13 to 1.78 nm, was a sufficient confirmation that the surfactant cations were intercalated within the interlayer spaces of bentonite (BA). Batch adsorption experiments were performed to evaluate the adsorption efficiencies of Methylene Blue (MB), Bezathren Red (BzR) and Telon Blue (TB) dyes on the surfactant-modified bentonite from an aqueous solution. Moreover, the effects of several factors, such as the contact time, pH of dye solution, adsorbent dosage, initial dye concentrations, and temperature, on the adsorption capacity were investigated. In addition, the kinetic data were found to follow the pseudo second-order model for the adsorption processes of all three dyes. Afterwards, the equilibrium data were analyzed using the Langmuir and Freundlich isotherm models, and the Langmuir isotherm model turned out to be the most suitable to describe the adsorption of these dyes. It is worth indicating that the calculated Langmuir maximum adsorption capacities increased from 74 to 166.67 mg g^{-1} for Methylene Blue, from zero to 111.1 mg g^{-1} for Bezathren Red, and from zero to 500 mg g^{-1} for Telon Blue. The adsorption process was found to be endothermic in nature, in all cases.

Keywords: Inorganic/organic hybrid materials, Adsorption mechanism, Cationic, Anionic, Vat dyes

INTTRODUCTION

One of the major future challenges facing humanity is to secure the supply of clean water to the world population. It is widely admitted that population growth and pollution have a strong impact on water quality. Indeed, nowadays, dyes utilized in industrial activities are increasingly becoming a problematic class of pollutants to the environment. Due to the complex structure of dyes, their discharge to water bodies engenders bad aesthetic and health consequences [1]. Over the last few years, several classes of dyes have been used in many industrial sectors such as rubber, textiles, cosmetics, plastics, leather, food

and paper making [2]. Wastewater discharged from these industries contains a variety of dyes and the majority of them are stable to light, heat and oxidizing agents and are usually non-biodegradable [3], hence the urgent need to remove them from the environment. Dyes can be classified as cationic, anionic, and nonionic (disperse/vat). These three kinds of dyes are the most widely used dyes in many industries. Due to their complex structures, they are not easily biodegradable and can therefore have destructive impacts on the environment [4]. Today, adsorption is viewed as a viable procedure for the removal of dyes from the environment; it is a simple process that is economically feasible and can help to recycle the adsorbents without any harmful residues. Indeed, a large number of studies have investigated the use of various adsorbents intended for the

*Corresponding author. E-mail: bismetdz@yahoo.fr

purpose of reducing dye concentrations in aqueous solutions. Materials like walnut husk [5], modified chitosan composite [6], biochars from crop residues [7], natural zeolite [8], cross-linked succinyl chitosan [9], modified bentonite [10], quaternized poly(4-vinylpyridine) copolymers [11], natural clinoptilolite [12], activated carbon [13], chromium-intercalated montmorillonite [14] and metal oxides [15-18] have been used to remove dyes from aqueous solutions. Clays, such as bentonite, have exhibited high removal efficiency; it was found that their adsorption capacities may exceed that of activated carbon, under the same temperature and pH conditions [19]. The adsorption and desorption of organic molecules on clays depend primarily on the surface properties of these materials and on the chemical properties of their molecules as well [20]. Note that the net negative charge on clays provides them with a high adsorption capacity toward positively charged cations such as cationic dyes, heavy metals, *etc*. However, clays have a poor affinity for negatively charged anionic dyes. It is worth indicating that a simple modification of clays can help to improve their adsorption capacities by the use of cationic polymers or surfactants through straightforward ion-exchange reactions which generate some interactions between the cationic species and the adsorbate [21]. Previous studies have shown that the removal of acid dyes can be better enhanced by the use of modified montmorillonite, in comparison with untreated montmorillonite. It is worth mentioning that modified montmorillonites have previously been prepared and used for Congo red dye adsorption. It was also found that the adsorption efficiency is influenced by the length of alkyl chains present in a series of alkyl ammonium bromides [22]. Several authors have successfully modified montmorillonite using some unconventional modifiers [23], such as gemini surfactants, for the adsorption of organic contaminants [24]. The results obtained showed that the adsorption capacity of surfactant-modified montmorillonites for organic contaminants was greatly improved in comparison with that of natural montmorillonite. The present work aims to investigate the possibility of interposing HDTMA-Br molecules into clay for the purpose of obtaining BAS materials. A BAS is employed as an adsorbent for the removal of three kinds of dyes, namely Methylene Blue

(cationic dye), Telon Blue (anionic dye), and Bezathren Red (nonionic dye), from aqueous solutions. Optimization of the adsorption conditions was possible by investigating the influence of different parameters. The equilibrium data obtained were then assessed using various adsorption isotherm models. Some kinetic studies were also conducted in order to evaluate the adsorption mechanism.

EXPERIMENTAL

Materials

The hexadecyltrimethylammonium bromide (HDTMA-Br) was purchased from Sigma Aldrich (99% purity) and used as received. Sodium chloride (NaCl) was provided by Aldrich and used without further purification. Likewise, Methylene Blue (MB), Bezathren Red (BzR) and Telon Blue (TB) were purchased from Sigma-Aldrich and utilized without further purification. Some specific characteristics of these three dyes are summarized in Table 1.

Bentonite Sample

The starting material used in this study was natural bentonite (NB), provided by the National Company of Non-Ferrous Mining Products and Useful Substances (ENOF-Algeria). Natural bentonite, which is essentially composed of montmorillonite (80%), contains a large number of impurities. The chemical composition of natural bentonite (NB) was determined by X-ray fluorescence (XRF) spectrometry, and the data obtained are reported in Table 2.

Raw bentonite was purified under laboratory conditions [25]. In order to remove impurities, such as carbonates, quartz, and organic matter, the bentonite was dispersed in bidistilled water, and the clay fraction ($< 2 \mu m$) was recovered through sedimentation. In order to obtain sodium bentonite, the solid phase was then saturated with sodium ions in a 1 M sodium chloride solution and stirred; this operation was repeated three times. When saturation was achieved, the resulting solid was washed with bidistilled water several times in order to remove excess salt; the final product was sodium bentonite (BA). Then, the hexamminecobalt (III) chloride was used to determine the cation exchange capacity (CEC) which was found equal to 85 meq g/100 g.

Table 1. Physicochemical Characteristics of Dyes Used in this Study
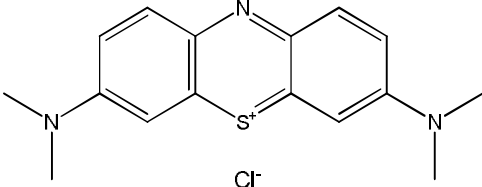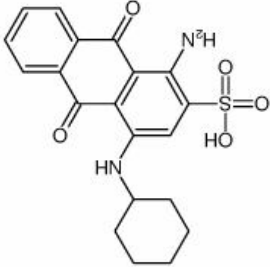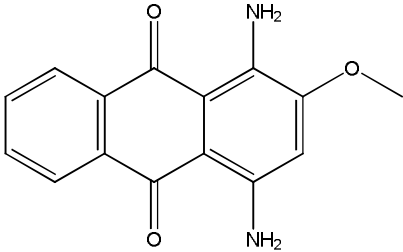
Name	Molecular structure	Nature	M_w (g mol^{-1})	λ_{max} (nm)
Methylene Blue (Basic Blue 9)		Cationic	319.851	664
Telon Blue (Acid Blue 62)		Anionic	400.44	640
Bezathren Red FBB EPS (Disperse 11)		Disperse	268.272	505

Table 2. Chemical Composition of Natural Bentonite

Species	SiO_2	Al_2O_3	Fe_2O_3	CaO	MgO	Na_2O	K_2O	TiO_2	LOI
%(w/w)	65.2	17.25	2.10	1.20	3.10	2.15	0.60	0.20	8.20

Preparation of Organo-clays (BAS)

The amount of 2 g of sodium bentonite (BA) was dispersed into 50 ml of distilled water. Then, 200 ml of the HDTMA-Br solution was added dropwise to this suspension, and the mixture was shaken using a mechanical shaker for 4 h at 80 °C. Note that the initial amounts of HDTMA-Br in the aqueous phase were equivalent to various percentages of CEC (from 50 to 200 meq g/100 g BA). The resulting material was centrifuged at 4000 rpm, for 30 min, to yield a clear supernatant. Afterwards, the solid was washed several times with warm distilled water, until complete disappearance of bromide anions, as indicated by the silver nitrate ($AgNO_3$) test. Next, the ensuing organo-clay was dried at 60 °C, then crushed and

sieved for particles less than 100 μm. The organo-clays obtained were labeled as BAS 0.5, BAS 1, BAS 1.2, BAS 1.5 and BAS 2, according to the percentage of CEC.

Batch Adsorption Studies

The adsorption capacities of the prepared composites for MB, TB and BzR dyes were evaluated using a batch equilibrium procedure. For doing so, the stock dyes solutions (1000 mg l^{-1}) were first prepared by dissolving MB and TB in deionized water. For the vat dye BzR, a sodium hydroxide solution and hydrosulfite salts were used for the preparation of the aqueous solution. The stock solutions were then diluted in deionized water to achieve the desired concentration ranges. Subsequently, the dried sample (25 mg) was immersed in each dye solution (40 ml). The dye solutions containing the adsorbents were then shaken at 400 rpm. Finally, each solution was centrifuged at 4000 rpm for a period of 15 min, and the ensuing supernatant was analyzed using a UV-Vis spectrophotometer (OPTIZEN 1412 UV/VIS) at their maximum wavelengths (664, 495 and 505 nm for MB, TB and BzR, respectively).

Furthermore, adsorption experiments were conducted in conical flasks, at a constant agitation speed of 400 rpm, while varying the pH of the solution from 2 to 11, the adsorbent dosage from 10 to 100 mg, the contact time from 2 to 180 min, the initial dye concentration from 5 to 200 mg l^{-1} and the temperature from 25 to 50 °C.

The adsorption capacity and removal efficiency of the prepared composite were calculated based on the initial and final concentrations of dyes present in the solution, using the following Eq. (1):

$$q_e = \frac{(C_0 - C_e) \cdot V}{m} \tag{1}$$

where C_0 and C_e are the initial and equilibrium dye concentrations, respectively, V is the volume of dye aqueous solution (l) and m is the mass of adsorbent (g).

Characterization

The XRD patterns of the samples were obtained with X-ray diffractometer ULTIMA IV (Rigaku, Tokyo, Japan), operating with Copper K$_\alpha$ radiation (λ = 1.54 Å) at 40 kV

and 30 mA. All experiments were carried out at ambient temperature with 2θ varying between 2 and 40°, a scan speed of 2°/min and a step size of 0.02°.

Infrared (IR) spectra of the samples were obtained using an Agilent Cary 600 Series FTIR Spectrometer equipped with DRIFT (diffuse reflectance infra-red Fourier transform) spectroscopy. Spectra over the 4,000-400 cm^{-1} range were obtained by the co-addition of 64 scans with a resolution of 4 cm^{-1} and a mirror velocity of 0.6329 cm s^{-1}.

Thermogravimetric analyses of the samples were obtained using High-resolution TGA (TA Instruments Q Series Q600 SDT). 10 mg of finely ground sample was heated in an open platinum crucible with a heating rate of 10 °C min^{-1} and temperature from 50 to 800 °C under a nitrogen atmosphere flow rate of 100 ml min^{-1}.

Determination of pH$_{pzc}$

The point of zero charge (pH$_{pzc}$) is the pH for which the net surface charge of the adsorbent is equal to zero. This is an important parameter in determining the adsorption capacity of the surface and the type of surface active centers. In the present work, the pH$_{pzc}$ of the adsorbent (BA and BAS 1.5) was determined using a batch equilibrium method, following the procedures previously outlined by Monvisade *et al.* [26].

RESULTS AND DISCUSSION

X-Ray Diffraction

The X-ray diffraction patterns of the absorbents BA and BAS are presented in Fig. 1a, while the variation of the interlamellar distance (Δd) as a function of the amount of intercalated surfactant molecules is depicted in Fig. 1b.

The interlayer spacing values d$_{(001)}$ of the parent BA and of BAS clay samples were determined using low-angle XRD. For BA, as can be seen in Fig. 1a, a broad peak was observed at 2θ = 7.76° which corresponds to montmorillonite. This result suggests an interlamellar distance d$_{(001)}$ of 11.37 Å. For BAS 0.5 sample (Fig. 1a), corresponding to 0.5 CEC of BA, a sharp peak was observed at 2θ = 6.58°, which corresponds to d$_{(001)}$ = 13.41 Å. Upon the addition of HDTMA molecules, the peak positions shifted to lower angles, in accordance with the HDTMA loading. A displacement of the angle 2θ
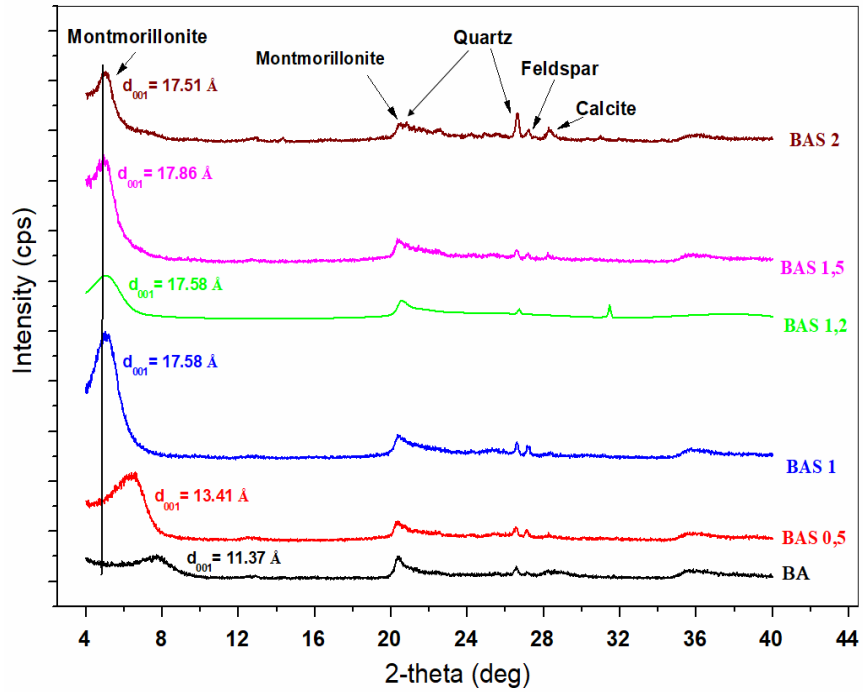
(a)
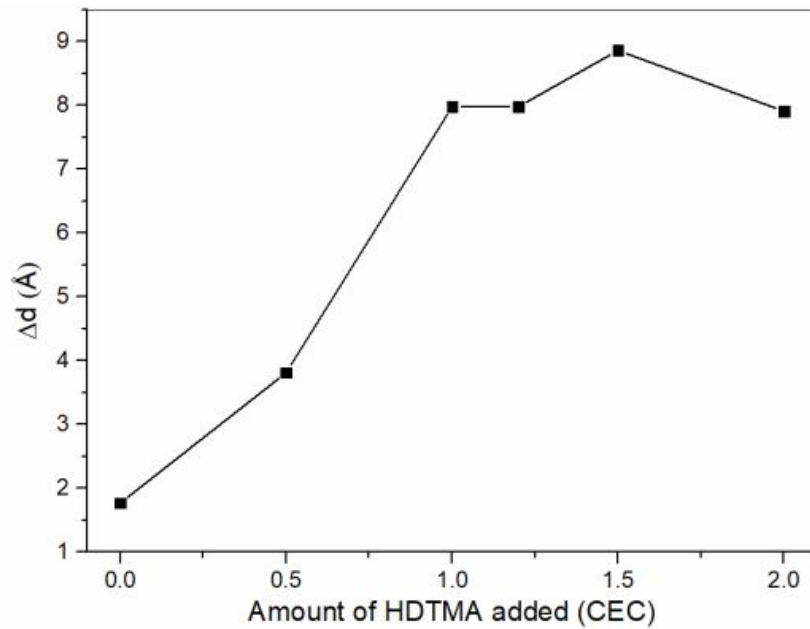
(b)

Fig. 1. XRD analysis of BA and BAS samples and values of their interlamellar distances $d_{(001)}$ at different surfactant concentrations (a) and Δd (b).

was observed from 7.76° to 5.04° with an increase in $d_{(001)}$ values from 11.37 Å for BA to 17.86 Å for the organophilic clay BAS 1.5, confirming the intercalation of ammonium ions in the interlayer space [27]. However, for higher HDTMA loadings, the peak position remained nearly constant, which means that a saturation limit was reached for the intercalation of the HDTMA molecules inside the BA material. These findings are in accordance with the FTIR and TGA results.

A cation exchange process was used to compensate for the excess negative charges, and the sodium ions were replaced by the positively charged surfactant molecules. The thickness of a layer in a single unmodified montmorillonite structural unit was considered to be equal to 9.6 Å [28]. By subtracting the thickness of the single montmorillonite unit (9.6 Å) from the $d_{(001)}$ spacing of the surfactant-modified clay, the interlamellar spacing Δd, occupied by the HDTMA molecules, can be deduced. It is worth noting that the Δd values increased from 3.81 Å in the case of BAS 0.5 to reach 8.26 Å in the case of BAS 1.5; it then remained almost unchanged with greater HDTMA loadings (Fig. 1b).

Infrared Spectroscopy

The IR spectra of BA and BAS, depicted in Fig. 2a, indicate that modification of clay was successfully achieved. It should be noted that the FTIR spectra were characterized by an important absorption band reduction, between 3300 and 3750 cm^{-1}, indicating the new hydrophobic behavior of the BAS samples. The bands corresponding to hydroxyl groups indicated the progressive replacement of water molecules by those of the cationic surfactant [29].

The presence of cationic surfactant molecules in BAS composites was confirmed by the appearance of new absorption bands. The spectra (Fig. 2a) showed additional absorption bands, at 2927 cm^{-1} and 2854 cm^{-1}, which are assigned to the asymmetric and symmetric stretching vibrations of -CH_2 groups, respectively.

Another new band appeared at 1464 cm^{-1} was attributed to the bending vibrations of methyl group C-H in the ammonium groups.

When the surfactant loadings were increased, the peak intensity and peak area of the absorption bands at 2927 cm^{-1}

and 2854 cm^{-1} for BAS samples became stronger and sharper, exhibiting a sudden initial increase in the incorporation of HDTMA molecules. By increasing the amount of HDTMA loading, these bands shifted towards lower frequencies (Fig. 2b), suggesting a transition from a disordered liquid-like conformation of alkyl chains at low HDTMA loadings to a more ordered state at higher loadings where the modifier alkyl chains exhibited highly ordered all-trans conformations [30].

Thermogravimetric Analysis

In order to investigate the structural properties of modified clays and to estimate the surfactant adsorbed onto sodium bentonite, some thermogravimetric analysis (TGA) experiments were conducted under a nitrogen atmosphere. The TGA and DTG results obtained, presented in Fig. 3a and 3b, indicate that unmodified sodium bentonite (BA) exhibited a mass loss of 5.31% at 64 °C, corresponding to the loss of the interlayer water. A second mass loss of 5.26%, between 170 °C and 800 °C, was related to the dehydration of the BA layers, including condensation of both the intralamellar Al(OH) and structural Al(OH) in clay [31]. The TGA and DTG data of all BAS samples showed a similar degradation profile (Fig. 3a), indicating the presence of both surface bound and intercalated organic modifiers. However, for BAS 0.5 sample, only one peak at around 407 °C was observed, suggesting that at low modifier loadings, intercalation occurs only within the BA interlayers. For BAS samples, the resulting thermograms suggested the occurrence of additional weight losses within the temperature range between 170 and 460 °C. The corresponding degradations could not be observed in the thermogram of the BA sample. These findings indicate that the surfactant molecules adsorbed onto the external surface of the BA sample and intercalated in the interlayer spaces helped to improve the thermal stability of the corresponding composites [32]. Note also that the DTG curves of surfactant-modified sodium bentonite samples (BAS 0.5, BAS 1, BAS 1.2, BAS 1.5 and BAS 2) presented four kinds of weight losses (Table 3). The first one was assigned to the vaporization of free water. It is worth indicating that when the HDTMA loading goes up, these weight losses get smaller. Moreover, the presence of Alkylammonium leads to the conversion of hydrophilic surfaces to hydrophobic
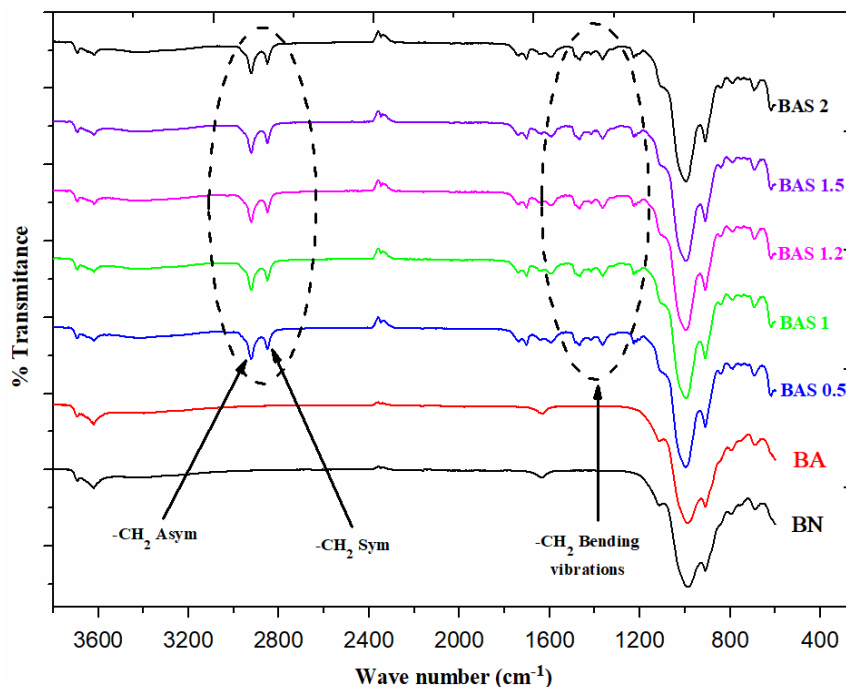
(a)
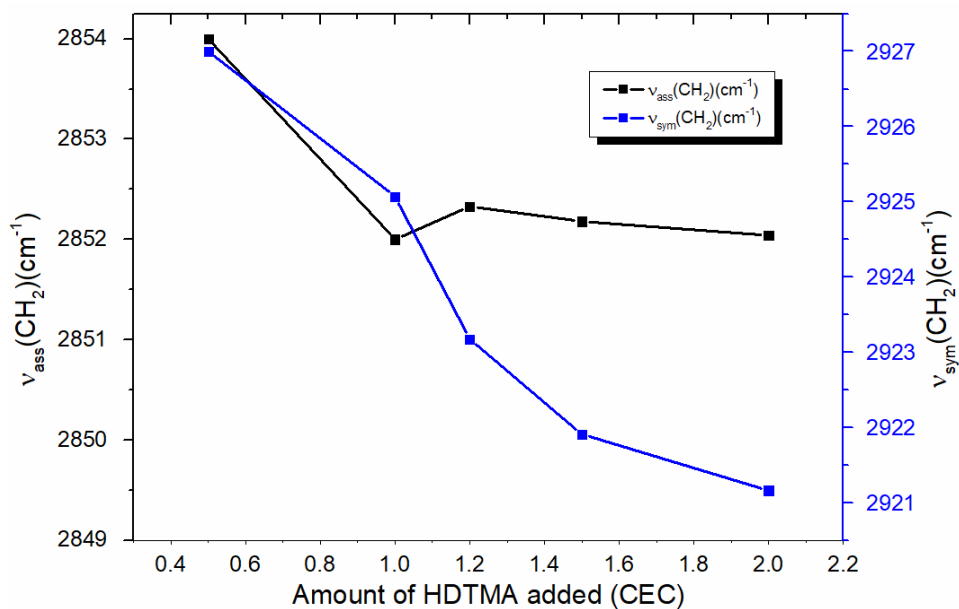
(b)

Fig. 2. (a) IR spectra of BN, BA and BAS samples. (b) Variation of vas(-CH$_2$-) and vs. (-CH$_2$-) as a function of HDTMA loading.
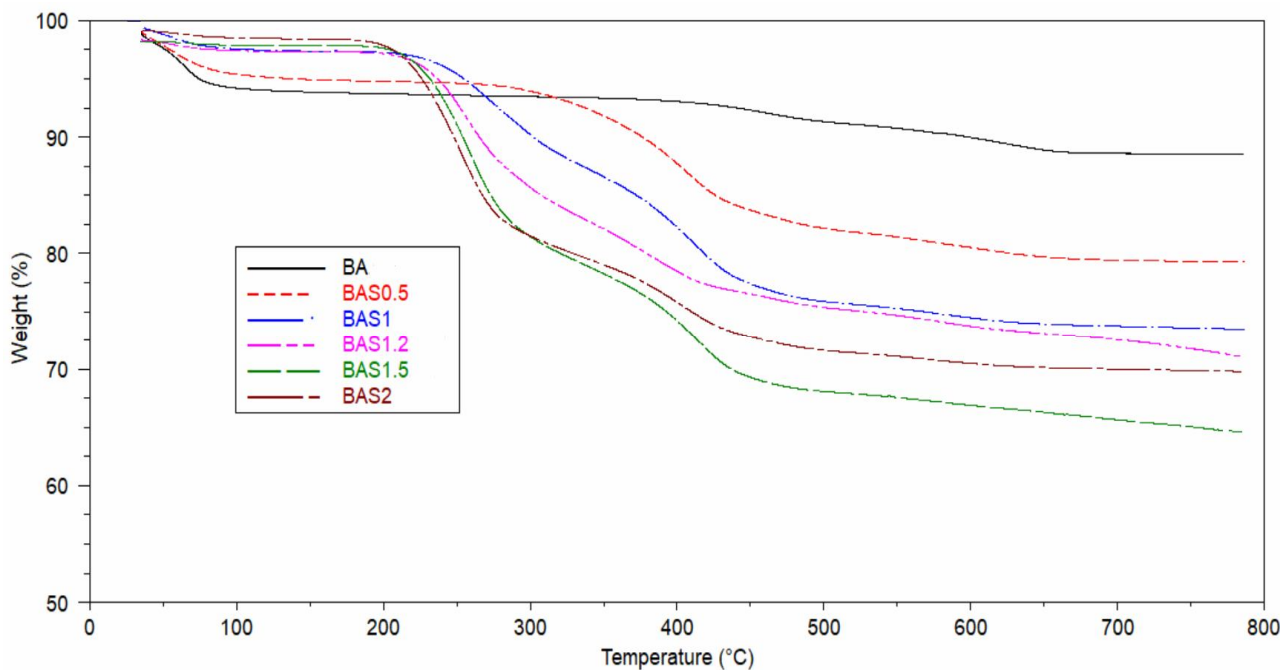
(a)
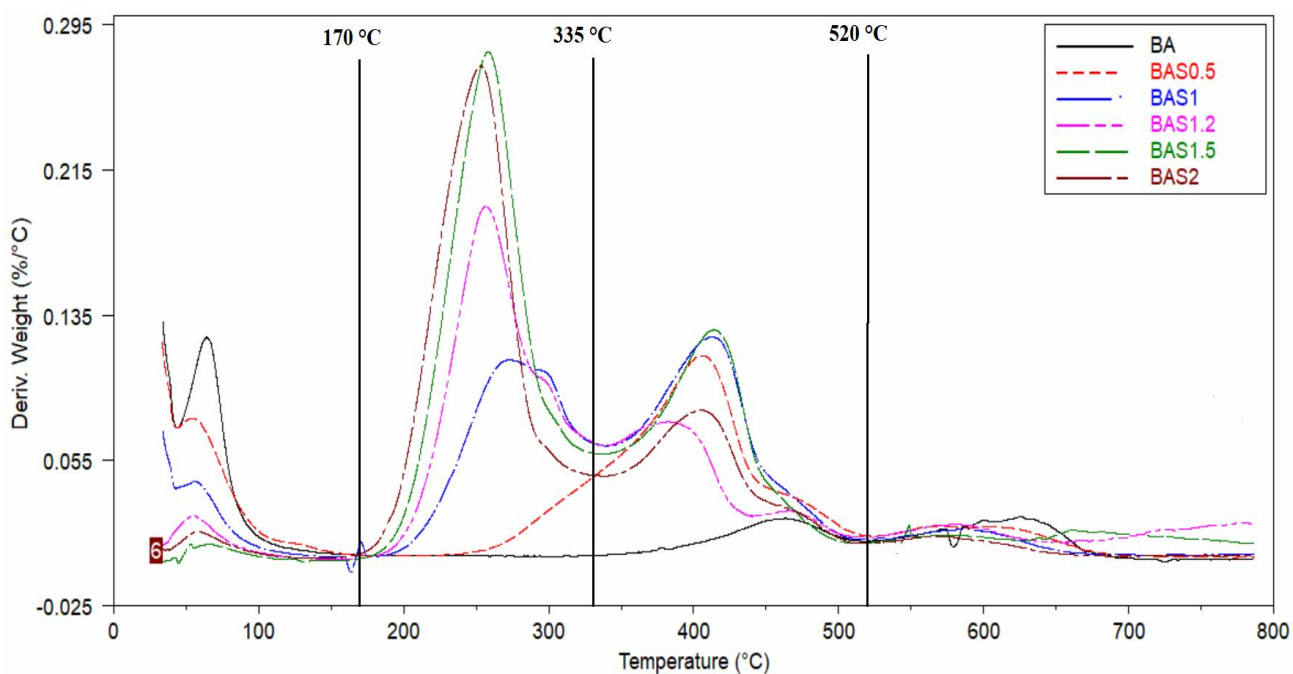
(b)

Fig. 3. TGA (a) and DTG (b) thermograms of BA and BAS samples.

Table 3. Summary of TGA Analysis of BA and BAS Samples, at Different Surfactant Concentrations

Sample	Dehydratation (water adsorbed by metal cations)	Adsorbed surfactant decomposition	Intercalated surfactant decomposition	Dehydroxylation	%Surfactant
	T < 170 °C	170 °C < T < 335 °C	335 °C < T < 520 °C	T > 520 °C	
	%mass- loss	%mass- loss	%mass- loss	%mass- loss	
BA	5.31	0.41	2.3	2.55	-
BAS 0.5	4.45	2.27 - 0.41 = 1.86	10.74 - 2.3 = 8.44	2.6	10.3
BAS 1	2.26	9.8 - 0.41 = 9.39	11.88 - 2.3 = 9.58	2.2	18.97
BAS 1.2	1.05	14.25 - 0.41 = 13.84	7.98 - 2.3 = 5.68	4	19.52
BAS 1.5	0.35	18.75 - 0.41 = 18.34	11.23 - 2.3 = 8.51	1.68	26.85
BAS 2	0.78	18.68 - 0.41 = 18.27	8.3 - 2.3 = 6.0	1.62	24.27

Fig. 4. Effect of pH on the adsorption of dyes onto BAS 1.5 composite.

and organophilic ones. These findings confirm the hydrophilicity loss of BAS samples [33].

The second greatest mass loss, observed within the range of 170-335 °C, turned out to be more pronounced in BAS than in BA. Since pure HDTMA bromide decomposes at about 250 °C [34], the peak observed corresponds to the decomposition of some cationic surfactant molecules adsorbed on the external surface of clay. The third most important weight loss occurred between 335 and 520 °C; it is certainly due to the decomposition of cationic surfactants

intercalated within the BA layers [35]. The last weight loss occurred between 520 and 800 °C; it corresponds to the dehydroxylation of the aluminosilicates [33].

Adsorption Studies

Effect of pH. The pH of the aqueous solution is an important parameter in the adsorption process. It is important to identify the effect of pH on adsorption, as it helps to determine the optimized operational parameters and consequently establish the most appropriate adsorption mechanism. Adsorption experiments of three different dyes onto BAS 1.5 were carried out to examine the effect of pH (in a range from 2-11) on the removal efficiency of these three dyes from an aqueous solution. The results obtained are given in Fig. 4.

It was found that the pH has no significant effect on the adsorption efficiency of methylene blue (BM). In addition, the absorption capacity at equilibrium (q_e) increased slightly (about 1 mg g^{-1}) as the pH value rose from 2 to 11.

These results are in good agreement with those described in the previous study [36]. Moreover, non-ionic dyes, like BzR, are generally water-insoluble dyes which are generally found in colloidal form [37]; they are negatively charged in solution [38]. The pH of zero point charge (pH$_{PZC}$) of BAS 1.5 was about 6.34 (results not shown). At pH values below and above the PZC, the organo-clay exhibited a positive and negative charge, respectively. It was found that for a pH value of about 11, the BAS 1.5 surface was less negative. Moreover, for a pH less than the PZC, BAS 1.5 composite exhibited a net positive surface charge that was attributed to the presence of ammonium groups N$^+$(CH$_3$)$_3$. For lower pH values, the removal efficiency was enhanced because of the electrostatic attraction between the negative charges of dye molecules and the positively charged surface of the adsorbent. Obviously, functional groups exhibited different degrees of ionization at different pH values. For pH values greater than the PZC, the BAS surface charge tended to be negative. When the pH value rose from 2 to 11, the adsorption of Bezathren Red (BzR) dropped. This was certainly due to the competitive adsorption between the OH$^-$ ions and BzR dye molecules [39]. However, Telon Blue (TB) dye exhibited a different adsorption behavior.

As clearly seen in the representative curve, the adsorption capacity q_e reached two maximum values of 82.5 and 77.25 mg g^{-1}, corresponding to two pH values of 2 and 11, respectively. At pH = 2, protons were available, giving rise an increased electrostatic attraction between the negatively charged TB dye anions and the positively charged BAS 1.5 adsorption sites. The noted high adsorption capacity was certainly due to the strong electrostatic interaction between the ammonium cations of composite BAS 1.5 and the dye anions. It is important to note that the adsorption capacity decreased as the pH value augmented. Moreover, the positive charge on the composite decreased gradually and consequently the surface became negatively charged [40]. Note also that for pH values greater than 8, the adsorption capacity went up. It is worth mentioning that the surface charge of composite BAS 1.5 was less negative at pH = 11, which favored the adsorption of anionic dye molecules, probably due to hydrophobic interactions.

Effect of Contact Time

The effect of contact time on the adsorption of MB, BzR, and TB dyes, at various time points, onto the composite BAS 1.5 were investigated using a fixed adsorbent dose of 25 mg. As shown in Figure 5, the adsorption of dyes onto the organo-clay increased for longer contact time.

The result obtained is consistent with those reported in previous studies [41,42]. It is clearly noted that at the beginning, the adsorption rate of dyes was fast. After this rapid dye adsorption, the adsorbent surface became saturated and this adsorption rate dropped. The adsorption efficiency reached 80% in less than 20 min. Saturation of the BAS 1.5 composite substrate was observed at 60 min, suggesting that the aggregation of dye molecules took place around the BAS 1.5 particles. After 60 min, no significant increase in the adsorption efficiency was detected. Therefore, the contact time of 60 min was selected for all subsequent measurements.

Adsorption Kinetic Models

A kinetic study was carried out with the pseudo-first order and pseudo-second order kinetic models for the purpose of studying the adsorption process of dyes onto BAS 1.5 composite. These models are presented by Eqs.
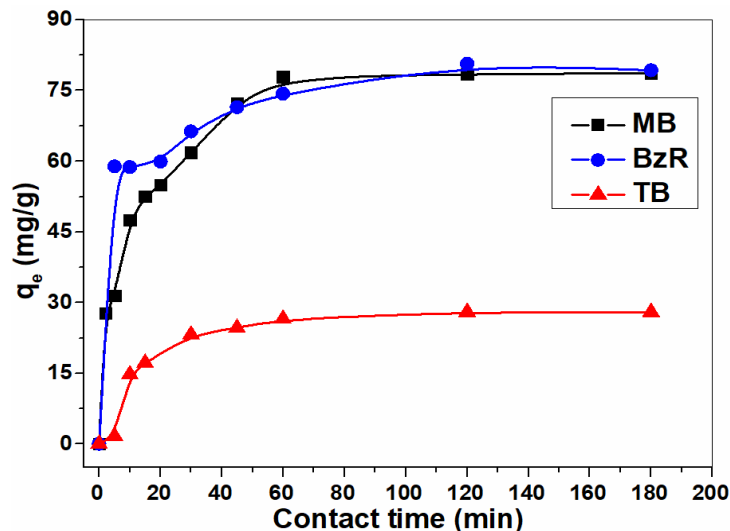
Fig. 5. Effect of time on the adsorption of dyes onto BAS 1.5 composite.

(2) and (3).

$$\ln(q_e - q_t) = \ln q_e - k_1 t \qquad (2)$$

$$\frac{t}{q_t} = \frac{1}{k_2 q_e^2} + \frac{t}{q_e} \qquad (3)$$

where q_e is the adsorption capacity at equilibrium (mg g^{-1}), q_t (mg g^{-1}) is the amount of dye adsorbed at time t; k_1 (min^{-1}) and k_2 (g mg^{-1} min^{-1}) are the pseudo-first and pseudo-second order rate constants, respectively.

The adsorption kinetic plots are shown in Fig. 6a and Fig. 6b. The kinetic parameters and correlation coefficient (R^2) of the two models are given in Table 4.

Regarding the pseudo-first order model, it was noted that R^2 increased from 0.781 to 0.985, and the equilibrium capacity (q_e, cal), calculated by the equation of the model, was much smaller than the experimental value (q_e, exp) for both dyes MB and TB but not for BzR. Thereby, the pseudo-first order kinetic model was not suitable to model the sorption process of MB and TB dyes onto the BAS 1.5 composite. However, the pseudo-second order kinetic model described better the adsorption processes of MB and TB based on the correlation coefficient values which were found above 0.99 and greater than those of the pseudo-first order model, except for BzR (Table 4).

Regarding the adsorption of MB and BT dyes, the suggested mechanism involved valence forces through the exchange of electrons between dye molecules and BAS 1.5 composite [43].

The adsorption mechanism of BzR which behaved as an anionic dye was probably due to the electrostatic attractions between the charged surface and charged dye molecules, considering the chemical characteristics of the surfactant-modified clay and dye molecules [44,45].

Effect of Adsorbent Dosage

The effect of the adsorbent dose on the adsorption of MB, TB and BzR dyes was studied by varying the amount of BAS 1.5 composite adsorbent. Figure 7 presents the adsorption of dyes by BAS 1.5 composite, at different adsorbent doses (10-100 mg) for the dye solution volume of 40 ml, at dye concentrations of 20, 50 and 100 mg l^{-1}, for MB, TB, and BzR, respectively.

The results presented in Fig. 7 indicate clearly that the adsorption efficiency started increasing with the adsorbent dosage at the beginning, suggesting that a greater surface area and more adsorption sites are available. The optimal BAS composite adsorbent dose for the adsorption of TB and BzR dyes was found to be 40 mg; however, a better dose (25 mg) was needed for the adsorption of MB. Moreover, for m > 25 mg, no significant variation in the adsorption
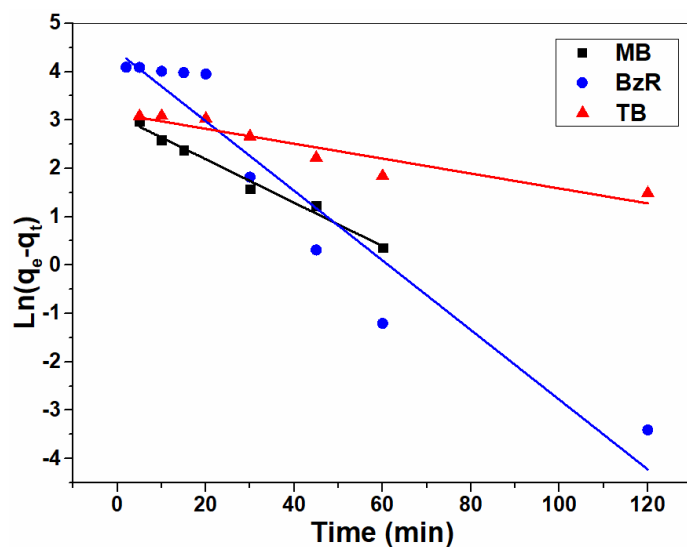
(a)
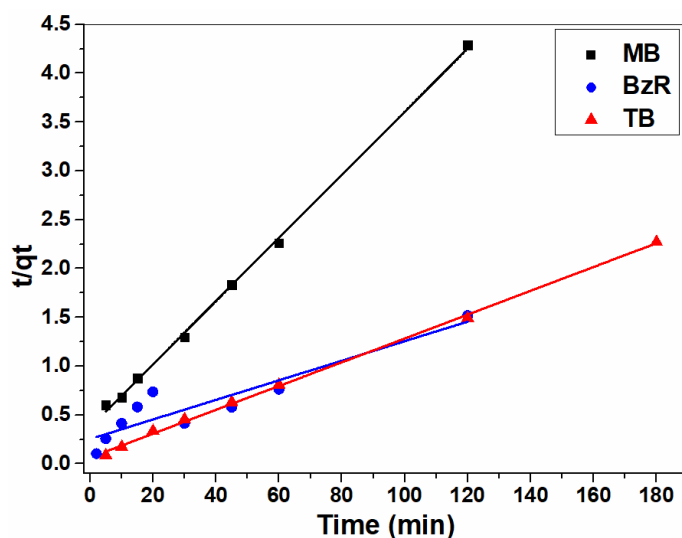
(b)

Fig. 6. a) Pseudo-first-order kinetics model (a) and pseudo-second-order kinetics model (b) for the adsorption of different dyes on BAS 1.5 composite.

efficiency was observed for MB. Therefore, the dose of 25 mg of BAS 1.5 composite was selected for all subsequent measurements.

Adsorption Isotherm Studies

The adsorption isotherms were studied by mixing 25 mg of the composite with a series of MB, TB, and BzR solutions, at different initial concentrations (from 5 to 200 mg l^{-1}); the mixtures thus obtained were stirred for 60 min. Figure 8 indicates that at low equilibrium concentrations, the adsorption capacities increased quickly. Note that the values of q_e increased slowly when C_e was

Table 4. Pseudo-first and Pseudo-second Order Kinetic Parameters for the Adsorption of Dyes onto BAS 1.5
Composite

Dye	q_e (exp) (mg g^{-1})	Pseudo-first order			Pseudo-second order		
		k_1 (min^{-1})	q_e (cal) (mg g^{-1})	R^2	k_2 (min^{-1})	q_e (cal) (mg g^{-1})	R^2
BM	28	0.044	21.86	0.985	0.0034	31.25	0.998
BzR	79.73	0.072	82.59	0.923	0.00039	100	0.852
TB	80.64	542	5.002	0.781	0.2	100	0.999
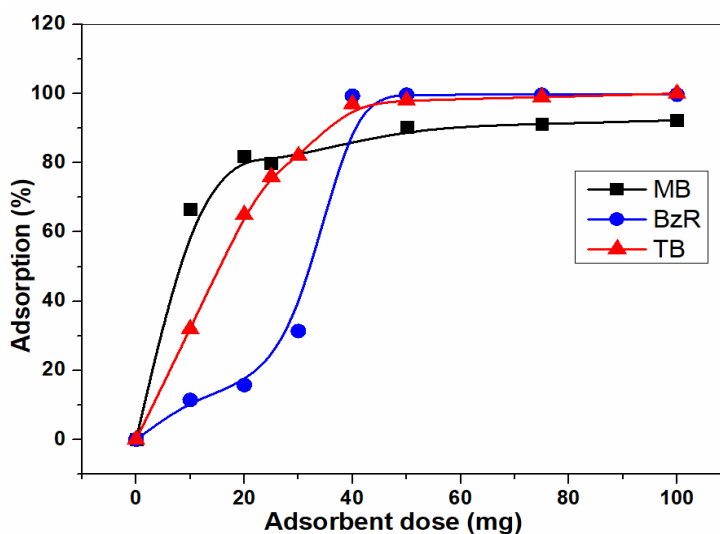
Fig. 7. Effect of adsorbent dose on the adsorption of dyes onto BAS 1.5 composite.

within the range [10-20 mg l^{-1}] for adsorption of all dyes. However, when C_e increased beyond 100 mg l^{-1}, the q_e values remained nearly unchanged. These findings suggest that the initial dye concentration is an important parameter in the adsorption process.

Langmuir and Freundlich isotherms are presented by Eqs. (4) and (5):

$$\frac{C_e}{q_e} = \frac{C_e}{q_{max}} + \frac{1}{q_{max}.K_L} \tag{4}$$

$$\ln q_e = \ln K_F + \frac{1}{n}\ln C_e \tag{5}$$

where C_e is the equilibrium concentration of dye (mg l^{-1}), q_e is the amount of dye adsorbed on BAS 1.5 composite (mg g^{-1}), K_L is the Langmuir adsorption constant (l mg^{-1}), q_{max} is the maximum monolayer adsorption capacity of the adsorbent (mg g^{-1}), K_F is the Freundlich adsorption constant, which is related to the adsorption capacity, and n is the heterogeneity factor. The Langmuir and Freundlich
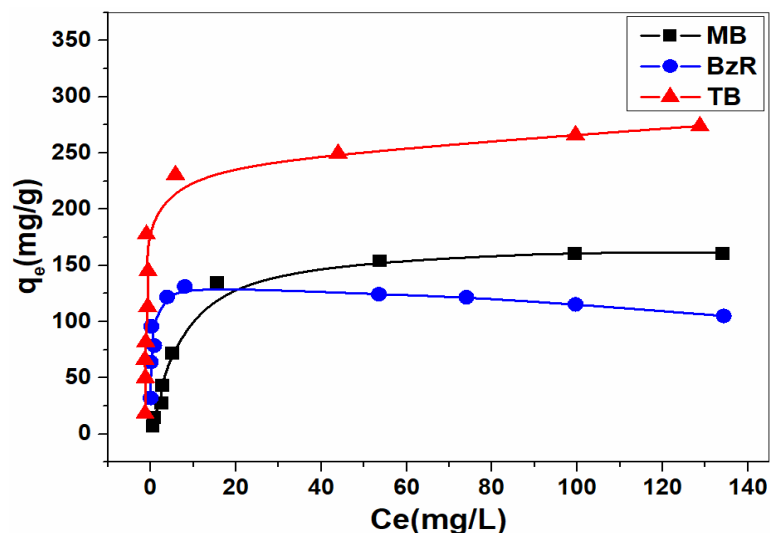
Fig. 8. Effect of initial dye concentration on the adsorption of dyes onto BAS 1.5 composite

Table 5. Langmuir and Freundlich Isotherm Parameters for the Adsorption of MB, TB and
BzR Dyes *onto* BAS1.5 Ccomposite

Dye	pH	Langmuir			Freundlich		
		K_L (l mg^{-1})	q_m (mg g^{-1})	R^2	K_F (l g^{-1})	$1/n$	R^2
MB	6.4	0.139	166.67	0.997	20.106	0.542	0.895
TB	11	0.125	500	0.971	116.62	0.210	0.537
BzR	2.5	225.00	111.11	0.994	89.57	0.103	0.614

adsorption isotherms for dyes adsorbed onto BAS 1.5 composite are presented in Fig. 9. The isotherm parameters obtained from these models are summarized in Table 5. The equilibrium data were fit better to the Langmuir model than to the Freundlich model, as can be seen in Fig. 9. This is indicative of the homogeneity of the adsorption sites on the BAS 1.5 composite particles. In addition, as clearly indicated in Table 5, all 1/n values are below 1, indicating a normal Langmuir isotherm. However, the 1/n value above unity is indicative of the cooperative adsorption [46], and

the values of 1/n between 0.103 and 0.542 are indicative of a favorable adsorption [47].

Thermodynamic Studies

The influence of temperature on the adsorption behavior of different dyes onto BAS 1.5 composite was also investigated under optimized conditions, at the temperatures of 298, 303, 313 and 323 K. A thermodynamic analysis was conducted to understand the characteristics and mechanisms of adsorption. The thermodynamic parameters $\Delta G°$, $\Delta H°$,
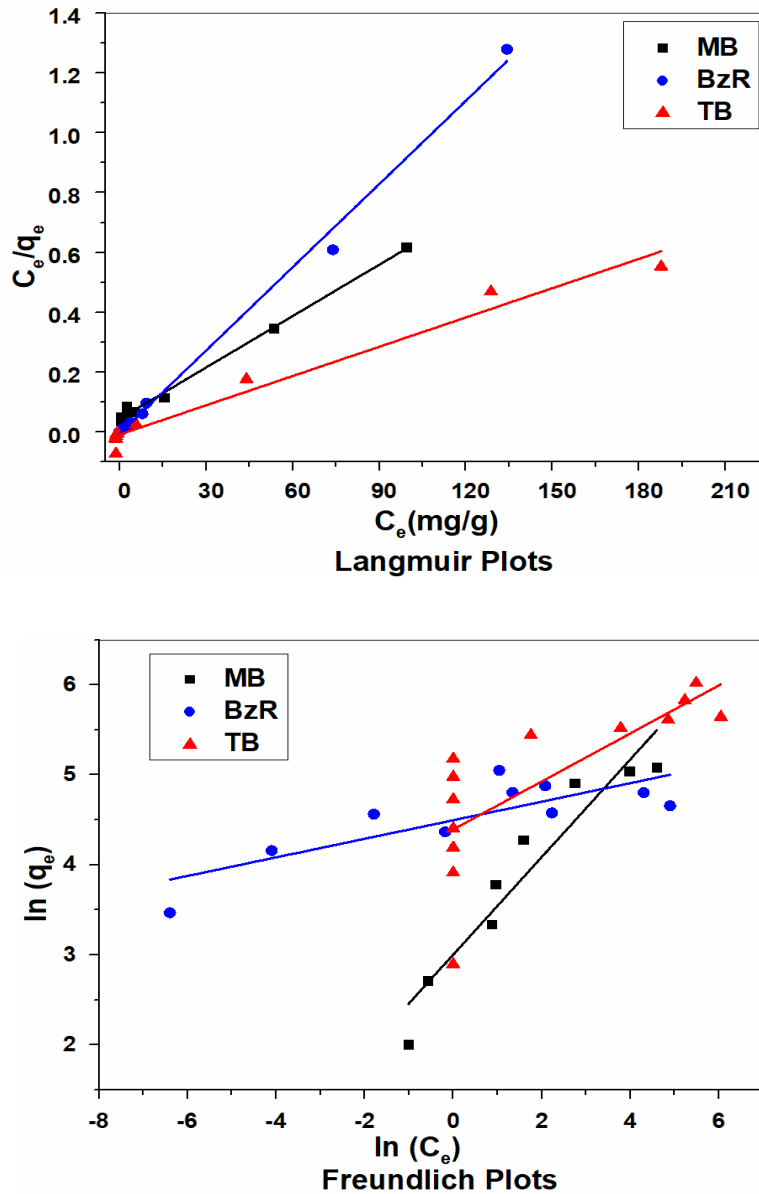
Fig. 9. Isotherm plots for the adsorption of dyes onto BAS1.5.

and $\Delta S°$ were calculated using Eqs. (6), (7) and (8).

$$K_d = q_e/C_e \qquad (6)$$

$$\Delta G° = -RT\ln K_d \qquad (7)$$

$$\ln K_d = \frac{\Delta S°}{R} - \frac{\Delta H°}{RT} \qquad (8)$$

where K_d is the distribution coefficient (l g^{-1}), T is the temperature (K), and R is the gas constant (8.314 J mol^{-1} K^{-1}). The enthalpy change ($\Delta H°$ (kJ mol^{-1})) and the entropy change ($\Delta S°$ (J mol^{-1} K^{-1})) were computed from the slope and intercept of the linear plot of $\ln K_d$ *vs.* $1/T$, as presented in Fig. 10.

The previously calculated thermodynamic parameters $\Delta G°$, $\Delta H°$ and $\Delta S°$ are summarized in Table 6. Generally,
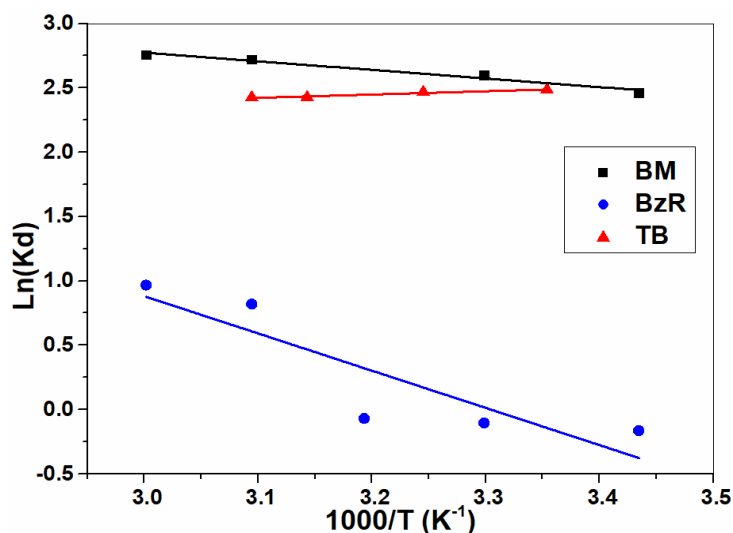
Fig. 10. The Van't Hoff plots for the adsorption of dyes onto BAS1.5 composite.

Table 6. Thermodynamic Parameters for the Adsorption Process of dyes onto BAS1.5 Composite at Various Temperatures

Dye	$\Delta H°$ (kJ mol^{-1})	$\Delta S°$ (J mol^{-1} K^{-1})	$\Delta G°$ (kJ mol^{-1})			
			298 K	303 K	313 K	323 K
MB	12.11	58.6	-5.36	-5.65	-6.24	-6.83
TB	2.09	13.64	-1.98	-2.04	-2.18	-2.32
BzR	24.04	79.46	0.36	-0.048	-0.84	-1.64

the absolute magnitude of free energy change for physisorption is between -20 and 0 kJ mol^{-1} [48].

The results concerning the adsorption process of BM, BT and BzR dyes, at 298, 303, 313, 323 K, show that the free energy values were negative, indicating a spontaneous and favorable adsorption process onto BAS 1.5 composite, except for BzR at 298 K. The positive $\Delta G°$ value suggests that the adsorption is non-spontaneous and less favorable at that temperature. It is worth recalling that positive values of $\Delta H°$ imply an endothermic reaction. The positive values of $\Delta S°$ indicate an increase in entropy and the solid-liquid interface becomes more random during the adsorption process of dyes.

In conclusion, the adsorption capacity of BM, BzR and TB dyes at 298 K obtained in this study is compared with those determined by other authors [48-51]. These results are given in Table 7.

Proposed Adsorption Mechanism

The composite under study consists of bentonite clay and surfactant. According to the literature [52,53], and based on the composite structure, the hydrophilic adsorption occurs between the composite and different dyes, as shown in Fig. 11. It is worth mentioning that the quaternary ammonium cationic surfactant turns the composite hydrophilic. It is widely acknowledged that cationic

Table 7. Comparison of the Mmaximum Adsorption Capacities for BM, BzR and TB Adsorption on
BAS 1.5 with Those of other Adsorbents

Dye	Adsorbent	Maximum adsorption capacity (mg g^{-1})	Ref.
MB	Montmorillonite	74	[48]
	Acid modified clay beads	223.19	[49]
	BAS 1.5	166.67	Present study
TB	Mesoporous silicate/polypyrrole	55.55	[50]
	BAS 1.5	500	Present study
BzR	Sodic Montmorillonite	48.52	[51]
	BAS 1.5	111.11	Present study
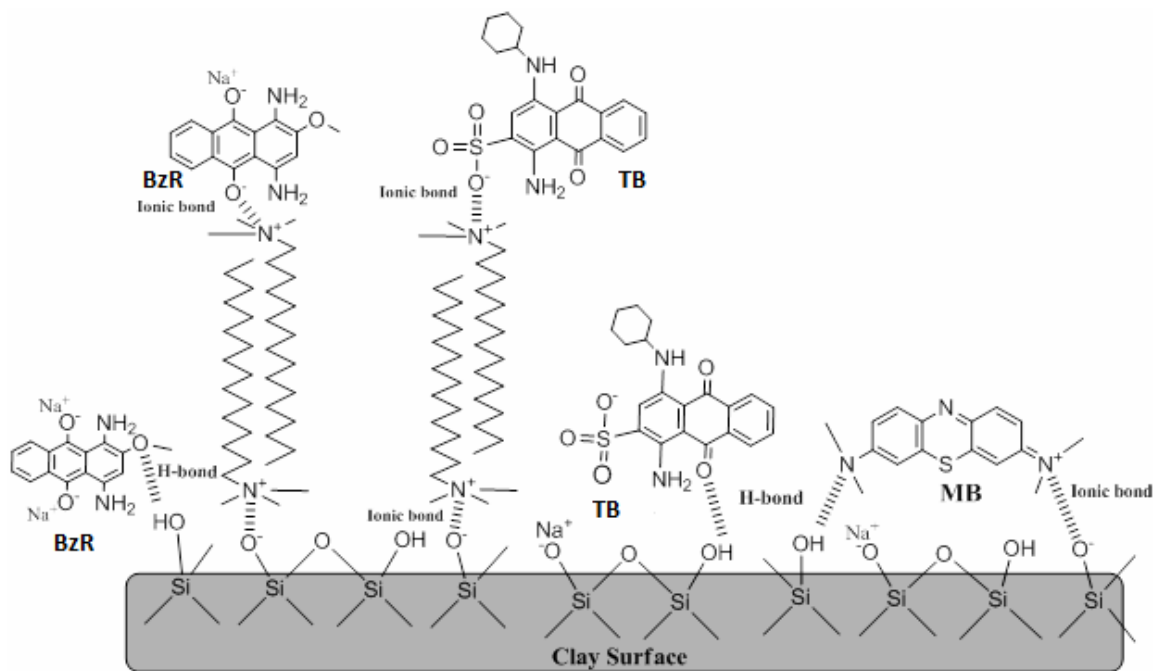
Fig. 11. Proposed mechanism for the adsorption of Telon Blue, Bezathren Red and Methylene Blue onto
BAS1.5 composite.

surfactants can produce strong electrostatic adsorption of anionic dyes. This process leads to ultrahigh adsorption capacities of the composite for BzR and TB molecules.

Moreover, hydrogen bonding may occur between the oxygen silanol groups of bentonite and both of nitrogen and oxygen atoms of dyes. Therefore, the excellent adsorption

properties of BAS composite can be attributed to the synergistic effect of hydrogen bonding and the electrostatic interactions between the adsorbent and MB, TB and BzR dyes.

CONCLUSIONS

In this study, the BAS composite was prepared by the modification of bentonite with the HDTMA surfactant loadings from 50 to 200% of CEC. The resulting composites were characterized by X-ray diffraction (XRD), infrared spectroscopy (FTIR) and thermal analysis (ATG/DTG).

The adsorption of Methylene Blue (MB), Bezathren Red (BzR), and Telon Blue (TB) dyes onto BAS 1.5 composite were studied using batch tests conducted under different experimental conditions, while the parameters such as the contact time, pH of dye solution, adsorbent dosage, initial dye concentrations, and temperature changed. The kinetic study showed that the adsorption process of all dyes can be described by the pseudo-second order model.

The equilibrium data were analyzed using the Langmuir and Freundlich models, but the first one was found more appropriate for describing the adsorption of MB, BzR and TB dyes. In addition, the calculated Langmuir maximum adsorption capacities of MB, BzR, and TB were found equal to 166.67, 111.11 and 500 mg g^{-1}, respectively, and the adsorption process turned out to be endothermic in nature in all cases (MB, TB and BzR). The adsorption capacities of BM, BzR, and TB dyes at 298 K, obtained in this study, were found to be more effective than those reported by other authors in the literature. These findings allow stating that BAS composite can be employed as a low-cost material for the removal of cationic, anionic and vat dyes from effluents.

REFERENCES

[1] De Jesus da Silveira Neta, J.; Costa Moreira, G.; da Silva, C. J.; Reis, C.; Reis, E. L., Use of polyurethane foams for the removal of the direct red 80 and reactive blue 21 dyes in aqueous medium. *Desalination* **2011**, *281*, 55-60, DOI: 10.1016/j.desal.2011.07.041.

[2] Kono, H., Preparation and characterization of amphoteric cellulose hydrogels as adsorbents for the anionic dyes in aqueous solutions. *Gels* **2015**, *1*, 94-116, DOI: 10.3390/gels1010094.

[3] Ngulube, T.; Gumbo, J. R.; Masindi, V.; Maity, A., An update on synthetic dyes adsorption onto clay based minerals: A state-of-art review. *J. Environ. Manage.* **2017**, *191*, 35-57, DOI: 10.1016/j.jenvman.2016.12.031.

[4] Kuppusamy, S.; Thavamani, P.; Megharaj, M.; Venkateswarlu, K.; Lee, Y. B.; Naidu, R., Potential of melaleuca diosmifolia as a novel, non-conventional and low-cost coagulating adsorbent for removing both cationic and anionic dyes. *J. Ind. Eng. Chem.* **2016**, *37*, 198-207, DOI: 10.1016/j.jiec.2016.03.021.

[5] Çelekli, A.; Birecikligil, S. S.; Geyik, F.; Bozkurt, H., Prediction of removal efficiency of lanaset red G on walnut husk using artificial neural network model. *Bioresour. Technol.* **2012**, *103*, 64-70, DOI: 10.1016/j.biortech.2011.09.106.

[6] Zhu, H. Y.; Jiang, R.; Fu, Y. Q.; Jiang, J. H.; Xiao, L.; Zeng, G. M., Preparation, characterization and dye adsorption properties of γ-Fe$_2$O$_3$/SiO$_2$/Chitosan Composite. Appl. Surf. Sci. 2011, 258, 1337-1344, DOI: 10.1016/j.apsusc.2011.09.045.

[7] Xu, R. Kou; Xiao, S. Cheng; Yuan, J. Hua; Zhao, A. Zhen., Adsorption of methyl violet from aqueous solutions by the biochars derived from crop residues. *Bioresour. Technol.* **2011**, *102*, 10293-10298, DOI: 10.1016/j.biortech.2011.08.089.

[8] Akgül, M.; Karabakan, A., Promoted dye adsorption performance over desilicated natural zeolite. *Microporous Mesoporous Mater.* **2011**, *145*, 157-164, DOI: 10.1016/j.micromeso.2011.05.012.

[9] Huang, X. Y.; Bu, H. T.; Jiang, G. B.; Zeng, M. H., Cross-linked succinyl chitosan as an adsorbent for the removal of methylene blue from aqueous solution. *Int. J. Biol. Macromol.* **2011**, *49*, 643-651, DOI: 10.1016/j.ijbiomac.2011.06.023.

[10] Heddi, D.; Benkhaled, A.; Boussaid, A.; Choukchou-Braham, E., Adsorption of anionic dyes on poly(N-vinylpyrrolidone) modified bentonite. *Phys. Chem. Res.* **2019**, *7*, 731-749, DOI: 10.22036/pcr.2019.179510.1625.

[11] Medjahed, K.; Tennouga, L.; Mansri, A.; Chetouani,

A.; Hammouti, B.; Desbrières, J., Interaction between poly(4-vinylpyridine-graft-bromodecane) and textile blue basic dye by spectrophotometric study. *Res. Chem. Intermed.* **2013**, *39*, 3199-3208, DOI: 10.1007/s11164-012-0832-2.

[12] Ghaedi, M.; Hossainian, H.; Montazerozohori, M.; Shokrollahi, A.; Shojaipour, F.; Soylak, M.; Purkait, M. K., A Novel Acorn Based Adsorbent for the Removal of Brilliant Green. *Desalination* **2011**, *281*, 226-233, DOI: 10.1016/j.desal.2011.07.068.

[13] Elmoubarki, R.; Mahjoubi, F. Z.; Tounsadi, H.; Moustadraf, J.; Abdennouri, M.; Zouhri, A.; El Albani, A.; Barka, N., Adsorption of textile dyes on raw and decanted moroccan clays: Kinetics, equilibrium and thermodynamics. *Water Resour. Ind.* **2015**, *9*, 16-29, DOI: 10.1016/j.wri.2014.11.001.

[14] Bouberka, Z.; Khenifi, A.; Benderdouche, N.; Derriche, Z., Removal of supranol yellow 4GL by adsorption onto Cr-intercalated montmorillonite. *J. Hazard. Mater.* **2006**, *133*, 154-161, DOI: 10.1016/j.jhazmat.2005.10.003.

[15] Mousavi, S. M.; Babapoor, A.; Hashemi, S. A.; Medi, B. C. Adsorption and removal characterization of nitrobenzene by graphene oxide coated by polythiophene nanoparticles. *Phys. Chem. Res.* **2020**, *8*, 225-240, DOI: 10.22036/pcr.2020.208780.1700.

[16] Ait Himi, M.; El Ghachtouli, S.; Amarray, A.; Zaroual, Z.; Bonnaillie, P.; Azzi, M., Removal of azo dye calcon using polyaniline films electrodeposited on SnO_2 substrate. *Phys. Chem. Res.* **2020**, *8*, 111-124, DOI: 10.22036/pcr.2019.203023.1680.

[17] Salari, H.; Kohantorabi, M., Fabrication of novel $Fe_2O_3/MoO_3/AgBr$ nanocomposites with enhanced photocatalytic activity under visible light irradiation for organic pollutant degradation. *Adv. Powder Technol.* **2020**, *31*, 493-503, DOI: 10.1016/j.apt.2019.11.005.

[18] Salari, H.; Kohantorabi, M., Facile template-free synthesis of new α-MnO_2 nanorod/silver iodide p-n junction nanocomposites with high photocatalytic performance. *New J. Chem.* **2020**, *44*, 7401-7411, DOI: 10.1039/d0nj01033b.

[19] Ali, I.; Asim, M.; Khan, T. A., Low cost adsorbents for the removal of organic pollutants from wastewater. *J. Environ. Manage.* **2012**, *113*, 170-183, DOI: 10.1016/j.jenvman.2012.08.028.

[20] Özcan, A. S.; Erdem, B.; Özcan, A., Adsorption of acid blue 193 from aqueous solutions onto Na-bentonite and DTMA-bentonite. *J. Colloid Interface Sci.* **2004**, *280*, 44-54, DOI: 10.1016/j.jcis.2004.07.035.

[21] Kaya, E. M. Ö.; Özcan, A. S.; Gök, Ö.; Özcan, A., Adsorption kinetics and isotherm parameters of naphthalene onto natural- and chemically modified bentonite from aqueous solutions. *Adsorption* **2013**, *19*, 879-888, DOI: 10.1007/s10450-013-9542-3.

[22] Wang, L.; Wang, A., Adsorption properties of congo red from aqueous solution onto surfactant-modified montmorillonite. *J. Hazard. Mater.* **2008**, *160*, 173-180, DOI: 10.1016/j.jhazmat.2008.02.104.

[23] Açışlı, Ö.; Karaca, S.; Gürses, A., Investigation of the alkyl chain lengths of surfactants on their adsorption by montmorillonite (Mt) from aqueous solutions. *Appl. Clay Sci.* **2017**, *142*, 90-99, DOI: 10.1016/j.clay.2016.12.009.

[24] Yang, S.; Gao, M.; Luo, Z., Adsorption of 2-naphthol on the organo-montmorillonites modified by gemini surfactants with different spacers. *Chem. Eng. J.* **2014**, *256*, 39-50, DOI: 10.1016/j.cej.2014.07.004.

[25] Makhoukhi, B.; Djab, M.; Amine Didi, M., Adsorption of telon dyes onto bis-imidazolium modified bentonite in aqueous solutions. *J. Environ. Chem. Eng.* **2015**, *3*, 1384-1392, DOI: 10.1016/j.jece.2014.12.012.

[26] Monvisade, P.; Siriphannon, P., Chitosan intercalated montmorillonite: Preparation, characterization and cationic dye adsorption. *Appl. Clay Sci.* **2009**, *42*, 427-431, DOI: 10.1016/j.clay.2008.04.013.

[27] Huang, P.; Kazlauciunas, A.; Menzel, R.; Lin, L., Determining the mechanism and efficiency of industrial dye adsorption through facile structural control of organo-montmorillonite adsorbents. ACS *Appl. Mater. Interfaces* **2017**, *9*, 26383-26391, DOI: 10.1021/acsami.7b08406.

[28] Darder, M.; Colilla, M.; Ruiz-Hitzky, E., Biopolymer-clay nanocomposites based on chitosan intercalated in montmorillonite. *Chem. Mater.* **2003**, *15*, 3774-3780, DOI: 10.1021/cm0343047.

[29] Parolo, M. E.; Pettinari, G. R.; Musso, T. B.; Sánchez-Izquierdo, M. P.; Fernández, L. G., Characterization of organo-modified bentonite sorbents: The effect of modification conditions on adsorption performance. *Appl. Surf. Sci.* **2014**, *320*, 356-363, DOI: 10.1016/j.apsusc.2014.09.105.

[30] Vaia, R. A.; Teukolsky, R. K.; Giannelis, E. P., Interlayer structure and molecular environment of alkylammonium layered silicates. *Chem. Mater.* **1994**, *6*, 1017-1022, DOI: 10.1021/cm00043a025.

[31] Xie, W.; Gao, Z.; Pan, W. P.; Hunter, D.; Singh, A.; Vaia, R., Thermal degradation chemistry of alkyl quaternary ammonium montmorillonite. *Chem. Mater.* **2001**, *13*, 2979-2990, DOI: 10.1021/cm010305s.

[32] Zhu, J.; Morgan, A. B.; Lamelas, F. J.; Wilkie, C. A., Fire properties of polystyrene-clay nanocomposites. *Chem. Mater.* **2001**, *13*, 3774-3780, DOI: 10.1021/cm000984r.

[33] Xi, Y.; Mallavarapu, M.; Naidu, R., Preparation, characterization of surfactants modified clay minerals and nitrate adsorption. *Appl. Clay Sci.* **2010**, *48*, 92-96, DOI: 10.1016/j.clay.2009.11.047.

[34] Erdem, B.; Özcan, A. S.; Özcan, A., Preparation of HDTMA-bentonite: Characterization studies and its adsorption behavior toward dibenzofuran. *Surf. Interface Anal.* **2010**, *42*, 1351-1356, DOI: 10.1002/sia.3230.

[35] Majdan, M.; Pikus, S.; Gajowiak, A.; Sternik, D.; Zieba, E., Uranium sorption on bentonite modified by octadecyltrimethylammonium bromide. *J. Hazard. Mater.* **2010**, *184*, 662-670, DOI: 10.1016/j.jhazmat.2010.08.089.

[36] Jourvand, M.; Shams Khorramabadi, G.; Omidi Khaniabadi, Y.; Godini, H.; Nourmoradi, H., Removal of methylene blue from aqueous solutions using modified clay. *J. Basic Res. Med. Sci.* **2015**, *2*, 32-41.

[37] Gupta, V. K.; Suhas, Application of low-cost adsorbents for dye removal-A review. *J. Environ. Manage.* **2009**, *90*, 2313-2342, DOI: 10.1016/j.jenvman.2008.11.017.

[38] Kim, T. H.; Park, C.; Shin, E. B.; Kim, S., Decolorization of disperse and reactive dye solutions using ferric chloride. *Desalination* **2004**, *161*, 49-58, DOI: 10.1016/S0011-9164(04)90039-2.

[39] Binaeian, E.; Seghatoleslami, N.; Chaichi, M. J., Synthesis of oak gall tannin-immobilized hexagonal mesoporous silicate (OGT-HMS) as a new super adsorbent for the removal of anionic dye from aqueous solution. *Desalin. Water Treat.* **2016**, *57*, 8420-8436, DOI: 10.1080/19443994.2015.1020513.

[40] Zohra, B.; Aicha, K.; Fatima, S.; Nourredine, B.; Zoubir, D., Adsorption of Direct Red 2 on Bentonite Modified by Cetyltrimethylammonium Bromide. *Chem. Eng. J.* **2008**, *136*, 295-305, DOI: 10.1016/j.cej.2007.03.086.

[41] Rajabi, M.; Mirza, B.; Mahanpoor, K.; Mirjalili, M.; Najafi, F.; Moradi, O.; Sadegh, H.; Shahryari-ghoshekandi, R.; Asif, M.; Tyagi, I.; Agarwal, S.; Gupta, V. K., Adsorption of Malachite Green from Aqueous Solution by Carboxylate Group Functionalized Multi-Walled Carbon Nanotubes: Determination of Equilibrium and Kinetics Parameters. *J. Ind. Eng. Chem.* **2016**, *34*, 130-138, DOI: 10.1016/j.jiec.2015.11.001.

[42] Bhatt, A. S.; Sakaria, P. L.; Vasudevan, M.; Pawar, R. R.; Sudheesh, N.; Bajaj, H. C.; Mody, H. M., Adsorption of an Anionic Dye from Aqueous Medium by Organoclays: Equilibrium Modeling, Kinetic and Thermodynamic Exploration. *RSC Adv.* **2012**, *2*, 8663-8671, DOI: 10.1039/c2ra20347b.

[43] Orucoglu, E.; Haciyakupoglu, S., Bentonite modification with hexadecylpyridinium and aluminum polyoxy cations and its effectiveness in Se(IV) removal. *J. Environ. Manage.* **2015**, *160*, 30-38, DOI: 10.1016/j.jenvman.2015.06.005.

[44] Keyhanian, F.; Shariati, S.; Faraji, M.; Hesabi, M., Magnetite nanoparticles with surface modification for removal of methyl violet from aqueous solutions. *Arab. J. Chem.* **2016**, *9*, S348-S354, DOI: 10.1016/j.arabjc.2011.04.012.

[45] Muthukumaran, C.; Sivakumar, V. M.; Thirumarimurugan, M., Adsorption isotherms and kinetic studies of crystal violet dye removal from aqueous solution using surfactant modified magnetic nanoadsorbent. *J. Taiwan Inst. Chem. Eng.* **2016**, *63*, 354-362, DOI: 10.1016/j.jtice.2016.03.034.

[46] Jović-Jovičić, N.; Milutinović-Nikolić, A.; Gržetic, I.; Jovanović, D., Organobentonite as efficient textile dye

sorbent. *Chem. Eng. Technol.* **2008**, *31*, 567-574, DOI: 10.1002/ceat.200700421.

[47] Hameed, B. H.; Din, A. T. M.; Ahmad, A. L., Adsorption of methylene blue onto bamboo-based activated carbon: Kinetics and equilibrium studies. *J. Hazard. Mater.* **2007**, *141*, 819-825, DOI: 10.1016/j.jhazmat.2006.07.049.

[48] Yu, Y.; Zhuang, Y. Y.; Wang, Z. H., Adsorption of water-soluble dye onto functionalized resin. *J. Colloid Interface Sci.* **2001**, *242*, 288-293, DOI: 10.1006/jcis.2001.7780.

[49] Zhou, K.; Zhang, Q.; Wang, B.; Liu, J.; Wen, P.; Gui, Z.; Hu, Y., The integrated utilization of typical clays in removal of organic dyes and polymer nanocomposites. *J. Clean. Prod.* **2014**, *81*, 281-289, DOI: 10.1016/j.jclepro.2014.06.038.

[50] Auta, M.; Hameed, B. H., Acid modified local clay beads as effective low-cost adsorbent for dynamic adsorption of methylene blue. *J. Ind. Eng. Chem.* **2013**, *19*, 1153-1161, DOI: 10.1016/j.jiec.2012.12.012.

[51] Belbachir, I.; Makhoukhi, B., Adsorption of bezathren dyes onto sodic bentonite from aqueous solutions. *J. Taiwan Inst. Chem. Eng.* **2017**, *75*, 105-111, DOI: 10.1016/j.jtice.2016.09.042.

[52] Errais, E.; Duplay, J.; Elhabiri, M.; Khodja, M.; Ocampo, R.; Baltenweck-Guyot, R.; Darragi, F., Anionic RR120 dye adsorption onto raw clay: Surface properties and adsorption mechanism. *Colloids Surfaces A Physicochem. Eng. Asp.* **2012**, *403*, 69-78, DOI: 10.1016/j.colsurfa.2012.03.057.

[53] Mahmoodi, N. M.; Abdi, J.; Taghizadeh, M.; Taghizadeh, A.; Hayati, B.; Shekarchi, A. A.; Vossoughi, M., Activated carbon/metal-organic framework nanocomposite: Preparation and photocatalytic dye degradation mathematical modeling from wastewater by least squares support vector machine. *J. Environ. Manage.* **2019**, *233*, 660-672, DOI: 10.1016/j.jenvman.2018.12.026.

Abstract

Main results obtained from the structural evolution of cost-effective Organo-Bentonite (Bentonite modified with different loadings of Hexadecyltrimethylammonium Bromide) from 50 to 200% of the CEC with CMC (CarboxyMethyl Cellulose) in different percentages is investigated and linked to the adsorption uptake and mechanism of an important industrial dyes (Methylene Blue (MB), Bezathren Red (BzR) and Telon Blue (TB) in single and mixture system from the aqueous solution. The prepared materials were characterized by X-ray diffraction XRD, infrared spectroscopy measurements FT-IR, and thermal analysis ATG/DTG. The influence of several factors on the adsorption capacity such as contact time, dye solution pH, adsorbent dosage, initial dyes concentrations, and the temperature was investigated. The equilibrium data were analyzed using the Langmuir and Freundlich models. The Langmuir isotherm model is the most suitable to describe MB, BzR and TB dyes adsorption.

Key words: Inorganic/organic hybrid materials, Adsorption, Cationic, Anionic, Vat dyes.

ملـخـص

في اطروحـة الـدكتوره هـذه قمنـا بـالتطرق إلـى موضـوع هـو مـن الأهميـة بمكـان، موضـوع تلـوث الميـاه بالأصـبغة الصـناعية المستعملة فـي معامـل دباغـة الملابـس. حاولنـا مـن خـلال هـذا البحـث العلمـي توليـف وتوصـيف مـواد ماصـة لثلاثـة اصـبغة عضـوية مختلفـة مـن حيـث تصـنيفها والمهمـة جـدا فـي عـالم الدباغـة والمسـمات بـ أزرق الميثـيلان، أزرق التِـيلـون، وأحمـر البِزتـران بإسـتعمال طـين البنتونيـت الجزائـري المتواجـد بولايـة تلمسـان فـي دائـرة حمـام بـوغرارة ومزجـه مـع مـادة السـيتيل ثلاثـي الميثيـل بروميـد الأمونيـوم وبـوليمير الكاربوكسـي ميثيـل سـليلوز بنسـب مختلفـة وإسـتعمله لإمتـزاز هـذه الأصـبغة مـن المـاء .تـم متابعـة ومعاينـة المـواد المصـنعة بإسـتعمال تقنيـات الأشـعة السـينية، التحليـل الـوزني الحـراري والأشـعة تحـت الحمـراء. كمـا تـم متابعـة عمليـة إمتـزاز الاصـباغ فـي نظـام الدفعـة الواحـدة بإسـتعمال تقنيـة الأشـعة فـوق البنفسـجية والمرئيـة وفـي المرحلـة الثانيـة عنـد مـزج الأصـبغة مـع بعضـها بطريقـة حسـاب الطلـب الكيميـائي للأكسـجين .خـلال هـذه الدراسـات تـم معاينـة عـدة عوامـل مـؤثرة علـى سـعة الإمتـزاز منهـا درجـة حموضـة الوسـط، تراكيـز الأصـبغة الابتدائيـة، كميـة الممتـز المسـتخدمة ودرجـة حـراة الوسـط .تـم تحليـل البيانـات المستخلصـة مـن هـذه التجـارب بإسـتخدام نمـادج لـونغمير و فرانـدليش و النمـادج الحركية المقترحة من طرف لاجيرجرين.

الكلمات المفتاحية :البنتونيت ,اصبغة عضوية ,إمتزاز,تلوث الماء .

Résumé

Les travaux réalisés dans le cadre de cette thèse visent à synthétiser des Bioadsorbants à base de bentonite locale et de biopolymère afin d'éliminer trois colorants industriels nommés: Bleu de Méthylène (MB), Rouge de Bézathrène (BzR) et Bleu de Telon (TB) séparément et dans des solutions mixtes. L'évolution structurelle de l'Organo-Bentonite (Bentonite modifiée avec différents pourcentages de bromure d'hexadécyltriméthylammonium (HDTMA-Br) et de Carboxyméthylcellulose CMC) ont été étudiés. Les matériaux préparés (BAS et BAS/CMC) ont été caractérisés par la diffraction des rayons X (XRD), la spectroscopie infrarouge (FTIR) et l'analyse thermogravimétrique (ATG/DTG). Plusieurs facteurs qui influencent la capacité d'adsorption, tels que le temps de contact, le pH, la concentration initiale de la solution de colorant, la masse de l'adsorbant et la température, ont été étudiés. Les isothermes d'adsorption des colorants par les adsorbants préparés sont décrites de manière satisfaisante par le modèle de Langmuir, alors que le modèle de Freundlich ne peut décrire nos résultats expérimentaux sur tout le domaine de concentration étudié. Les résultats obtenus sont encourageants, de sorte que les adsorbants préparés peuvent être testés et évalués à l'échelle industrielle avec des eaux usées plus complexes.

Mots clés : Organo/Bentonite, Colorants, Adsorptions, Biopolymères, Composites